EXPERIMENTAL AND MOLECULAR MODELING INSIGHTS ON THE THERMOLYTIC DEHYDROGENATION OF AMINE BORANES WITH IONIC LIQUIDS AND DEEP EUTECTIC SOLVENTS

A Thesis Submitted in Partial Fulfilment of the

Requirements for the Degree of

DOCTOR OF PHILOSOPHY

By

DHIRENDRA KUMAR MISRA

DEPARTMENT OF CHEMICAL ENGINEERING INDIAN INSTITUTE OF TECHNOLOGY GUWAHATI-781039, Assam, India

FEBRUARY, 2022

Dedicated to My Late Grandparents, Parents, Teachers, and Friends

Indian Institute of Technology Guwahati
Department of Chemical Engineering

Statement

I hereby declare that the content embodied in this thesis entitled "**Experimental and Molecular Modeling Insights on the Thermolytic Dehydrogenation of Amine Boranes with Ionic Liquids and Deep Eutectic Solvents**" is the result of investigations carried out by me at the Department of Chemical Engineering, Indian Institute of Technology Guwahati, Guwahati, India, under the supervision of **Prof. Tamal Banerjee and Prof. G. Pugazhenthi**.

In keeping with the general practice of reporting scientific observations, due acknowledgements have been made wherever the work described is based on the findings of other investigators.

Guwahati,
February 2022

Dhirendra Kumar Misra

Indian Institute of Technology Guwahati

Department of Chemical Engineering

Certificate

It is certified that the work presented in the thesis entitled **"Experimental and Molecular Modeling Insights on the Thermolytic Dehydrogenation of Amine Boranes with Ionic Liquids and Deep Eutectic Solvents"** is a bonafide work of **Mr. Dhirendra Kumar Misra (Roll No. 166107108),** has been carried out in the Department of Chemical Engineering, Indian Institute of Technology Guwahati, under our supervision and this work has not been submitted elsewhere for any other degree.

Dr. Tamal Banerjee
Professor
Department of Chemical Engineering
IIT Guwahati, Guwahati-781039
Assam, India

Dr. G. Pugazhenthi
Professor
Department of Chemical Engineering
IIT Guwahati, Guwahati-781039
Assam, India

ACKNOWLEDGEMENTS

My doctoral dissertation would not have come to successful completion without the help of several people. I take this opportunity to express my sincere gratitude to all of them.

To begin, I would like to express my gratitude to my thesis supervisors, **Prof. Tamal Banerjee Sir** and **Prof. G. Pugazhenthi Sir**, from the **Department of Chemical Engineering**, for motivating and building my confidence, as well as for their insightful suggestions, astute thinking, and coherent and logical counsel throughout the research period. Their constant support, constructive criticism, and meticulous planning have all contributed significantly to the development of the dissertation. Their true scientific zeal, autonomy, and self-reliance have aided considerably in improving the quality of my research. This feat was only achieved as a result of their unwavering support. I shall be eternally grateful to them for granting me the freedom to explore many research possibilities without worrying about achieving a successful conclusion as a result of my efforts. They encouraged me to visit many organizations as part of my research, which aided my maturation as a newbie to the research fraternity. I have always been certain that God has endowed me with the opportunity to pursue a doctoral degree under their supervision. To be very candid, whatever knowledge I got during my research period was entirely due to them. It was an absolute privilege to work alongside them. Many thanks, sir, for your wonderful assistance and support.

I would like to extend my sincere gratitude to my doctoral committee members, **Prof. Mahuya De**, **Dr. R. Prasanna Venkatesh**, and **Prof. Gopal Das**, for their incisive ideas and comments throughout the Ph. D. program's evaluation process. I would also like to extend my thanks to **Prof. Mahuya De**, **Dr. R. Prasanna Venkatesh**, and **Prof. Vaibhav Vasant Goud**, members of my comprehensive committee. I also thank **Prof. Bishnupada Mandal**, **Prof. Anugrah Singh**, Ex-Head, and **Prof. Kaustubha Mohanty** Head, Department of Chemical

Engineering, for his administrative support. Furthermore, I would like to thank other faculty members, research scholars, support staff of the Department of Chemical Engineering, IIT Guwahati, for their kind cooperation in all aspects.

I take this time to express my sincere gratitude to our collaborators **Prof. Nagarajan Sivaraman** (Director, Materials Chemistry & Metal Fuel Cycle Group), **Prof. Brahmmananda Rao** (Head, Solution Chemistry & Mass Spectrometry Section), and **Dr. Gopinadhanpillai Gopakumar** (Scientist D) at the Indira Gandhi Centre for Atomic Research, for their immense support and motivation during my visit to the organization. I would especially thank **Dr. Gopinadhanpillai Gopakumar** for sharing his immense knowledge, which inspired me to learn various quantum and computational chemistry prospects and move forward to take computational chemistry as my future research area. I would also like to thank **Prof. Brahmmananda Rao** for his valuable and constructive discussions on various topics of chemistry over lunch and tea, which helped me apply them in my thesis work.

I owe my sincere thanks to **Prof. Aditya Narayan Panda** (Department of Chemistry, Indian Institute of Technology, Guwahati) for helping me with various computational scripts during my research duration at IIT Guwahati.

I would also like to thank Central Instruments Facility (CIF) IIT Guwahati for providing NMR Analysis. Computational time from *PARAM-ISHAN* supercomputer (162 nodes and 3024 cores in each node), and Karplus (3 nodes, 12 cores in each node), facility of Institute, and Department of Chemical Engineering, IIT Guwahati is highly acknowledged. I acknowledge the Ministry of Human Resource Development (MHRD) and our institute for providing fellowship throughout the Ph.D. program. I would also like to thank the Department of

Chemical Engineering, IIT Guwahati, India for financially supporting attending an International Conference “COIL 2019” held in Beijing, China.

I sincerely acknowledge my research group members **Mr. Nikhil Kumar**, **Mr. Nabendu Paul**, **Mr. Arindam Dutta**, **Mr. Nipu Kumar Das**, **Mr. Raghibul Hussain**, **Mr. Harish G**, **Mr. Harsh Thakur** for providing a cooperative research environment.

I would like to express my profound gratitude to my previous group members **Dr. Basudhrity Banerjee**, **Dr. Mood Mohan**, **Dr. Anand Bharti**, **Dr. Papu Kumar Naik**, **Dr. Pyarimohan Dehury**, **Dr. Upasana Mahanta**, **Dr. Debashis Kundu**, **Dr. Rima Biswas**, **Mr. Janardan Singh**, **Mr. Ashvini Upadhayay**, **Mr. Harish Bhupathi**, **Mr. Sai Dileep Kumar Seera**, **Ms. Sambita Choudhary** for their immense support, encouragement, and help.

My sincere thanks to IIT Guwahati friends **Dr. Rahul Saha, Mr. Rahul Kumar, Mr. Nilesh Khalse, Mr. Ramanujan Pandey, Mr. Prateek Pranab, Mr. Rahul Tiwari, Mr. Kuldeep Sharma, Dr. Shyam Trivedi, Dr. Kishore Gajrani, Mr. Bastav Borah, Dr. Jogen Dutta** and many more for making my stay at IIT Guwahati memorable.

Finally, but certainly not least, I want to convey my sincere gratitude to my parents and family members for their sustained help and encouragement in all my personal and academic ventures. I feel proud and blessed to have such parents as my mother, **Mrs. Urmila Mishra,** and my father, **Mr. Raghvendra Mishra**, uncle and aunt. Special thanks to my loving brothers **Shivendra**, **Manvendra,** and **Varun,** who always strengthened my morale by standing by me in all situations. I'd want to express my heartfelt thanks to the owner of "**DEEDRAWS**," who has been encouraging me for several months and teaches me how to remain focused on my work each day.

I sincerely express my wholehearted gratitude to **Prof. Dhananjay Kumar Singh** (I.E.T Lucknow) for seeing my potential to pursue research as a career. I will be thankful to

him, and I promise I shall never forget his uncountable help and encouragement. Today, I am in this position just because of my parents. I do not find words to express my gratitude to them, and they are always in my heart. I feel deeply indebted to them for whatever I have achieved so far.

I wish to thank many other people whose names are not mentioned here, but this does not mean that I have forgotten their help. Above all, I am thankful to GOD for giving me a wonderful and healthy life.

DHIRENDRA KUMAR MISRA

भारतीय प्रौद्योगिकी संस्थान गुवाहाटी
रासायनिक अभियांत्रिकी विभाग
गुवाहाटी ७८१ ०३९, असम, भारत

INDIAN INSTITUTE OF TECHNOLOGY GUWAHATI
Department of Chemical Engineering
Guwahati 781039, Assam, India

Thesis Title : Experimental and Molecular Modeling Insights on the Thermolytic Dehydrogenation of Amine Boranes with Ionic Liquids and Deep Eutectic Solvents

Roll No : **166107008**

Name of the Candidate : **Dhirendra Kumar Misra**

Month/Year of Submission: February, 2022

Ph.D. Synopsis

The scientific community has identified hydrogen energy as a potential fuel for the foreseeable future. The hunt for hydrogen storage materials capable of storing hydrogen efficiently while remaining compact and lightweight is one of the most difficult tasks facing the emerging hydrogen economy. Using solid chemical hydrides with high gravimetric and volumetric hydrogen densities, it may be possible to overcome the difficulties associated with hydrogen storage. The solid-phase nature of these hydrogen storage devices provides key advantages such as ease of discharge, a greater kinetic, and controlled release of hydrogen equivalents at moderate temperatures.

However, solid-state dehydrogenation of AB has significant restrictions, including the need to modify the structure of AB molecules by employing carbon derivatives or adducts. Ionic liquids (ILs) and Deep Eutectic Solvents (DESs), a class of environmentally friendly solvents, have several potential usages because of their physicochemical features. ILs and DESs can be utilized to sidestep the issue of thermolysis of AB and its adducts due to their low

vapor pressure, superior thermal stability, and molecular tunability. Due to their solubilizing capabilities, ILs/DESs tend to stabilize the polar and transition intermediates produced during the dehydrogenation process, and they effectively inhibit the onset phase of the dehydrogenation process of AB and its adducts. Consequently, they foster a conducive environment for dehydrogenation to take place.

This thesis investigates the usage of ionic liquids (ILs) as a catalytic solvent media for the dehydrogenation of amine borane complexes. For the dehydrogenation study, a set of ILs based on methyl, ethyl, and butyl substituted pyrrolidinium, ammonium, and imidazolium cations with methyl carbonate [CH_3COO^-], methylsulfate [$MeSO_4^-$], methanesulfonate [$MeSO_3^-$], tetrafluoroborate [BF_4^-], and hexafluorophosphate [PF_6^-] anions have been selected for further investigation. Additionally, this work utilizes ionic liquid-based Deep Eutectic Solvents (IL-based DESs) and metal salt-based Deep Eutectic Solvents (Type 1 DESs). 1-butyl-3-methylimidazolium methanesulfonate ([BMIM][$MeSO_3$]) here is used as the hydrogen bond acceptor (HBA) for DESs in order to synthesize novel ionic liquid-based Deep Eutectic Solvents (IL-based DESs). In this case, Urea (U) and Imidazole (Im) are assumed to be the appropriate hydrogen bond donors (HBDs). Additionally, for the synthesis of Type 1 metal salt-based Deep Eutectic Solvents, choline chloride (ChCl) was considered as a hydrogen bond acceptor (HBA), whilst metal (II) chloride based on zinc and tin atoms was used as a metal halide salt, resulting in the design of Type 1 DESs.

The thesis begins by discussing the use of pyrrolidinium and ammonium-based ILs. Initially, ILs were employed to aid in the dehydrogenation of chemical hydrides, specifically ammonia borane (AB) and ethylene diamine bisborane (EDAB). Additionally, a conductor-like Screening Model-Segment Activity Coefficient (COSMO-SAC) thermodynamic model is utilized to screen out potential solvents from a large number of cations and anions. The dehydrogenation assays conducted in the presence of pyrrolidinium and ammonium cation-

based ILs revealed that ammonium-based ILs outperformed pyrrolidinium-based ILs, releasing 1.46 and 3.50 equivalents of hydrogen from AB and EDAB, respectively. In addition, ^{1}H and ^{11}B NMR validates the catalytic activity of ILs and the reaction mechanism for the dehydrogenation of chemical hydrides. However, as previously documented, the effect of anions' hydrogen bond basicity (β) on the catalytic process was non-existent during the preliminary dehydrogenation process. This prompted us to investigate the dehydrogenation reaction in the presence of imidazolium-based ILs and anions with varying β-value. Following dehydrogenation experiments on AB and EDAB in the presence of imidazolium-based ILs, it was determined that the effect of anions basicity on the dehydrogenation process is a controlling parameter in the presence of imidazolium cation. [$MeSO_4^-$] anion with a β-value of 0.71 coupled with $[Bmim]^+$ cation was capable of releasing 2.18 and 3.66 equivalents of hydrogen from AB and EDAB, respectively. Furthermore, a DFT-based calculation was performed to verify the origin of anion's basicity and its effect on the dehydrogenation process at the molecular level.

The economics of ILs are impeding their industrial deployment. Whereas in dehydrogenation, the inability to regenerate chemical hydrides in on-board devices necessitates us to use DESs. Due to the solubility of the polymer species formed during the reaction in ILs, the regeneration of chemical hydrides or the catalytic solvent is complicated. This transition focuses on the possibility of DESs as a catalytic solvent in the dehydrogenation reaction. The investigation continues by examining the type 1 metal salt-based DES formation mechanism, which was previously unknown. The design of DESs was thoroughly investigated using a combination of experimental and DFT-based computational methodologies. To validate the synthesis of DES, FTIR spectroscopy was used. Optimized geometries, interaction energies, and atom in molecules (AIM) and reduced gradient (RDG) analysis demonstrated the presence of electrostatic and hydrogen bond interactions in DES systems.

Additionally, higher dehydrogenation rates were observed with AB and EDAB in IL-based DESs due to their ionic nature and increased thermal stability. TGA analysis demonstrates no mass loss above 150°C, indicating that IL-based DES can be used as a catalytic solvent for the dehydrogenation of amine boranes at elevated temperatures. By stabilizing the transition species formed during the dehydrogenation process, [BMIM][$MeSO_3$]:[Urea], IL-based DES offered an optimal catalytic environment. [BMIM][$MeSO_3$]:[Urea] produces 3.2 equivalents of hydrogen gas, which is significantly less than its IL component [BMIM][$MeSO_3$]. In the next part, a type 1 metal salt-based DES constituted of ChCl and metal (II) halide salts was used as a catalytic solvent in the dehydrogenation process. ChCl: $ZnCl_2$ produced 3.89 equivalents of H_2, which was significantly more than the solvent systems used in this investigation. This study leads to the establishment of DES as a novel catalytic media for the thermolytic dehydrogenation of chemical hydrides.

The present thesis also investigated a novel hydrogen storage carrier, morpholine borane complex (MBC). Experimental investigations were conducted to verify the dehydrogenation of MBC in its solid-state, which resulted in the release of 0.6 equivalents of hydrogen gas and a more extended induction period compared to AB and EDAB. MBC was dehydrogenated for the first time in the presence of protic ILs, which are well-known for their catalytic activity. The addition of protic ILs improved the dehydrogenation of MBC, resulting in the release of 1.62 equivalents of hydrogen gas via an intramolecular and intermolecular dehydrogenation that was confirmed using ^{11}B NMR and DFT-based transition state calculations. Figure S1 provides an overview of the thesis.

Keywords: Ionic Liquids, Deep Eutectic Solvents, AB, EDAB, MBC, DFT, AIM, NCI

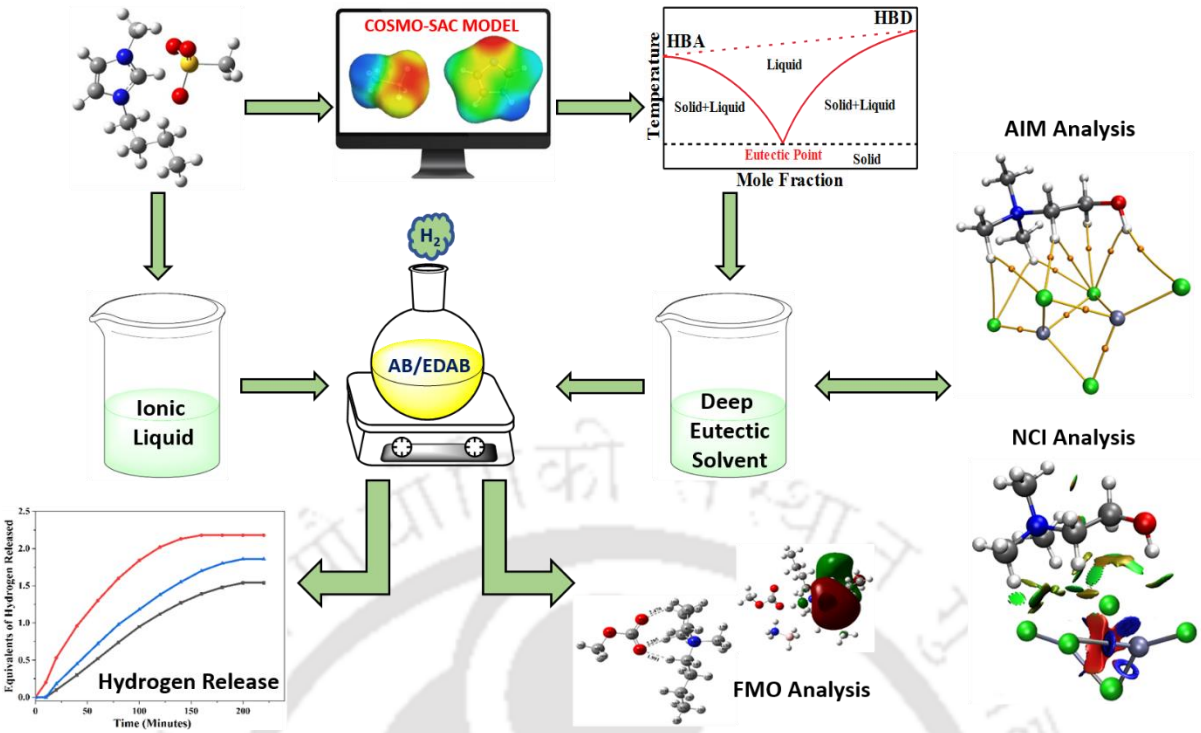

Figure S1: Schematic outline of the current thesis

Table of Contents

List of Figures

List of Tables

List of Schemes

List of Abbreviations and Symbols

Abbreviations

AB	Ammonia Borane
AIM	Atoms in Molecules
BCP	Bond Critical Point
B3LYP	Becke three-parameter, Lee-Yang-Parr
B3LYP-D3 (BJ)	Dispersion corrected density functional theory (Becke Johnson)
BP86	Becke 1988 exchange functional and the Perdew 86 correlation
BSSE	Basis Set Superposition Error
CCSD(T)	Coupled Cluster Single-Double and Triple
ChCl	Choline Chloride
CHELPG	CHarges from Electrostatic Potentials using a Grid-based method
COSMO-RS	COnductor like Screening MOdel for Real Solvents
COSMO-SAC	COnductor like Screening MOdel for segment activity coefficient
DES	Deep Eutectic Solvents
DFT	Density Functional Theory
DGA1	Density Gradient Approximation
FMO	Frontier Molecular Orbital
FTIR	Fourier transform spectroscopy

HBA	Hydrogen Bond Acceptor
HBD	Hydrogen Bond Donor
HF	Hartree Fock Theory
HOMO	Higher Occupied Molecular Orbital
IDAC	Infinite Dilution Activity Coefficient
IL	Ionic Liquid
IEFPCM	Integral Equation Formalism Polarizable Continuum Model
IE	Interaction Energy
IP	Ionization Potential
LUMO	Lower Unoccupied Molecular Orbital
MD	Molecular Dynamics Simulation
MS	Metal Salts
NBO	Natural Bonding Orbitals
NCI	Non-Covalent Interaction
NMR	Nuclear Magnetic Resonance
NPA	Natural Population Analysis
QC	Quantum Chemical
RDG	Reduced Density Gradient
RESP	Restrained Electrostatic Potential

SCRF	Self-Consistent Reaction Field
$SnCl_2$	Tin (II) Chloride
TGA	Thermo-Gravimetric Analysis
TZVP	Triple Zeta Valence Potential
QAS	Quaternary Ammonium Salt
QTAIM	Quantum Theory of Atoms in Molecules
VMD	Visual Molecular Dynamics
ZORA	Zero-Order Regular Approximation
$ZnCl_2$	Zinc (II) Chloride

Ionic Liquids

[AmPyr][CH_3CO_3]	1-Allyl-1-methylpyrrolidium methylcarbonate
[HmPyr][CH_3CO_3]	1-Hexyl-1-methylpyrrolidinium methylcarbonate
[PentPyr][CH_3CO_3]	1-Pentyl-1-methylpyrrolidinium methylcarbonate
[PropPyr][CH_3CO_3]	1-Propyl-1-methylpyrrolidinium methylcarbonate
[BmPyr][CH_3CO_3]	1-Butyl-1-methylpyrrolidinium methylcarbonate
[EtPyr][CH_3CO_3]	1-Ethyl-1-methylpyrrolidinium methylcarbonate
[HxPyr][CH_3CO_3]	1-Hexadecyl-1-methylpyrrolidinium methylcarbonate
[TMA][CH_3CO_3]	Tetramethylammonium methylcarbonate
[TEA][CH_3CO_3]	Tetraethylammonium methylcarbonate
[TBA][CH_3CO_3]	Tetrabutylammonium methylcarbonate
[TPA][CH_3CO_3]	Tetrapentylammonium methylcarbonate
[THA][CH_3CO_3]	Tetrahexylammonium methylcarbonate
[TBMA][CH_3CO_3]	Tributylmethylammonium methylcarbonate
[TEMA][CH_3CO_3]	Triethylmethylammonium methyl carbonate
[EMIM][SCN]	1-Ethyl-3-methylimidazolium thiocyanate
[AMIM][Cl]	1-Allyl-3-methylimidazolium chloride
[AMIM][Br]	1-Allyl-3-methylimidazolium bromide
[BMIM][HSO4]	1-Butyl-3-methylimidazolium hydrogensulfate

[EMIM][OAc]	1-Ethyl-3-methylimidazolium acetate
[BMIM][Cl]	1-Butyl-3-methylimidazolium chloride
[EMIM][MeSO3]	1-Ethyl-3-methylimidazolium methanesulfonate
[BMIM][$MeSO_3$]	1-Butyl-3-methylimidazolium methanesulfonate
[EMIM][MeSO4]	1-Ethyl-3-methylimidazolium methylsulfate
[BMIM][$MeSO_4$]	1-Butyl-3-methylimidazolium methylsulfate
[BMIM][BF4]	1-Butyl-3-methylimidazolium tetrafluoroborate
[BMIM][PF6]	1-Butyl-3-methylimidazolium hexafluorophosphate

List of Symbols

a_{eff}	Effective contact surface area of a segment in Å^2
C_{hb}	Effective contact surface area of a segment in Å^2
E_{misfit}	Misfit interaction energy
E_{vdW}	Van der Waals (vdW) interaction energy
$p_s(\sigma)$	Probabilistic surface charge distribution for mixture (S)
p^{Xi} (σ)	Sigma profile of the pure component i
r_{n}	Radius of the nth segment
r_{eff}	Radius of the standard surface segment (a_{eff}) in Å
r	Pure component volume
q	Pure component area
r_{avg}	Average radius in Å
R	Universal gas constant in (kcal mol^{-1} K^{-1})
T	Temperature in K
Q	Normalized area parameter
x_i	Mole fraction of species 'i'
d_{mn}	Distance between the mth and nth segment
A^{PCM}	Molecular surface area in Polarizable Continuum Model, in^2
A_{ws}	Standard segment area, cm^2 mol^{-1}

V^{PCM}	Molecular surface volume in Polarizable Continuum Model, in^3
V_{ws}	Standard segment volume, $cm^3\ mol^{-1}$

Greek Symbols

$\Gamma_s(\sigma)$	Segment activity coefficient for mixture (S)
$\Gamma_i(\sigma)$	Segment activity coefficient for pure component (i)
γ_i/s	Component activity coefficient in the mixture (S)
Φ_i	Fugacity coefficient of the component in mixture
A	Non-randomness parameter
α'	Misfit constant in kJ mol^{-1} Å^{-2}
σ, σ'	Screening charge density in e Å^{-2}
σ_{don}	Screening charge density for hydrogen-bond donor in e Å^{-2}
σ_{acc}	Screening charge density for hydrogen-bond acceptor in e Å^{-2}
σ_{hb}	Screening charge density for hydrogen-bond in e Å^{-2}
τ_{vdW}	Dispersion coefficient in kJ mol^{-1} Å^{-2}
$\mu_s(\sigma)$	Sigma potential in kJ mol^{-1} Å^{-2} for a surface segment in solution S

CHAPTER 1

Introduction and Literature Review for the Thermal Dehydrogenation of Amine Boranes in Ionic Liquids and Deep Eutectic Solvents

1.1. Hydrogen as a Future Fuel

The term "hydrogen economy" has gained traction in recent years. To put it another way, a hydrogen economy is a picture of the future in which electric power will be created not by direct combustion of fossil fuels or nuclear fission but rather through the electrochemical oxidation of hydrogen in a fuel cell device.[1] There are significant prospects of replacing conventional power plants with hydrogen-powered fuel cells, whether on the grid or distributed energy applications. Aside from that, there is a great deal of interest in discovering alternatives to fossil fuels for use in transportation applications.[2] Internal combustion engines (ICEs) powered by hydrogen are also an alternative for transportation, which is the reason that this hydrogen consumption method is included in the hydrogen economy vision.[3] Finally, several ventures are researching tiny fuel cells as a potential replacement for batteries in portable/mobile applications such as laptop computers and mobile phones.

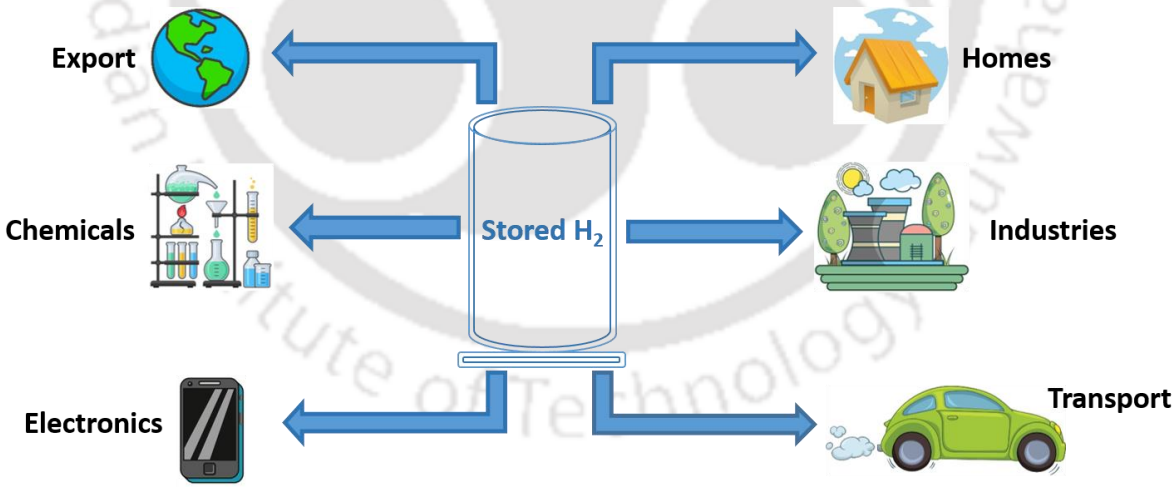

Figure 1.1: Different applications of hydrogen as a fuel source

Hydrogen storage and delivery must be resolved prior for the hydrogen economy to be accomplished on a national or global scale, regardless of the use.[4] Other critical concerns include developing low-cost, sustainable, and effective methods for hydrogen production and

distribution, as well as enhancing the efficiency and dependability of the fuel cell and lowering its cost. International research is being conducted on these critical concerns, and a list of possible science and technology reviews are accessible.[5]

When it comes to petrochemical applications, hydrogen production, storage, transport, and use are well matured and well-developed. However, hydrogen storage and generation for the hydrogen economy, as stated above, are now under development.[6] In addition to the ways to hydrogen storage and transport that are currently under active study and development, there are various other approaches that have been discussed in studies that are both scientific and application-oriented.[7] A multitude of chemical processes can release hydrogen, which can then be used in a fuel cell or an ICE.[8] Complex chemical hydrides have also been found to be capable of storing hydrogen in the solid form at temperatures and pressures that are close to ambient.[9] The thermophysical properties of chemical hydrides and reaction products are particularly important for sizing storage and heat management equipment.[10] The selection of catalysts and the design of the reactor for hydrogen delivery to the power conversion device is ultimately dictated by the kinetic characteristics of the hydrogen, in conjunction with the thermochemistry.[11] Naturally, economic analysis, security, and transportation infrastructure all play a role in the hydrogen economy, and these concerns can be handled through the use of various hydrogen storage materials.[12] In comparison to alternative hydrogen storage technologies, chemical hydrides will be our primary emphasis, primarily due to their high hydrogen content and ability to release a significant amount of hydrogen at moderate temperatures and a faster reaction rate.[13]

1.2. Chemical Hydrides

Hydrogen, one of the cleanest sources of energy, is gaining a lot of attention lately since it has the potential to replace fossil fuels and petrochemical resources.[14] In our pursuit of a hydrogen-powered economy as a long-term solution to the world's energy concerns, one of the

most difficult hurdles is the discovery of effective hydrogen storage materials.[15] One of the major obstacles is the lack of onboard hydrogen storage, which limits the use of hydrogen as a fuel for vehicular applications and fuel cells.[16] As a result, much research has been conducted to exploit promising hydrogen storage materials, such as metal-organic frameworks, chemical hydrides, and metal hydrides, in order to overcome this barrier.[17]

This resulted in the investigation of a number of chemical hydrides, which, upon heat disintegration, release a significant amount of hydrogen gas.[18] The amine borane family of compounds, commonly known as B-N compounds, may be considered a contender for hydrogen storage.[13] It is well established that B-N compounds have hydrogen linked to the B and N moieties, which can be desorbed at a moderate temperature in the presence of a solvent or a catalytic system.[19] In the amine borane family, ammonia borane (AB) is the most basic compound and has been discovered as a promising chemical hydride storage medium due to its high hydrogen weight percent (19.6 wt%) and probable regenerability.[20] As illustrated in Fig.1.2, AB has a higher gravimetric density than the majority of other documented chemical systems. This combined capacity and stability has rekindled interest in ammonia borane as a hydrogen storage carrier.[21] An ample study has been carried out during the initial years after the first synthesis and characterization of Ammonia Borane (NH_3BH_3) by Sheldon Shore in the late '50s.[22] The polar nature of ammonia borane (5.2 debye) thus contributes to the physical properties where an extensive network of dihydrogen bonding between amine and boron species of adjacent ammonia borane molecules has been suggested as a key phenomenon that dictates dehydrogenation from ammonia borane in the solid-state.[23]

The breakdown of AB can also result in the production of borazine and ammonia gas, both of which are highly hazardous in nature and can congest fuel cells.[24] Numerous attempts have been made to resolve this issue, many of which entail altering the structure of ammonia borane via the use of carbon derivatives or adducts of AB molecules.[25] Although partial

dehydrogenation of ammonia borane can be generated thermally in the solid-state, milder conditions and more controlled reactions are required for the process to be beneficial for hydrogen storage. Given these considerations, it is known that carbon substituted amine boranes such as ethylene diamine bisborane (EDAB),[26] tert-butyl amine borane (TBAB),[27] methyl amine borane (MeAB),[28] and sec-butyl amine borane (SBAB)[29] exist. These amine boranes release less hydrogen but do not produce volatile or hazardous compounds.

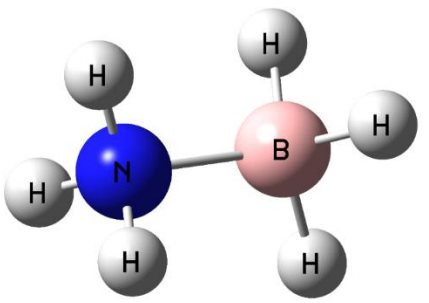

Ammonia Borane (AB) (19.6 wt%)

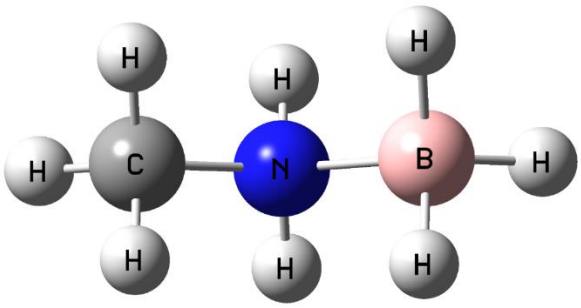

Methylamine Borane (MeAB) (11.23 wt%)

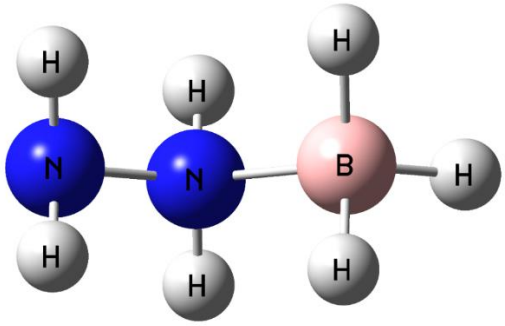

Hydrazine Borane (HAB) (15.38 wt%)

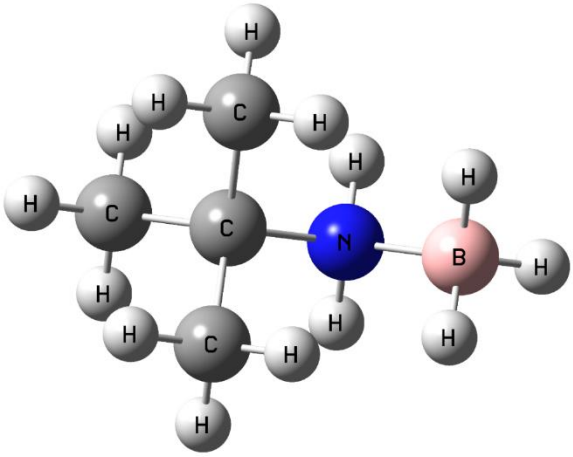

Tert-Butylamine Borane (TBAB) (5.80 wt%)

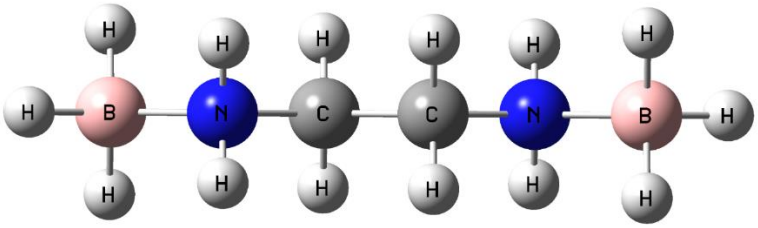

Ethylenediamine bisborane (EDAB) (11.49 wt%)

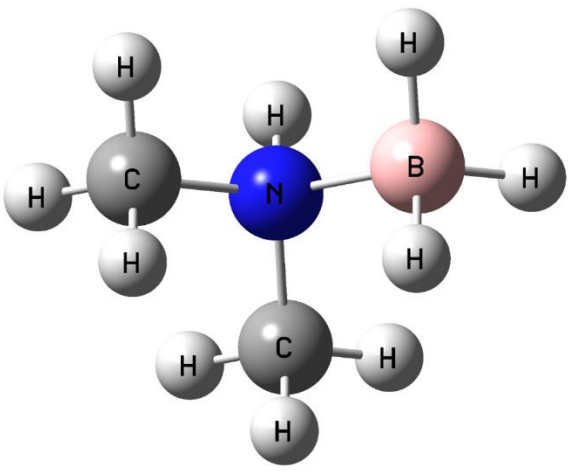

Dimethylamine Borane (DMAB) (6.84 wt%)

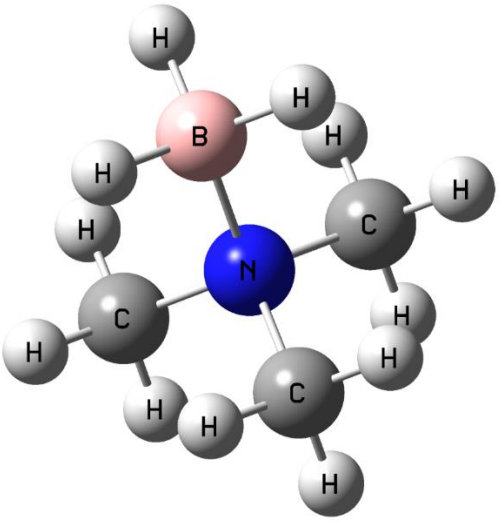

Trimethylamine Borane (TMAB) (5.53 wt%)

Figure 1.2: Various chemical hydrides and their hydrogen content

Carbon replacements for amine borane complexes were introduced into practice with the advancement of technology and resources. Despite the fact that it contains a high amount of hydrogen, hydrazine borane (HAB) cannot be used as a hydrogen storage carrier due to its instability and explosive nature at higher temperatures.[30] Given its higher gravimetric density (11.5 weight percent), EDAB was adopted for the dehydrogenation reaction in this application.

Ethylene diamine bisborane (EDAB), a white crystalline molecule with outstanding kinetic stability, is a hydrogen storage carrier with the promise to be a credible alternative to ammonia borane.[31] In comparison to AB, it is more stable at temperatures below 100°C and releases approximately 10.0 wt% of molecular hydrogen without discernible toxins between 100 and 200°C, at ambient pressure.[32] At temperatures greater than 120°C, Neiner et al. demonstrated that EDAB releases hydrogen at a quicker rate than ammonia diborane.[33] However, as a potential solid-state hydrogen carrier, EDAB confronts a shorter induction period than AB. To circumvent the problems associated with solid-state dehydrogenation, solvent-assisted dehydrogenation approaches induced by environment-conscious solvents such as ionic liquids (ILs)[34], and Deep Eutectic Solvents (DESs)[35] have been developed.

1.3. Ionic Liquids and their Usage as a Thermal Dehydrogenation Media

ILs can be defined as a substance that is solely made up of ions, organic cations, and organic/inorganic anions, which is liquid at temperatures close to the ambient temperature and does not crystallize at room temperature.[36] Additionally referred to as room temperature ionic liquids (RTILs), these solvents have been proven to be peculiar solvents owing to the distinctive features dictated by their structure and interactions occurring within the system. RTILs are usually made up of large organic cations and inorganic or organic anions.[37] The cations based on imidazolium or pyridinium rings with one or more alkyl groups linked to the nitrogen or carbon atoms are the most usually regarded for extraction and synthesis, while quaternary ammonium salts have been widely implemented for electrochemical applications.[38] The most frequently employed ions are halide (Cl, Br), tetrafluoroborate (BF_4), tetrafluoroaluminate ($AlCl_4$), hexafluorophosphate (PF_6), and bis(perfluoromethyl-sulfonyl)imide anion $(CF_3SO_2)_2N$. [39]

Since a long time, the catalytic abilities of ILs have been considered in a wide variety of applications.[40] Since their inception, ILs have been routinely employed in the catalytic dissolution of lignocellulosic biomass. Due to the solvent's ability to dissolve pure cellulose, lignin, and hemicellulose, the researchers investigated the solvent's potential to dissolve raw lignocellulosic biomass.[41] Moyna and colleagues first described the use of [Bmim][Cl] and its capacity to dissolve a variety of wood species with differing degrees of hardness.[42] Li and Zhao demonstrated that raw cellulose might be hydrolyzed in [Bmim][Cl] in the presence of mineral acids such as H_2SO_4, HCl, HNO_3, and H_2PO_4.[43] The research revealed that the acidity of the acids in the presence of IL is a critical parameter in the hydrolysis of cellulose. Several other fields of research demonstrate the broad utility of ILs in homogeneous and heterogeneous catalysis.[44]

The first homogeneous catalysis reaction to utilize RTILs was a transition metal catalysis reaction. Using a Ziegler-Natta catalyst, the reaction involved the use of weakly acidic imidazolium-based chloroaluminates for the polymerization of ethylene.[45] However, chloroaluminate-based ILs are notoriously moisture-sensitive and rapidly hydrolyze to hydrochloric acid and aluminum oxides, which is a significant disadvantage for a process. To make the process more efficient, researchers also opted to substitute the chloroalumiante anions with tetrafluoroborate or nitrate anions, known as hydrolytic stable anions. Emphasis is being placed on expanding the anions accessible for modifying and optimizing the catalytic performance of ILs. Numerous heterogeneous catalytic reactions have benefited from the use of task-specific ILs (TSILs), which are composed of various cations and anions.[46] In general, regardless of its nature, the use of an IL in heterogeneous catalysis results in an increase in reaction activity. There are just a few instances where adverse impacts are documented when IL is used, owing to mass transportation constraints. However, these concerns can be solved

by gaining a better understanding of the IL system required for a specific reaction, which can have a positive effect on the reaction's desired yield.[47]

Due to their physicochemical properties, IL's are advantageous for a variety of applications in the field of hydrogen storage.[48] In their initial work, Sneddon et al. have demonstrated that IL's are capable of acting as promoting solvents for the dehydrogenation of amine boranes.[49] Due to their low vapor pressure, excellent thermal stability, and molecular tunability, ionic liquids can be used to circumvent the problem of thermolysis of amine borane and its adducts (Figure 1.3). Since ILs have a solubilizing property, they are an excellent alternative for use as solvents in a broad array of applications. Due to their solubilizing properties, ILs tend to stabilize the polar and transition intermediates generated during the dehydrogenation process, and they are effective in suppressing the onset phase of the dehydrogenation process of ammonia borane and its adducts. Consequently, it creates favorable conditions for dehydrogenation to occur.

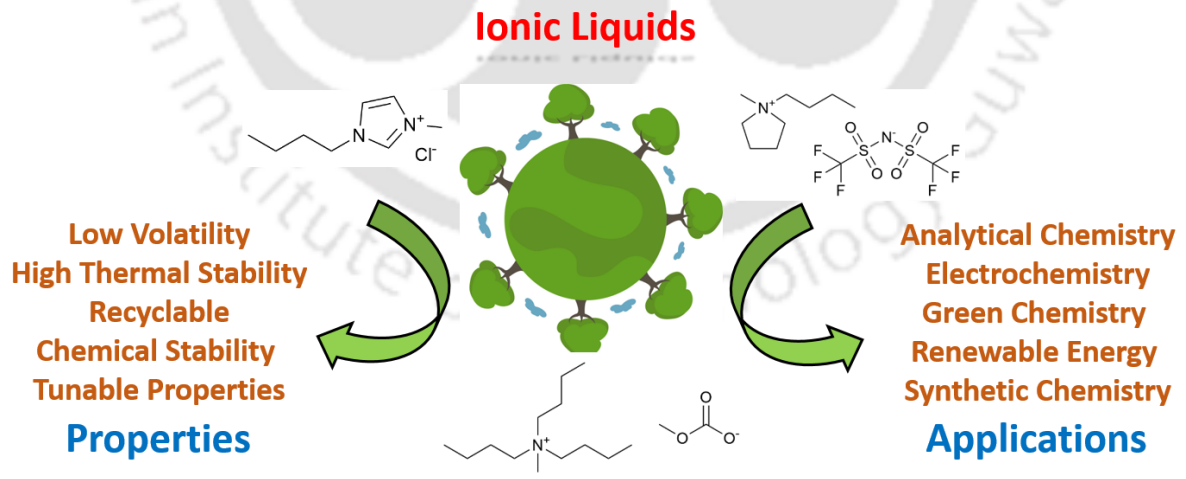

Figure 1.3: Various applications and properties of Ionic Liquids (ILs)

Himmelberger and colleagues demonstrated in another study that the release of hydrogen equivalents from ammonia borane can be significantly increased by the addition of ionic liquids.[50] These systems facilitate the generation of hydrogen gas at low temperatures, with high reaction rates and total hydrogen yields. The addition of ILs lowers the activation energy required to initiate the rate-determining reaction, namely the formation of an ionic intermediate species diammoniate of diborane [DADB]. It was discovered that the rate-determining step is the formation of DADB.[51] The increased reaction rate and decreased operating temperature are attributed to the stabilization of DADB in a more bronsted basic environment offered by some task-specific ionic liquids (TSILs). When compared to solid-state dehydrogenation of AB, the time required for hydrogen liberation is significantly reduced when employing ILs for the solvent-assisted dehydrogenation of AB. On dehydrogenation, solid-state AB generated 0.9 equivalents after an induction period of 3hrs when operated at 85°C, but a mixture of AB/IL produced 1.0 equivalent of hydrogen gas within 67 minutes; and 2.2 equivalents of hydrogen in 330 minutes at 85°C with a minimal induction duration.[52]

The study of reaction kinetics in both domains, namely solid-state ammonia borane and ammonia borane with ionic liquids, has been limited due to the fact that each domain requires a unique modeling strategy.[53] Sahler and his colleagues carried out studies with a variety of ionic liquids to determine their catalytic influence on the dehydrogenation of ethylene diamine bisborane (EDAB). They investigated the catalytic activity of many different catalytic solvents based on imidazolium and pyrrolidinium cations. This system is capable of delivering around 6.5 wt% hydrogen at 140°C, which is comparable to the capacity of traditional hydrogen storage systems. The authors explored the relationship between the polarity of the ILs and the amount of hydrogen produced, where an analysis of the appropriateness of the results for hydrogen storage devices were discussed.[54]

As part of the same field of research, Zhang et al. reported the hydrogen (H_2) production and reaction rate measurements of ammonia borane (AB) thermolysis in both its pure form and with the addition of an ionic solvent, 1-butyl-3-methylimidazolium chloride ([bmim][Cl]).[55] All measurements were carried out under quasi-isothermal conditions at varying temperatures ranging from 85°C to 120°C. For the first time, the specifics of rapid hydrogen evolution at the initial step of the thermolysis process have been documented. As a result of their investigation, they concluded that the addition of [bmim][Cl] resulted in a considerable increase in both the rate and amount of hydrogen equivalents emitted compared to the same amounts at equal temperatures for neat thermolysis of AB. Ahluwalia et al. proposed a model for ammonia borane dehydrogenation facilitated by imidazolium-based IL on the basis of data from an isothermal batch reaction.[56] The proposed system was capable of releasing 2.35 equivalents of H_2 at a temperature greater than 200°C. Modifications were done to the Avrami-Erofeyev model to account for the two-step dehydrogenation scheme. The Adams-Bashforth-Moulton method was used to solve the ordinary differential equations.

In a recent work, Banerjee et al. demonstrated the dehydrogenation of ethylene diamine bisborane (EDAB) using allyl-based imidazolium cations at three distinct temperatures and under vacuum circumstances.[57] The allyl-based ionic liquid (IL) was chosen based on its infinite dilution activity coefficient (IDAC), which was predicted using the COSMO-SAC (COnductor-like Screening MOdel-Segment Activity Coefficient) model. At 115°C, the EDAB/[AMIM][Br] system produced the maximum amount of hydrogen (3.25 equivalents). Kundu et al. proposed ionic liquid (IL) aided dehydrogenation of tert-butylamine borane (TBAB) at a moderate temperature of 90°C and 105°C.[58] For the purpose of screening probable IL solvents, (COSMO-SAC) based thermodynamic model was used to predict the solubility of TBAB in various ILs. At 105°C, TBAB/[Bmim][OAc] released 1.95 equivalents of hydrogen, while TBAB/[TDTHP][Phosph] produced 1.63 equivalents after 360 minutes of

dehydrogenation. Banerjee et al. devised a strategy for screening ILs for subsequent EDAB dehydrogenation. Initially, the ILs were screened using the quantum chemical-based COSMO-SAC model. To avoid the existence of impurities and moisture, the thermal dehydrogenation of EDAB was carried out at 95°C and 105°C in a vacuum.[59] At 105°C, desorption of EDAB/[BMIM][OAc] and EDAB/[EMIM][OAc] resulted in the release of a total of 3.96 and 3.52 equivalents of hydrogen, respectively. The released gases during the dehydrogenation experiment were analyzed using the gas chromatographic (GC) analysis. A brief quantum chemical-based DFT calculations were performed to understand the mechanism of IL-induced dehydrogenation of EDAB. The capacity to dissolve polar and non-polar organic, inorganic, and polymeric molecules is a well-known property of imidazolium cation-based ILs. They are used widely in catalytic reactions such as biomass treatment, extraction, and separation.[55] Despite their lower cost and documented physicochemical features, ammonium and pyrrolidinium cation-based ILs have not been explored in the accessible literature for dehydrogenation of AB and EDAB.[46]

However, ILs are not commonly used in industrial applications at the moment due to their high cost and toxicity concerns. It is possible that the continuous development and usage of these solvents will result in inadvertent discharge and pollution, which has not been explored so far. Chemical and thermal stability, as well as non-volatility, are among the characteristics that make them attractive as a prospective industrial target. However, degradation and persistence in the environment are two issues that they may encounter. In general, a lack of knowledge and uncertainty about the environmental impact of ILs is a significant impediment for use in industry.[60] Attempts have been undertaken to circumvent this limitation and gain a rudimentary understanding of how ILs respond in aqueous environments.

Recently, DESs have been discovered as novel IL analogues developed as green solvent substitutes to regular ILs because of their ease of preparation, high purity, and low cost

compared to more traditional ILs.[61] This is precisely the domain in which we desire to investigate these solvents.

1.4 Deep Eutectic Solvents

DESs are defined as the formation of particular interactions, primarily hydrogen bonds, between two molecules, specifically a Hydrogen Bond Donor (HBD) and a Hydrogen Bond Acceptor (HBA).[63] This results in the formation of a new chemical entity with a lower melting point than the precursor compounds. DESs, in particular those derived from natural sources, have been discovered, and it is anticipated that these compounds will be converted into a new class of chemicals appropriate for a wide variety of applications in the near future. Overall experimental studies have assessed both environmental concerns and energy conservation.[35] The latter is attainable through the design of novel eutectic systems based on their structure and properties, with the ultimate goal of inventing and optimizing industrial processes based on thermal dehydrogenation of amine boranes. An important advantage lies in the fact that DESs have solvent qualities similar to those of RTILs while being significantly less expensive, more readily synthesized, highly pure, nontoxic, and biodegradable.

DESs can be generally divided into four groups based on the nature of the complexing agent that is used in their synthesis. DESs of type I are formed of quaternary ammonium salt (QAS) and metal halide salts, while DESs of type II are composed of QAS and metal salt hydrate. DESs of type III are composed of QAS and hydrogen bond donors (HBD), such as amides, alcohols, and carboxylic acids. The final class of DESs, namely type IV, comprises metal halide salts and HBD.[62] The various types of reported DESs are mentioned in Table 1.1.

Table 1.1: Types of DESs, their general formula, terms and examples

Types	*General Formula*	*Terms*	*Example*
Type I	$Cat^+X^- + zMCl_x$	*M = Zn, In, Sn, Al, Fe*	*ChCl + $ZnCl_2$*
Type II	$Cat^+X^- + zMCl_x.yH2O$	*M = Cr, Ni, Cu, Fe, Co*	*ChCl + $CoCl_2.6H_2O$*
Type III	$Cat^+X^- + zRZ$	*M = Cr, Ni, Cu, Fe, Co*	*ChCl + Urea*
Type IV	$MCl_x + zRZ$	*M = Zn, Al and Z = OH, $CONH_2$*	*$ZnCl_2$ + Urea*

The physicochemical properties of type III eutectics produced from choline chloride and hydrogen bond donors have drawn attention because of their capacity to solvate a wide spectrum of transition metal species, including transition metal chlorides and transition metal oxides.[63] In 2004, Abbot et al. identified the type III deep eutectic phenomena for a 1:2 molar ratio combination of choline chloride (ChCl) and urea (U).[64] ChCl is a QAS that acts as an HBA with a melting temperature of 302°C, while urea is an HBD with a melting point of 133°C. The result of the mixture is a eutectic that freezes at 12°C. Thus, the eutectic mixture's freezing point is lowered by 178°C. A limitless number of DESs can be synthesized from the chemicals now accessible because there is a vast number of salts and HBDs that can be employed in the DES synthesis process. They have proven to be quite versatile, with a diverse variety of potential applications being examined, including the removal of glycerol from biodiesel, the processing of metal oxides, and the synthesis of cellulose derivatives, among others.[65] Until yet, only a limited number of DESs have been used. The future holds tremendous promise for expanding the types of salts and hydrogen bond donors used, hence expanding the applications of these solvents, most notably as a thermal medium, catalytic media, and separation, and extraction solvent.[66]

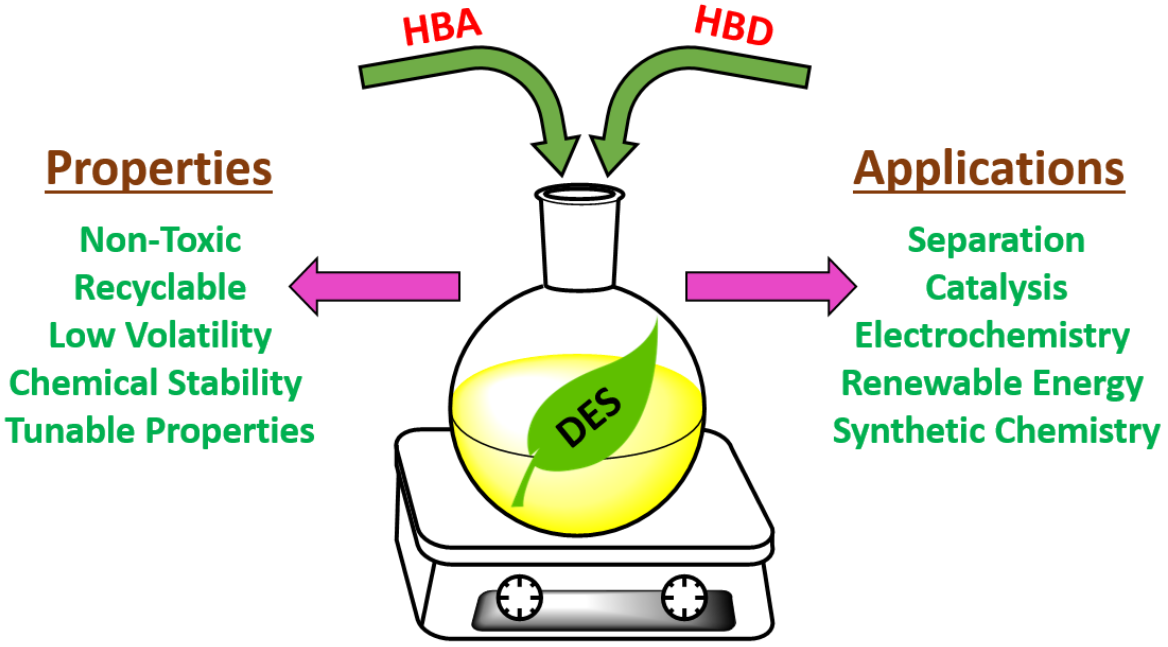

Figure 1.4: Various properties and applications of Deep Eutectic Solvents (DESs)

It has been demonstrated that ILs and molten salts may be utilized in redox flow batteries (RFBs) in the past, and Sandia National Laboratories has suggested and deployed metal ion-based ILs.[67] Recently, Chakrabarti et al. proposed that Deep Eutectic Solvents (DESs) might be used in a variety of applications, including electrolytes for lithium-ion batteries and possibly fuel cells.[68] The work provides an overview of distributed energy systems and analyzes the feasibility of incorporating them into renewable energy storage and load balancing applications at the utility scale. It begins with a review of energy storage technologies and the RFB and then goes on to provide information about ILs and DESs, as well as their applications in electrochemistry and energy conversion, among other things.[69]

In general, the literature review reveals that the majority of work is conducted with imidazolium-based ionic liquids.[49,52,54,55] Due to their advantageous properties, such as low densities, viscosities, and melting points, ammonium and pyrrolidinium cation-based ILs are investigated in detail in this work to verify their application in the dehydrogenation of amine borane compounds, a process that has remained unexplored to date. With the investigation of

dehydrogenation of amine borane derivatives in the presence of ionic liquids, several significant effects such as hydrogen bond basicity of anions, the effect of anions, and the effect of cations are uncovered. Further thermal dehydrogenation of ammonia borane and its derivatives using Deep Eutectic Solvents (DESs) have yet to be investigated.

1.5. Objective of the Thesis

The aim of this thesis is to investigate the dehydrogenation of amine-borane complexes in the presence of non-toxic solvents such as Ionic liquids (ILs) and Deep Eutectic Solvents (DESs). To gain a better knowledge of the dehydrogenation process and to design solvents that will address future requirements, comprehensive experimental work and accurate computational models are essential. As a result, this thesis addresses both experimental and theoretical aspects. In view of the existing literature and knowledge gap indicated in the previous sections, the following objectives have been established for the thesis study.

a) *Assessment of prospective ionic liquid systems using COSMO-SAC model for solubilizing ammonia borane (AB) and ethylene diamine bisborane (EDAB) and their effect in thermal dehydrogenation of chemical hydrides.*
b) *Screening of potential Deep Eutectic Solvents, i.e., hydrogen bond acceptor (HBA) and hydrogen bond donor (HBD) for the thermal dehydrogenation of amine boranes.*
c) *To understand the formation mechanism of type 1 Deep Eutectic Solvents and their interaction with chemical hydrides using quantum chemical calculations.*
d) *Preparation and characterization of DESs and their application in thermal dehydrogenation of ammonia borane (AB) and ethylene diamine bisborane (EDAB) complexes.*

e) *Thermal dehydrogenation of novel hydrogen storage material morpholine borane in the presence of acidic ILs and obtain the transition state search for the onset of dehydrogenation of morpholine borane using DFT calculations.*

1.6. Outline of Thesis

The current thesis is organized into the following chapters. The schematic outline of the current thesis is presented in Figure S1.

A variety of scaffolds which exist to serve for the dehydrogenation of chemical hydrides in solid form are described in **Chapter 1**. Scaffolds can be catalytic, non-catalytic, or solvent systems. Dehydrogenation of chemical hydrides in the solvent state provides a number of advantages over catalytic and hydrolytic dehydrogenation. Significant technical hurdles remain unanswered despite using ionic liquids (ILs) in prior reported studies. When it comes to their catalytic effect in the dehydrogenation process, only a small number of ILs have been studied thus far. Additionally, until now, a precise molecular level understanding of the dehydrogenation mechanism is unknown. As an alternative, the possibility of Deep Eutectic Solvents (DESs) as a catalytic solvent for dehydrogenation has not been investigated to date. To address this knowledge gap, we have explored the dehydrogenation of amine boranes in ionic liquids (ILs) and innovative solvents, including Deep Eutectic Solvents (DESs).

In **Chapter 2**, ammonia borane (AB) and ethylene diamine bisborane (EDAB) are dehydrogenated using ionic liquids (ILs). The COSMO-SAC model was used to predict the solubility of hydrides AB and EDAB in ILs. A comparative set of experiments were conducted to verify the effect of anions' basicity and its impact on the dehydrogenation of amine boranes. We performed density functional theory (DFT) calculations on the ILs to get additional insight into the ion-pair interaction between chemical hydrides and various functional groups of cations and anions. Following the dehydrogenation of amine boranes in the presence of ILs,

we have concentrated on the dehydrogenation of AB and EDAB in the presence of solvents that have not been used in this process, namely Deep Eutectic solvents (DESs).

Chapter 3 focuses on understanding the mechanism involved in the formation of Type I-based Deep Eutectic Solvents at the molecular level. We have described the molecular mechanism of the formation of metal salt-based Deep Eutectic Solvents (DESs) in this chapter and their charge transfer analysis and thermodynamics related to their formation, using density functional theory (DFT) calculations. The experimental approach of FTIR spectroscopy was used to validate the mechanism involved into the formation of DES. Additionally, the atom-in-molecules (AIM) and non-covalent interactions (NCI) analyses indicate that DES systems exhibit a significant electrostatic connection. The frontier molecular orbital analysis was used to determine the chemical stability and reactivity of the investigated DES complexes. This experimental and computational investigation revealed key chemical details about the design of these inexpensive ionic liquid mimics.

Chapter 4 advances with the knowledge of the formation mechanism of DESs that will facilitate its future use in dehydrogenation experiments. This chapter discusses the dehydrogenation of chemical hydrides, specifically ammonia borane (AB) and ethylene diamine bisborane (EDAB), in the presence of newly synthesized ionic liquid-based Deep Eutectic Solvents, referred to as. In the introductory section, the COSMO-SAC model was used to predict the solubility of AB and EDAB in the given DES. Following the selection of an appropriate solvent, the DES was prepared in the desired molar ratio. It also investigated the dehydrogenation of AB and EDAB systems in DES. A comprehensive examination was conducted to compare the dehydrogenation capacities of ILs and IL-based DESs. It also compared the dehydrogenation capacities of ILs and IL-based DESs. The findings revealed the fact that Deep Eutectic Solvents based on ionic liquids might be employed as a solvent-catalytic media in the thermolytic dehydrogenation of amine borane derivatives. The investigation of

thermolytic dehydrogenation prompted us to investigate dehydrogenation in the presence of Type I DESs. During the initial stages of the dehydrogenation reaction, a shorter induction period was noted, which can be linked to the high viscosity of the DES systems'. This lag is visible in our DES-facilitated dehydrogenation experiment, and it prevents the prospect of developing a lower viscosity solvent capable of enhancing both reaction and dehydrogenation rates concurrently.

With an eye on developing innovative hydrogen storage carriers, **chapter 5** discusses the dehydrogenation of morpholine borane (MB), a novel chemical hydride that has the potential to be exploited as a hydrogen storage carrier in the future. For the first time, we compared solid-state and ionic liquid-mediated dehydrogenation of the morpholine borane complex. To identify the optimal ionic liquid solvent for the dehydrogenation experiment, the COSMO-SAC model was used. In order to predict the mechanism responsible for the hydrogen release from MB, ^{1}H, and In-situ ^{11}B NMR experiments were conducted. It also reports the intramolecular process of hydrogen release from the MB complex using density functional theory (DFT)-based transition state calculations. Finally, **chapter 6** summarizes the major findings of this thesis work and a discussion of potential avenues for future research.

References

(1) Vezirolu, T. N.; Barbir, F. Hydrogen: The Wonder Fuel. *Int. J. Hydrogen Energy* **1992**. https://doi.org/10.1016/0360-3199(92)90183-W.

(2) Schlapbach, L.; Züttel, A. Hydrogen-Storage Materials for Mobile Applications. *Nature* **2001**, *414* (6861), 353–358. https://doi.org/10.1038/35104634.

(3) Falcone, P. M.; Hiete, M.; Sapio, A. Hydrogen Economy and Sustainable Development Goals: Review and Policy Insights. *Current Opinion in Green and Sustainable Chemistry*. 2021. https://doi.org/10.1016/j.cogsc.2021.100506.

(4) Rivard, E.; Trudeau, M.; Zaghib, K. Hydrogen Storage for Mobility: A Review. *Materials*. 2019. https://doi.org/10.3390/ma12121973.

(5) Kojima, Y. Hydrogen Storage Materials for Hydrogen and Energy Carriers. *Int. J. Hydrogen Energy* **2019**. https://doi.org/10.1016/j.ijhydene.2019.05.119.

(6) Vinoth Kanna, I.; Paturu, P. A Study of Hydrogen as an Alternative Fuel. *International Journal of Ambient Energy*. 2020. https://doi.org/10.1080/01430750.2018.1484803.

(7) Yang, Y.; Xu, H.; Lu, Q.; Bao, W.; Lin, L.; Ai, B.; Zhang, B. Development of Standards for Hydrogen Storage and Transportation. In *E3S Web of Conferences*; 2020. https://doi.org/10.1051/e3sconf/202019402018.

(8) Verhelst, S.; Wallner, T. Hydrogen-Fueled Internal Combustion Engines. *Progress in Energy and Combustion Science*. 2009. https://doi.org/10.1016/j.pecs.2009.08.001.

(9) Hirscher, M.; Yartys, V. A.; Baricco, M.; Bellosta von Colbe, J.; Blanchard, D.; Bowman, R. C.; Broom, D. P.; Buckley, C. E.; Chang, F.; Chen, P.; et al. Materials for Hydrogen-Based Energy Storage – Past, Recent Progress and Future Outlook. *J. Alloys Compd.* **2020**. https://doi.org/10.1016/j.jallcom.2019.153548.

(10) Orimo, S. I.; Nakamori, Y.; Eliseo, J. R.; Züttel, A.; Jensen, C. M. Complex Hydrides for Hydrogen Storage. *Chemical Reviews*. 2007. https://doi.org/10.1021/cr0501846.

(11) Wong, B. M.; Lacina, D.; Nielsen, I. M. B.; Graetz, J.; Allendorf, M. D. Thermochemistry of Alane Complexes for Hydrogen Storage: A Theoretical and Experimental Investigation. *J. Phys. Chem. C* **2011**. https://doi.org/10.1021/jp112258s.

(12) Boretti, A. The Hydrogen Economy Is Complementary and Synergetic to the Electric

Economy. *International Journal of Hydrogen Energy*. 2021. https://doi.org/10.1016/j.ijhydene.2021.09.121.

(13) Moussa, G.; Moury, R.; Demirci, U. B.; Şener, T.; Miele, P. Boron-Based Hydrides for Chemical Hydrogen Storage. *Int. J. Energy Res.* **2013**. https://doi.org/10.1002/er.3027.

(14) Peraldo Bicelli, L. Hydrogen: A Clean Energy Source. *Int. J. Hydrogen Energy* **1986**. https://doi.org/10.1016/0360-3199(86)90121-7.

(15) Kustov, L. M.; Tarasov, A. L.; Sung, J.; Godovsky, D. Y. Hydrogen Storage Materials. *Mendeleev Communications*. 2014. https://doi.org/10.1016/j.mencom.2013.12.001.

(16) Semelsberger, T.; Graetz, J.; Sutton, A.; Rönnebro, E. C. E. Engineering Challenges of Solution and Slurry-Phase Chemical Hydrogen Storage Materials for Automotive Fuel Cell Applications. *Molecules* **2021**. https://doi.org/10.3390/molecules26061722.

(17) Matus, M. H.; Grant, D. J.; Switzer, J. R.; Davis, B. L.; Stephens, F. H.; Dixon, D. A. Computational Studies on Regeneration of Boron-Nitrogen Compounds for Hydrogen Fuel Cells. In *ACS National Meeting Book of Abstracts*; 2008.

(18) David, W. I. F. Effective Hydrogen Storage: A Strategic Chemistry Challenge. *Faraday Discussions*. 2011. https://doi.org/10.1039/c1fd00105a.

(19) Luconi, L.; Tuci, G.; Giambastiani, G.; Rossin, A.; Peruzzini, M. H2 Production from Lightweight Inorganic Hydrides Catalyzed by 3d Transition Metals. *International Journal of Hydrogen Energy*. 2019. https://doi.org/10.1016/j.ijhydene.2019.08.017.

(20) Akbayrak, S.; Özkar, S. Ammonia Borane as Hydrogen Storage Materials. *Int. J. Hydrogen Energy* **2018**. https://doi.org/10.1016/j.ijhydene.2018.02.190.

(21) Demirci, U. B. Ammonia Borane, a Material with Exceptional Properties for Chemical Hydrogen Storage. *International Journal of Hydrogen Energy*. 2017. https://doi.org/10.1016/j.ijhydene.2017.01.154.

(22) Shore, S. G.; Parry, R. W. The Crystalline Compound Ammonia-Borane, H3NBH3. *Journal of the American Chemical Society*. 1955. https://doi.org/10.1021/ja01627a103.

(23) Li, H.; Yang, Q.; Chen, X.; Shore, S. G. Ammonia Borane, Past as Prolog. *J. Organomet. Chem.* **2014**. https://doi.org/10.1016/j.jorganchem.2013.08.044.

(24) Denney, M. C.; Pons, V.; Hebden, T. J.; Heinekey, D. M.; Goldberg, K. I. Efficient

Catalysis of Ammonia Borane Dehydrogenation. *J. Am. Chem. Soc.* **2006**. https://doi.org/10.1021/ja062419g.

(25) Sun, C. H.; Yao, X. D.; Du, A. J.; Li, L.; Smith, S.; Lu, G. Q. Computational Study of Methyl Derivatives of Ammonia Borane for Hydrogen Storage. *Phys. Chem. Chem. Phys.* **2008**. https://doi.org/10.1039/b807776b.

(26) Sahler, S.; Scott, M.; Gedig, C.; Prechtl, M. H. G. Transfer Hydrogenation Employing Ethylene Diamine Bisborane in Water and Pd- and Ru-Nanoparticles in Ionic Liquids. *Molecules* **2015**. https://doi.org/10.3390/molecules200917058.

(27) Sanna, C.; Sodo, A.; Laguzzi, G.; Mancini, G.; Bicchieri, M. Tert-Butyl Amine Borane Complex: An Unusual Application of a Reducing Agent on Model Molecules of Cellulose Based Materials. *J. Cult. Herit.* **2009**. https://doi.org/10.1016/j.culher.2008.10.008.

(28) Ma, N.; Song, M.; Meng, Q.; Wei, C.; Zhang, G. Theoretical Insight into the Solvent Effect on the Stoichiometric Reduction of Carbonyl Compounds by Ammonia Borane and N-Methyl Amine Borane. *Int. J. Quantum Chem.* **2020**. https://doi.org/10.1002/qua.26162.

(29) Mal, S. S.; Stephens, F. H.; Baker, R. T. Transition Metal Catalysed Dehydrogenation of Amine-Borane Fuel Blends. *Chem. Commun.* **2011**. https://doi.org/10.1039/c0cc03585h.

(30) Zhang, S.; Yao, Q.; Lu, Z. Synthesis and Dehydrogenation of Hydrazine Borane. *Progress in Chemistry*. 2017. https://doi.org/10.7536/PC161234.

(31) Ting, H. Y.; Watson, W. H.; Kelly, H. C. The Molecular and Crystal Structure of Ethylenediamine-Bisborane, C2H14B2N2. *Inorg. Chem.* **1972**. https://doi.org/10.1021/ic50108a034.

(32) Kelly, H. C. Electronic Effects of the NH2BH3 Group. The Hydrolysis of Diamine Bisboranes. *Inorg. Chem.* **1966**. https://doi.org/10.1021/ic50046a020.

(33) Neiner, D. .; Karkamkar, A. .; Bowden, M. .; Joon Choi, Y. .; Luedtke, A. .; Holladay, J. .; Fisher, A. .; Szymczak, N. .; Autrey, T. . Kinetic and Thermodynamic Investigation of Hydrogen Release from Ethane 1,2-Di-Amineborane. *Energy Environ. Sci.* **2011**, *4* (10), 4187–4193. https://doi.org/10.1039/c1ee01884a.

(34) Welton, T. Ionic Liquids in Catalysis. *Coord. Chem. Rev.* **2004**, *248* (21–24), 2459–2477. https://doi.org/10.1016/j.ccr.2004.04.015.

(35) Martins, M. A. R.; Pinho, S. P.; Coutinho, J. A. P. Insights into the Nature of Eutectic and Deep Eutectic Mixtures. *J. Solution Chem.* **2019**. https://doi.org/10.1007/s10953-018-0793-1.

(36) Ludwig, R. Ionic Liquids in Synthesis. Edited by Peter Wasserscheid and Tom Welton. *ChemSusChem* **2008**. https://doi.org/10.1002/cssc.200800126.

(37) Kar, M.; Tutusaus, O.; MacFarlane, D. R.; Mohtadi, R. Novel and Versatile Room Temperature Ionic Liquids for Energy Storage. *Energy Environ. Sci.* **2019**. https://doi.org/10.1039/c8ee02437e.

(38) Wei, D.; Ng, T. W. Application of Novel Room Temperature Ionic Liquids in Flexible Supercapacitors. *Electrochem. commun.* **2009**. https://doi.org/10.1016/j.elecom.2009.08.037.

(39) Abe, H.; Tsuzuki, S.; Ozawa, S. Anion Effects on Amorphization and Crystallization in Room-Temperature Ionic Liquids. *Chem. Phys. Lett.* **2018**. https://doi.org/10.1016/j.cplett.2018.09.046.

(40) Brandt, A.; Gräsvik, J.; Hallett, J. P.; Welton, T. Deconstruction of Lignocellulosic Biomass with Ionic Liquids. *Green Chemistry*. 2013. https://doi.org/10.1039/c2gc36364j.

(41) Clough, M. T.; Geyer, K.; Hunt, P. A.; Son, S.; Vagt, U.; Welton, T. Ionic Liquids: Not Always Innocent Solvents for Cellulose. *Green Chem.* **2015**. https://doi.org/10.1039/c4gc01955e.

(42) Fort, D. A.; Remsing, R. C.; Swatloski, R. P.; Moyna, P.; Moyna, G.; Rogers, R. D. Can Ionic Liquids Dissolve Wood? Processing and Analysis of Lignocellulosic Materials with 1-n-Butyl-3-Methylimidazolium Chloride. *Green Chem.* **2007**. https://doi.org/10.1039/b607614a.

(43) Li, C.; Zhao, Z. K. Efficient Acid-Catalyzed Hydrolysis of Cellulose in Ionic Liquid. *Adv. Synth. Catal.* **2007**. https://doi.org/10.1002/adsc.200700259.

(44) Yan, N. The Nature of Metal Catalysts in Ionic Liquids: Homogeneous vs Heterogeneous Reactions. *Top. Organomet. Chem.* **2015**.

https://doi.org/10.1007/3418_2013_59.

(45) Kadokawa, J. I.; Iwasaki, Y.; Tagaya, H. Ring-Opening Polymerization of Ethylene Carbonate Catalyzed with Ionic Liquids: Imidazolium Chloroaluminate and Chlorostannate Melts. *Macromol. Rapid Commun.* **2002**. https://doi.org/10.1002/1521-3927(20020901)23:13<757::AID-MARC757>3.0.CO;2-0.

(46) Giernoth, R. Task-Specific Ionic Liquids. *Angewandte Chemie - International Edition*. 2010. https://doi.org/10.1002/anie.200905981.

(47) Davis, J. H. Task-Specific Ionic Liquids. *Chemistry Letters*. 2004. https://doi.org/10.1246/cl.2004.1072.

(48) Lombardo, L.; Yang, H.; Züttel, A. Study of Borohydride Ionic Liquids as Hydrogen Storage Materials. *J. Energy Chem.* **2019**. https://doi.org/10.1016/j.jechem.2018.08.011.

(49) Himmelberger, D. W.; Alden, L. R.; Bluhm, M. E.; Sneddon, L. G. Ammonia Borane Hydrogen Release in Ionic Liquids. *Inorg. Chem.* **2009**, *48* (20), 9883–9889. https://doi.org/10.1021/ic901560h.

(50) Himmelberger, D. W.; Alden, L. R.; Bluhm, M. E.; Sneddon, L. G. Ammonia Borane Hydrogen Release in Ionic Liquids. *Inorg. Chem.* **2009**, *48* (20), 9883–9889. https://doi.org/10.1021/ic901560h.

(51) Zhao, Q.; Li, J.; Hamilton, E. J. M.; Chen, X. The Continuing Story of the Diammoniate of Diborane. *Journal of Organometallic Chemistry*. 2015. https://doi.org/10.1016/j.jorganchem.2015.05.027.

(52) Bluhm, M. E.; Bradley, M. G.; Butterick, R.; Kusari, U.; Sneddon, L. G. Amineborane-Based Chemical Hydrogen Storage: Enhanced Ammonia Borane Dehydrogenation in Ionic Liquids. *J. Am. Chem. Soc.* **2006**, *128* (24), 7748–7749. https://doi.org/10.1021/ja062085v.

(53) Valero-Pedraza, M. J.; Martín-Cortés, A.; Navarrete, A.; Bermejo, M. D.; Martín, Á. Kinetics of Hydrogen Release from Dissolutions of Ammonia Borane in Different Ionic Liquids. *Energy* **2015**. https://doi.org/10.1016/j.energy.2015.08.106.

(54) Sahler, S.; Konnerth, H.; Knoblauch, N.; Prechtl, M. H. G. Hydrogen Storage in Amine Boranes: Ionic Liquid Supported Thermal Dehydrogenation of Ethylene Diamine

Bisborane. *Int. J. Hydrogen Energy* **2013**, *38* (8), 3283–3290. https://doi.org/10.1016/j.ijhydene.2012.12.150.

(55) Basu, S.; Zheng, Y.; Gore, J. P. An Experimental Study of Neat and Ionic Liquid-Aided Ammonia Borane Thermolysis. *J. Power Sources* **2011**, *196* (2), 734–740. https://doi.org/10.1016/j.jpowsour.2010.07.085.

(56) Ahluwalia, R. K.; Peng, J. K.; Hua, T. Q. Hydrogen Release from Ammonia Borane Dissolved in an Ionic Liquid. *Int. J. Hydrogen Energy* **2011**, *36* (24), 15689–15697. https://doi.org/10.1016/j.ijhydene.2011.09.016.

(57) Banerjee, B.; Pugazhenthi, G.; Banerjee, T. Experimental Insights into the Thermal Dehydrogenation of Ethylene Diamine Bisborane Using Allyl-Based Ionic Liquids. *Energy and Fuels* **2017**, *31* (5), 5428–5440. https://doi.org/10.1021/acs.energyfuels.6b02823.

(58) Kundu, D.; Chakma, S.; Pugazhenthi, G.; Banerjee, T. Ionic Liquid Facilitated Dehydrogenation of Tert-Butylamine Borane. *ACS Omega* **2018**. https://doi.org/10.1021/acsomega.7b01781.

(59) Banerjee, B.; Kundu, D.; Pugazhenthi, G.; Banerjee, T. Quantum Chemical and Experimental Insights for the Ionic Liquid Facilitated Thermal Dehydrogenation of Ethylene Diamine Bisborane. *RSC Adv.* **2015**, *5* (104), 85280–85290. https://doi.org/10.1039/c5ra10625g.

(60) Khoo, K. S.; Tan, X.; Ooi, C. W.; Chew, K. W.; Leong, W. H.; Chai, Y. H.; Ho, S. H.; Show, P. L. How Does Ionic Liquid Play a Role in Sustainability of Biomass Processing? *Journal of Cleaner Production*. 2021. https://doi.org/10.1016/j.jclepro.2020.124772.

(61) Qin, H.; Hu, X.; Wang, J.; Cheng, H.; Chen, L.; Qi, Z. Overview of Acidic Deep Eutectic Solvents on Synthesis, Properties and Applications. *Green Energy and Environment*. 2020. https://doi.org/10.1016/j.gee.2019.03.002.

(62) Smith, E. L.; Abbott, A. P.; Ryder, K. S. Deep Eutectic Solvents (DESs) and Their Applications. *Chem. Rev.* **2014**, *114* (21), 11060–11082. https://doi.org/10.1021/cr300162p.

(63) Abranches, D. O.; Martins, R. O.; Silva, L. P.; Martins, M. A. R.; Pinho, S. P.; Coutinho,

J. A. P. Liquefying Compounds by Forming Deep Eutectic Solvents: A Case Study for Organic Acids and Alcohols. *J. Phys. Chem. B* **2020**. https://doi.org/10.1021/acs.jpcb.0c02386.

(64) Abbott, A. P.; Boothby, D.; Capper, G.; Davies, D. L.; Rasheed, R. K. Deep Eutectic Solvents Formed between Choline Chloride and Carboxylic Acids: Versatile Alternatives to Ionic Liquids. *J. Am. Chem. Soc.* **2004**, *126* (29), 9142–9147. https://doi.org/10.1021/ja048266j.

(65) Liu, Y.; Friesen, J. B.; McAlpine, J. B.; Lankin, D. C.; Chen, S. N.; Pauli, G. F. Natural Deep Eutectic Solvents: Properties, Applications, and Perspectives. *Journal of Natural Products*. 2018. https://doi.org/10.1021/acs.jnatprod.7b00945.

(66) Hansen, B. B.; Spittle, S.; Chen, B.; Poe, D.; Zhang, Y.; Klein, J. M.; Horton, A.; Adhikari, L.; Zelovich, T.; Doherty, B. W.; et al. Deep Eutectic Solvents: A Review of Fundamentals and Applications. *Chem. Rev.* **2021**, *121* (3), 1232–1285. https://doi.org/10.1021/acs.chemrev.0c00385.

(67) Cao, X.; Wang, S.; Xue, X. A Zn−Ce Redox Flow Battery with Ethaline Deep Eutectic Solvent. *ChemSusChem* **2021**. https://doi.org/10.1002/cssc.202100077.

(68) Chakrabarti, M. H.; Mjalli, F. S.; Alnashef, I. M.; Hashim, M. A.; Hussain, M. A.; Bahadori, L.; Low, C. T. J. Prospects of Applying Ionic Liquids and Deep Eutectic Solvents for Renewable Energy Storage by Means of Redox Flow Batteries. *Renewable and Sustainable Energy Reviews*. 2014. https://doi.org/10.1016/j.rser.2013.10.004.

(69) Zhang, L.; Zhang, C.; Ding, Y.; Ramirez-Meyers, K.; Yu, G. A Low-Cost and High-Energy Hybrid Iron-Aluminum Liquid Battery Achieved by Deep Eutectic Solvents. *Joule* **2017**. https://doi.org/10.1016/j.joule.2017.08.013.

CHAPTER 2

Ionic Liquid-based Thermal Dehydrogenation of Amine Borane Complexes

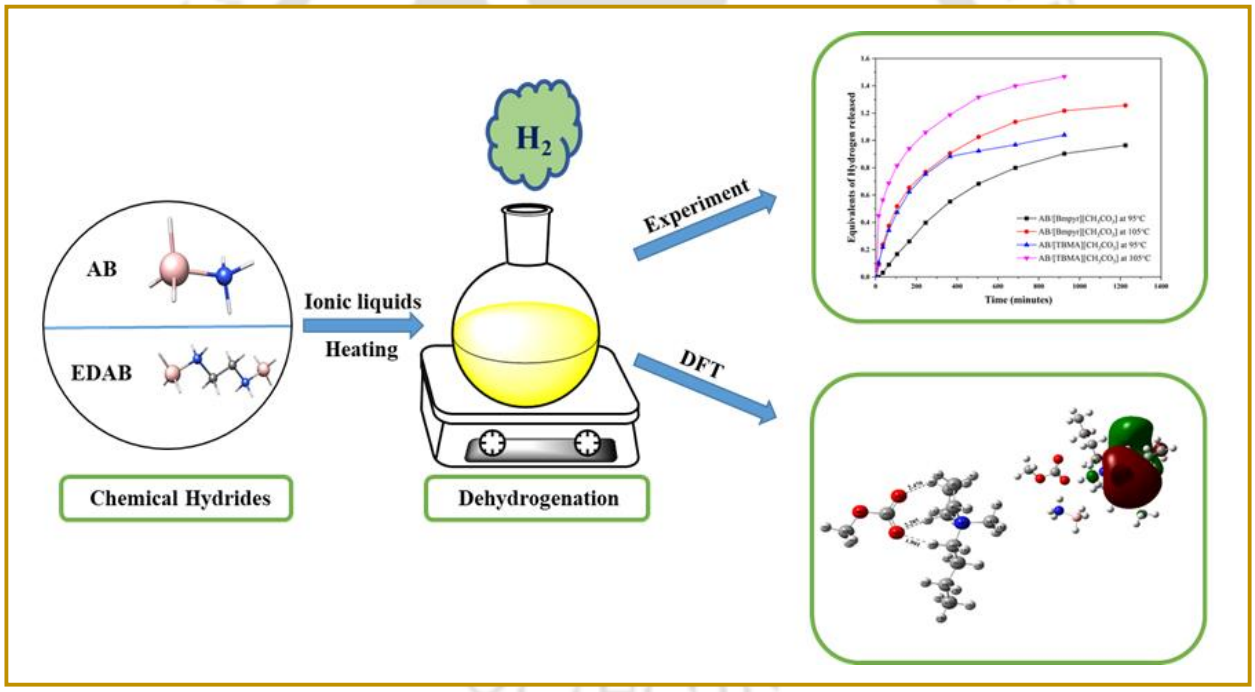

2.1. Chapter Abstract

This chapter reports the thermal dehydrogenation of chemical hydrides, namely ammonia borane (AB) and ethylene diamine bisborane (EDAB), in the presence of neoteric ionic liquids based on methyl carbonate anions. Initially, the COSMO-SAC model was performed to predict the Infinite dilution activity coefficient (IDAC) values for the solubility of AB and EDAB on the pyrrolidinium and ammonium-based cations. Based on the screening study, 1-butyl-1-methylpyrrolidinium methyl carbonate[Bmpyr][CH_3CO_3] and tributylmethylammonium methyl carbonate[TBMA][CH_3CO_3] were selected for our dehydrogenation studies. It was observed that the latter performed remarkably well in terms of equivalents of hydrogen released, which is primarily due to the higher stability of the intermediate in the polar medium of IL. Here [TBMA][CH_3CO_3] gave a cumulative release of 3.50 equivalents of hydrogen with EDAB at 105°C. The ^1H NMR spectroscopy technique confirmed the catalytic sum solvent role of IL. The electronic structure elucidation of individual ILs and ILs-chemical hydrides complexes was then performed at the M06-2X/6-311++G(d,p) level of theory. The DFT calculations, along with the HOMO-LUMO analysis, pointed out the fact that the active sites mainly existed within the methyl carbonate anions. Overall the dehydrogenation pathway was initiated by the formation of hydrogen-bonded interactions between the protic moieties of the hydrides and the anionic part of the ILs, respectively.

In the later section, a detailed study on the dehydrogenation of chemical hydrides was performed using the imidazolium-based ILs, to verify the effect of hydrogen bond basicity of the anionic moiety on the dehydrogenation process. The imidazolium-based ILs coupled with anions having higher β values are believed to be a better catalytic solvent for the process, whereas this effect is found to be negligible in the absence of imidazolium-based ILs. It was observed that methylsulfate-based anions AB/EDAB-[Bmim][$MeSO_4$] system produced 2.18 and 3.66 equivalents of hydrogen with a lower induction time when compared to other studied

AB/EDAB-IL systems. This trend was also confirmed through COSMO-SAC predictions, where the infinite dilution activity coefficient values for the solubility of chemical hydrides on the examined IL systems were computed. The solubility of chemical hydrides (AB and EDAB) is shown to be linearly related to the hydrogen-bond basicity value (β). A quantum-chemical parameter, namely the most negative surface electrostatic potential ($V_{s,min}$), was used to explore the electrostatic properties of ILs' basicity at the microscopic level. It was observed that the ILs' basicity originates from their anionic moiety and that its value changes with the anion. Further DFT-based calculations were carried out to elucidate the interactions between the anionic moiety of the ILs and chemical hydrides, followed by an NBO charge analysis to further clarify the interaction within the complexes. Quantum mechanical calculations revealed that the acidic protons of chemical hydrides form strong hydrogen bonds and electrostatic interactions with the highly basic anions of ILs. The electronic structure elucidation and charge analysis revealed that the anions of the ILs are the primary reactive sites that initiate the dehydrogenation reaction and result in the release of hydrogen equivalents.

2.2. Introduction

The need for clean fuel as hydrogen is no longer an option but a necessity.[1] Hydrogen has been established as a possible alternative energy carrier for future energy supplies because it is pure, sustainable, and environmentally friendly and has a high-energy density of 142 MJ/Kg.[2] Based on these merits, hydrogen production could replace the scarcity of fossil fuel and lower hydrocarbon-based combustion emissions. This would invariably benefit economic growth to cater to the sustainable development objective. The technical obstacles, including the manufacture of hydrogen, storage, transport, and service, should be addressed in advance to achieve a hydrogen economy. Thus, hydrogen production feedstock and hydrogen production methods such as hydrocarbon reforming, hydrocarbon pyrolysis, biomass

processes, and photocatalytic water splitting are well known. Moreover, the well-developed fuel cell paves the way for the practical application of hydrogen in portable electronic devices or vehicles. Nevertheless, the hydrogen economy still has an impediment in terms of its safety and effective storage.[3]

Since safety in terms of transportation is a major issue, the shift towards hydrogen-generating materials is gaining momentum. Several hydrogen storage materials, including metal hydrides, carbon-based materials, MOFs, organic and inorganic hydrides, have been extensively studied in recent decades, with significant challenges still remaining. Due to its significantly higher gravimetric and volumetric hydrogen density, chemical hydrogen storage has attracted considerable attention.[4] Boron and nitrogen-based hydrides (namely amine boranes) were considered one of the most promising hydrogen storage materials due to their high hydrogen content. The capability to release hydrogen under mild conditions makes it an attractive candidate. Ammonia borane (AB) is a parent member of the amine borane family.[5] As a result of its high capacity (19.6% wt.) and ambient temperature stability, it is known as a secure and efficient storage medium. But the dehydrogenation of AB allows for a significant volume of ammonia and borazine to intoxicate the release of hydrogen, which is a significant challenge to fuel cell activity. A solution to the inherent limitations of AB involves the use of chemical modification to improve its hydrogen desorption properties.[6] A sequence of ammonia borane adducts can be synthesized to replace the BH_3 and NH_3 portions of AB with alkyl chains. The carbon derivative of ammonia borane, namely ethylene diamine bisborane (EDAB), has been investigated in this context.

Initially, several research on the synthesis and physiological properties of EDAB demonstrated that the material is capable of releasing two hydrogen equivalents during a two-step thermolysis process.[7,8] Dehydrogenation at elevated temperatures up to 1000°C under varying air conditions resulted in the production of four H_2 equivalents.[9] To alleviate the

shortcomings caused by the thermal decomposition of hydrides, processes such as nano-scaffolding, mixing of hydrides with metal halides, and metal catalysis of hydrides dissolved in organic solvents were employed.[10] Traditional organic solvents have been found to influence the evolved hydrogen gas's catalytic activity, leading to contamination of fuel cell electrodes.[11] In this context, the application of Ionic liquids (ILs) and their unique properties promise considerable advantages.

Ionic Liquids are chemically and thermally stable and are thus regarded as environmentally friendly solvents relative to volatile organic solvents.[12] Furthermore, by alternating the substituent cation group or the combined anion, the ionic liquid's physicochemical properties can be varied. Due to their environment-friendly perception, ILs have been proposed as possible substitutes for volatile organic compounds (VOCs) in industrial separation methods,[13] catalytic reactions,[14] electrochemical,[15] biochemistry,[16] and nanotechnology applications.[17] The use of ionic liquids in chemical hydride dehydrogenation is well known for greatly enhancing hydrogen release and reducing the induction time. The use of ILs improves the formation of diammoniate of diborane ($[NH_3BH_2NH_3]^+[BH_4]^-$), which is the main intermediate ionic species in AB thermolysis, by providing a controlled reaction media and milder reaction temperature.[18] Bluhm et al. proposed the use of ILs as solvents that could overcome the issue of amine borane thermolysis by preventing the formation of unwanted products.[19] Zheng et al. reported that the use of IL [Bmim][Cl] significantly improved the H_2 release rate and its yield from AB.[20] In another work, Banerjee et al. stated that a maximum of 3.96 hydrogen equivalents was released using an acetate-based IL, namely, [Bmim][OAc] at 105°C in a solvent-state dehydrogenation of EDAB.[21] In a recent study, Sahler compared the release of hydrogen equivalents using IL to that using neat EDAB and found them to be much higher when using IL.[22] Various solid-state and solution-state studies

were carried out to figure out and understand the role of ILs in promoting the hydrogen release from AB and EDAB, respectively.[7-12,18-22]

Polar solvents such as IL dissolve and stabilize solutes and intermediates in a reaction media by dipolar hydrogen bonding and ionic interactions.[23] One of the most desirable features of polarity is through the solvatochromic probes, which allows us to rank these solvents in terms of the Kamlet-Taft descriptors.[24] Here, the hydrogen-bond basicity was chosen in this work for the selection of the anion since it is one of the essential parameters reflecting the hydrogen-bond accepting ability of the IL anion.[25] Methylcarbonate [CH_3COO^-] is one of the most rarely explored anions in ILs, despite its immense acceptable physicochemical and thermal properties. ILs based on [CH_3COO^-] anions are usually liquid above 0°C and exhibit low viscosity, rendering them as beneficial solvents for various applications. The low melting point, high conductivity, and low viscosity accord the methyl carbonate anions with better fluidity.[26] In light of a recent study, it is anticipated that the ILs composed of the same group of anions can act as a catalytic solvent. In the dehydrogenation study of amine boranes to date, imidazolium and phosphonium-based ILs have so far been extensively investigated.[27] This study is the first attempt at studying the effect of pyrrolidinium and ammonium cations coupled with methyl carbonate anions. The ammonium and pyrrolidinium cations have favorable documented physicochemical and catalytic properties.[28,29]

Over the last decade, the usage of ILs in various domains of chemistry, most notably catalysis, has expanded considerably. The basicity of ILs is a crucial metric for a variety of applications, as higher basicity often leads to enhanced process selectivity and efficiency. As a result, increasing the basicity of ILs enhances the efficiency of numerous processes, which is why basicity is crucial for a variety of IL-derived applications.[30] Additionally, current strategies for adjusting the basicity of ILs are confined to modifying the type and amount of basic sites within the ILs' structure.[31] As a result, it is exceptionally beneficial to investigate a

new method of adjusting and enhancing the basicity of ILs from both a scientific and a practical perspective.[32] The selective dehydrogenation of amine-borane complexes using ILs is based on the interaction of the basic anions with the acidic or protic hydrogen atom/s in the amine-borane compounds, which is entirely reliant on the basicity of the ILs.

This chapter provides a comparative investigation of the dehydrogenation of chemical hydrides (AB and EDAB) in the presence of two selected aprotic ionic liquids (AILs). To predict the solubility of hydrides AB and EDAB in ILs, the COSMO-SAC model was used to predict the IDAC values. The residual reaction mixture was characterized using the ^{1}H NMR technique, ensuring IL's role as a catalytic solvent media. In the following sections, to gain further insight, we performed density functional theory (DFT) calculation of the aprotic ionic liquids (AILs) to study the ion-pair interaction between chemical hydrides and different functional groups of the cations and anions. Quantum chemical (QC) calculations were employed to obtain the chemical potential (μ) and chemical hardness (η) of the AILs. HOMO-LUMO calculations were performed on ionic liquid as well as ionic liquid-chemical hydride complexes to predict the active sites available in the ionic liquid systems. Therefore, we assume that a combination of theoretical and experimental aspects would provide a detailed overview of the dehydrogenation of chemical hydrides by the ILs.

Furthermore, the hydrogen bond basicity (β) of the anions was used to envisage the ability of imidazolium-based ionic liquids for thermal dehydrogenation of amine borane complexes (AB and EDAB) which has not been documented yet. The polar reaction media offered by some ILs facilitates enhanced dehydrogenation by varying the anions and increasing the amount of hydrogen released. Based on the hydrogen bond basicity of the anions investigated, the dehydrogenation capacities of the chemical hydrides AB and EDAB were determined.

In the preceding section, DFT calculations were performed to procure an additional insight into the hydrogen bond basicity of IL systems and its effect on the dehydrogenation capabilities of the chemical hydrides. It has been demonstrated that the strength of the cation-anion interaction and the approach used to tether basic functional groups with imidazolium-based cations have a significant effect on the basicity of the ILs. The most negative surface electrostatic potential ($V_{s,min}$), a critical quantum-chemical descriptor, has been selected as a unique approach for comprehending the basicity of the ILs. The promoting effect of the imidazolium-based ionic liquids in enhancing thermal dehydrogenation of amine borane complexes was investigated using a combination of experimental and quantum chemical simulations, with a particular emphasis on the anion-hydride interaction. The study's distinctiveness emanates from the fact that it emphasizes the role of imidazolium-based ILs' hydrogen bond basicity (β) on the thermolytic dehydrogenation of amine-borane complexes.

2.3. Computational Details

2.3.1. COSMO-SAC Modeling

2.3.1.1. Computational Details for the Generation of COSMO Files

COSMO-SAC model is used for predicting the solubility of AB and EDAB in ILs and DESs, which can be used for amine borane complex dehydrogenation.[33] Using GaussView 5.0 visualization package, the initial structures of AB, EDAB, ILs (ion-pair approach), and DESs were drawn.[34] The geometry of all compounds was optimized at B3LYP level and 6-311++G(d) basis set using the Gaussian 09 package.[35,36] From the optimized geometry of all species, a single point energy calculation was performed with another set of DFT calculations using the BVP86 level of theory for the generation of ***.cosmo*** file. Standard global adjustable parameters such as surface area of the segment (=6.32 $Å^2$), misfit energy interaction constant [=8419 kcal $Å^4$ /(mol e^2)], cutoff for hydrogen-bonding interaction (=0.0084 e/$Å^2$), and

hydrogen-bonding interaction constant [=75006 kcal Å^4 /(mol e^2)] were adopted to compute the activity coefficient. Thereafter, ***.cosmo*** file was used to predict the IDAC value (denoted as γ^{∞}).[37]

The details of the COSMO-SAC calculation are presented below:

```
%mem=540MW
%chk= Bmpyr_CH3CO3
#P BVP86/svp/DGA1 scf=tight
Comment Line
0  1            (Charge and Multiplicity)
Z-Matrix
--link1--
%chk= Bmpyr_CH3CO3
#P BVP86/svp/DGA1 scf=(tight,novaracc) SCRF=COSMORS guess=read geom=checkpoint
Comment line
0  1                    (Charge and Multiplicity)

Bmpyr_CH3CO3.cosmo  (The COSMO file which will be created)
```

Figure 2.1: Input file for COSMO File generation in Gaussian 09

The various terms and its meaning are as follows:

1. % mem = 540 MW

   This gives the total amount of internal memory needed for this calculation.

2. # P BVP86/SVP/DGA1

   This indicates the DFT Theory being used (i.e.,#P BVP86), the basis set (SVP), and the density fitting function. The SVP orbital coefficients and its expansion can be obtained by the *GFprint* and *GFInput* command in Gaussian 09

   The DGA1 or the Density Gradient Approximation expands the electron density in a set of atom-centered functions when computing the Coulomb interaction instead of computing all the two-electron integrals. It provides significant performance gains for

pure DFT calculations on medium-sized systems too small to take advantage of the linear scaling algorithms without significant degradation in the accuracy of predicted structures, relative energies, and molecular properties.

3. SCF = tight. This indicates a full convergence of energy.

The calculation procedure for IDAC are listed below:

The COSMO-SAC model determines the segment coefficient from an independent segment activity coefficient equation.[38] The surface characteristics are determined from the induced screening charge densities developed by placing a molecule in a perfect conductor. Due to the polarization, charge densities are divided into a certain number of segments over the interface of the solute and the conductor. The charge is then calculated by defining solvation energy (E_{solv}) which takes into consideration (Equation A1).

$$4\pi\varepsilon_o E^{solv} = \sum_A \sum_\alpha Z_A q_\alpha B_{A\alpha} + \sum_\alpha q_\alpha C_\alpha + \frac{1}{2}\sum_\alpha \sum_\beta q_\alpha q_\beta D_{\alpha\beta} \qquad (2.1)$$

Here, q_α represents the screening charge of the α^{th} segment solved by minimizing the equation with respect to the segment's charge. The equation takes a form of:

$$\left(\frac{dE^{solv}}{dq_\alpha}\right) = \sum_A Z_A B_{A\alpha} + C_\alpha + \sum_\beta q_\beta D_{\alpha\beta} = 0 \qquad (2.2)$$

This process is also known as “SCF” or “COSMO” calculation. The optimized geometries, energies, surface screening charge densities of the solute molecule are stored within the COSMO file. Histogram distribution of these obtained charges (-0.03 to +0.03 e/ $Å^2$) are obtained, which are known as sigma profile (σ-profile). The ‘SAC’ component is usually the mathematical, mechanical structure that measures simply the energy needed to restore the molecule to its original state, which is Gibb’s free energy and can be related to the activity coefficient.

$$\ln\left(x_{i/s}\gamma_{i/s}\right)=\frac{\Delta G_{i/S}^{solv}-\Delta G_{i/i}^{solv}}{kT}=\frac{\Delta G_{i/S}^{*solv}-\Delta G_{i/i}^{*solv}}{kT}+\ln\left(\frac{V_{i/i}}{V_{i/S}}\right) \quad (2.3)$$

Gibb's Free energy of solvation (ΔG^{*solv}) comprises the electrostatic (ES) and van der Waals (vdW) forces. Activity coefficients can be computed by the difference in Gibb's Free energy of solvation of the entire mixture and the individual component.

$$\Delta G_{i/S}^{*solv}=\left(\frac{\Delta G_{i/S}^{*ES}-\Delta G_{i/i}^{*ES}}{kT}\right)+\ln\left(\gamma_{i/S}^{comb}\right) \quad (2.4)$$

The first term of Eq. 2.4 is the dominating energy term and can be referred to as the restoring free energy

$$\begin{aligned} G\left(N-mol_i,P,T\right)&=G\left(N,P,T\right)-\mu_{mol,i}\\ G\left(N-seg_\alpha,P,T\right)&=G\left(N,P,T\right)-\mu_{seg,\alpha}\end{aligned} \quad (2.5)$$

In our work, we have computed Eq. 2.3 at infinite dilution, i.e. ($x\to 0$).The higher the deviation of values from unity, the higher the solubility of AB/EDAB in IL. The solubility of a solute in a solvent can be measured by the logarithmic value of IDAC. AB/EDAB solubility in ILs is predicted based on the IDAC value as the negative value of logarithmic IDAC denotes solubility, whereas positive value denotes insolubility.

2.3.2. Ionic Liquid Selection

The solubility of the chemical hydrides in ILs is assessed based on the IDAC values obtained, as the negative logarithmic IDAC value implies solubility, whereas the positive value implies insolubility among the screened solvents (ILs). This work predicted the solubility of AB and EDAB in IL-based on methyl carbonate anion coupled with pyrrolidinium and ammonium-based cations.[39] Among the screened solvents, both AB and EDAB have the highest predicted solubility in the ILs: 1-butyl-1-methylpyrrolidinium methyl carbonate

[Bmpyr][CH_3CO_3] and tributylmethylammonium methyl carbonate[TBMA][CH_3CO_3]. The higher solubility of the hydrides in the respective solvents initiated us selecting the respective ILs for the dehydrogenation experiments. Figure 2.2 and Figure 2.3 below summarize AB and EDAB logarithmic IDAC values in various screened ionic liquids (ILs), where the alkyl chain length of the respective cations was varied.

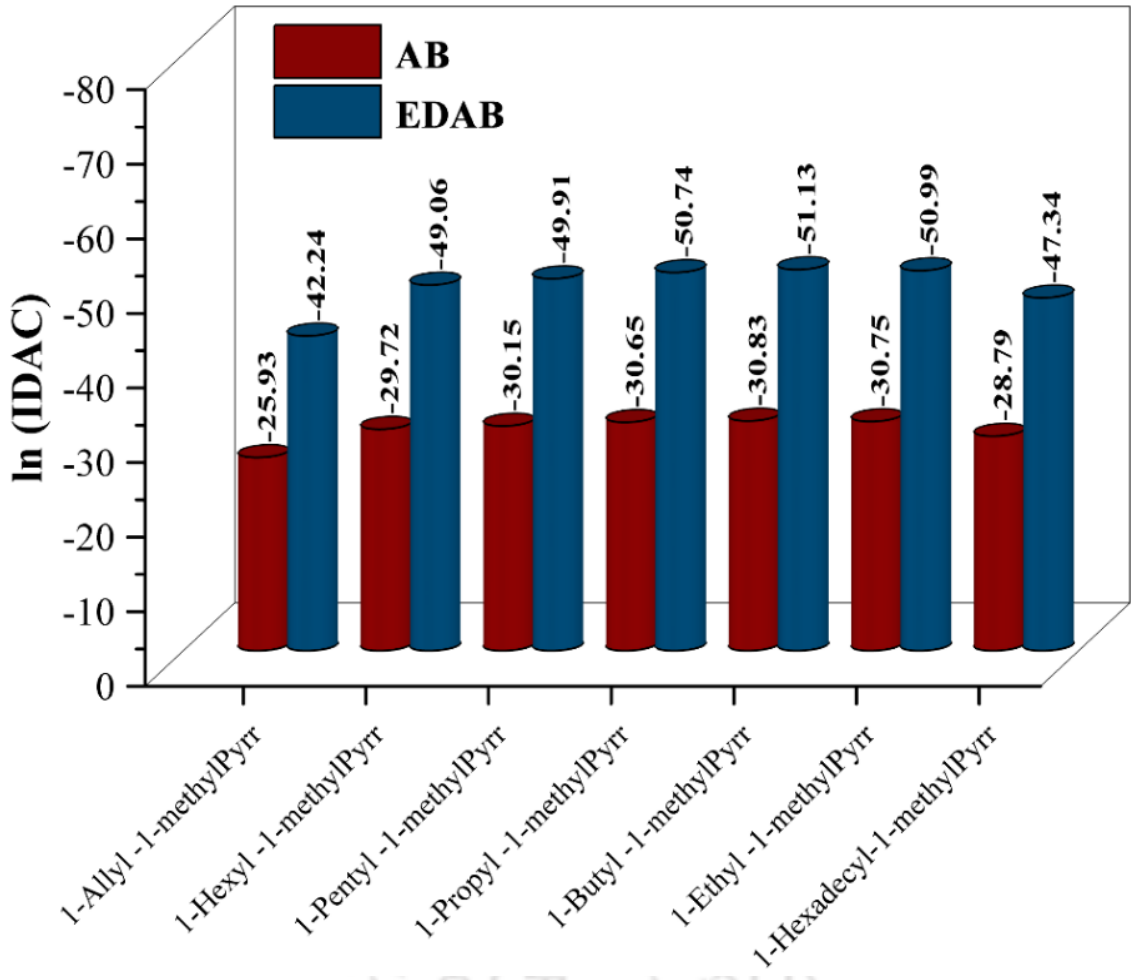

Figure 2.2: COSMO-SAC model predicted logarithmic IDAC values of AB and EDAB in Pyrrolidinium methyl carbonate-based Ionic liquids (ILs). (The Ionic Liquids acronym on the x-axis is represented by (1) *1-Allyl-1-methylPyrrolidium*, (2) *1-Hexyl-1-methylPyrrolidinium*, (3) *1-Pentyl-1-methylPyrrolidinium*, (4) *1-Propyl-1-methylPyrrolidinium*, *(5) 1-Butyl-1-methylPyrrolidinium*, *(6) 1-Ethyl-1-methylPyrrolidinium*, *(7) 1-Hexadecyl-1-methylPyrrolidinium*. All the cations are coupled with a common methyl carbonate-based anion.

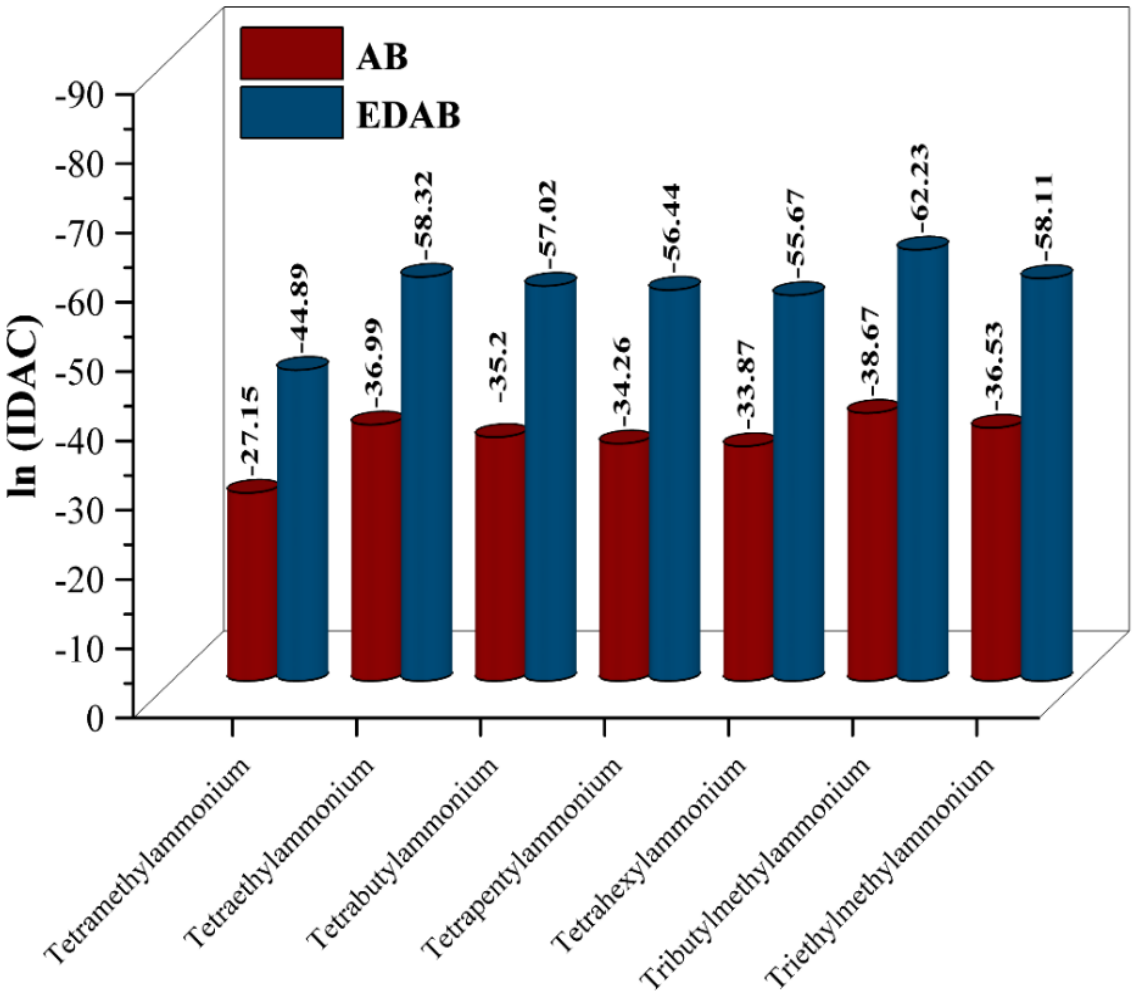

Figure 2.3: COSMO-SAC model predicted logarithmic Infinite dilution activity coefficient of AB and EDAB in tetra alkyl ammonium methyl carbonate-based Ionic liquids (ILs). All the cations are coupled with a common methyl carbonate-based anion.

2.3.3. Quantum Chemical Calculations

DFT-based calculations were employed to optimize the geometries of the individual pyrrolidinium and ammonium cation, methyl carbonate anions, ion-pair, and chemical hydrides using the Gaussian 09 software package.[35] The geometry optimizations of IL-chemical hydride systems have been carried out using the hydride molecules positioned around IL's with different orientations in and out of the plane. The initial optimizations were carried out at the B3LYP/6-31G(d,p) level, followed by re-optimizing the model at the higher M06-2X/6-311++G(d,p) level of theory.[40] To confirm the minima state in PES, vibrational frequency

calculations were performed at the same level of theory. The chemical reactivity of the hydrides, ILs, and IL-chemical hydrides complex systems were investigated using frontier molecular orbital (FMO) analysis.[41]

Additional quantum chemical calculations have been performed in the subsequent section to study the effect of hydrogen bond basicity within imidazolium-based cations and their effect on thermal dehydrogenation. Herein, DFT-based quantum chemical calculations were used to investigate the cation-anion interactions, the impact of anions on the ion-ion (cation-anion) interactions, and the basicity of ILs. To better understand the geometric and electronic structures of the investigated IL systems, density functional theory (DFT) calculations were carried out. The geometry optimization of the IL systems was carried out using various starting orientations of the ions, i.e., co-planar and out-of-plane around imidazolium cation, with the anions placed at various positions (Figure 2.23). This step employed the widely used B3LYP density functional in conjunction with 6-31g(d,p) basis sets.[36,42] Further re-optimization was performed on the optimized geometries at the higher B3LYP-D3(BJ)/6-311++G(d,p) level of theory.[43] Additionally, the optimized structures were employed to perform vibrational frequency calculations at the same level of theory in order to classify all stationary points as minima.[44]

Interaction energies (E) of the examined IL systems were calculated as the difference between the energies of the cation-anion pair and the sum of the energies of the individual cation and anion moieties (Equation 2.6). The obtained interaction energies were subjected to a counterpoise correction scheme (CP), a method developed by Boys and Bernardi.[45] To gain a more in-depth understanding within the ILs, Multiwfn 3.8 software package was employed to perform atoms-in-molecules (AIM) calculations.[46] $V_{s,min}$ was computed by the Multifunctional wavefunction analyzer (Multiwfn) 3.8 program utilizing optimized geometries and wave functions from Gaussian 16 at B3LYP-D3(BJ)/6-311++G(d,p) level.[47] As proposed

by Bader et al., the molecular surface was characterized using the 0.001 au (electrons/bohr^3) contour of the electronic density.[48] The contour maps of $V_{s,min}$ were obtained by the VMD visualization program.[49]

$$E_{AB}(kJ/mol) = 2625.5\,\{E_{AB}(au) - [E_A\,(au) + E_B\,(au)] + E_{BSSE}\} \quad (2.6)$$

In the consequent section, the interactions within the IL-chemical hydride systems were studied to gain a deep insight into the dehydrogenation mechanism of amine-borane complexes in the presence of ILs. The charge transfer behavior of individual ILs, chemical hydrides, and IL-chemical hydride complex systems was explored using a natural bond orbital (NBO) analysis approach.[50]

2.4. Experimental Details

2.4.1. Materials

The following chemicals were used as base agents for hydrogen release, namely ammonia borane (AB) and ethylene diamine bisborane (EDAB). Methyl carbonate anion-based ILs in the form of [Bmpyr][CH_3CO_3] and [TBMA][CH_3CO_3] were used as a catalytic solvent to enhance the dehydrogenation process. These ILs were pretreated to remove moisture by keeping them under vacuum at 70°C for 24 hours before experiments. Dimethyl sulfoxide-d6 (deuteration degree of minimum 99.9%, DMSO) and $CDCl_3$-d_6 (deuteration degree of minimum 99.8%, $CDCl_3$) were used as the deuterated solvent for recording NMR spectra. The molecular structures of the compounds employed in this study are depicted in Figure 2.4 below.

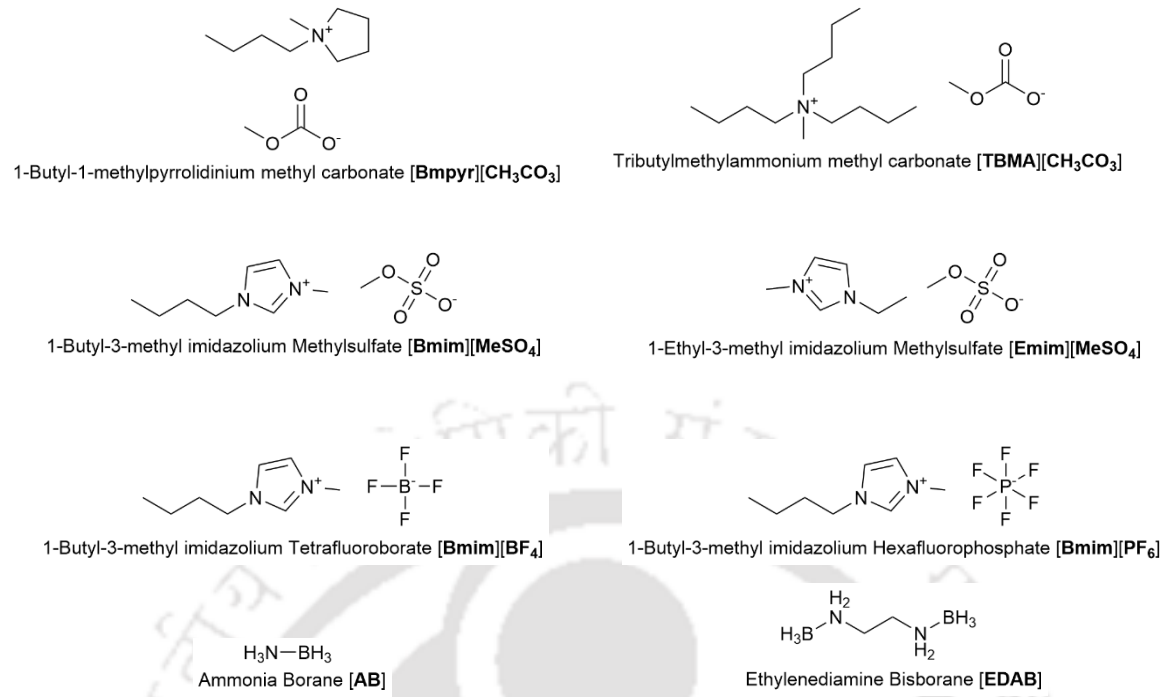

Figure 2.4: Structures of different Ionic liquids (ILs) and chemical hydrides employed in this work for dehydrogenation of amine-borane complexes

2.4.2. Thermal Dehydrogenation Apparatus

A schematic diagram of the glass apparatus for the dehydrogenation experiment is given in Figure 2.5. The entire setup can be divided into two separate parts. The right side of the setup, collectively known as the "gas chamber side" includes the condenser where liquid nitrogen is used as a cold trap (with stopper). The other apparatus are collecting flask, gas burette, mercury vessel, and mercury leveler. The left side of the setup, which is known as the "reactor side" comprises the reactor with input, oil bath, and filter adapter ports.

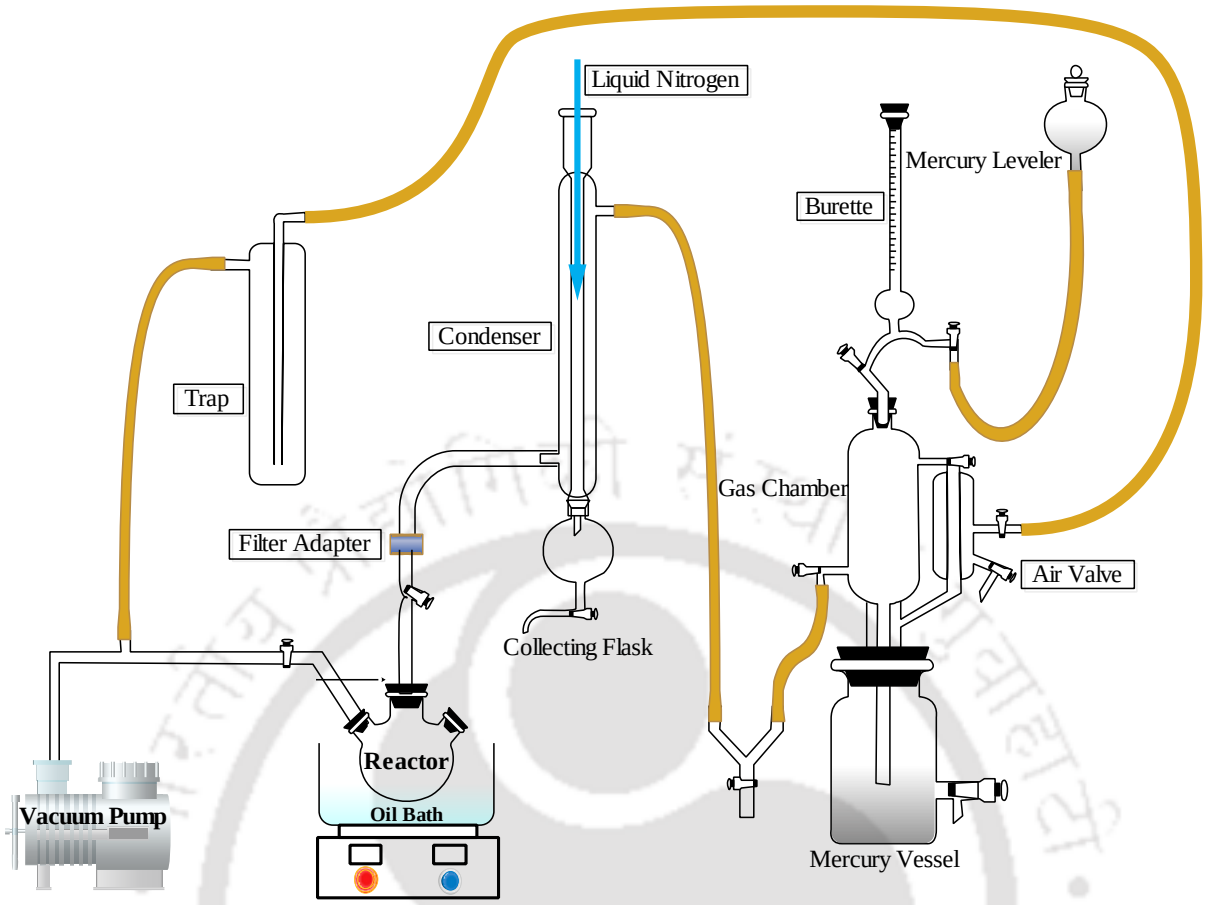

Figure 2.5: Schematic diagram of the experimental setup

All the dehydrogenation experiments were performed under different temperatures (95 °C and 105 °C) at a maintained vacuum pressure of 4.5 $\times 10^{-2}$ mbar. The high vacuum is a vital part of the operation as it minimizes the presence of undesirable materials such as air and moisture as they can affect the rate of reaction. The AB/EDAB, along with IL mixtures (15 mg of AB/EDAB and 0.5 mL of IL/DES), was stored within the reactor and heated for various cumulative time intervals in an oil bath at different temperatures. In the next step, the condenser was loaded with liquid nitrogen. The reactor side was opened at different time intervals, and the gas was allowed to move to the other part of the glass setup. The primary reason for using liquid nitrogen as a coolant was to trap unwanted gases and moisture content in the collecting flask. Only hydrogen is able to pass through the gas valve as it is the lightest gas component. After a specific period of time, the gas valve was closed at the opening of the gas chamber

resulting in the isolation of the collected gas from the "reactor side". In the next step, the air valve is opened gradually so that ambient air at 1 bar pushes the mercury piston upwards and thus moves the collected gas from the gas chamber into the gas burette. A fixed needle gas syringe (5.0 ml HAMILTON GASTIGHT® Syringe) was then used to extract the released hydrogen gas from the gas burette, followed by a gas chromatography test. A Bruker 450-GC-TCD was then used to detect the presence and purity of the released hydrogen gas. The obtained residual products were then characterized using the ^{1}H and ^{11}B NMR spectroscopy techniques.

2.5. Pyrrolidinium and Ammonium-based Ionic Liquid aided Dehydrogenation Experiment of Chemical Hydrides and its Mechanism

The thermal dehydrogenation of AB and EDAB were performed separately in [Bmpyr][CH_3CO_3] and [TBMA][CH_3CO_3] at two different temperatures of 95°C and 105°C. The working temperature preferred in the study was nearly around the melting point of AB and EDAB, which is approximately 106 °C and 116 °C, respectively.[21,51,52] In this work, we have reported the dehydrogenation of solid-state AB and EDAB.[53] When heated at 105°C, 0.90 and 1.89 equivalents of hydrogen are released by solid-state dehydrogenation of pure AB and EDAB. A maximum of 3 and 4 equivalents of hydrogen gas may be available for desorption from AB and EDAB, especially through the B-N attachment or the $–NH_2$ and $–BH_3$ moieties. It is stated that there is an induction time in the AB and EDAB solid-state dehydrogenation, which is suppressed with the usage of IL. No induction periods were observed for both the amine borane-IL complexes. However, the release of hydrogen for EDAB/[Bmpyr][CH_3CO_3] as well as EDAB/[TBMA][CH_3CO_3] from each time step were greater than that of AB/[Bmpyr][CH_3CO_3] and AB/[TBMA][CH_3CO_3] at the same conditions. A cumulative 0.96 and 1.25 equivalent hydrogen was released from AB/[Bmpyr][CH_3CO_3] at 95°C and 105°C, respectively. AB/[TBMA][CH_3CO_3] released 1.04 and 1.46 equivalent hydrogen at 95°C and 105°C respectively (Figure 2.6). A cumulative release of equivalent hydrogen from

EDAB/[Bmpyr][CH_3CO_3] was found to be 1.72 at 95°C, 2.72 at 105°C; while for EDAB/[TBMA][CH_3CO_3] it was 3.01 and 3.50 equivalents of hydrogen at 95°C and 105°C respectively (Figure 2.7). The cumulative equivalent release of hydrogen of both AB and EDAB into different IL systems at 95°C and 105°C is shown in Figure 2.8. The equivalents of hydrogen released belongs to the hydride molecules and can be termed as mole hydrogen per mole of complex.

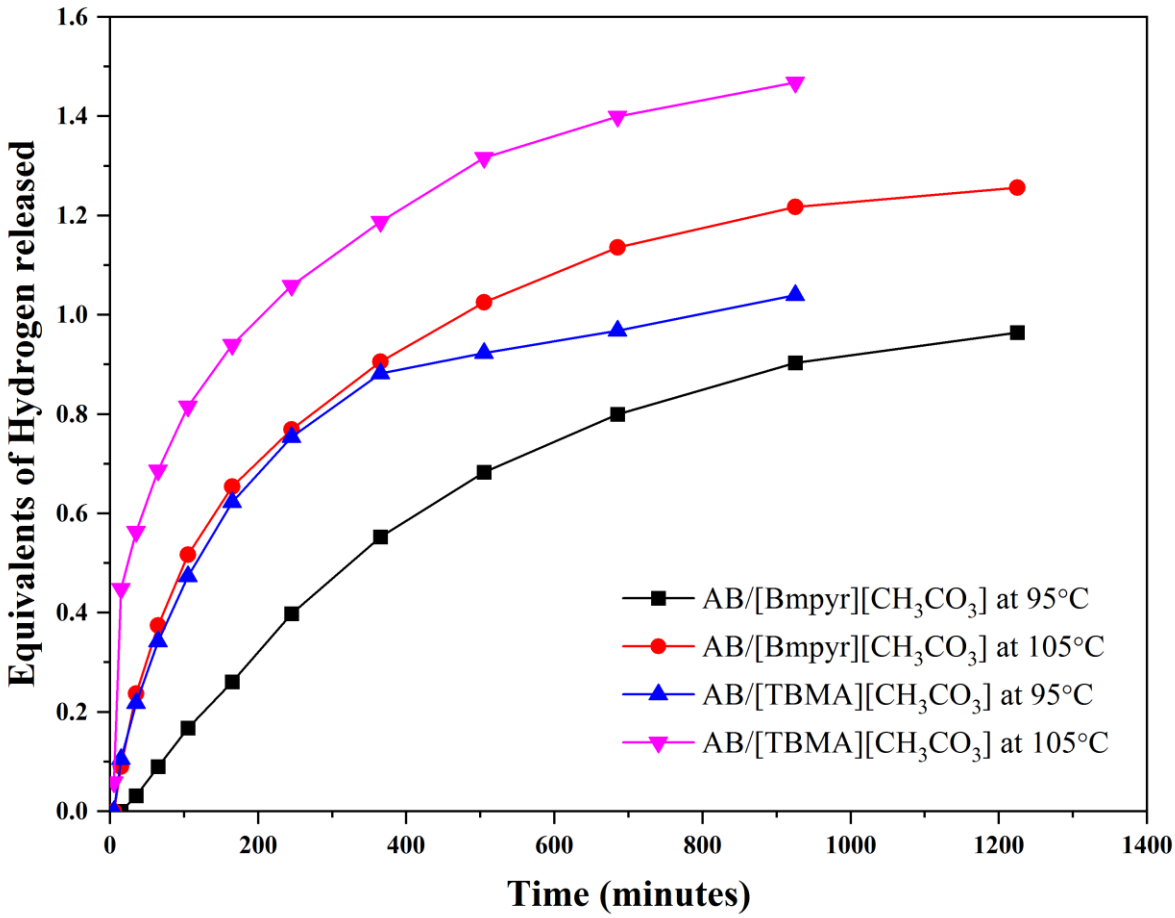

Figure 2.6. Equivalents of Hydrogen released from AB/[Bmpyr][CH_3CO_3] and AB/[TBMA][CH_3CO_3] at 95°C and 105°C

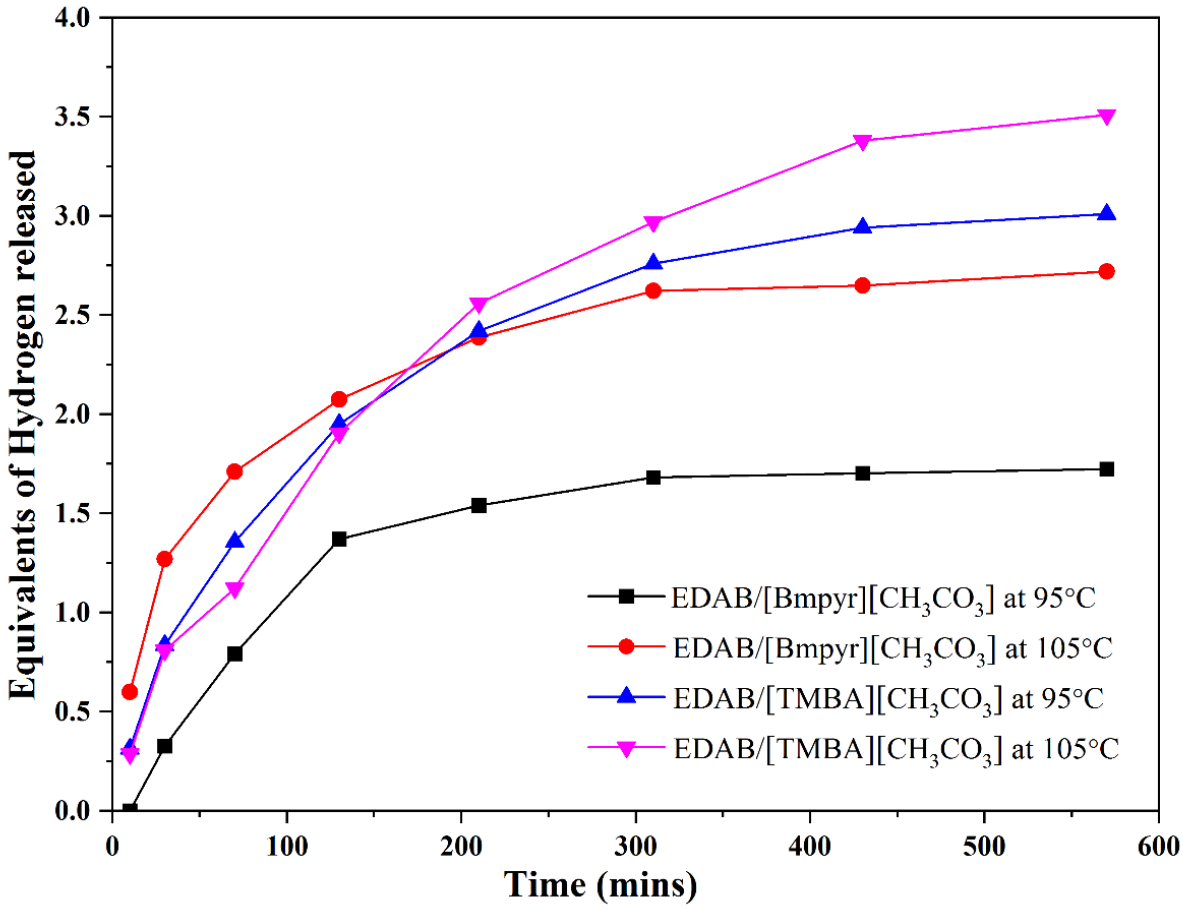

Figure 2.7. Equivalents of Hydrogen released from EDAB/[Bmpyr][CH_3CO_3] and EDAB/[TBMA][CH_3CO_3] at 95°C and 105°C

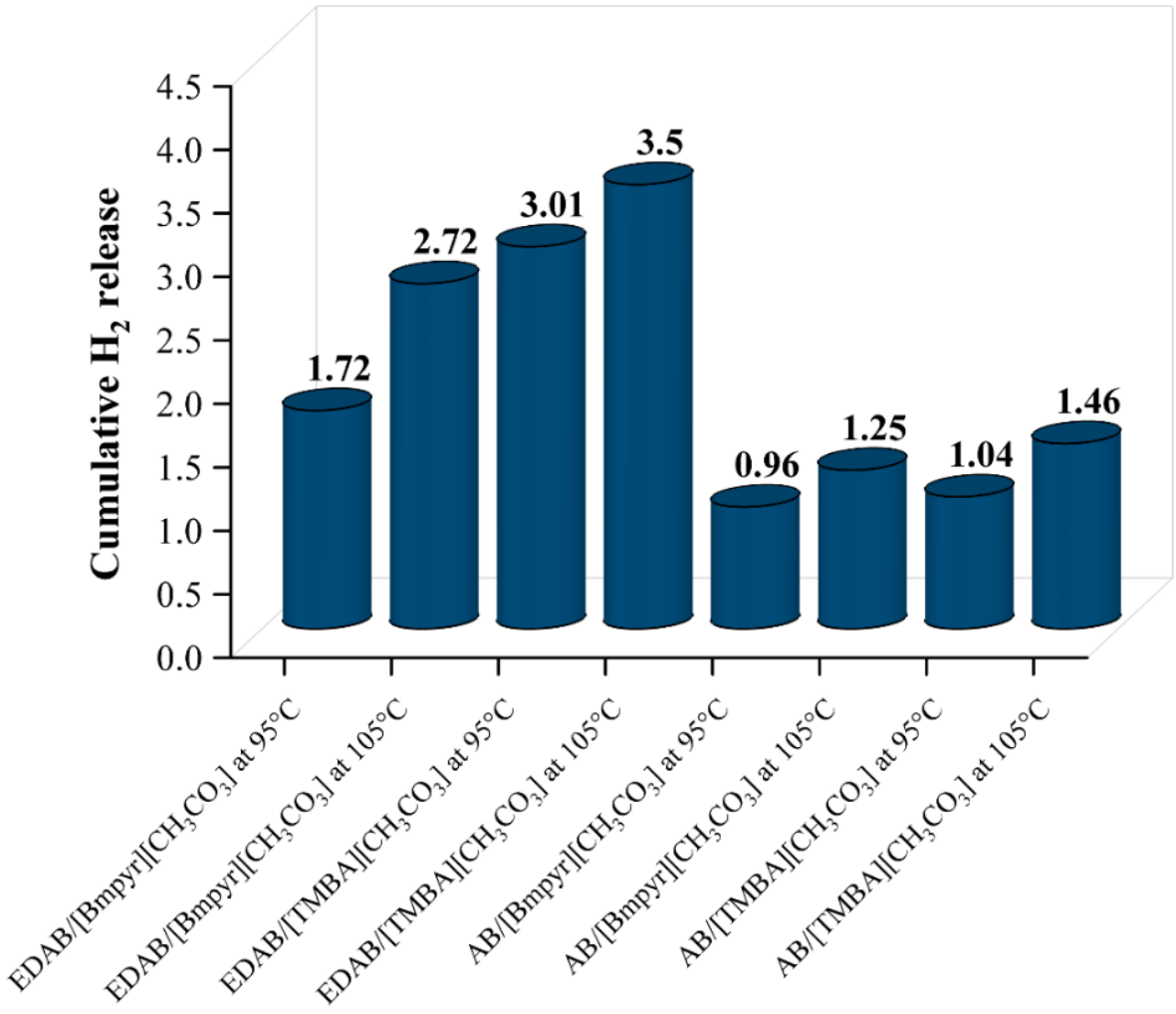

Figure 2.8. Cumulative hydrogen generation from AB and EDAB facilitated by ILs at 95 °C and 105 ˚C

The mechanism usually depends on the fundamental parameter hydrogen bond basicity (β) of the IL, which determines an anion's ability to accept protons. Strong non-covalent interactions between anions and the protic nitrogen moiety of chemicals are attributable to chemical hydrides solubility. Conversely, the higher the solubility of amine-borane compounds in IL, the easier is the deliverance of hydrogen gas. Thus, IL must possess strong basic anions to dissolve chemical hydrides. These strong, non-covalent interactions disrupt the intramolecular linkage between the hydride chains and lead to hydrogen bonds between the hydrides and ILs. Sahler and co-workers linked the hydrogen bond basicity (β) of various IL

anions with hydrogen release in one of the previously reported works.[22] The basic characteristics of the anionic moiety of ILs are as follows: methyl carbonate > acetate > dicyanamide > halides. The hydrogen bond basicity trend (β) is an essential parameter for the release of higher H_2 equivalents using methyl carbonate-based anion ILs.

Table 2.1 describes the comparative study with the previously published literature for IL-aided dehydrogenation of AB and EDAB. The reported literature with their equivalents hydrogen released at their operating temperatures has been compared with our present study. Bluhm et al. in their pioneer work used ILs as solvent cum catalyst media. They documented a release of 1.6 hydrogen equivalents at an operating temperature of 95 °C.[19] Himmelberger et al. proposed a comprehensive mechanism of ammonia borane hydrogen release combined with IL.[18] They demonstrated the existence of various dehydrogenation oligomers (DADB, PAB, and PB) in the residual products. At an operating temperature of 110°C, the authors reported a release of 2.2 equivalents for the AB/[Bmim][Cl] complex system. In our earlier work, the EDAB/IL efficiency was elucidated and was correlated to the catalytic behavior of highly basic anions, including acetate and bromide.[54,51] The authors reported the effect of increasing the length of the cation alkyl chain. [Bmim]-based cations were found to be superior in terms of its catalytic cum solvent behavior when compared to their lower alkyl cation counterpart [EMIM]. According to the aforementioned study, increasing the alkyl chain of the cationic moiety considerably affects the dehydrogenation efficiency of chemical hydrides. The weaker cation-anion interaction with an increased alkyl chain length results in the interaction between the basic anions and the hydrides. This makes it responsible for the catalytic activity of ILs. Kundu et al. also presented a mechanistic study of EDAB with ILs with phosphonium cations.

In contrast to the acetate-based systems, the phosphonium cation-based ILs facilitate the selective formation of higher repeating units, thereby regulating the formation of EDAB oligomers. Kundu et al. reported that imidazolium-based ILs incorporated with thiocyanate and

hydrogen sulfate-based anions contributed to the dehydrogenation of AB and EDAB.[52,55] The authors reported the selection of highly basic anions, which leads to higher chemical hydride solubilities. The authors also reported the effect of temperature conditions. The dehydrogenation efficiency of the ILs was found to enhance as the reaction temperature was increased, as reported by the authors. The protic nature of the hydrogen sulfate anions resulted in a faster dehydrogenation at 40°C.[52] In contrast, the thiocyanate ions produced an appreciable induction period with a lower release of hydrogen equivalents. The acidic nature of the imidazolium cations makes it the most favorable group of ionic liquids compared to other IL groups (ammonium, pyrrolidinium, pyridinium, etc.). Additionally, the ammonium and pyrrolidinium-based ILs reported some advantageous properties over imidazolium-based ILs such as thermally stable, electrochemical, economic, and less hazardous media.[56] Thus, their usage as solvents in thermal dehydrogenation procedures needs to be investigated. In this context, we have screened [TBMA][CH_3CO_3] and [Bmpyr][CH_3CO_3] ILs from a pool of methyl carbonate-based ILs, to assist the thermolytic dehydrogenation of both AB and EDAB. The former being a non-ring cation, combined with a highly basic anion, has provided a significant inductive effect. No induction period was observed with our chosen ILs, making it a favorable media for the dehydrogenation reaction.

Table 2.1: Comparison of ionic liquid assisted dehydrogenation of amine borane complexes with previously reported literature

S.No	Ionic Liquids Used	Operating Temperature	Hydrides/ILs Complexes	Highest Equivalents Released	References
1.	[BMIM][OAc]	105 °C	EDAB/ [BMIM][OAc]	3.96	(21)
	[EMIM][OAc]		EDAB/[EMIM][OAc]	3.52	
2.	[BMIM][HSO_4]	100°C	EDAB/[BMIM][HSO_4]	3.92	(52)
	[EMIM][HSO_4]		EDAB/ [EMIM][HSO_4]	3.90	
3.	Present Study	105 °C	EDAB/[TBMA][CH_3CO_3]	3.50	-
			EDAB/[Bmpyr][CH_3CO_3]	1.46	
4.	[TDTHP][Phosph]	105 °C	EDAB/[TDTHP][Phosph]	3.25	(27)
	[TDTHP][DCA]		EDAB/[TDTHP][DCA]	3.04	
5.	[EMIM][SCN]	105°C	AB/[EMIM][SCN]	1.64	(55)
			EDAB/[EMIM][SCN]	2.37	
			AB+EDAB/[EMIM][SCN]	0.43	
6.	[BMIM][Cl]	95 °C	AB/[BMIM][Cl]	1.6	(19)
7.	[BMIM][Cl]	110 °C	AB/[BMIM][Cl]	2.2	(18)
8.	[AMIM][Br]	115 °C	EDAB/[AMIM][Br]	3.25	(51)
	[AMIM][$N(CN)_2$]		EDAB/[AMIM][$N(CN)_2$]	1.32	
	[AMIM][Tf_2N]		EDAB/[AMIM][Tf_2N]	2.08	

Abbreviations: [Bmim][OAc]: 1-butyl-3-methylimidazolium Acetate, [Emim][OAc]: 1-Ethyl-3-methylimidazolium Acetate, [TDTHP][Phosph]: Trihexyl(tetradecyl)phosphonium Phosphinate [TDTHP][DCA]: Trihexyl(tetradecyl)phosphonium Dicyanamide [EMIM][SCN]: 1-Ethyl-3-methylimidazolium Thiocyanate, [BMIM][Cl]: 1-butyl-3-methylimidazolium Chloride, [AMIM][Br]: 1-Allyl-3-methylimidazolium Bromide, [AMIM][$N(CN)_2$]: 1-Allyl-3-methylimidazolium dicyanamide, [AMIM][Tf_2N]1-Allyl-3-methylimidazolium bis-(trifluoromethylsulfonyl)imide, [BMIM][HSO_4]: 1-butyl-3-methylimidazolium Hydrogen Sulfate, [EMIM][HSO_4]: 1-Ethyl-3-methylimidazolium Hydrogen Sulfate, [AB]: Ammonia Borane, [EDAB]: Ethylenediamine bisborane

2.6. Ionic Liquid aided Reaction Mechanism

The dehydrogenation of pure AB and EDAB by two potential pathways, i.e., intramolecular and intermolecular mechanism which was initially postulated by previous authors.[8,18,19] The mechanism of AB and EDAB are identical to each other and progress in the same manner. In both cases, the formation of ionic intermediates was observed. Intramolecular dehydrogenation does not result in the formation of oligomeric dehydrogenated AB/EDAB structures; rather, it results in the production of cyclic dehydrogenated AB/EDAB structures. Here the formation of the AB/EDAB dimer initiates the intermolecular dehydrogenation. This dimerization results in the first step of dehydrogenation. The dehydrogenation reaction begins with the creation of an ionic intermediate of AB/EDAB dimer, similar to the formation of diammoniate of diborane (DADB). Following subsequent polymerization of this dimer, larger chains are formed. Each repeat unit then loses further hydrogen as BH_2 cyclic groups and B=N bonds are formed. The dehydrogenation mechanism follows the same path as previous literature (Scheme 2.1 and 2.2). The hydrogen release mechanism of amine borane complexes with ILs remains the same and varies only in the molecular weight of repeated polymer chains.[51]

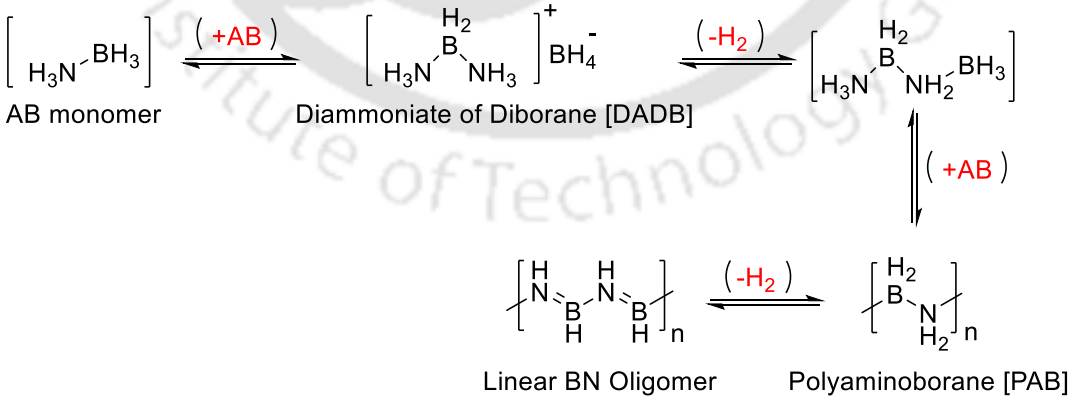

Scheme 2.1: Dehydrogenation Mechanism of Ammonia Borane/IL Complexes

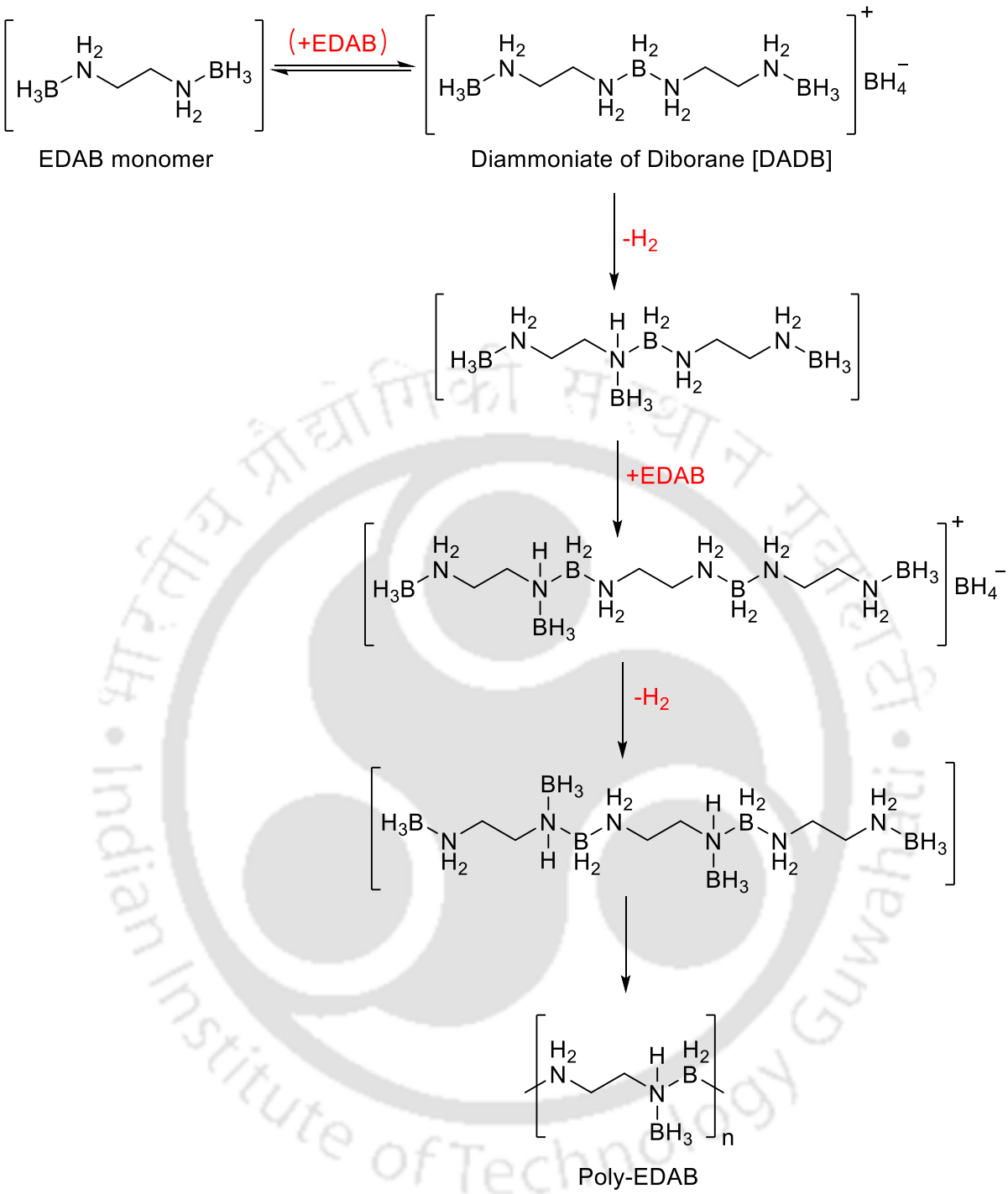

Scheme 2.2: Dehydrogenation Mechanism of Ethylene diamine bisborane/IL Complexes

2.7. Reusability of Ionic Liquid aided Dehydrogenation

Another critical issue is the recyclability of these environmentally friendly solvents. Solvents such as diethyl ether and tetrahydrofuran can be used to isolate reported ILs from solutes. However, in the case of thermal dehydrogenation of the chemical hydrides, the reaction is coupled with the formation of linear poly(aminoborane) $(NH_2BH_2)_n$, in the presence of solvents such as ILs. Due to the fact that these oligomers are soluble in IL media, they cannot be separated from their solute-IL mixtures. Augmenting antisolvents is one way to circumvent this issue. Anti-solvents such as lower alcohols, acetonitrile, dimethyl sulfoxide, and tetrahydrofuran were demonstrated in a recent study.[57] DMSO was found to be the most promising solvent for recovering amine boranes. A strategy similar to this one could also be recommended for our work. This will eventually solubilize the hydrides or linear poly(aminoborane), leaving the solvent behind, which will be easily recoverable.

2.8. ^{1}H NMR Plots of AB and EDAB with Methyl Carbonate Anion based IL's

We conducted the ^{1}H NMR study to characterize AB/IL and EDAB/IL complexes before and after the hydrides' dehydrogenation in the presence of ILs. ^{1}H NMR plots of pure AB/IL and EDAB/IL complexes will negate the presence of any reaction after dehydrogenation and further IL's role in dehydrogenation. Here we have used the referred literature to locate the peak of the compounds only.[21,39] Though there is a chemical shift, which varies with concentration, the trend remains the same.

2.8.1. AB/[Bmpyr][CH_3CO_3]

Figure 2.9.(a) represents the ^{1}H NMR spectra for AB/[Bmpyr][CH_3CO_3] (before reaction). The accurate identification of peaks in a pure compound will help us locate the peak for functional groups in the mixture. Due to the addition of AB and EDAB in IL, the peaks have shifted, but their nature remains the same. AB's peaks can be located at their positions as

NH_3 (4.44 ppm) and BH_3 (1.31 ppm). The peaks for the IL systems can also be related to their positions as N-CH_2 (3.20ppm), N-CH_2-$\underline{CH_2}$ (1.65 ppm), CH_2 (1.30 ppm), CH_3 (0.92 ppm). The peak at 2.50 ppm represents the solvent DMSO-D_6, respectively. The O-CH_3 group of the anion is at a peak location of 3.48 ppm. Ar-H can be located at 3.29, 3.15, 1.68, and 1.66 ppm. Figure 2.9.(b) represents the ^{1}H NMR spectra for AB/[Bmpyr][CH_3CO_3] (after reaction). It is observed that all the peaks of IL have retained their original entity, and the peaks are within their initial assigned position. An important observation is the absence of a peak corresponding to NH_3, suggesting that AB is the active hydrogen releasing moiety that has reacted and initiates the pathway for liberating hydrogen.

2.8.2. EDAB/[Bmpyr][CH_3CO_3]

Figure 2.10.(a) represents the ^{1}H NMR spectra for EDAB/[Bmpyr][CH_3CO_3] (before reaction). The peaks for EDAB can be located at their positions as BH_3 (1.32 ppm), CH_2 (2.61 ppm), and NH_2 (5.40 ppm). The peaks for the IL systems can also be related to their positions as N-CH_2 (3.20 ppm), N-CH_2-$\underline{CH_2}$ (1.66 ppm), CH_2 (1.30 ppm), CH_3 (0.92 ppm). The O-CH_3 group of the anion is at a peak location of 3.47 ppm. The ring hydrogens can be located at 3.29, 3.15, 1.67, and 1.68 ppm. Figure 2.10.(b) represents EDAB/[Bmpyr][CH_3CO_3] (after reaction), where we can observe that the IL have retained its original structure and all the peak are nearby its original assigned position. However, the NH_2 bond of EDAB is absent, which ensures that it is only the EDAB that is taking part in the reaction and liberating hydrogen. Thus IL in all aspects is acting merely as a solvent.

2.8.3. AB/[TBMA][CH_3CO_3]

Similarly, ^{1}H NMR spectra for AB/[TBMA][CH_3CO_3] (before and after) and EDAB/[TBMA][CH_3CO_3] (before and after) reaction have been recorded. Figure 2.11.(a) represents the ^{1}H NMR spectra of AB/[TBMA][CH_3CO_3] (before). Similarly, in Figure 2.9.(a),

the peaks for AB can be located at their positions as H_3N (4.42 ppm) and BH_3 (1.31 ppm). For the IL-[TBMA][CH_3CO_3], the peaks can be located at their positions as N-CH_2 (3.20 ppm, 3.16 ppm, and 3.18 ppm), N-CH_3 (3.20 ppm), N-CH_2-$\underline{CH_2}$ (1.61 ppm, 1.61 ppm, 1.59 ppm), CH_2 (1.28 ppm, 1.29 ppm, and 1.31 ppm), CH_3 (0.91 ppm, 0.92 ppm, and 0.93 ppm). The O-CH_3 group of the anion is at a peak location of 3.58 ppm. Figure 2.11.(b) shows the chemical shifts of AB/[TBMA][CH_3CO_3] (after reaction). All the [TBMA][CH_3CO_3] peaks are in the same position as their initial structure.

2.8.4. EDAB/[TBMA][CH_3CO_3]

Figure 2.12.(a) represents the ^{1}H NMR spectra for EDAB/[TBMA][CH_3CO_3] (before reaction), whereas Figure 2.12.(b) represents EDAB/[TBMA][CH_3CO_3] (after reaction). The peaks for EDAB can be located at their positions as BH_3 (1.30 ppm), CH_2 (2.62 ppm), and NH_2 (5.36 ppm). For the IL - [TBMA][CH_3CO_3], the peaks can be located at their positions as N-CH_2 (3.20 ppm, 3.16 ppm, and 3.18 ppm), N-CH_3 (3.20 ppm), N-CH_2-$\underline{CH_2}$ (1.61 ppm, 1.61 ppm, 1.59 ppm), CH_2 (1.28 ppm, 1.29 ppm, and 1.31 ppm), CH_3 (0.91 ppm, 0.92 ppm, and 0.93 ppm). The O-CH_3 group of the anion is at a peak location of 3.58 ppm. Again we observe that the IL has not gone through any deterioration and retained its original structure. The significant and desired missing hydrogen was found in the NH_2 bond of EDAB, ensuring that only the EDAB is taking part in the reaction and liberating hydrogen.

In all the ^{1}H NMR study of the amine borane complexes and the methyl carbonate anion-based ILs, a similar trend of thermal dehydrogenation of EDAB/AB has been observed.

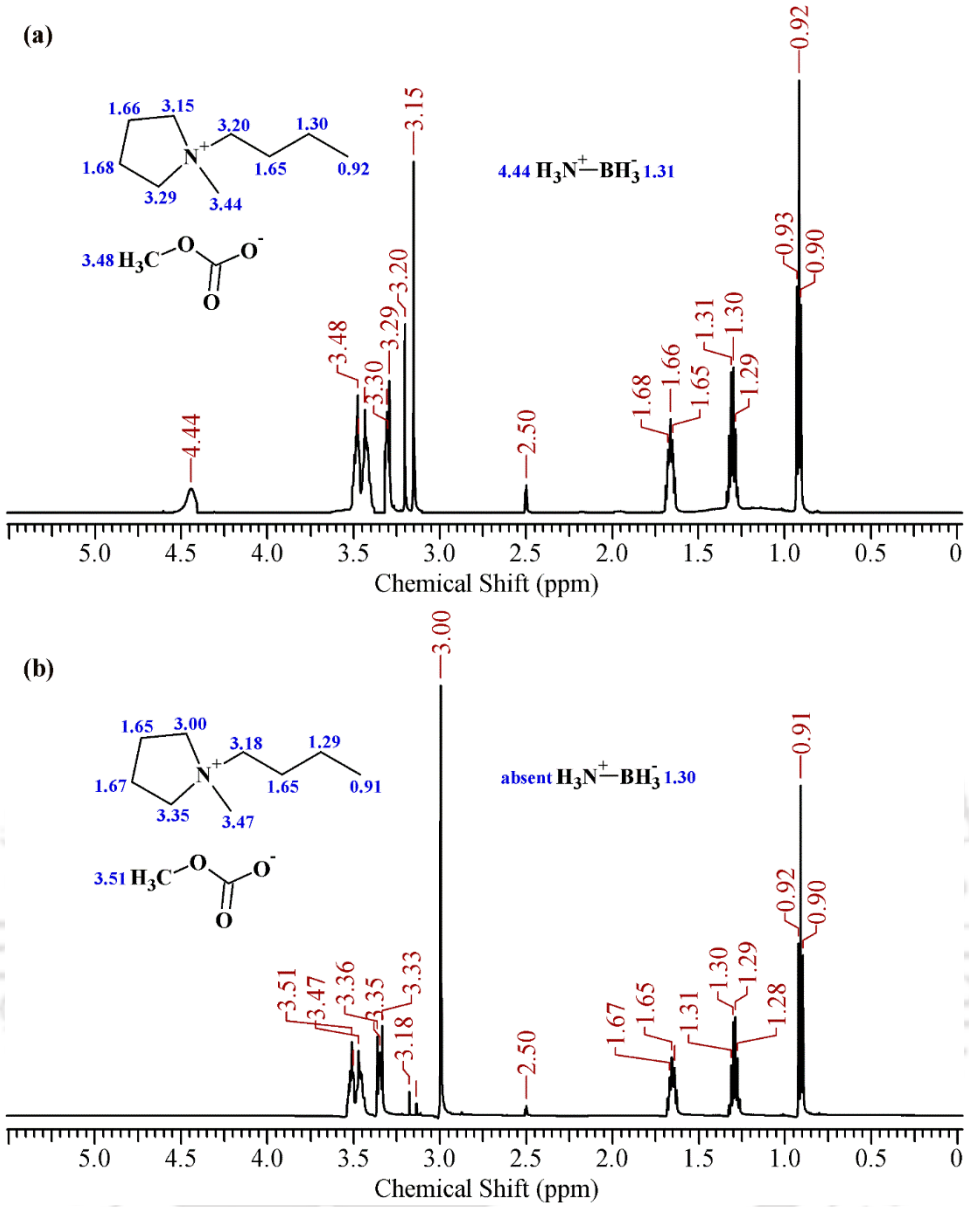

Figure 2.9: ^{1}H NMR spectra of (a) AB/[Bmpyr][CH_3CO_3] (before reaction) and (b) AB/[Bmpyr][CH_3CO_3] (after reaction)

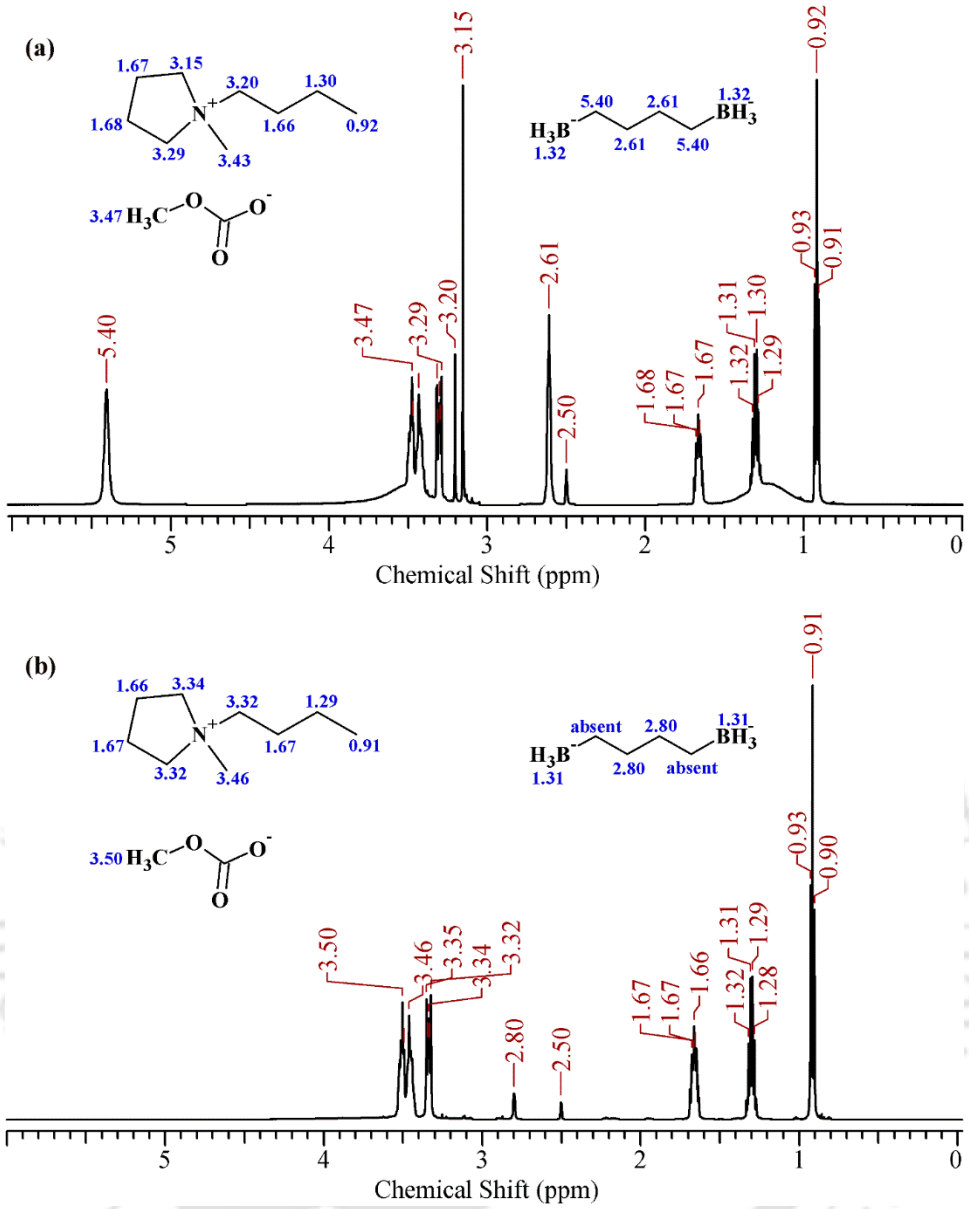

Figure 2.10: ^{1}H NMR spectra of (a) EDAB/[Bmpyr][CH_3CO_3] (before reaction) and (b) EDAB/[Bmpyr][CH_3CO_3] (after reaction)

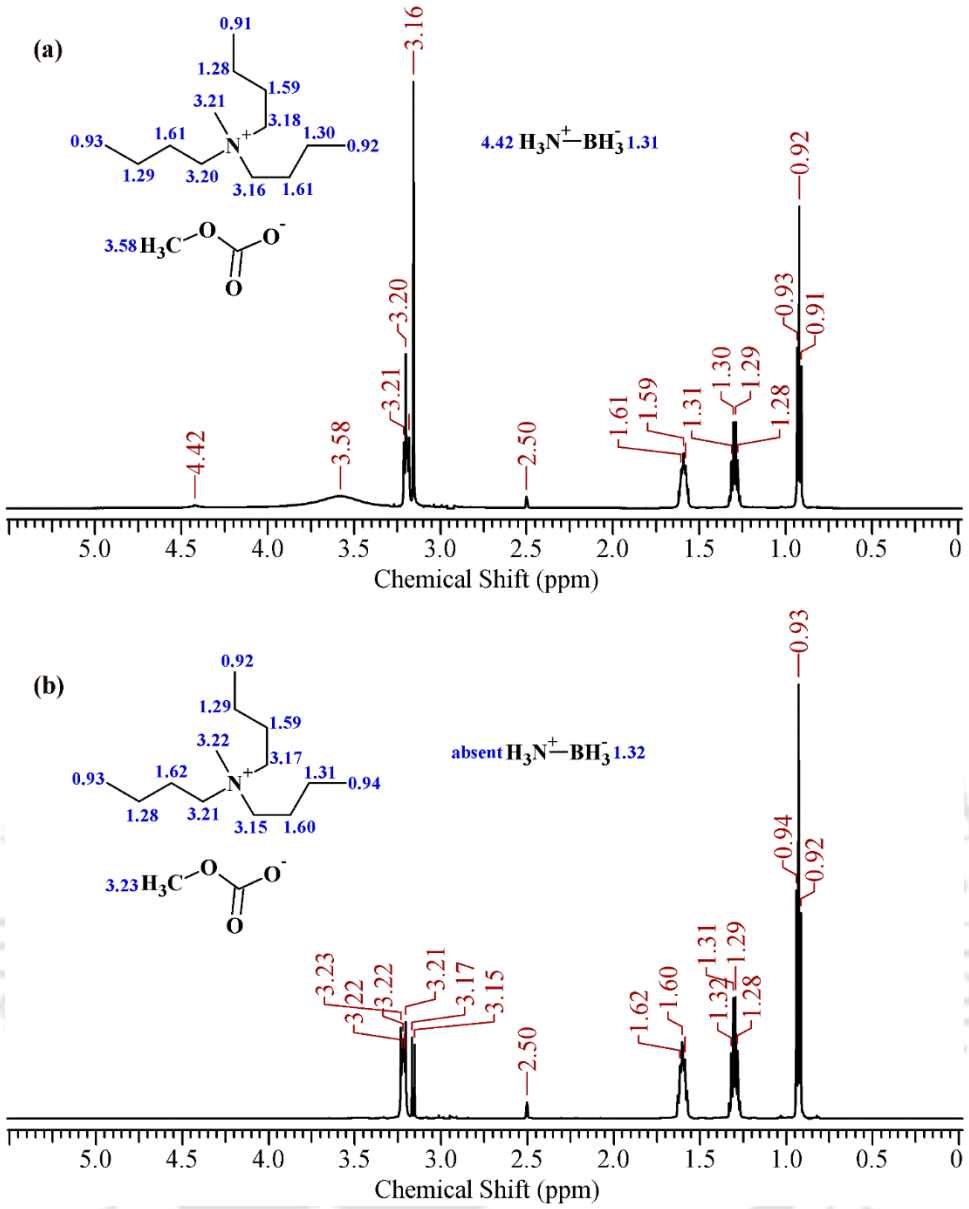

Figure 2.11: ^{1}H NMR spectra of (a) AB/[TBMA][CH_3CO_3] (before reaction) and (b) AB/[TBMA][CH_3CO_3] (after reaction)

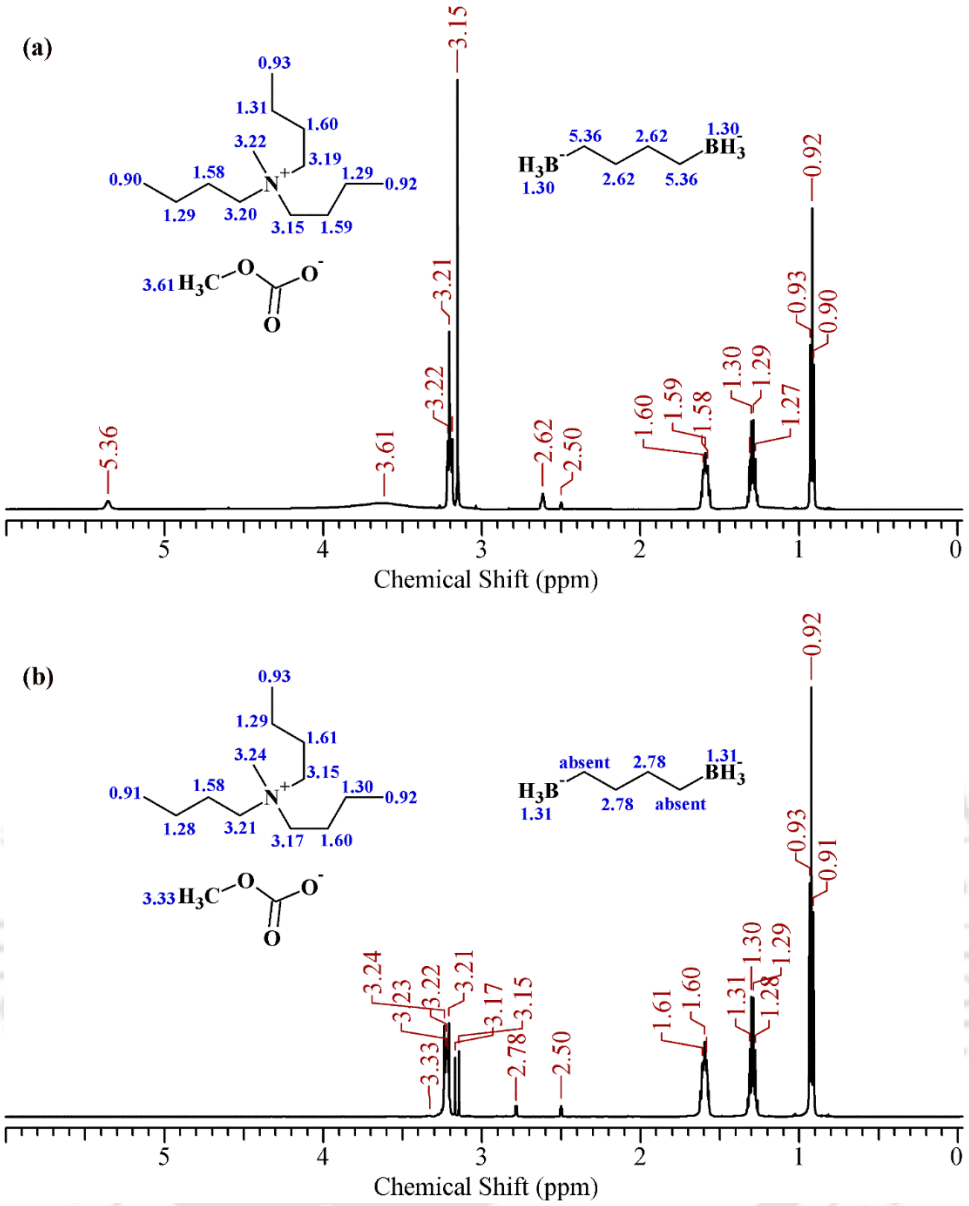

Figure 2.12: ^{1}H NMR spectra of (a) EDAB/[TBMA][CH_3CO_3] (before reaction) and (b) EDAB/[TBMA][CH_3CO_3] (after reaction)

2.9. Quantum Chemical Insights

2.9.1. DFT Studies

In the beginning, density functional theory (DFT) calculations were performed to compare interactions between chemical hydrides (AB and EDAB) and [BMPYR][CH_3CO_3] at the M06-2X/6-311++G(d,p) level of theory.[40] The optimized geometries of the pyrrolidinium cation-based methyl carbonate IL [Bmpyr][CH_3CO_3] are presented in Figure 2.13.(a). As evident from the optimized geometries, the strong ionic interactions between the cationic and anionic moieties are responsible for the formation of the ILs. Further, the chemical hydrides molecules are optimized with the respective IL.

Figure 2.13 (a), (b) represents the optimized structures of the AB/[Bmpyr][CH_3CO_3] and EDAB/[Bmpyr][CH_3CO_3] complex clusters. Further, as shown in Figure 2.13.(c), the distance between the positive charged H attached to the NH_3 moiety in the closest AB molecule and the negatively charged O atoms in the [Bmpyr][CH_3CO_3] were measured at 1.736 Å. This indicates that the O···NH_3 interaction propagated the reactive dehydrogenation by [Bmpyr][CH_3CO_3], which concurs with the previous reports.[58] This is also evident from Figure 2.13.(a), which represents the optimized structure of isolated IL molecule [Bmpyr][CH_3CO_3], where the predicted distance between O atom of the anion and H atom of the cation (33O···8H, 32O···5H, and 32O···20H) are 2.470 Å, 2.285 Å, and 1.991 Å, respectively.

The optimization of AB/[Bmpyr][CH_3CO_3] resulted in the increase of interatomic distances between the cation and anion moiety of the IL, which was due to the addition of chemical hydrides. The negatively charged oxygen in the IL's anionic fragment interacts favorably towards the positively charged NH_3 part of the chemical hydrides. In the similar analogy for [EDAB]·[Bmpyr][CH_3CO_3] Figure 2.13.(d), the distances between the positive charged N in the closest EDAB molecules and O atom in the IL [Bmpyr][CH_3CO_3] were predicted as 1.991 and 1.778 Å respectively. These were equivalent to the corresponding

distances in AB/[Bmpyr][CH_3CO_3]. These findings not only indicated stronger interactions in AB/[Bmpyr][CH_3CO_3] and EDAB/[Bmpyr][CH_3CO_3] but also predicted that the O atom was the most active anion location.

The interactions between chemical hydrides and [TBMA][CH_3CO_3] have been further examined by DFT measurement, using M06-2X/6-311++G(d,p) level of theory,[40] and each optimization for the isolated IL, isolated chemical hydride, and each IL-chemical hydride complex was performed. Figure 2.13.(e) shows optimized structures that reflect the interactions between the chemical hydride molecule and the IL [TBMA][CH_3CO_3] active sites. It is possible to note that the distance between the H of the NH_3 moiety of the AB molecule and the O and H atoms in [Bmpyr][CH_3CO_3] is expected to be 2.542, 1.691, and 2.226 Å, which indicated an interaction between the O···NH3 and that the later was stronger than the former. The optimized [TBMA][CH_3CO_3]·AB/EDAB structures Figure 2.13.(e) and (f) were compared to [Bmpyr][CH_3CO_3]·AB/EDAB Figure 2.13.(c),(d), the shorter intermolecular distances in the [TBMA][CH_3CO_3]·AB/EDAB proposed the stronger interactions between the H atoms of the NH_3 moiety in both the chemical hydrides (AB and EDAB) and the active sites in the [TBMA][CH_3CO_3]. Overall, the study of optimized geometry of chemical hydrides-IL complexes reveals that shorter inter-molecular interactions between IL [TBMA][CH_3CO_3] and the studied chemical hydrides can be suggested as the fundamental explanation for the higher release of hydrogen equivalents using the same catalytic solvent at different temperatures, which is strongly supported by our experimental studies.

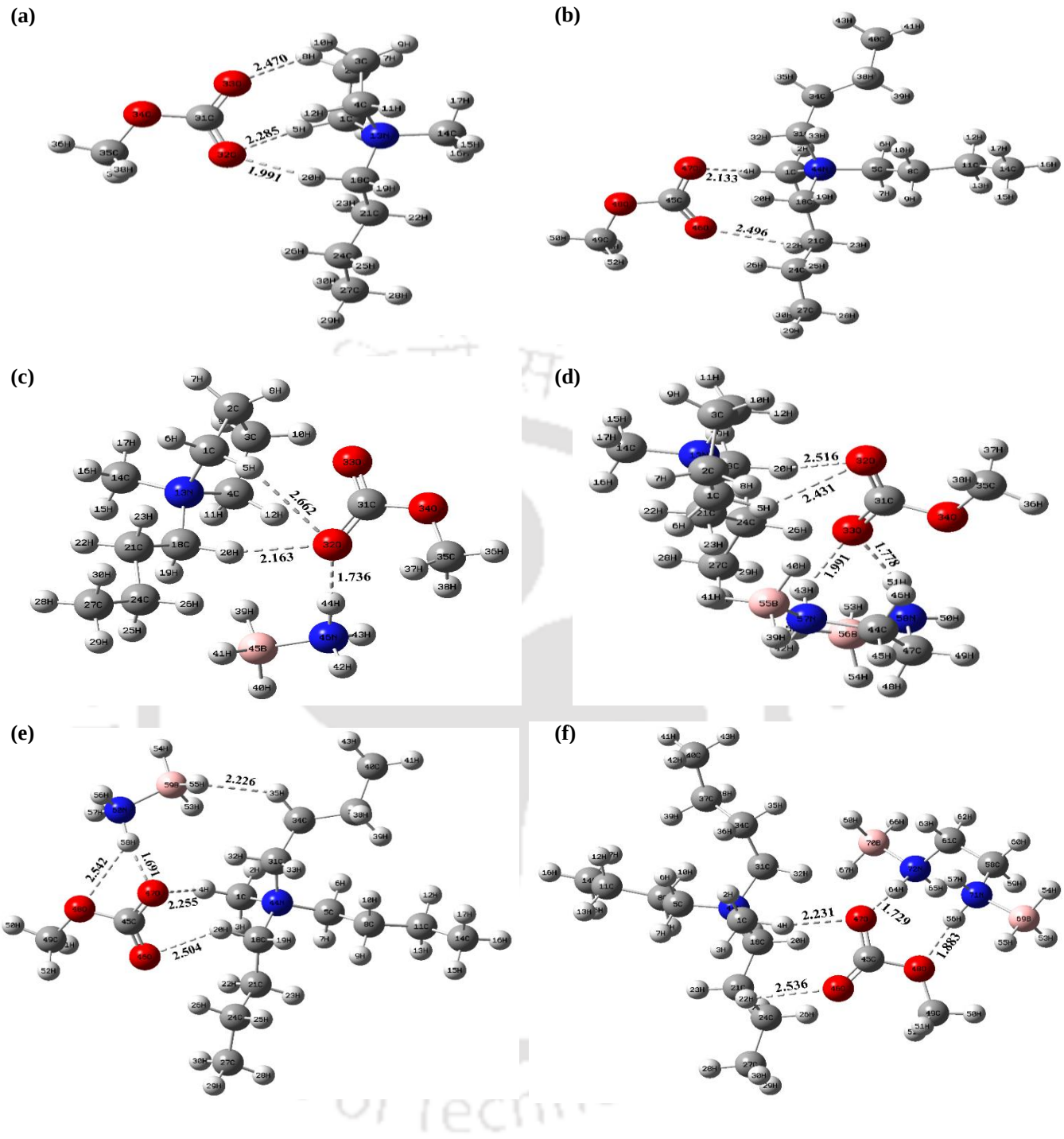

Figure 2.13: Optimized geometries at M06-2X level of theory (a) [Bmpyr][CH_3CO_3], (b) [TBMA][CH_3CO_3], (c) AB/[Bmpyr][CH_3CO_3], (d) EDAB/[Bmpyr][CH_3CO_3], (e) AB/[TBMA][CH_3CO_3], and (f) EDAB/[TBMA][CH_3CO_3].

2.9.2. NBO Charge Analysis

To investigate the interactions between chemical hydrides and the methyl carbonate-based ILs such as [Bmpyr][CH_3CO_3], and [TBMA][CH_3CO_3], the natural bond orbital (NBO) charge distribution of chemical hydrides-ILs complexes were calculated using the Gaussian 09 program.[50,35] It has been demonstrated that the NBO charge analysis provides accurate estimates of atomic charges for IL and chemical hydride systems. The NBO natural charges on the individual components of the ILs and the hydrides studied were assessed before and after the formulation of the complex to decipher the magnitude and direction of the charge transfer (CT) process among specific parts of the chemical hydrides-IL complexes. This analysis identified the components of the ILs that are specifically involved in interaction with a target hydride and aided in quantifying the strength of these interactions.

We observe (Table 2.2) that interaction with the chemical hydrides results in considerable disruption of the CT process occurring within an initial (hydride-free) IL cluster. In IL1 **[**Bmpyr**][**CH_3CO_3**]** and IL2 **[**TBMA**][**CH_3CO_3**]**, the chemical hydrides (AB and EDAB) gain electron density upon interaction with the ILs. The gain or loss of electron density of hydrides tends to be loosely associated with the distance between methyl carbonate anions and chemical hydrides (AB and EDAB).

Table 2.2: Calculated NBO charge on studied chemical hydrides in the presence and absence of the ILs

	AB	**EDAB**
NO IL	**0.0000**	**0.0000**
IL 1 [Bmpyr**][**CH_3CO_3**]**	**-0.0359**	**-0.0611**
IL 2 [TBMA**][**CH_3CO_3**]**	**-0.0517**	**-0.0753**

Table 2.3: Calculated NBO charges on the components of IL in the presence and absence of chemical hydrides

Charge on the cationic part of IL in IL-chemical hydrides complexes			
	AB	**EDAB**	**Neat IL**
IL1 [Bmpyr**][**CH_3CO_3**]**	**0.9594**	**0.9604**	**0.9486**
IL2 [TBMA**][**CH_3CO_3**]**	**0.9575**	**0.9614**	**0.9458**
Charge on the anionic part of IL in IL-chemical hydrides complexes			
	AB	**EDAB**	**Neat IL**
IL1 [Bmpyr**][**CH_3CO_3**]**	**-0.9235**	**-0.8992**	**-0.9486**
IL2 [TBMA**][**CH_3CO_3**]**	**-0.9058**	**-0.8861**	**-0.9458**

The closer the anion is to the hydride molecule, the greater the loss of electron density from the chemical hydrides. The methyl carbonate anion generally displaced the electron density when most chemical hydrides–IL-complexes are formed. For the chemical hydrides-to-anionic part of ILs, CT is accompanied by a weakening of the interaction between the cation and anionic moieties, concomitant with an increased number of chemical hydrides−anion interactions (Table 2.3). In addition, cations lose electron density from the cationic species in the chemical hydrides-ILs complexes. We attribute these trends in CT behavior due to the higher interaction between the IL and chemical hydrides' cationic moiety. Overall, full NBO charge analysis reveals that the presence of the chemical hydrides significantly alters the CT interactions between the constituents of the ILs in a complex manner that depends on the choice of anions in the ILs.

2.10. Frontier Molecular Orbital (FMO) Analysis

2.10.1. FMO Analysis of the Ionic Liquids (ILs)

Frontier Molecular Orbital (FMO) analysis is a potent tool to study donor-acceptor interaction and molecular reactivity. The interactions in a given chemical system can be classified into hydrogen bond interactions, electrostatic interactions, and orbitals between the HOMO and LUMO species. HOMO stands for the highest occupied molecular orbitals, while LUMO stands for the lowest unoccupied molecular orbitals. The molecule's HOMO-LUMO energy gap can determine the energy involved in adding or extracting electrons from a molecule. HOMO characterizes a species nucleophilicity, namely its tendency to donate electrons, while LUMO defines a species' electrophilicity, i.e., its tendency to receive electrons. FMO analysis of aprotic ionic liquids (AILs) with pyrrolidinium and ammonium cations coupled with methyl carbonate as the anion was carried out.

In this work, using the frontier molecular orbital (FMO) analysis, i.e., the HOMO–LUMO gap, the most appropriate IL system for the dehydrogenation of chemical hydrides was again confirmed. In the first instance, kinetic stability and reactivity of a particular IL system were computed from the value of HOMO-LUMO energy band gaps for the cation and anion of the certain IL system. The FMO diagrams of the ILs and pure hydrides with their energy band gaps are shown in Figures 2.14 and 2.15. The green and red isosurfaces represent positive and negative amplitudes of the HOMOs and LUMOs of the ILs, respectively. From the FMO diagrams, it can be observed that while HOMO electrons are located predominantly over methyl carbonate anions, LUMO electrons are primarily clustered around the pyrrolidinium and ammonium cation moiety, with the nitrogen atoms contributing significantly to it. With the interaction of the cation's electron-deficient portion, the negatively charged methyl carbonate anion contributes to the formation of the corresponding ILs.

A molecule with a higher HOMO-LUMO energy gap has a low chemical reactivity and high kinetic stability. For instance, compounds with a high energy gap in HOMO-LUMO are stable and therefore chemically harder than compounds than a lower value of the HOMO-LUMO energy gap. It is important to note that AB and EDAB need electron acceptors due to a higher negative value for HOMO energy. In this way, AB and EDAB can interact with the LUMO of the cation. Based on the FMO analysis on ILs isolated structures, it can be partially predicted that [TBMA][CH_3CO_3] is stable due to its higher energy bandgap and lower negative LUMO energy in comparison to [Bmpyr][CH_3CO_3]. The calculated values of the HOMO, LUMO, bandgap, chemical hardness, and chemical potential are given in Table 2.4. The energy band difference of pure ILs is almost identical. The preference for the suitable solvent for dehydrogenation between the two ILs can therefore not be determined. Thus the FMO analysis of the isolated IL systems left us with an oddity and led us to study the FMO analysis of chemical hydrides/IL complexes. In the ensuing section, FMO analysis was performed on the Ionic liquids and Chemical hydrides complex systems.

2.10.2. FMO Analysis of the Ionic Liquids with Chemical Hydrides

The orbital analysis of reported ILs with chemical hydrides, namely AB and EDAB, was studied. The frontier molecular orbital analysis was performed to determine the stability of the hydrides/ILs clusters. Using the HOMO–LUMO energy band gap, we could decide the optimal IL for the dehydrogenation of chemical hydrides. As reported by Fukui et al., HOMO-LUMO's energy band gap indicates the electrical transport characteristics and mobility.[41] HOMO-LUMO plots of the chemical hydrides/ILs complexes are reported in Figures 2.16 and 2.17, respectively.

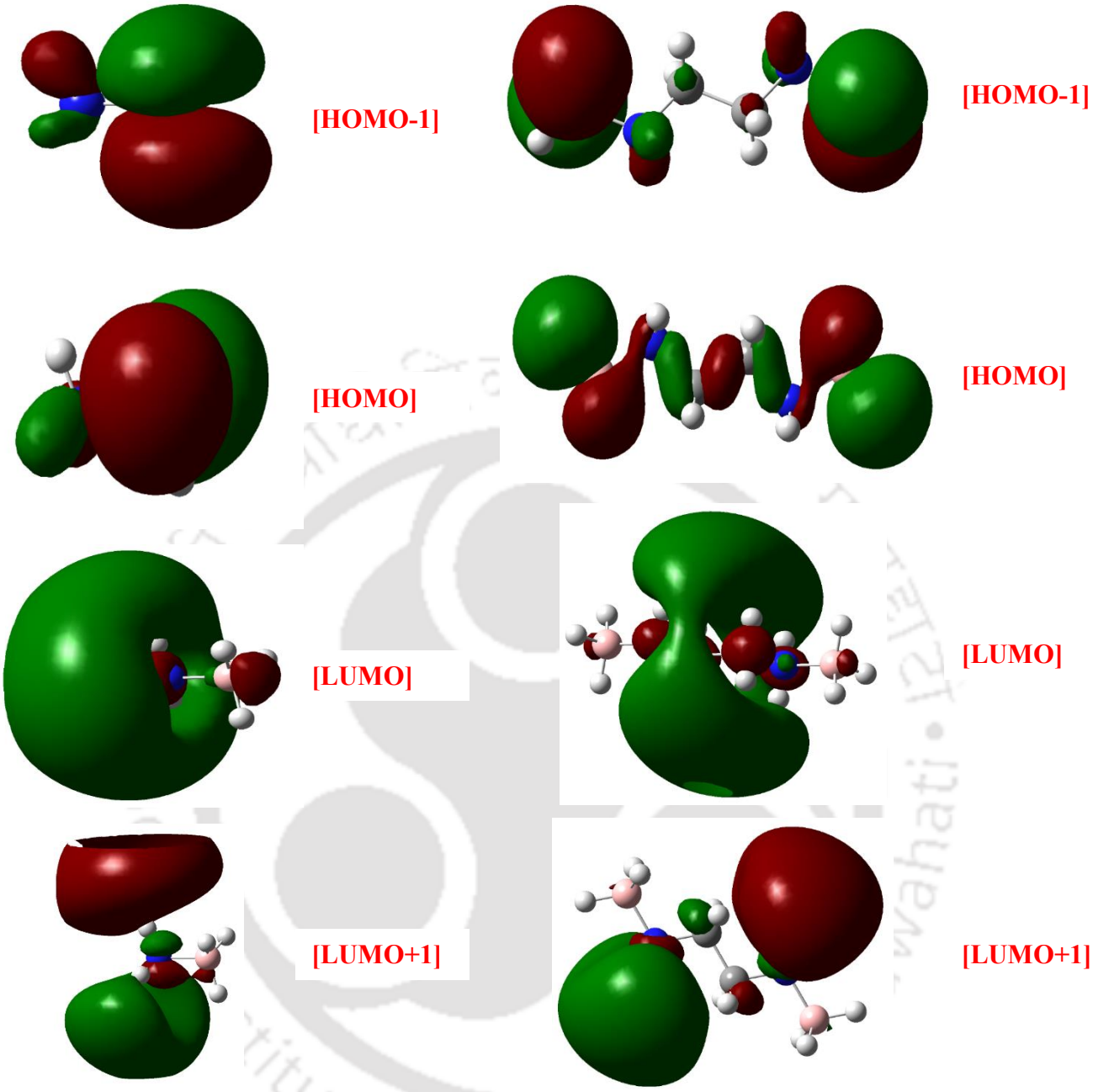

Figure 2.14: HOMO-LUMO isosurfaces of (a) Ammonia Borane (AB) and (b) Ethylene diamine bisborane (EDAB)

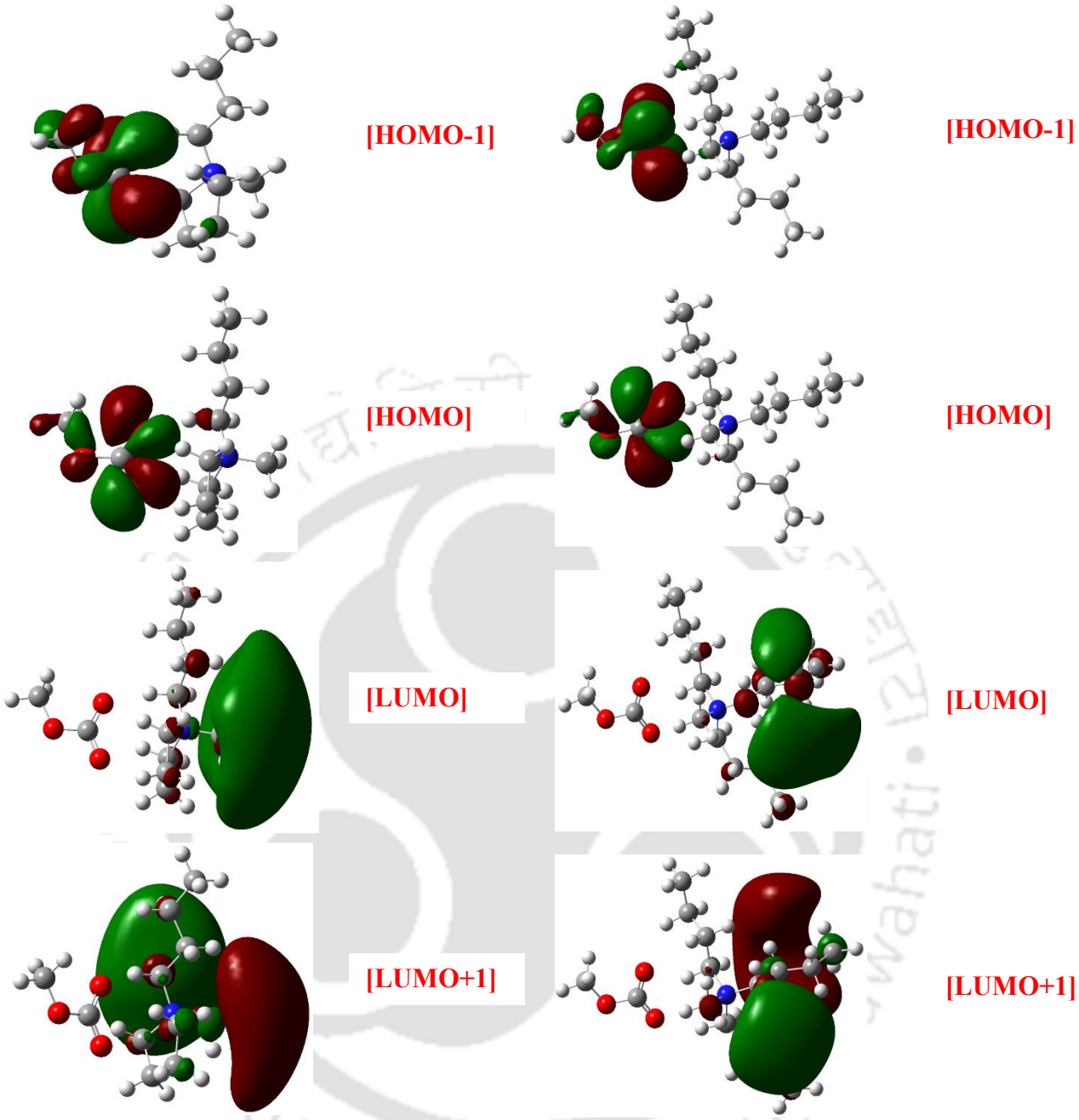

Figure 2.15: HOMO-LUMO isosurfaces of (a) [Bmpyr][CH_3CO_3] (IL1) and (b) [TBMA][CH_3CO_3] (IL2)

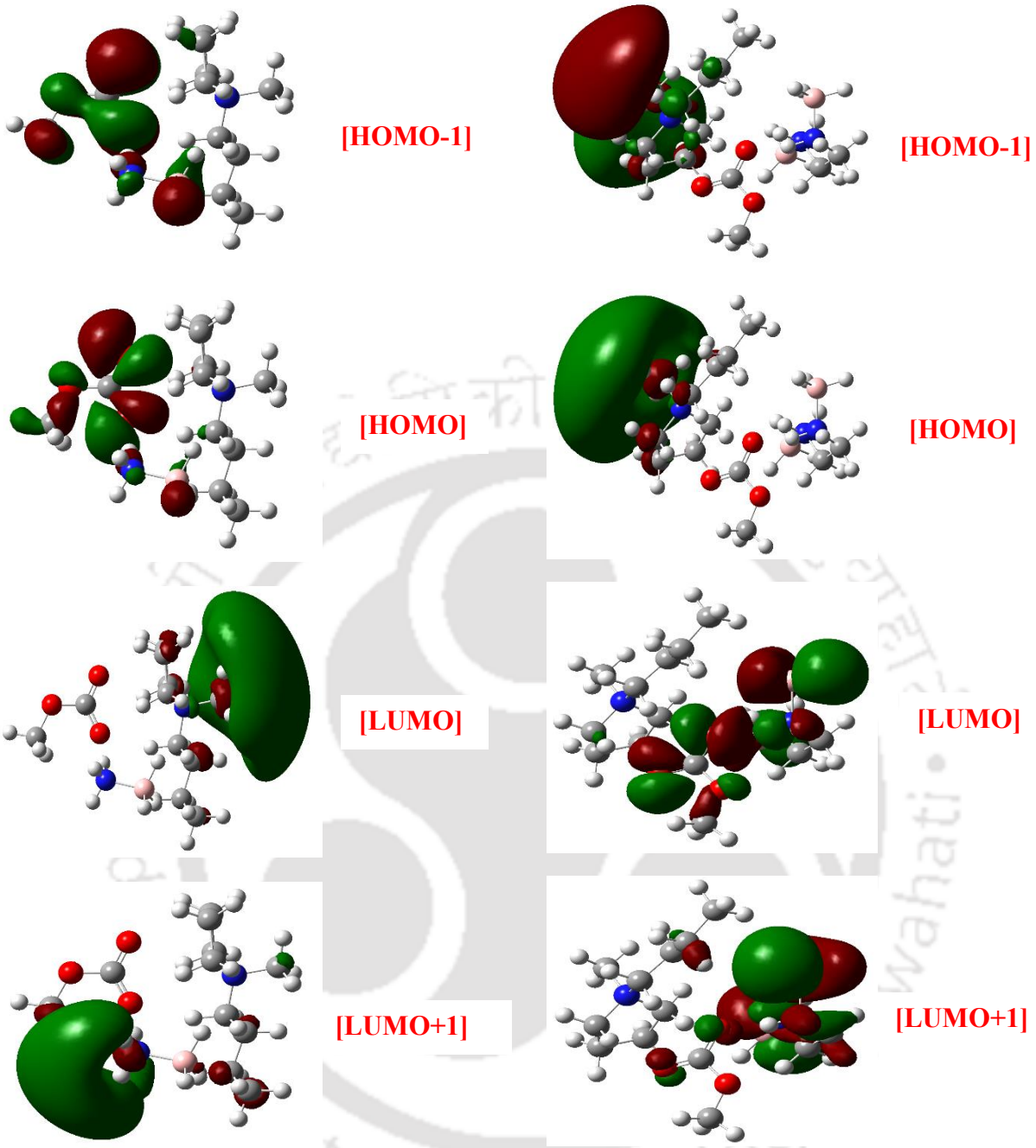

Figure 2.16: HOMO-LUMO isosurfaces of (a) AB/[Bmpyr][CH_3CO_3] and (b) EDAB/[Bmpyr][CH_3CO_3]

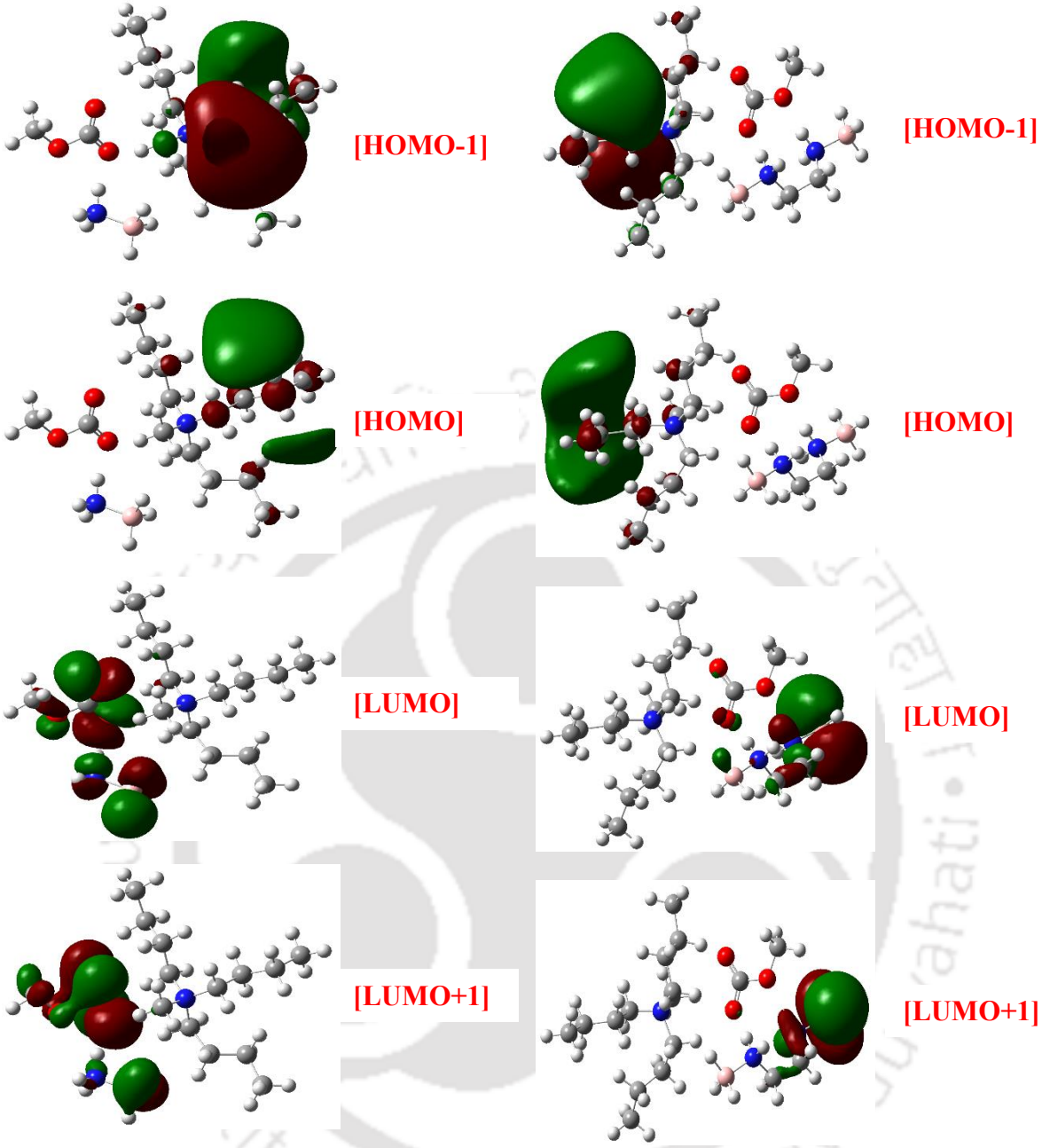

Figure 2.17. HOMO-LUMO isosurfaces of (a) AB/[TBMA][CH_3CO_3] and (b) EDAB/[TBMA][CH_3CO_3]

From Figures 2.16 and 2.17, the HOMO-LUMO energy band gap can be analyzed for the reported ILs and chemical hydrides (AB and EDAB) complex systems. As similar to the isolated ionic liquid system, in both systems, LUMOs are located on the cationic part of the IL, irrespective of being a ring or non-ring cation. This can be attributed to the presence of nitrogen

atoms in both the cations of the respective ILs, making the cations a favorable location to create a transition or intermediate species with the hydrides. On the other hand, the HOMO localized electrons lie on the anionic methyl carbonate moiety. The HOMO-LUMO energy gap of the complex hydrides/ILs systems can be predicted from the band energy gap, which can measure chemical reactivity and stability. However, based on the band energy gap analysis, hydrides and [TBMA][CH_3CO_3] systems come out with a smaller band energy gap. This implies that AB/[TBMA][CH_3CO_3] and EDAB/[TBMA][CH_3CO_3] are less stable than the corresponding hydride/ILs systems. Thus we presume that the combined effect of nitrogen-based cations coupled with basic methyl carbonate anions lowers the LUMO energy significantly and influences the hydrogen yield. Based on the HOMO-LUMO energy gap, which is a representation of the chemical reactivity of a solvent towards its solute and in complex system configuration, [TBMA][CH_3CO_3] is more favorable than [Bmpyr][CH_3CO_3] for hydrogen release from AB and EDAB both, respectively.

The HOMO and LUMO energies are given in Table 2.4 along with the energy of highest (HOMO), second highest (HOMO-1), lowest (LUMO), and second-lowest (LUMO+1) unoccupied orbital with their corresponding orbital energy gap. The pictorial view of the frontier molecular orbital and their respective positive and negative region are shown in Figure 2.16 and Figure 2.17. The HOMO-LUMO energy band gap for IL-AB and IL-EDAB may throw open further evidence as discussed above. In the case of [Bmpyr][CH_3CO_3] cluster coupled with AB and EDAB, second highest (HOMO-1) and second-lowest (LUMO+1), unoccupied orbital with their corresponding orbital energy gap was considered for FMO analysis. It should be noted that the combination of higher LUMO of IL's along with lower HOMO orbital values of AB and EDAB will invariably give the best IL. Thus combining both the results, a lower band gap for EDAB/[Bmpyr][CH_3CO_3] and EDAB/[TBMA][CH_3CO_3] systems suggest that both the reported ILs have a higher tendency towards EDAB. This higher

reactivity and low stability predicted using frontier molecular (FMO) analysis favors the obtained experimental results as discussed previously.

Table 2.4: Theoretical calculated LUMO, HOMO (ground and excited state), chemical hardness (η), and chemical potential (μ)

Complex systems	LUMO energy (a.u.)	HOMO energy (a.u.)	Energy Gap (a.u.)	LUMO+1 energy (a.u.)	HOMO-1 energy (a.u.)	Energy Gap (a.u.)	(η) (a.u.)	(μ) (a.u.)
AB	-0.02469	-0.33430	0.30961	0.01861	-0.33430	0.35291	0.15480	-0.17949
EDAB	-0.02826	-0.34546	0.31720	-0.02122	-0.34779	0.32657	0.15860	-0.18686
[Bmpyr][CH_3CO_3] [IL1]	-0.02509	-0.27333	0.24824	-0.00729	-0.28388	0.27659	0.12412	-0.14921
[TBMA][CH_3CO_3] [IL2]	-0.02293	-0.27141	0.24848	-0.01475	-0.28227	0.26752	0.12424	-0.14717
AB+[Bmpyr][CH_3CO_3]	-0.02077	-0.29712	0.27635	-0.00532	-0.30719	0.30187	0.13817	-0.15894
EDAB+[Bmpyr][CH_3CO_3]	-0.01926	-0.29739	0.27813	-0.01101	-0.30997	0.28896	0.13906	-0.15832
AB+[TBMA][CH_3CO_3]	-0.02309	-0.31304	0.28995	-0.00467	-0.31913	0.31446	0.14497	-0.16806
EDAB+[TBMA][CH_3CO_3]	-0.02508	-0.30909	0.28401	-0.01647	-0.30987	0.29340	0.14200	-0.16708

2.11. Imidazolium-based Ionic Liquid Expedited Dehydrogenation Experiment of Chemical Hydrides

Prior to the dehydrogenation experiment, an IDAC study was conducted to obtain the solubility of chemical hydrides in the studied IL systems (Table 2.5). The thermal dehydrogenation experiment of AB and EDAB was conducted at 100 °C in the presence of the investigated IL systems. When heated to 100 °C, the dehydrogenation of AB and EDAB in their solid-state can yield up to 0.90 and 1.89 equivalents of hydrogen gas, respectively. When AB and EDAB are dehydrogenated in their solid state, an induction period occurs prior to the release of hydrogen. The use of IL as a reaction medium in the dehydrogenation of amine borane complexes aims to minimize the induction period. From Figures 2.19 and 2.20, we can see that in the presence of ILs, such as [Bmim][BF_4] and [Bmim][PF_6], the induction period

for both AB and EDAB is approximately 20 minutes, with an essentially negligible amount of hydrogen being produced at the beginning of the experiment. However, the thermolytic dehydrogenation in the presence of [Bmim][$MeSO_4$] can release hydrogen gas equivalents without an induction period at the same working temperature. A cumulative of 1.86 and 2.69 equivalents of hydrogen was released from AB/[Bmim][BF_4] and EDAB/[Bmim][BF_4] at 100°C, respectively. AB/[Bmim][PF_6] and EDAB/[Bmim][PF_6] systems were capable of releasing a cumulative of 1.54 and 2.41 equivalents of hydrogen. Until 100 minutes, the hydrogen desorption rate for both ILs is nearly identical, indicating that both hydrides are dehydrogenating at approximately the same rate. [Bmim][PF_6] is the IL with the lowest overall performance in the analyzed subsection. Despite the induction period, the system has a greater yield than the pure AB and EDAB systems, demonstrating the advantage of AB/EDAB dehydrogenation with ILs over pure AB and EDAB systems.

Table 2.5: COSMO-SAC Predicted Solubility of AB and EDAB in Studied ILs at T= 25°C

Ammonia Borane (AB)		
IL system and its abbreviation	$(IDAC)_{AB}$	$\ln(IDAC)_{AB}$
1-Butyl-3-methylimidazolium methylsulfate [Bmim][$MeSO_4$]	0.0099	-4.615
1-Butyl-3-methylimidazolium tetrafluorborate [Bmim][BF_4]	0.6873	-0.374
1-Butyl-3-methylimidazolium hexafluorphosphate [Bmim][PF_6]	3.7756	1.328
Ethylenediamine Bisborane (EDAB)		
IL system and its abbreviation	$(IDAC)_{EDAB}$	$\ln(IDAC)_{EDAB}$
1-Butyl-3-methylimidazolium methylsulfate [Bmim][$MeSO_4$]	0.0127	-4.366
1-Butyl-3-methylimidazolium tetrafluorborate [Bmim][BF_4]	0.8332	-0.182
1-Butyl-3-methylimidazolium hexafluorphosphate [Bmim][PF_6]	2.5969	0.9543

It is plausible that EDAB/[Bmim][$MeSO_4$] and AB/[Bmim][$MeSO_4$] outperformed all other systems when used in conjunction with [Bmim][BF_4] and [Bmim][PF_6]-based ILs (Figure 2.19 and 2.20). We noticed that 0.55 equivalent of hydrogen equivalents was liberated from the AB/[Bmim][$MeSO_4$] system within 10 minutes of dehydrogenation. In contrast, the

EDAB/[Bmim][$MeSO_4$] system was capable of releasing nearly 2.0 equivalents of hydrogen gas within the first 20 minutes of dehydrogenation. Following the release of a total of 3.66 equivalents of hydrogen gas by the EDAB/[Bmim][$MeSO_4$] system, the system became stable, indicating that the system had reached its limit and could no longer release extra hydrogen. The system AB/[Bmim][$MeSO_4$] produces 2.18 equivalents of hydrogen, with the rate of release decreasing after the formation of the second hydrogen equivalent. In part, this performance of the [BMIM][$MeSO_4$] IL can be attributed to the greater basicity of the methylsulfate anions. The higher basicity is considered to distort the hydrogen bond network of the amine borane complexes, thereby allowing the dissolution of chemical hydrides in methylsulfate-based ILs. This nature of methylsulfate-based ILs can be visualized in the images provided below in Figure 2.18.

Figure 2.18 demonstrates the images of 2 ml Eppendorf tube with materials of (a) neat hydride, (b) neat IL [Bmim][$MeSO_4$], (c) hydride-IL mixture right before the reaction, and (d) hydride-IL mixture of thermolysis right after the reaction. As it is evident from image (c), the hydride-IL mixture is a slurry at room temperature. As the solvent is added to the chemical hydride, a sudden frothing is observed, and the reaction mixtures expand, as shown in the image (c). Further, the reaction mixture changes into a stable liquid phase with the completion of the dehydrogenation reaction as most of the dehydrogenation process was completed in the first 120 minutes (image (d)). This initial frothing of the reaction mixture initiates the rapid hydrogen release in the case of the AB/EDAB-[Bmim][$MeSO_4$] mixture. In the studied case, released hydrogen equivalents can be referred to as the hydrogen of hydride molecules, expressed as "moles of hydrogen per moles of the complex."

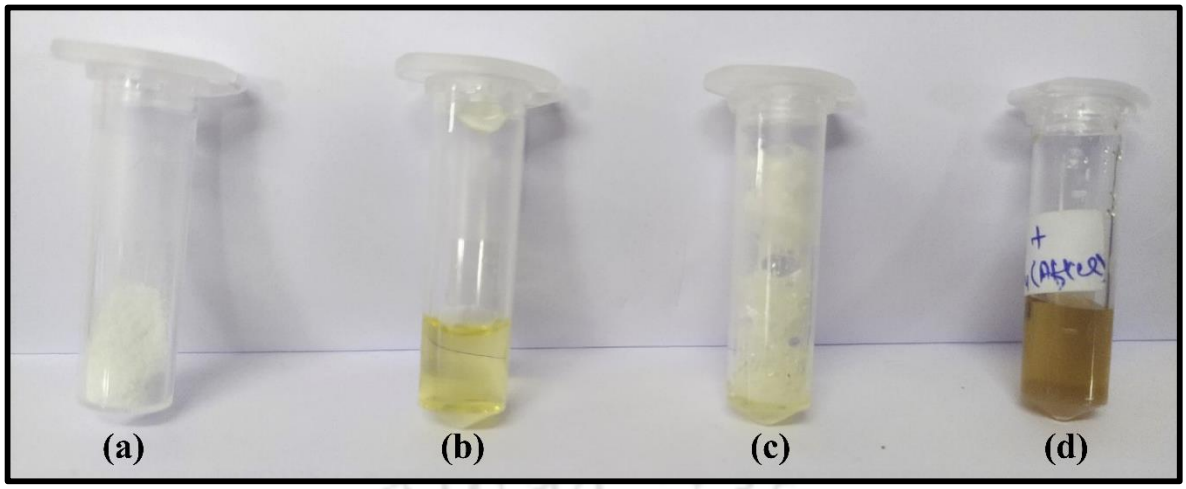

Figure 2.18: Images of a 2 mL Eppendorf tube with materials of (a) neat hydride, (b) neat IL [Bmim][$MeSO_4$], (c) hydride-IL mixture right before the reaction, (d) hydride-IL mixture of thermolysis right after the reaction

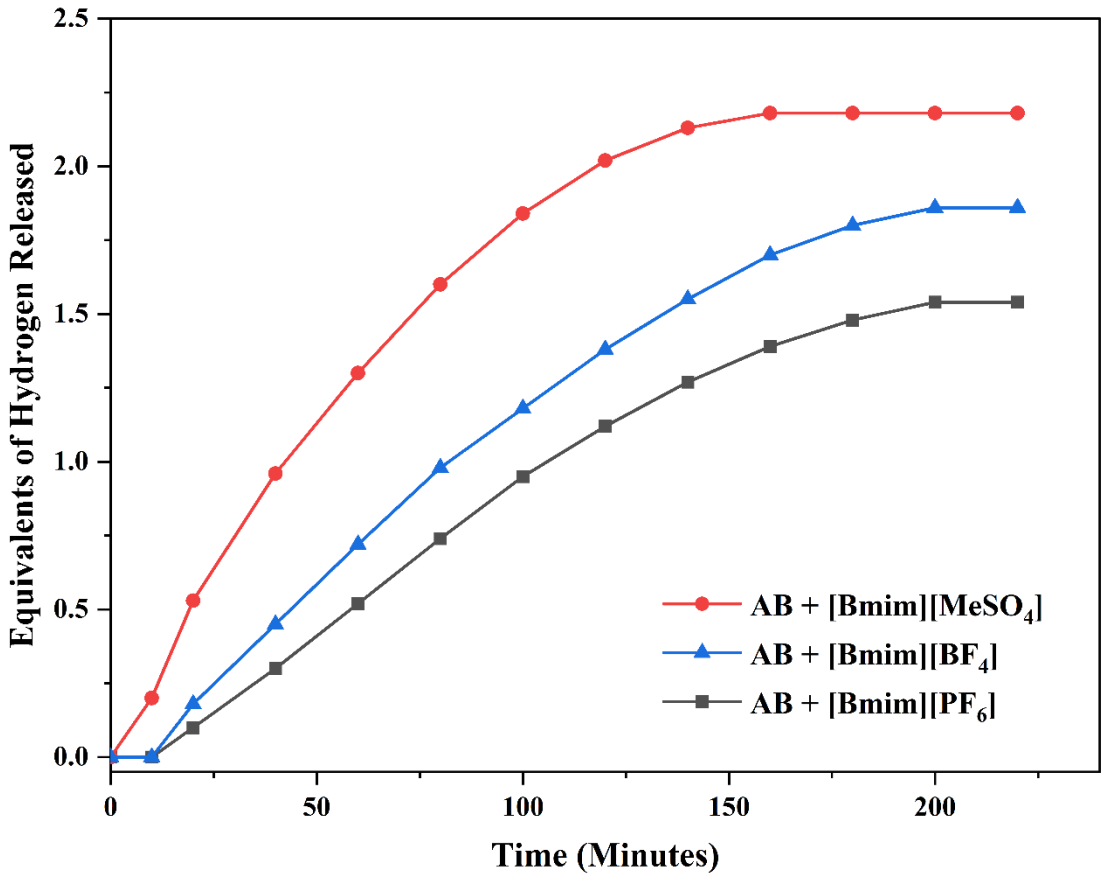

Figure 2.19: Equivalents of hydrogen released from AB/IL mixture at 100°C

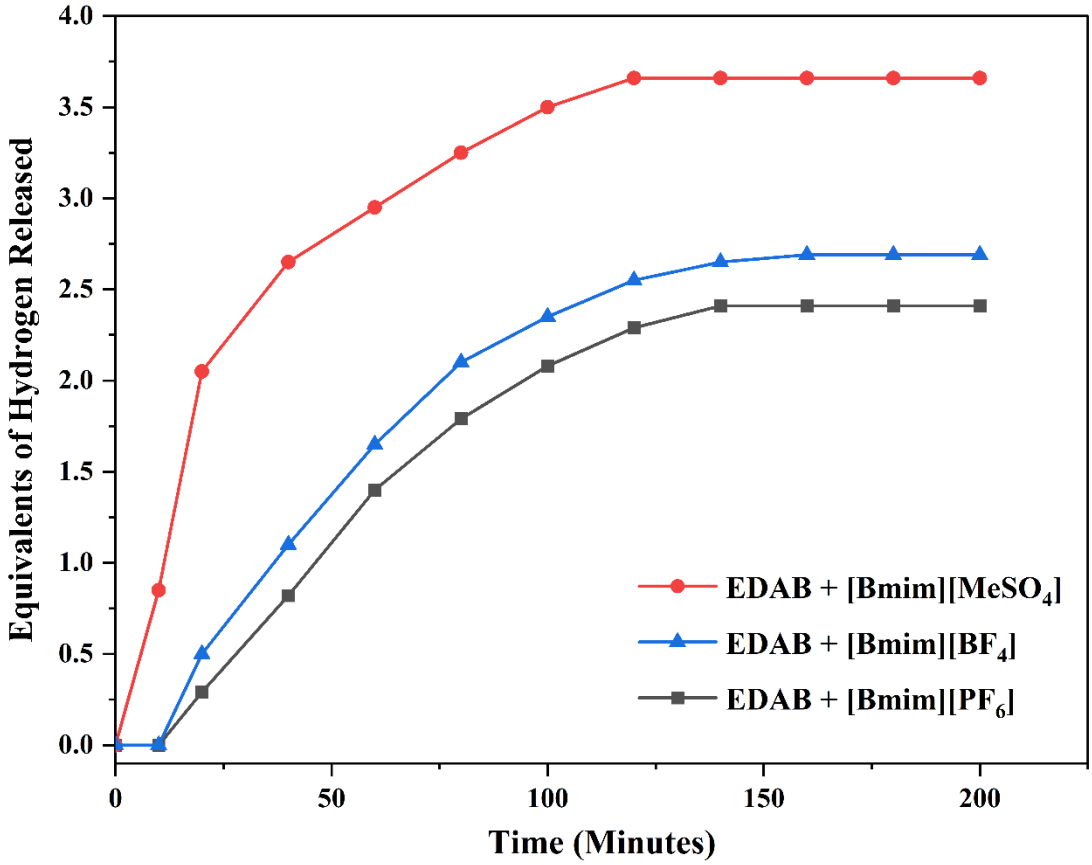

Figure 2.20: Equivalents of hydrogen released from EDAB/IL mixture at 100°C

2.12. Effect of Ion Choice on Thermal Dehydrogenation of Chemical Hydrides

The hydrogen bond basicity, or the β-value specified by Kamlet and Taft, is a crucial metric for classifying an ionic liquid or solvent for subsequent usage in a variety of applications.[59,60] According to the standard IL-based catalytic mechanism, which states that the ability of deprotonation of chemical hydrides controls the reactive activity, the hydrogen bond basicity of a traditional ILs is assumed to be responsible for the activity of the solvent.[61,24]

The effect of modulating the anion was tested (in conjunction with a $[Bmim]^+$ cation) using tetrafluoroborate [BF_4^-], hexafluorophosphate [PF_6^-], and methylsulfate [$MeSO_4^-$] anion using chemical hydrides bearing the same RTIL as the sample. The subset of ILs possessing imidazolium cations exhibits a specific pattern that is implied by the anion. According to the study reported by Jessop et al. on the trend in mean β-values of the Kamlet-

Taft parameters, hydrogen yields are related to the basicity of the ILs.[62] The ILs containing anions with extremely low mean β-values, such as [PF_6^-], and [BF_4^-], as well as those containing anions with larger mean β-values, such as [$MeSO_4^-$], carrying the identical cationic species [Bmim] $^+$, precisely fit the pattern, as shown in Figure 2.21. Thermal dehydrogenation in the presence of methylsulfate [$MeSO_4^-$] ILs enhances the yield and reaction rates. The presence of ILs with lower basicity values, tetrafluoroborate [BF_4^-], hexafluorophosphate [PF_6^-], in combination with [Bmim]$^+$ cation exhausts with the lower release of hydrogen equivalents. This correlation states that the higher the hydrogen bond basicity of an anion, the higher it will contribute to the amount of hydrogen equivalents released.

The catalytic effect of the anions correlated with the basicity was in the sequence as follows: [Bmim][$MeSO_4$] > [Bmim][BF_4] >[Bmim][PF_6], which implied that the anion moieties dominated the dehydrogenation of chemical hydrides. The hydrogen bond basicity also contributes to the solubility of chemical hydrides in the IL system. The strong non-covalent interactions between the basic anions and the protic nitrogen moiety of the hydrides in the ILs are responsible for the higher chemical hydride solubility in the ILs.[31] The delay in breaking dihydrogen bonds formed in the solid-state of amine borane complexes results in an enhanced induction period. The solubilizing property of ILs, breaks the dihydrogen network, hence shortening the induction period. Thus, the solubility of amine borane complexes in IL is proportional to the ease with which hydrogen can be released from the complex system.[63] The higher equivalent release of AB and EDAB in the presence of methylsulfate [$MeSO_4^-$] ILs would arise due to the higher solubility of hydrides in the IL. A COSMO-SAC model-based study performed in this work follows a trend related to the solubility of chemical hydrides with a higher hydrogen bond basicity value of the anion (Table 2.5). This trend for basicity value of anions pertaining to the release of hydrogen equivalents only lines in accordance with ILs with imidazolium-based cations.

Table 2.6 illustrates the comparison of the hydrogen equivalents released by incorporating different anions for the IL-mediated dehydrogenation of chemical hydrides. The previously reported literature has been compared to our work in terms of the amount of hydrogen released by incorporating different anions with higher and lower β-values at various operating temperatures (Table 2.6). All the reported earlier results incorporate the usage of a similar cationic moiety $[Bmim]^+$ and varying the anionic part. In one of the work reported by Banerjee et al., thermal dehydrogenation of EDAB in the presence of acetate anion-based IL (β=0.99) documented a release of 3.96 equivalents of hydrogen gas.[54] The benchmarking work reported by Bluhm and co-workers reported a release of 1.6 equivalents from IL-facilitated dehydrogenation of AB in the presence of chloride anion (β=0.93).[19] In one of our documented work, the efficiency of the EDAB/[Bmim][$MeSO_3$] system was elucidated and tended to release a cumulative of 3.7 equivalents of hydrogen, which can be attributed to the higher basicity value of the anionic moiety present in the IL.[64] This effect of ILs dependent on the anions' basicity can be only severely found in the presence of imidazolium cations.[22] This effect was not observed when there were no imidazolium cations present.

In the study performed in our initial section of this chapter, methyl carbonate anions with higher β-value were tuned with pyrrolidinium and ammonium cations.[63] The study could not correlate a distinct tendency of basicity and hydrogen release in the absence of imidazolium cations. This effect can be attributed to the acidic environment provided by the imidazolium-based ILs.[65] The presence of acidic hydrogen at the C^2, C^4, C^5 positions exerts a substantial effect on the catalytic activities in the presence of basic anions. Significantly, the presence of hydrogen at the C^2 position initiates the formation of intermediate carbene species.[66] The dehydrogenation of AB and EDAB begins with the formation of ionic species, namely diammoniate of diborane (DADB).[67,68] The formation of the intermediate moiety is proposed to be the rate-determining step. The acidic environment provided by imidazolium cations

initiates the dehydrogenation reaction by stabilizing the ionic intermediates formed during the reaction, which results in the increase of reaction rates and higher yield.[69]

Last, the effect of varying the cation was considered using the [$MeSO_4^-$] in each case. In addition to the anion, we observed that the nature of the cation impacts efficiency, particularly in terms of the reaction rate and total hydrogen production. A comparative study was conducted to study this effect of cation and alkyl chain length to elucidate its impact on the dehydrogenation of chemical hydrides. [Bmim][$MeSO_4$] was investigated above, and it outperformed all the counterpart ILs, incorporated with different anionic moieties. The catalytic performance of [Bmim][$MeSO_4$] with its lower alkyl chain length counterpart, namely 1-ethyl-3-methylimidazolium methylsulfate [Emim][$MeSO_4$], was performed. A cumulative of 1.97 and 3.17 equivalents of hydrogen was released from AB/[Emim][$MeSO_4$] and EDAB/[Emim][$MeSO_4$] at 100°C, respectively (Figure 2.22). The effect of increasing the alkyl chain length of the cation was found to be crucial. $[Bmim]^+$-based cations outperformed their lower alkyl cation analogues $[Emim]^+$ in terms of catalytic cum solvent activity. The release of hydrogen equivalents from [Bmim][$MeSO_4$] was two-fold higher than the latter. The increased catalytic activity with $[Bmim]^+$ cation can be attributed to weaker cation-anion interaction within the IL system. To put it another way, as the alkyl chain length rises, the cation-anion interaction within the ILs weakens by decreasing the cation's electron-donating capacity and augmenting the imidazolium ring's positive charge density. This results in an increase in the interaction between the anionic species and the desired molecules of the chemical hydrides investigated in this work, as well as a decrease in the amount of free anions.[70]

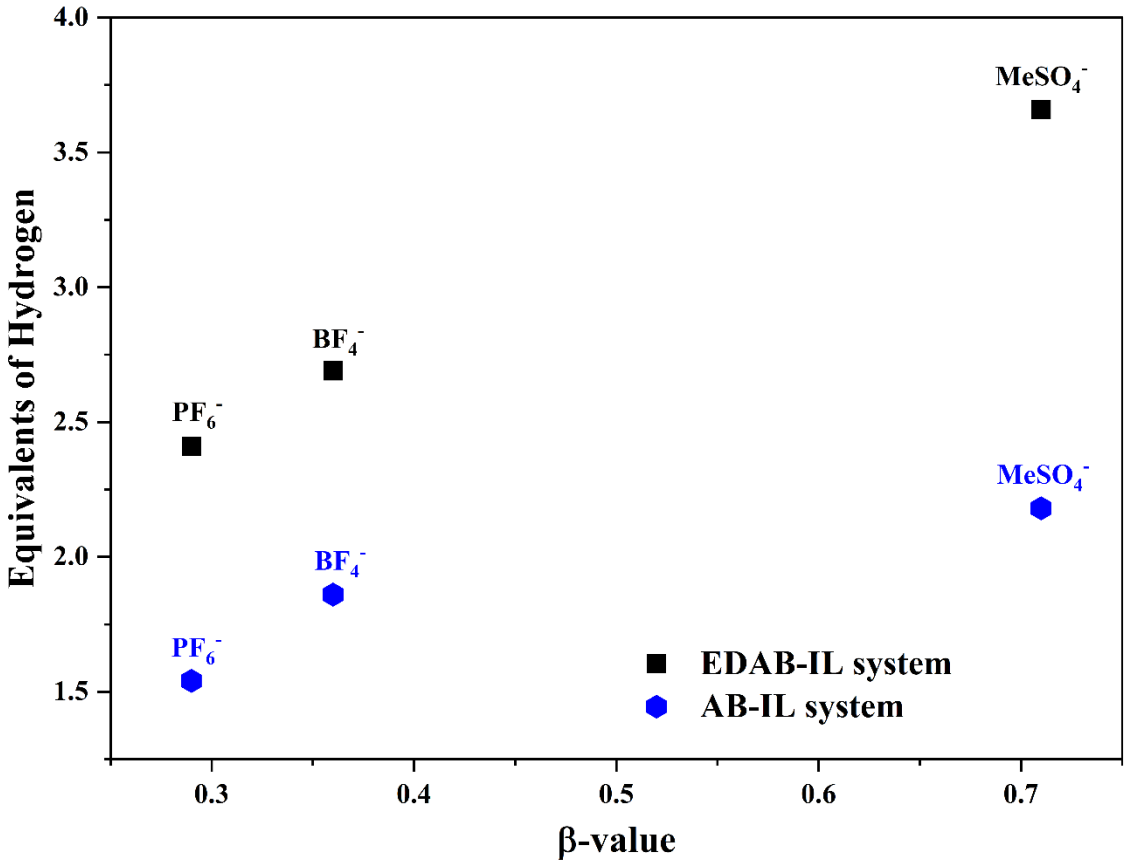

Figure 2.21: Plot of equivalents of hydrogen released in relation to mean β-value of anions of the studied ILs

Table 2.6: Comparison of hydrogen yield in AB and EDAB dehydrogenation to the mean β-value of the anion of the studied imidazolium ILs.

Anion	mean β-value	Equiv. H_2 from AB	Equiv. H_2 from EDAB	Reference
$MeSO_4^-$	0.71	2.18	3.66	Present Study
BF_4^-	0.36	1.86	2.69	Present Study
PF_6^-	0.29	1.54	2.41	Present Study
Cl^-	0.93	1.6	3.02	[50]
OAc^-	0.99	--	3.96	[49]
$MeSO_3^-$	0.77	--	3.70	[28]
Tf_2N^-	0.24	--	2.04	[20]

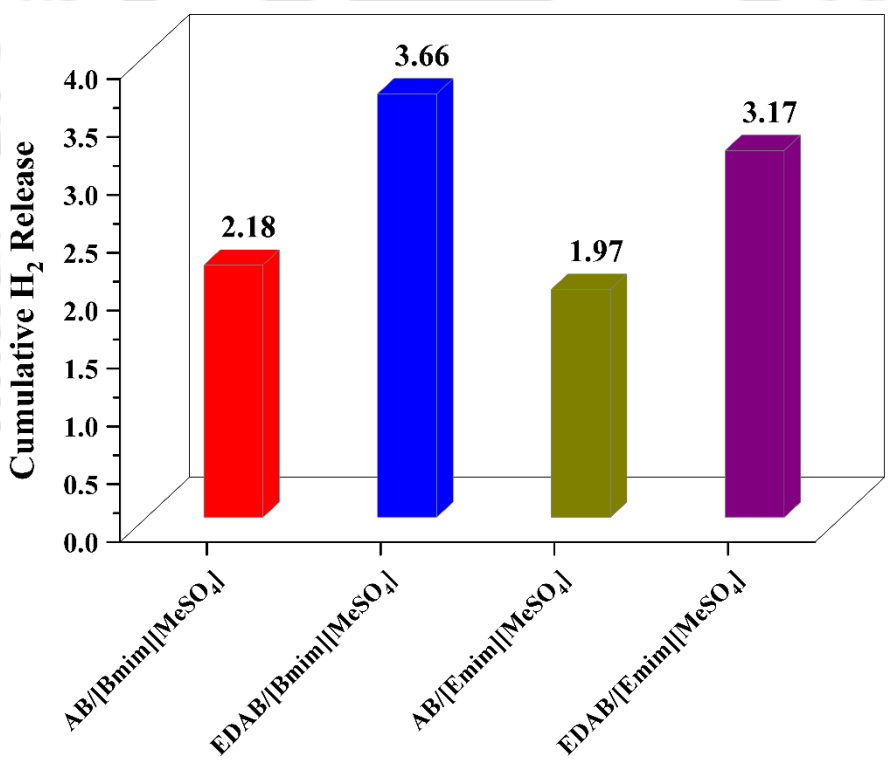

Figure 2.22: Cumulative release of hydrogen equivalents from AB and EDAB mediated by ILs at 100°C

2.13. Quantum Chemical Calculations

2.13.1. Geometry Optimization of Ionic Liquid Pairs

The advent of imidazolium-based ILs combined with a large variety of anions showed that ILs are a valuable domain of functional materials. A series of typical imidazolium-based ILs was chosen for this study. They are composed of 1-butyl-3-methylimidazolium cation $[Bmim]^+$ and a variety of coordinating and non-coordinating anions such as $[MeSO_4^-]$, $[BF_4^-]$, and $[PF_6^-]$ (Figure 2.4). The most stable ion pair geometries for these ILs are depicted in Figure. 2.24. All of the $[Bmim]^+$ cation-based ILs, namely $[Bmim][MeSO_4]$, $[Bmim][BF_4]$, and $[Bmim][PF_6]$, feature anions in the plane of the imidazolium ring, adjacent to the most acidic C^2-H group, culminating in strong hydrogen-bond interactions between the cation and anion moieties. As expected, the ion pair of the fluorine atoms in $[BF_4^-]$, and $[PF_6^-]$ anion exhibits at least one shortest H–(C^2)···F interaction distance, thus indicating one strong C^2–H···F H-bond interaction (Figure 2.24 (a, b)). A large number of interactions between the imidazolium cations and the fluorinated anions can be attributed to the front and top positions in the optimized geometries. The hydrogen bond interactions formed by fluorine (F) atoms with hydrogen (H) atoms are usually stronger. However, the large vdWs volume and delocalized charge of fluorinated anion make the interaction energies (E) of the IL system weaker. It is possible that the two ionic liquids, $[Bmim][BF_4]$ and $[Bmim][PF_6]$, acquire similar structural properties due to their classification as weakly coordinated ionic liquids.

On the other hand, the interaction between the acidic C^2–H group and $[MeSO_4^-]$ anions proceed further with the formation of H-bonding. The acidic C^2–H group of the $[Bmim]^+$ cation, has a strong affinity toward the oxygen atoms of the $[MeSO_4^-]$ anions (Figure 2.24(c)). The electronegative atoms have a stronger electrostatic interaction with the C^2–H position leading to a stronger electrostatic interaction. It has been shown that H-bond interactions with ILs can explain spatial patterns in both solid and liquid phases.[71] Anion and cation interactions

have traditionally been the focus of ab initio studies in the gaseous phase of the IL system. The imidazolium cation's peculiar chemical structure features several anion H-bonding sites, front, side, and rear, and co-planar with the ring, as well as two out-of-plane sites, top and bottom (Figure 2.23). As established by ab-initio investigations, the anion forms a favorable association with the C^2–H in both the co-planar front and out-of-plane top positions of $[C_nC_1Im]X$ ILs.[72]

The cation-anion interaction energies of the ILs given below were computed, as illustrated in Figure 2.24. A higher interaction energy indicates a stronger cation-anion interaction. The absolute value of the cation-anion interaction energy for the various IL systems exhibits the following trend: [Bmim][$MeSO_4$] (391.19 kJ/mol) > [Bmim][BF_4] (370.19 kJ/mol) > [Bmim][PF_6] (349.19 kJ/mol).

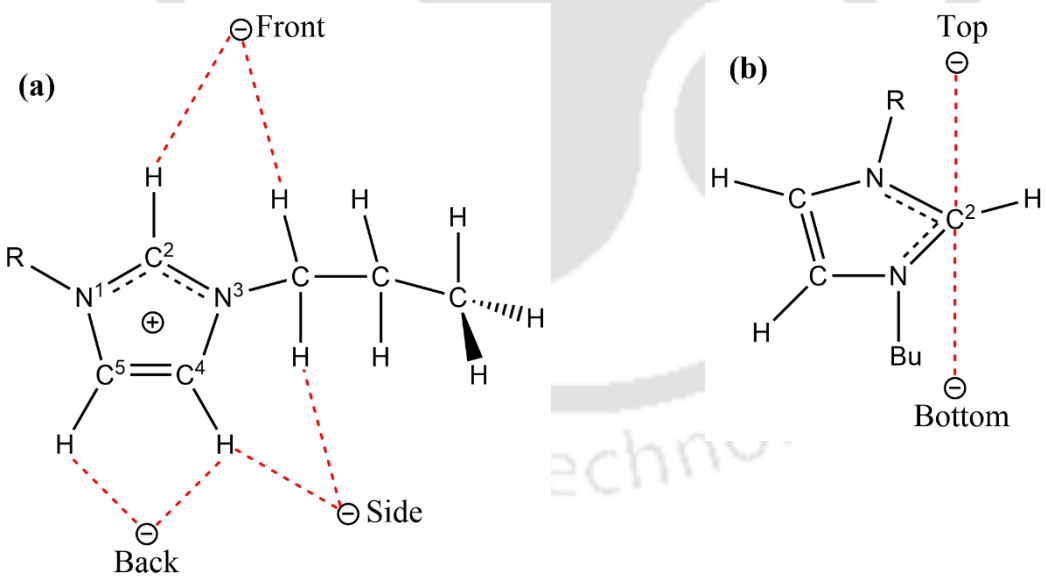

Figure 2.23: Possible anion positions around the $[C_4C_1Im]^+$ cation. (a) co-planar, and (b) out-of-plane anion interaction sites

2.13.2. Effect of Anion Type on Cation-Anion Interactions and Basicity of ILs

To acquire a greater comprehension of the anion's effect on the cation-anion interaction, the hydrogen-bonding interactions between different anions and cations were further investigated. The hydrogen bonding criteria defined by Popelier under the AIM theoretical framework were also used to distinguish existing H-bond interactions within a cation-anion pair.[73] As a result, it was observed that the $[Bmim]^+$ cation and the methylsulfate anion formed four hydrogen bonds in the $[Bmim][MeSO_4]$ ion pair (Table 2.7). The most significant bond exists between the cation's most acidic H atom, H_7, and the O in the anion, O_{29}. The rest of the interactions occur between the top methyl and lower butyl chain of the cation with the electron-withdrawing O atoms in the anionic moiety ($H_{11}\cdots O_{29}$, $H_{18}\cdots O_{27}$, $H_{14}\cdots O_{27}$). The presence of lone pair on the terminal oxygens of methylsulfate anion results in larger interactions with the cationic $[Bmim]^+$ moiety. Similarly, on the basis of H-bonding interactions occurring in the IL systems investigated between cations and anions, four H-bonds can be found in the other two IL systems. Compared to the $[Bmim][MeSO_4]$ IL, the latter two possess weaker H-bond interactions. The charge density at each hydrogen bond's bond critical point (BCP), ρ_c, was determined to assess the strength of the cation-anion hydrogen bonding interaction in the distinct ion pairs. The sum of the hydrogen bonds in $[Bmim][MeSO_4]$ is 0.0696, whereas the sums of the hydrogen bonds in $[Bmim][BF_4]$ and $[Bmim][PF_6]$ are 0.0585 and 0.0579, respectively.[74,75] With the understanding that a larger value for ρ_c indicates a stronger interaction, this result implies that the strength of the hydrogen-bonding interactions between the ion pair in the various imidazolium-based ILs is as follows: $[Bmim][MeSO_4]$ > $[Bmim][BF_4]$> $[Bmim][PF_6]$. The stronger hydrogen bonding interaction in ILs is consistent with the order of the overall cation-anion interaction strength, suggesting that the weaker interaction stems from the weak interatomic distances.[76]

Table 2.7: Bond Distances and Atoms in molecules (AIM) Parameters of ILs

			AIM parameters	
ILs	Bond	Distance (Å)	ρ_c	Sum of ρ_c
[Bmim][BF_4]	$H_7\cdots F_{29}$	1.914	0.0256	
	$H_{11}\cdots F_{27}$	2.224	0.0135	0.0585
	$H_{18}\cdots F_{29}$	2.372	0.0093	
	$H_{14}\cdots F_{30}$	2.341	0.0101	
[Bmim][$MeSO_4$]	$H_{11}\cdots O_{29}$	2.207	0.0161	
	$H_7\cdots O_{29}$	1.813	0.0298	0.0696
	$H_{18}\cdots O_{27}$	2.377	0.0124	
	$H_{14}\cdots O_{27}$	2.558	0.0113	
[Bmim][PF_6]	$H_{11}\cdots F_{31}$	2.273	0.0121	
	$H_7\cdots F_{32}$	1.943	0.0235	0.0579
	$H_{14}\cdots F_{28}$	2.350	0.0111	
	$H_{18}\cdots F_{32}$	2.320	0.0112	

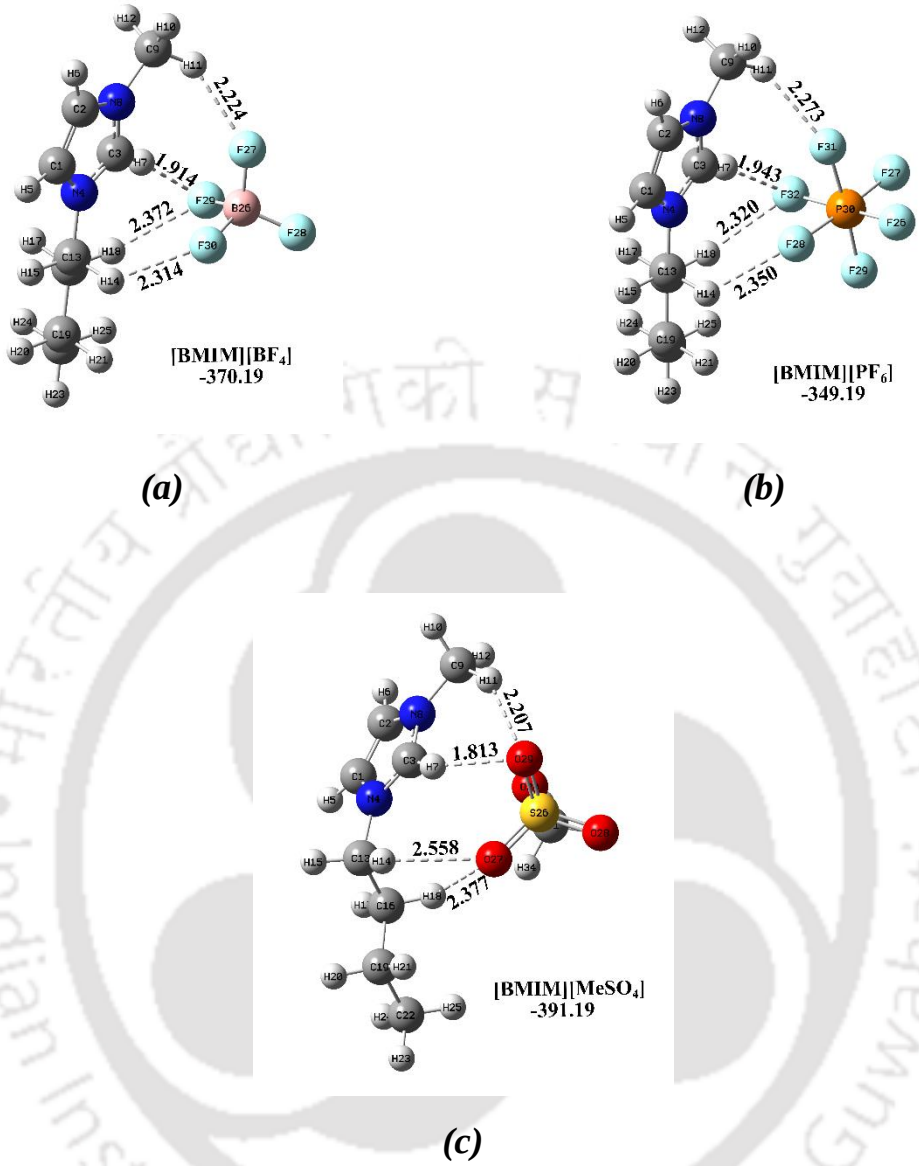

Figure 2.24: Optimized geometries of ILs at the DFT-D3(BJ)/B3LYP/6-311++G(d,p) level of theory. The interatomic distances mentioned are in angstroms (Å). The values under the abbreviations are the BSSE-corrected interaction energies between the cation and anions of the respective ILs (kJ/mol).

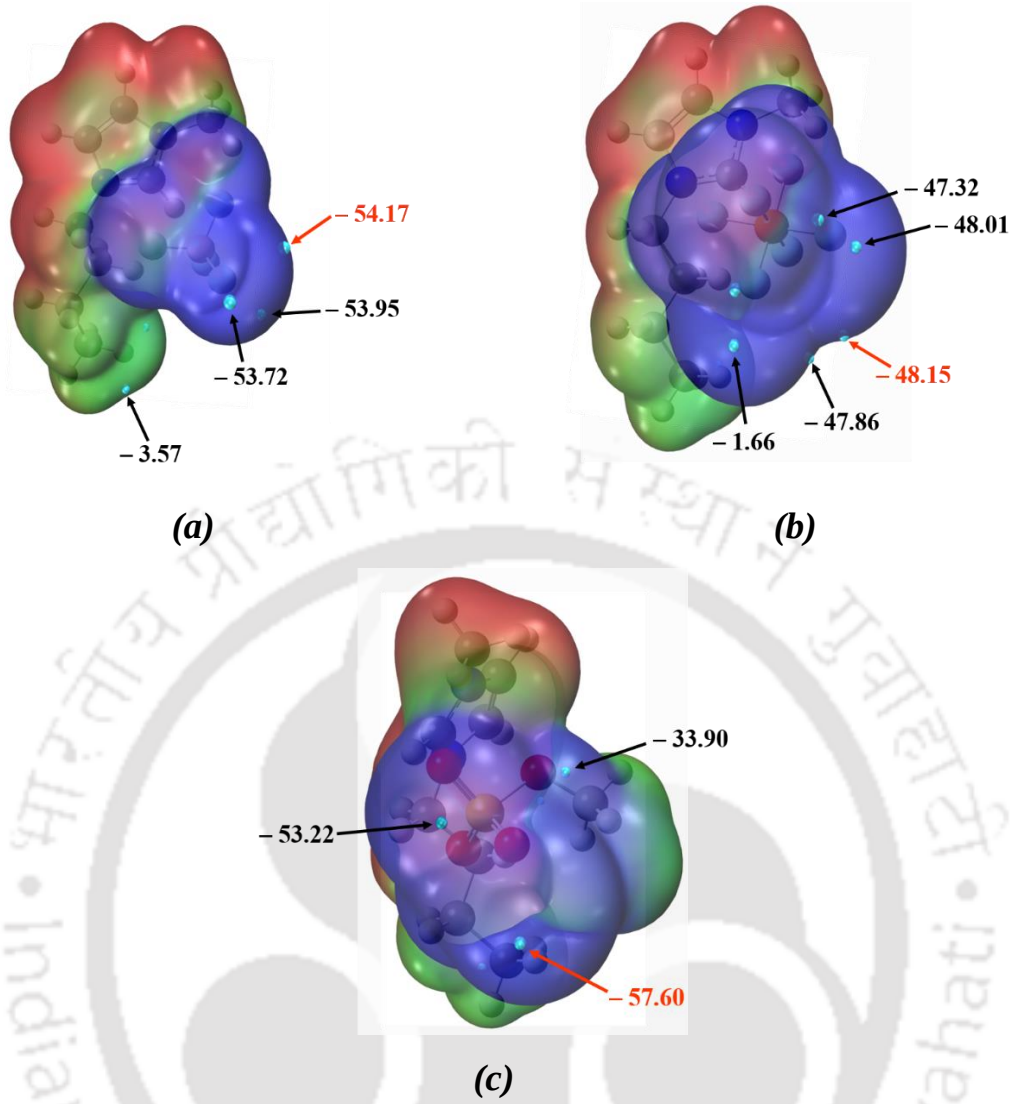

Figure 2.25: Computed electrostatic potential at the isodensity contour (0.001 au) surface of ILs. The position of $V_{s,min}$ is denoted by a red pointer. The values of $V_{s,min}$ are in (kcal/mol)

Electrostatic interactions are critical in intermolecular cation-anion interactions. The basicity of a molecule is governed mainly by its potential to form electrostatic interactions with other acidic moieties within the molecule. The most-negative-surface electrostatic potential ($V_{s,min}$) of the studied molecule is an effective criterion for deciphering and anticipating the electrostatically reactive ability of molecules at the microscopic level.[77,78] The electrostatic surface is defined as the 0.001 au isosurface of electron density, as proposed by Bader.[48] The negative sign of $V_{s,min}$ indicates an attractive interaction with a positive charge, and a larger magnitude of $V_{s,min}$ signifies a more strong interaction. As a result, the surface electrostatic

potentials of the various ILs depicted in Figure 2.25 were investigated, and the $V_{s,min}$ values for each IL were determined. As illustrated in Figure 2.25, the cation type has no discernible effect on the locations of the $V_{s,min}$ of the three studied IL systems. The $V_{s,min}$ sites are clustered around the oxygen and fluorine atoms in the anions, which is rooted in the idea that the basicity of ILs is often acquired from the anions. However, it is intriguing to note that when anion types vary, the corresponding magnitudes of $V_{s,min}$ are dramatically different. For imidazolium cation-containing ILs, the absolute value of $V_{s,min}$ for [Bmim][PF_6] is 48.15 kcal/mol, which is less than that of [Bmim][BF_4] (54.17 kcal/mol); the absolute value of $V_{s,min}$ for [Bmim][$MeSO_4$] is the highest of the three (57.60 kcal/mol).

2.13.3. Interaction of Chemical Hydrides with Anionic Moiety of ILs

As we have only assessed the effect of anions in the dehydrogenation of chemical hydrides, the quantum chemical calculation in the stemming section is only dedicated to the anionic moiety of the studied IL systems and chemical hydrides. In the next instance, a quantum chemical-based, dispersion corrected density functional theory (DFT-D3(BJ)) calculation at the B3LYP/6-311++G(d,p) level was performed to compare the interaction between chemical hydrides (AB and EDAB both) and active sites in [BF_4^-], [PF_6^-], and [$MeSO_4^-$] anions.[43] As illustrated in Figures 2.26 (a) and (b), the distance between the protic H atom attached to the NH_3 moiety in the nearest hydride molecules and the negatively charged F atoms in [BF_4^-] anion was anticipated to be 2.231 and 2.230, respectively. These interatomic distances suggest that the F···H contact played a significant role in thermal dehydrogenation by [BF_4^-] anion-based IL, which is consistent with prior results.[69] Similar results for [PF_6^-] anion are obtained by the optimized structures of [AB].[PF_6^-], where the F···H distance predicts to be 2.234 Å for both the interacting fluorine atoms. As for [$MeSO_4^-$]·AB (Figure 2.26 (c)), the distances between the positive charged H of the NH_3 moiety in the closest AB molecule and the O atoms in the [$MeSO_4^-$] anion were predicted as 2.012 Å, respectively, which were much shorter than

the corresponding distances in $[BF_4^-]$·AB and $[PF_6^-]$·AB. These results suggested the stronger interactions in $[MeSO_4^-]$·AB and conjectured that the O atom was the primary interaction site in the anion. The calculations were also performed by coupling the same anions with another chemical hydride, EDAB. This set of quantum chemical calculations elucidated the same trend as observed in the earlier case of AB with a similar set of anions. The optimized structures of EDAB with a different set of anions are illustrated below (Figure 2.27). The trends obtained are in accordance with the results of AB with $[BF_4^-]$, $[PF_6^-]$, and $[MeSO_4^-]$ anions. The higher basicity of $[MeSO_4^-]$ anion in comparison to the other studied anions provides the chemical hydrides to interact with multiple O atoms present in the structure. These stronger interatomic H-bond interactions between the $[MeSO_4^-]$ anion-based ILs with AB and EDAB present it as a better catalytic cum solvent for the dehydrogenation process in comparison to the latter two IL systems ($[BF_4^-]$, and $[PF_6^-]$). With shorter intermolecular distances between AB/EDAB and $[MeSO_4^-]$ anions (cf. Figure 2.26(c) and 2.27(c)), the dehydrogenation of the chemical hydrides propagates with N–H activation and interacts with the anion. This weakens B–N bonds, which subsidizes the formation of ionic species diammoniate of diborane [DADB], which is the rate governing step in the dehydrogenation reaction and initiates the hydrogen release.[78]

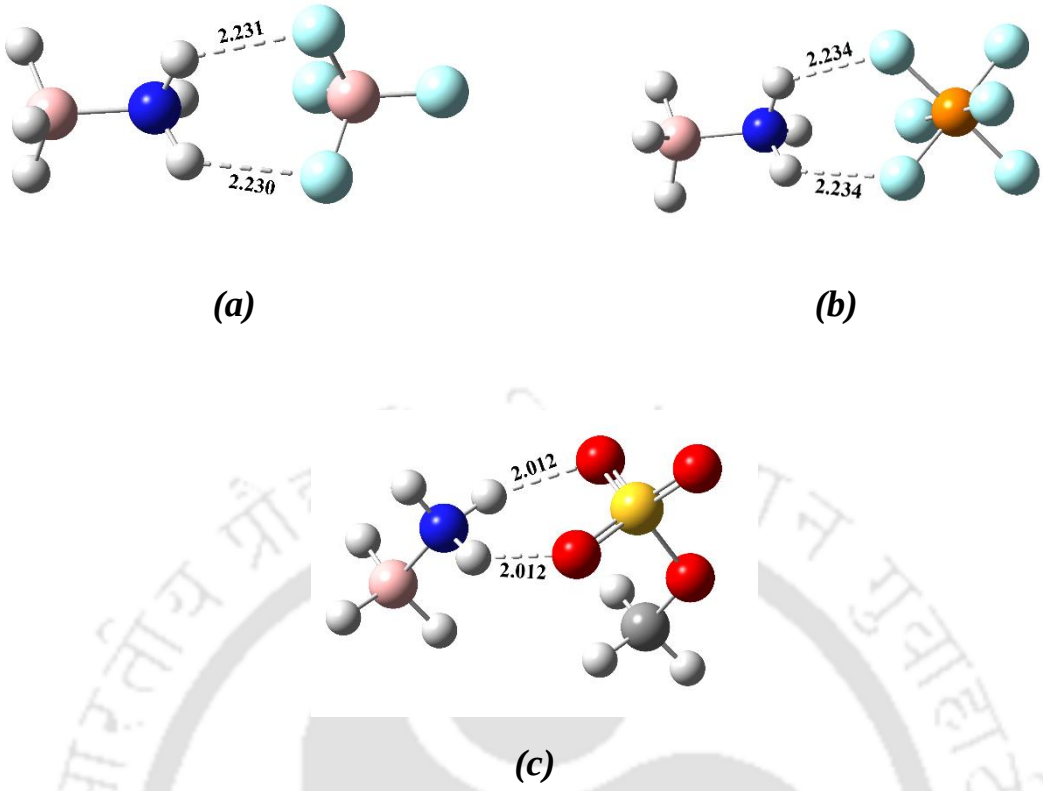

(a) ***(b)***

(c)

Figure 2.26: Optimized geometries at DFT-D3(BJ)/B3LYP/6-311++G(d,p) level of theory: (a) AB-[BF_4^-], (b) AB-[PF_6^-], and (c) AB-[$MeSO_4^-$]. The distance mentioned are in angstroms (Å).

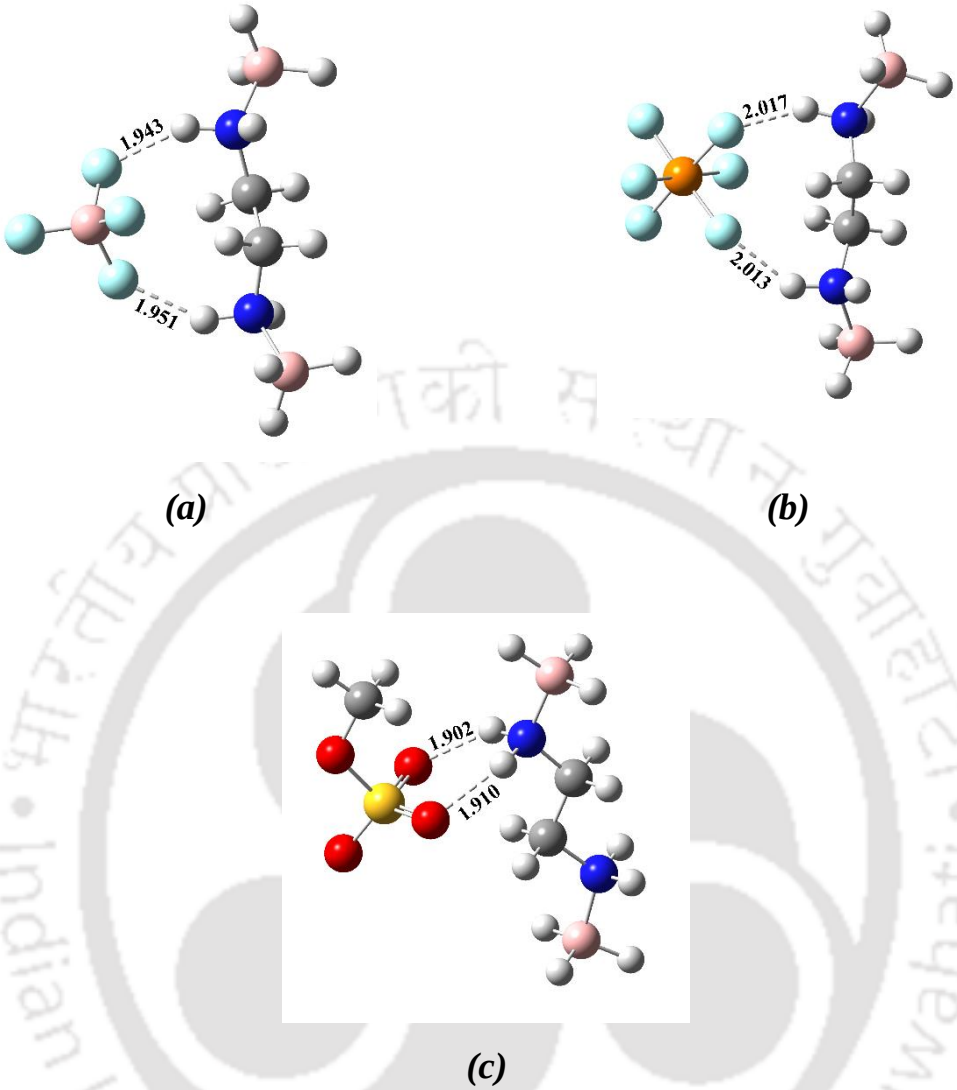

Figure 2.27: Optimized geometries at DFT-D3(BJ)/B3LYP/6-311++G(d,p) level of theory: (a) EDAB-[BF_4^-], (b) EDAB-[PF_6^-], and (c) EDAB-[$MeSO_4^-$]. The distance mentioned are in angstroms (Å).

Additionally, to examine the interactions between chemical hydrides and various anions such as [BF_4^-], [PF_6^-], and [$MeSO_4^-$], the Gaussian 16 package was used to determine the natural bond orbital (NBO) relative charge distribution of several active atoms in these anions.[79,50] To deeply investigate the charge redistribution of chemical hydrides and ILs upon mixing, we employed atomic charge to measure the electron variation on atoms, an intuitive representation of charge distribution in chemical systems. Atomic charge analysis using natural

bond orbital (NBO) charges has been demonstrated to be a reliable and appropriate method for studying charge distribution and transfer. Table A3-A8 (Appendix A) provides comprehensive data on the charge variation during the dehydrogenation process. This approach highlighted the ILs' components that are particularly involved in their interaction with a target chemical hydride and aided in evaluating the significance of these interactions. As can be seen from Figure 2.28 (a, and b), the electron-withdrawing fluorine atoms shared equal negative charge on the [BF_4^-], and [PF_6^-] anions, and consist of a positive atom in the centre. Whereas in the case of [$MeSO_4^-$] anion, the tertiary O atoms comprise of higher electron density (e^-), which reduces while moving towards anionic centre. For example, the NBO charges of the O atoms in [$MeSO_4^-$] were −0.987 and −0.966, whereas those in centre O atoms were decreased to both −0.768 (Figure 2.28 (c)). This is the reason for the interaction of tertiary higher electronegative O atoms with the protic NH_3 moiety in the hydrides.

While interacting with the chemical hydrides, it was observed that the interactions of anions or ILs with chemical hydrides result in complete disruption of the charge transfer process occurring within an initial IL cluster. The anionic moiety of the IL act as an active barrier for the charge transfer process between IL and the chemical hydrides (AB and EDAB). In one of our previous studies, we predicted that the closer the anion is to the hydride molecule, the greater the loss of electron density from the ILs to chemical hydrides.[63] The same charge transfer (CT) process can be intuited in our present study, where the charge transfer between the anionic species of ILs and chemical hydrides have been assessed, and similar trends are obtained. The shorter intermolecular distances between the anionic moiety and the chemical hydrides contribute to the greater loss of electron density from the anionic moiety of the ILs that is observed. In our present study, the shorter intermolecular distances between [$MeSO_4^-$] anion and chemical hydrides result in a higher loss of electron density from the anionic part of the IL. This charge transfer process occurs by weakening the interaction between the cation

and anion of the ILs, resulting in an increased number of anion-hydride interactions. The presence of electron-donating O atoms in [$MeSO_4^-$] anion, which provides the chemical hydrides with multiple interacting basic sites, can be attributed to the higher hydrogen bond basicity (β) of the particular IL.[30,24,31]

On the other hand, the fluorine-based anions consist of electron-withdrawing fluorine atoms that possess lower hydrogen bond basicity (β) and result in weaker intermolecular interactions between the anions and chemical hydrides. The strong and weak intermolecular distances between the studied anionic-hydride systems are directly proportional to the extent of charge transfer between the hydride and IL systems. It was observed (Table A1-Table A8, Appendix A) that in the presence of [$MeSO_4^-$] anions, chemical hydrides (AB and EDAB) gain a considerable amount of electron density, in comparison to other two counterpart anion systems, [BF_4^-], and [PF_6^-], respectively. The correlation of hydrogen bond basicity with the extent of charge transfer can be related to the presence of imidazolium-based ILs. The earlier predicted correlations were different in the reported studies where an anion comprised of higher hydrogen bond basicity coupled with ammonium and pyrrolidinium cations. The system failed to produce the exact correlation. A NBO charge analysis revealed that chemical hydrides dramatically alter charge transfer and interactions between their constituents in a nuanced manner that relies on the choice of anions when mated with imidazolium-based cations in ILs.

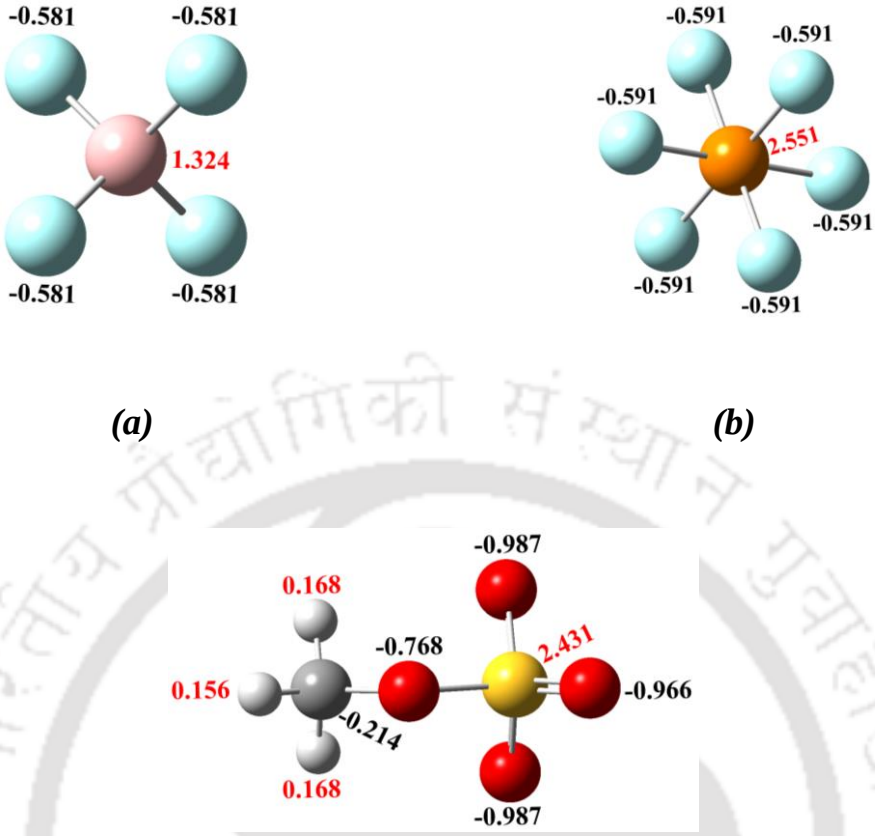

Figure 2.28: NBO charges on anions (a) [BF_4^-] anion, (b) [PF_6^-] anion, and (c) [$MeSO_4^-$] anion

2.14. Conclusions

A comparative study about the thermal decomposition of ammonia borane (AB) and ethylene diamine bisborane (EDAB) was conducted with methyl carbonate anion-based ILs at 95°C and 105°C. From the COSMO-SAC-based study, two ILs, namely 1-butyl-1-methylpyrrolidinium methyl carbonate [Bmpyr][CH_3CO_3] and Tributylmethyl ammonium methyl carbonate [TBMA][CH_3CO_3], were selected for the dehydrogenation experiment of chemical hydrides. The hydrogen released from AB/[TBMA][CH_3CO_3] (1.46 equivalents) and EDAB/[TBMA][CH_3CO_3] (3.50 equivalents) mixtures were subsequently higher in comparison to the other AB/EDAB-IL mixtures studied. Confirmation of IL as catalytic solvent was determined by ^{1}H NMR.

In comparison to ammonium and pyrrolidinium-based ionic liquids, imidazolium-based ionic liquids are the most extensively employed. This performance of imidazolium-based ILs is due to the presence of the carbene cation, which stabilizes the ionic complexes and has a significant effect on hydrogen yield when paired with basic anions. In the absence of imidazolium cations, the same action is absent.[22] The usage of ammonium and pyrrolidinium-based ILs provides a significant catalytic media for the thermal dehydrogenation of chemical hydrides. Despite lower equivalents of hydrogen release, the reported ILs proved to be an impressive replacement in comparison to the solid-state hydrogen release. Quantum chemical calculations revealed the electronic structural entity of the IL-chemical hydrides complex systems. HOMO-LUMO analysis was in good agreement with the experimental and theoretical predictions.

In the ensuing section, imidazolium-based ILs mediated thermal dehydrogenation of AB and EDAB was carried out in a high vacuum glass experimental setup at 100°C. A comparative analysis was conducted for the thermal decomposition of AB and EDAB in the

presence of three ILs different from their anions. The methylsulfate anion-based ILs [Bmim][$MeSO_4$] performed the best in this study, leading to increased reaction rates and yields. AB/[Bmim][$MeSO_4$] and EDAB/[Bmim][$MeSO_4$] released 2.18 and 3.66 equivalents of hydrogen with a negligible induction period. The solubility of chemical hydrides in ILs can be correlated to their higher β-value, resulting in higher hydrogen release. The catalytic effect of ILs is explained by their ability to stabilize ionic intermediates produced during the dehydrogenation of amine borane and further enhance hydrogen release by shortening the induction period.

The influence of basicity on anions was studied using cation-anion interactions and the cation-tethered approach. Atom in molecules (AIM) analysis was employed to distinguish the cation-anion hydrogen bonds in ILs. The most negative surface electrostatic potential ($V_{s,min}$), an efficient parameter that helps decipher the electrostatic reactivity, was employed. From the obtained ($V_{s,min}$) values, it can be predicted that the basicity of ILs emerges out from the anionic moieties. The higher negative ($V_{s,min}$) values simultaneously indicate an attractive interaction towards a positive charge and a stronger interaction.

Overall it is observed that the ILs have limited applicability in large-scale catalytic processes due to their higher cost. Deep Eutectic Solvents(DES) are known as the alternatives to ILs, which are more economical, and some of them are non-toxic. These neoteric solvents have the ability to perform the functions of ILs in a range of applications. The following chapter will examine the mechanism involved in the formation of these novel solvents.

References

(1) Poizot, P.; Dolhem, F. Clean Energy New Deal for a Sustainable World: From Non-CO2 Generating Energy Sources to Greener Electrochemical Storage Devices. *Energy and Environmental Science*. 2011. https://doi.org/10.1039/c0ee00731e.

(2) Eberle, U.; Felderhoff, M.; Schüth, F. Chemical and Physical Solutions for Hydrogen Storage. *Angew. Chemie - Int. Ed.* **2009**, *48* (36), 6608–6630. https://doi.org/10.1002/anie.200806293.

(3) Schlapbach, L.; Züttel, A. Hydrogen-Storage Materials for Mobile Applications. *Nature* **2001**, *414* (6861), 353–358. https://doi.org/10.1038/35104634.

(4) Rowsell, J. L. C.; Yaghi, O. M. Strategies for Hydrogen Storage in Metal-Organic Frameworks. *Angew. Chemie - Int. Ed.* **2005**, *44* (30), 4670–4679. https://doi.org/10.1002/anie.200462786.

(5) Hamilton, C. W.; Baker, R. T.; Staubitz, A.; Manners, I. B-N Compounds for Chemical Hydrogen Storage. *Chem. Soc. Rev.* **2009**, *38* (1), 279–293. https://doi.org/10.1039/b800312m.

(6) Stephens, F. H.; Pons, V.; Tom Baker, R. Ammonia–borane: The Hydrogen Source Par Excellence? *J. Chem. Soc. Dalt. Trans.* **2007**, No. 25, 2613–2626. https://doi.org/10.1039/b703053c.

(7) Kelly, H. C.; Edwards, J. O. Ethane 1,2-Diamineborane. *J. Am. Chem. Soc.* **1960**, *82* (18), 4842–4846. https://doi.org/10.1021/ja01503a023.

(8) Neiner, D. .; Karkamkar, A. .; Bowden, M. .; Joon Choi, Y. .; Luedtke, A. .; Holladay, J. .; Fisher, A. .; Szymczak, N. .; Autrey, T. . Kinetic and Thermodynamic Investigation of Hydrogen Release from Ethane 1,2-Di-Amineborane. *Energy Environ. Sci.* **2011**, *4* (10), 4187–4193. https://doi.org/10.1039/c1ee01884a.

(9) Leardini, F.; Valero-Pedraza, M. J.; Perez-Mayoral, E.; Cantelli, R.; Bañares, M. A. Thermolytic Decomposition of Ethane 1,2-Diamineborane Investigated by Thermoanalytical Methods and in Situ Vibrational Spectroscopy. *J. Phys. Chem. C* **2014**, *118* (31), 17221–17230. https://doi.org/10.1021/jp501964r.

(10) Biniwale, R. B.; Rayalu, S.; Devotta, S.; Ichikawa, M. Chemical Hydrides: A Solution to High Capacity Hydrogen Storage and Supply. *Int. J. Hydrogen Energy* **2008**, *33* (1),

360–365. https://doi.org/10.1016/j.ijhydene.2007.07.028.

(11) Karkamkar, A.; Aardahl, C.; Autrey, T. *Recent Developments on Hydrogen Release from Ammonia-Borane*; 2007. https://doi.org/10.1016/B978-0-12-385142-0.00015-5.

(12) Joglekar, H. G.; Rahman, I.; Kulkarni, B. D. The Path Ahead for Ionic Liquids. *Chem. Eng. Technol.* **2007**, *30* (7), 819–828. https://doi.org/10.1002/ceat.200600287.

(13) Taylor, A. W.; Lovelock, K. R. J.; Deyko, A.; Licence, P.; Jones, R. G. High Vacuum Distillation of Ionic Liquids and Separation of Ionic Liquid Mixtures. *Phys. Chem. Chem. Phys.* **2010**. https://doi.org/10.1039/b920931j.

(14) Hallett, J. P.; Welton, T. Room-Temperature Ionic Liquids: Solvents for Synthesis and Catalysis. 2. *Chem. Rev.* **2011**, *111* (5), 3508–3576. https://doi.org/10.1021/cr1003248.

(15) Endres, F. Physical Chemistry of Ionic Liquids. *Phys. Chem. Chem. Phys.* **2010**, *12* (8), 1648–1648. https://doi.org/10.1039/c001176m.

(16) Petkovic, M.; Ferguson, J.; Bohn, A.; Trindade, J.; Martins, I.; Carvalho, M. B.; Leitão, M. C.; Rodrigues, C.; Garcia, H.; Ferreira, R.; et al. Exploring Fungal Activity in the Presence of Ionic Liquids. *Green Chem.* **2009**. https://doi.org/10.1039/b823225c.

(17) Endres, F. Ionic Liquids: Solvents for the Electrodeposition of Metals and Semiconductors. *ChemPhysChem*. 2002. https://doi.org/10.1002/1439-7641(20020215)3:2<144::aid-cphc144>3.0.co;2-%23.

(18) Himmelberger, D. W.; Alden, L. R.; Bluhm, M. E.; Sneddon, L. G. Ammonia Borane Hydrogen Release in Ionic Liquids. *Inorg. Chem.* **2009**, *48* (20), 9883–9889. https://doi.org/10.1021/ic901560h.

(19) Bluhm, M. E.; Bradley, M. G.; Butterick, R.; Kusari, U.; Sneddon, L. G. Amineborane-Based Chemical Hydrogen Storage: Enhanced Ammonia Borane Dehydrogenation in Ionic Liquids. *J. Am. Chem. Soc.* **2006**, *128* (24), 7748–7749. https://doi.org/10.1021/ja062085v.

(20) Basu, S.; Zheng, Y.; Gore, J. P. An Experimental Study of Neat and Ionic Liquid-Aided Ammonia Borane Thermolysis. *J. Power Sources* **2011**, *196* (2), 734–740. https://doi.org/10.1016/j.jpowsour.2010.07.085.

(21) Banerjee, B.; Kundu, D.; Pugazhenthi, G.; Banerjee, T. Quantum Chemical and

Experimental Insights for the Ionic Liquid Facilitated Thermal Dehydrogenation of Ethylene Diamine Bisborane. *RSC Adv.* **2015**, *5* (104), 85280–85290. https://doi.org/10.1039/c5ra10625g.

(22) Sahler, S.; Konnerth, H.; Knoblauch, N.; Prechtl, M. H. G. Hydrogen Storage in Amine Boranes: Ionic Liquid Supported Thermal Dehydrogenation of Ethylene Diamine Bisborane. *Int. J. Hydrogen Energy* **2013**, *38* (8), 3283–3290. https://doi.org/10.1016/j.ijhydene.2012.12.150.

(23) Ab Rani, M. A.; Brant, A.; Crowhurst, L.; Dolan, A.; Lui, M.; Hassan, N. H.; Hallett, J. P.; Hunt, P. A.; Niedermeyer, H.; Perez-Arlandis, J. M.; et al. Understanding the Polarity of Ionic Liquids. *Phys. Chem. Chem. Phys.* **2011**. https://doi.org/10.1039/c1cp21262a.

(24) Cláudio, A. F. M.; Swift, L.; Hallett, J. P.; Welton, T.; Coutinho, J. A. P.; Freire, M. G. Extended Scale for the Hydrogen-Bond Basicity of Ionic Liquids. *Phys. Chem. Chem. Phys.* **2014**. https://doi.org/10.1039/c3cp55285c.

(25) Hunt, P. A.; Ashworth, C. R.; Matthews, R. P. Hydrogen Bonding in Ionic Liquids. *Chemical Society Reviews*. 2015. https://doi.org/10.1039/c4cs00278d.

(26) Papović, S.; Vraneš, M.; Tot, A.; Szilágyi, I.; Katana, B.; Alenezi, K.; Gadžurić, S. Physicochemical Investigations of a Binary Mixture Containing Ionic Liquid 1-Butyl-1-Methylpyrrolidinium Bis(Trifluoromethylsulfonyl)Imide and Diethyl Carbonate. *J. Chem. Eng. Data* **2020**. https://doi.org/10.1021/acs.jced.9b00738.

(27) Kundu, D.; Banerjee, B.; Pugazhenthi, G.; Banerjee, T. Reactive Insights into the Selective Dehydrogenation of Ethylene Diamine Bisborane Facilitated by Phosphonium Based Ionic Liquids. *Int. J. Hydrogen Energy* **2017**. https://doi.org/10.1016/j.ijhydene.2016.09.215.

(28) Fraser, K. J.; MacFarlane, D. R. Phosphonium-Based Ionic Liquids: An Overview. *Australian Journal of Chemistry*. 2009. https://doi.org/10.1071/CH08558.

(29) Papadopoulou, A. A.; Tzani, A.; Alivertis, D.; Katsoura, M. H.; Polydera, A. C.; Detsi, A.; Stamatis, H. Hydroxyl Ammonium Ionic Liquids as Media for Biocatalytic Oxidations. In *Green Chemistry*; 2016. https://doi.org/10.1039/c5gc02381e.

(30) Passos, H.; Dinis, T. B. V.; Cláudio, A. F. M.; Freire, M. G.; Coutinho, J. A. P. Hydrogen Bond Basicity of Ionic Liquids and Molar Entropy of Hydration of Salts as Major

Descriptors in the Formation of Aqueous Biphasic Systems. *Phys. Chem. Chem. Phys.* **2018**. https://doi.org/10.1039/c8cp01401a.

(31) Palgunadi, J.; Hong, S. Y.; Lee, J. K.; Lee, H.; Lee, S. D.; Cheong, M.; Kim, H. S. Correlation between Hydrogen Bond Basicity and Acetylene Solubility in Room Temperature Ionic Liquids. *J. Phys. Chem. B* **2011**. https://doi.org/10.1021/jp108351f.

(32) Yang, Q.; Xu, D.; Zhang, J.; Zhu, Y.; Zhang, Z.; Qian, C.; Ren, Q.; Xing, H. Long-Chain Fatty Acid-Based Phosphonium Ionic Liquids with Strong Hydrogen-Bond Basicity and Good Lipophilicity: Synthesis, Characterization, and Application in Extraction. *ACS Sustain. Chem. Eng.* **2015**. https://doi.org/10.1021/sc5006796.

(33) Klamt, A. Conductor-like Screening Model for Real Solvents: A New Approach to the Quantitative Calculation of Solvation Phenomena. *J. Phys. Chem.* **1995**, *99* (7), 2224–2235. https://doi.org/10.1021/j100007a062.

(34) Dennington, R.; Keith, T.; Millam, J. GaussView, Version 5. *Semichem Inc. Shawnee Mission. KS* **2009**.

(35) Frisch, M. J.; Trucks, G. W.; Schlegel, H. B.; Scuseria, G. E.; Robb, M. A.; Cheeseman, J. R.; Scalmani, G.; Barone, V.; Mennucci, B.; Petersson, G. A.; et al. Gaussian09 Revision D.01, Gaussian Inc. Wallingford CT. *Gaussian 09 Revision C.01*. 2010.

(36) Becke, A. B3LYP. *J. Chem. Phys.* **1993**.

(37) Gerber, R. P.; Soares, R. D. P. Prediction of Infinite-Dilution Activity Coefficients Using UNIFAC and COSMO-SAC Variants. *Ind. Eng. Chem. Res.* **2010**, *49* (16), 7488–7496. https://doi.org/10.1021/ie901947m.

(38) Hsieh, C. M.; Sandler, S. I.; Lin, S. T. Improvements of COSMO-SAC for Vapor-Liquid and Liquid-Liquid Equilibrium Predictions. *Fluid Phase Equilib.* **2010**, *297* (1), 90–97. https://doi.org/10.1016/j.fluid.2010.06.011.

(39) Kundu, D.; Chakma, S.; Pugazhenthi, G.; Banerjee, T. Ionic Liquid Facilitated Dehydrogenation of Tert-Butylamine Borane. *ACS Omega* **2018**. https://doi.org/10.1021/acsomega.7b01781.

(40) Zhao, Y.; Truhlar, D. G. The M06 Suite of Density Functionals for Main Group Thermochemistry, Thermochemical Kinetics, Noncovalent Interactions, Excited States, and Transition Elements: Two New Functionals and Systematic Testing of Four M06-

Class Functionals and 12 Other Function. *Theor. Chem. Acc.* **2008**. https://doi.org/10.1007/s00214-007-0310-x.

(41) Fukui, K. Theory of Orientation and Stereoselection. In *Orientation and Stereoselection*; Springer, 1970; pp 1–85.

(42) Lee, C.; Yang, W.; Parr, R. G. Development of the Colle-Salvetti Correlation-Energy Formula into a Functional of the Electron Density. *Phys. Rev. B* **1988**. https://doi.org/10.1103/PhysRevB.37.785.

(43) Tsuzuki, S.; Uchimaru, T. Accuracy of Intermolecular Interaction Energies, Particularly Those of Hetero-Atom Containing Molecules Obtained by DFT Calculations with Grimme's D2, D3 and D3BJ Dispersion Corrections. *Phys. Chem. Chem. Phys.* **2020**. https://doi.org/10.1039/d0cp03679j.

(44) Todorova, T. K.; Schreiber, M. W.; Fontecave, M. Thermochemistry in Gaussian. *ACS Catal.* **2020**.

(45) Gutowski, M.; Van Duijneveldt-Van De Rijdt, J. G. C. M.; Van Lenthe, J. H.; Van Duijneveldt, F. B. Accuracy of the Boys and Bernardi Function Counterpoise Method. *J. Chem. Phys.* **1993**. https://doi.org/10.1063/1.465106.

(46) Bader, R. F. W. Atoms in Molecules. *Acc. Chem. Res.* **1985**, *18* (1), 9–15. https://doi.org/10.1021/ar00109a003.

(47) Lu, T.; Chen, F. Multiwfn: A Multifunctional Wavefunction Analyzer. *J. Comput. Chem.* **2012**, *33* (5), 580–592. https://doi.org/10.1002/jcc.22885.

(48) Bader, R. F. W.; Carroll, M. T.; Cheeseman, J. R.; Chang, C. Properties of Atoms in Molecules: Atomic Volumes. *J. Am. Chem. Soc.* **1987**. https://doi.org/10.1021/ja00260a006.

(49) Humphrey, W.; Dalke, A.; Schulten, K. VMD: Visual Molecular Dynamics. *J. Mol. Graph.* **1996**. https://doi.org/10.1016/0263-7855(96)00018-5.

(50) Glendening, E. D.; Landis, C. R.; Weinhold, F. Natural Bond Orbital Methods. *Wiley Interdisciplinary Reviews: Computational Molecular Science*. 2012. https://doi.org/10.1002/wcms.51.

(51) Banerjee, B.; Pugazhenthi, G.; Banerjee, T. Experimental Insights into the Thermal

Dehydrogenation of Ethylene Diamine Bisborane Using Allyl-Based Ionic Liquids. *Energy and Fuels* **2017**, *31* (5), 5428–5440. https://doi.org/10.1021/acs.energyfuels.6b02823.

(52) Kundu, D.; Chakma, S.; Saikrishnan, S.; Pugazhenthi, G.; Banerjee, T. Molecular Modeling and Experimental Insights for the Dehydrogenation of Ethylene Diamine Bisborane Using Hydrogen Sulfate Based Ionic Liquid. *J. Ind. Eng. Chem.* **2019**. https://doi.org/10.1016/j.jiec.2018.11.010.

(53) Mishra, D. K.; Pugazhenthi, G.; Banerjee, T. Ionic Liquid-Based Deep Eutectic Solvents as Novel Solvent-Cum-Catalyst Media for Thermal Dehydrogenation of Chemical Hydrides. *Int. J. Hydrogen Energy* **2021**. https://doi.org/10.1016/j.ijhydene.2021.02.012.

(54) Banerjee, B.; Kundu, D.; Pugazhenthi, G.; Banerjee, T. Quantum Chemical and Experimental Insights for the Ionic Liquid Facilitated Thermal Dehydrogenation of Ethylene Diamine Bisborane. *RSC Adv.* **2015**, *5* (104), 85280–85290. https://doi.org/10.1039/c5ra10625g.

(55) Kundu, D.; Chakma, S.; Pugazhenthi, G.; Banerjee, T. Effect of Thiocyanate-Based Ionic Liquids on the Dehydrogenation of Amine Boranes: Experimental and Molecular Modeling Studies. *Asia-Pacific J. Chem. Eng.* **2019**. https://doi.org/10.1002/apj.2357.

(56) González, E. J.; Díaz, I.; Gonzalez-Miquel, M.; Rodríguez, M.; Sueiras, A. On the Behavior of Imidazolium versus Pyrrolidinium Ionic Liquids as Extractants of Phenolic Compounds from Water: Experimental and Computational Analysis. *Sep. Purif. Technol.* **2018**. https://doi.org/10.1016/j.seppur.2018.03.006.

(57) Confer, M. P.; DeSimone, A.; Burnham, H.; McLeod, W.; Klein, T. M.; Street, S. C.; Dixon, D. A. Solubility Thermodynamics of Amine Boranes in Polar Solvents. *Int. J. Hydrogen Energy* **2021**. https://doi.org/10.1016/j.ijhydene.2020.12.163.

(58) Kundu, D.; Pugazhenthi, G.; Banerjee, T. Low- To Room-Temperature Dehydrogenation of Dimethylamine Borane Facilitated by Ionic Liquids: Molecular Modeling and Experimental Studies. *Energy and Fuels* **2020**. https://doi.org/10.1021/acs.energyfuels.0c01896.

(59) Weiß, N.; Schmidt, C. H.; Thielemann, G.; Heid, E.; Schröder, C.; Spange, S. The

Physical Significance of the Kamlet-Taft: $\pi*$ Parameter of Ionic Liquids. *Phys. Chem. Chem. Phys.* **2021**. https://doi.org/10.1039/d0cp04989a.

(60) Crowhurst, L.; Falcone, R.; Lancaster, N. L.; Llopis-Mestre, V.; Welton, T. Using Kamlet-Taft Solvent Descriptors to Explain the Reactivity of Anionic Nucleophiles in Ionic Liquids. *J. Org. Chem.* **2006**. https://doi.org/10.1021/jo0615302.

(61) Niedermeyer, H.; Ashworth, C.; Brandt, A.; Welton, T.; Hunt, P. A. A Step towards the a Priori Design of Ionic Liquids. *Phys. Chem. Chem. Phys.* **2013**. https://doi.org/10.1039/c3cp50521a.

(62) Jessop, P. G.; Jessop, D. A.; Fu, D.; Phan, L. Solvatochromic Parameters for Solvents of Interest in Green Chemistry. *Green Chem.* **2012**. https://doi.org/10.1039/c2gc16670d.

(63) Mishra, D. K.; Banerjee, B.; Pugazhenthi, G.; Banerjee, T. Metal-Free, Ionic Liquid-Mediated Hydrogen Release from Amine Borane Complexes: An Experimental and Density Functional Theory Investigation. *Ind. Eng. Chem. Res.* **2021**, *60* (27), 9764–9776. https://doi.org/10.1021/acs.iecr.1c01507.

(64) Mishra, D. K.; Pugazhenthi, G.; Banerjee, T. Ionic Liquid-Based Deep Eutectic Solvent as Reaction Media for the Thermal Dehydrogenation of Ethylene Diamine- Bis -Borane . *ACS Sustain. Chem. Eng.* **2020**, *8* (12), 4910–4919. https://doi.org/10.1021/acssuschemeng.0c00220.

(65) Baek, C. S.; Lee, Y. J.; Lee, S. J.; Lee, S. G.; Kim, H. C.; Jeong, S. W. C2-Functionalized 1,3-Dialkylimidazolium Ionic Liquids for Efficient Cellulose Dissolution. *J. Mol. Liq.* **2017**. https://doi.org/10.1016/j.molliq.2017.03.086.

(66) Feroci, M.; Chiarotto, I.; Forte, G.; Vecchio Ciprioti, S.; Inesi, A. Stability and CO2 Capture Ability of Electrogenerated N-Heterocyclic Carbene in Parent 1-Butyl-3-Methylimidazoliun Ionic Liquid (BMIm-X): The Role of X-. *ChemElectroChem* **2014**. https://doi.org/10.1002/celc.201300269.

(67) Chen, X.; Bao, X.; Zhao, J. C.; Shore, S. G. Experimental and Computational Study of the Formation Mechanism of the Diammoniate of Diborane: The Role of Dihydrogen Bonds. *J. Am. Chem. Soc.* **2011**. https://doi.org/10.1021/ja203648w.

(68) Bowden, M.; Heldebrant, D. J.; Karkamkar, A.; Proffen, T.; Schenter, G. K.; Autrey, T. The Diammoniate of Diborane: Crystal Structure and Hydrogen Release. *Chem.*

Commun. **2010**. https://doi.org/10.1039/c0cc03249b.

(69) Rabideau, B. D.; Agarwal, A.; Ismail, A. E. The Role of the Cation in the Solvation of Cellulose by Imidazolium-Based Ionic Liquids. *J. Phys. Chem. B* **2014**. https://doi.org/10.1021/jp4115755.

(70) Banerjee, A.; Shah, J. K. Elucidating the Effect of the Ionic Liquid Type and Alkyl Chain Length on the Stability of Ionic Liquid-Iron Porphyrin Complexes. *J. Chem. Phys.* **2020**. https://doi.org/10.1063/5.0007815.

(71) Hunt, P. A. Quantum Chemical Modeling of Hydrogen Bonding in Ionic Liquids. *Topics in Current Chemistry*. 2017. https://doi.org/10.1007/s41061-017-0142-7.

(72) Matthews, R. P.; Ashworth, C.; Welton, T.; Hunt, P. A. The Impact of Anion Electronic Structure: Similarities and Differences in Imidazolium Based Ionic Liquids. *J. Phys. Condens. Matter* **2014**. https://doi.org/10.1088/0953-8984/26/28/284112.

(73) Zhang, Y.; Maginn, E. J. The Effect of C2 Substitution on Melting Point and Liquid Phase Dynamics of Imidazolium Based-Ionic Liquids: Insights from Molecular Dynamics Simulations. *Phys. Chem. Chem. Phys.* **2012**. https://doi.org/10.1039/c2cp41964e.

(74) Koch, U.; Popelier, P. L. A. Characterization of C-H-O Hydrogen Bonds on the Basis of the Charge Density. *J. Phys. Chem.* **1995**. https://doi.org/10.1021/j100024a016.

(75) Espinosa, E.; Alkorta, I.; Elguero, J.; Molins, E. From Weak to Strong Interactions: A Comprehensive Analysis of the Topological and Energetic Properties of the Electron Density Distribution Involving X-H···F-Y Systems. *J. Chem. Phys.* **2002**. https://doi.org/10.1063/1.1501133.

(76) Dhumal, N. R.; Kim, H. J.; Kiefer, J. Molecular Interactions in L-Ethyl-3-Methylimidazolium Acetate Ion Pair: A Density Functional Study. *J. Phys. Chem. A* **2009**. https://doi.org/10.1021/jp907394v.

(77) Devereux, M.; Popelier, P. L. A.; McLay, I. M. A Refined Model for Prediction of Hydrogen Bond Acidity and Basicity Parameters from Quantum Chemical Molecular Descriptors. *Phys. Chem. Chem. Phys.* **2009**. https://doi.org/10.1039/b816321a.

(78) Gao, P.; Huang, Z.; Yu, H. Exploration of the Dehydrogenation Pathways of Ammonia Diborane and Diammoniate of Diborane by Molecular Dynamics Simulations Using

Reactive Force Fields. *J. Phys. Chem. A* **2020**. https://doi.org/10.1021/acs.jpca.9b10441.

(79) Frisch, M. J.; Trucks, G. W.; Schlegel, H. B.; Scuseria, G. E.; Robb, M. A.; Cheeseman, J. R.; Scalmani, G.; Barone, V.; Petersson, G. A.; Nakatsuji, H.; et al. Gaussian 16, Rev. C.01. *Gaussian 16, Rev. C. 01*. 2016.

CHAPTER 3

Molecular and Spectroscopic Insights on a Metal Salt-Based Deep Eutectic Solvents: A Combined QTAIM, NCI and DFT Study

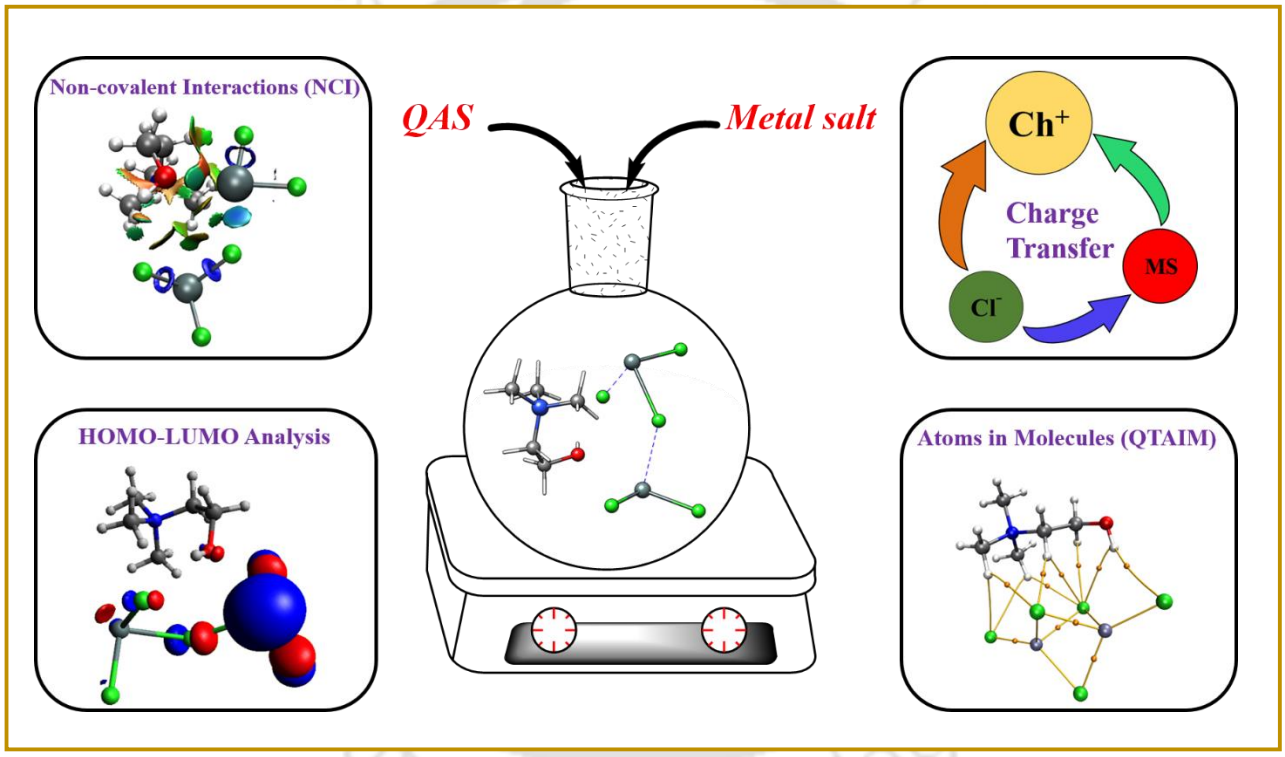

3.1. Chapter Abstract

Deep eutectic solvents based on metal halide salts are highly catalytic, low toxic, reusable, cost-effective, and have higher thermal stability than their analogue ionic liquids (ILs). In this work, we have reported the formation mechanism of metal salt-based Deep Eutectic Solvents (DESs) at the molecular level along with their charge transfer analysis and thermodynamics associated with its formation using density functional theory (DFT). The DES systems analyzed in the present work were Choline Chloride and Tin (II) Chloride (DES1) and Choline Chloride and Zinc (II) Chloride (DES2), both in a molar ratio of 1:2, respectively. An excellent correlation is obtained between the theoretically calculated IR spectra of the DES systems and the previously reported experimental findings for the formation of the complex systems. The DESs were found to be stable systems due to traditional hydrogen bonding and electrostatic interactions resulting in the ionic species $[Sn_2Cl_5]^-$ *and* $[Zn_2Cl_5]^-$*, and are elucidated with the help of electronic structure calculations. CHEPLG partial charge analysis and NBO analysis suggest a charge transfer from* Cl^- *(Chloride) to* Ch^+ *(Choline) and metal salts in the DESs structures. The atom-in-molecules (AIM) and non-covalent interactions (NCI) analysis suggest a strong electrostatic interaction within DES2 system as compared to DES1. Higher stability and reactivity is observed in DES2 system based on the frontier molecular orbital analysis. Our analysis offers important insights into the formation mechanism of these economic ionic liquid analogues.*

3.2. Introduction

The advent of Ionic Liquids (ILs) has revolutionized chemistry in the last two decades.[1,2] ILs are usually classified as compounds consisting of non-symmetric ions with low lattice energy making them liquid at an arbitrary threshold of 100°C. The ionic nature of ILs contributes to their desirable properties, such as high thermal stability, low vapor pressure, excellent chemical stability, and recyclability. [3-6] Recent developments in the field of green chemistry have unfortunately demonstrated significant toxicity and low biodegradability associated with several types of ILs.[7] Nevertheless, the high costs and purification related to the synthesis of ILs impede its application on a commercial scale. The drawbacks of the conventional ILs forced the researchers to develop a cheap and readily available solvent named Deep Eutectic Solvents (DESs). Deep eutectic solvents are the mixtures of quaternary ammonium salts (QAS) such as choline chloride mixed with a hydrogen bond donor (HBD) and form a low-temperature eutectic when mixed at a suitable molar ratio.[8,9] DES can be termed as a novel category of solvents that provides physicochemical properties suitable for various technical applications. Abbott et al. in the year 2003 reported the most popular mixture of quaternary ammonium salt and urea to be liquid at room temperature and had interesting solvent properties.[10] The interesting fact is the formation of DES that can form a eutectic mixture with a melting point well below that of the individual components and can be attributed to the charge transfer process resulting from the intermolecular hydrogen bonding.[11] The advantages of the neoteric solvents render them to replace the volatile organic solvents as well as conventional ILs in many applications such as electrochemistry, biomedical, extraction, catalytic solvent, etc. [12,13]

Several kinds of DESs incorporating different groups of hydrogen bond acceptors (HBAs) and hydrogen bond donors (HBDs) have been identified recently. Still, those based on choline chloride have so far been the most commonly investigated DES. Due to its low costs

and availability, choline chloride can be tuned up with several HBDs, including carboxylic acids, phenols, polyols, and amides, to form DES. The composition and the physicochemical properties, as anticipated, are the main factors affecting the application of the particular DES.[14]

With the growing demands and recognition of DES, a remarkable amount of experimental studies on the formation of DES from ChCl (Choline Chloride) with HBDs such as urea and glycerol have already been performed. The molecular-level understanding of the DES interactions and formation mechanism using computational methods are very scarce.[15] The hydrogen bond is critical in determining the DESs' physicochemical features. Ashworth et al. evaluated the importance of hydrogen bonding in DESs' using the Density Functional Theory (DFT) approach.[60] In earlier work, Sun et al. reported a molecular dynamics (MD) simulation study of ChCl based DES with urea in different molar ratios with an explanation for the depression in the melting point of the DES system.[16] Zhekenov et al. documented a combined experimental and computational approach to predict the importance of intermolecular hydrogen bonds in the formation of DES systems.[17] Similar work using infrared spectroscopy and MD simulations reported by Perkins et al., strong *trans*-type hydrogen-bonding interactions between chloride anion of ChCl and urea were predicted, which play a vital role in the depression of melting point of the DES system.[18] Zahn et al. made observations using *ab initio* MD simulations and concluded that charge delocalization through hydrogen bonding is not the only reason for the depression of the melting point in DES systems.[19] In a previous work based on ChCl/glycerol system, Wagle et al. predicted the linkage of glycerol with chloride anion and diffusion of Choline cation into the DES[20], and computational insights on the interaction and thermodynamics involved in the formation of various ChCl based DES systems.[21] Garcia et al., using quantum chemical calculations and AIM analysis, predicted the relationship between melting temperatures and electron density in ChCl based DESs.[22] Zhang et al. performed the experimental and computational analysis for the electrodeposition of

magnesium chloride hexahydrate in a Choline Chloride/magnesium chloride hexahydrate based DES.[23] Yang and co-workers investigated that the composition and molar ratio of HBA and HBD can have an impact on the freezing point of DES systems, as well as the physical and chemical properties of the system.[61] It can be concluded that all the previous work performed on the mechanism of formation and microstructure of DES systems were all based on the Type III DESs systems.

Recently, DESs consisting of choline chloride and metal salts (such as zinc (II) chloride and tin (II) chloride) have been described as a green and effective medium for polymerization, electrochemical process, dye-sensitized solar cells, metal electrodeposition, and organic synthesis.[24] Lin et al. reported the formation of eutectic mixtures by mixing the ionic liquids with metal halides such as zinc chloride.[25] Subsequently, it was reported by several authors that ionic liquids such as 1-butyl-3-methylimidazolium chloride could form a eutectic mixture with ferric and stannous salts. Abbott et al. reported the formation of Type I DES constituting of quaternary ammonium salts and metal halide salts such as $ZnCl_2$, $FeCl_3$, and $AlCl_3$, which can be termed as Deep Eutectic Solvents (DESs).[26] The presence of excess chloride ions in the QAS salt triggers its interaction with the metal cation, leading to the formation of the metal-chloride complex moiety. This is a unique formation and is not present in the metal halide salts. Abranches et al. reported that the charge transfer behavior of the chloride anion is responsible for the formation and properties of these mixtures.[27] Similarly, to optimize the design of Type I DESs for a particular chemical process, further information about their structural, physicochemical, and transport properties, as well as their relationship to temperature, is required, allowing for the accurate design of a task-specific solvent for a variety of applications.[62] The knowledge related to the interactions between choline chloride and metal halide salts is limited. Consequently, understanding the interaction of metal (II) halides and

ChCl is essential in studying the mechanism and charge transfer behavior involved in forming Type I-based DESs.

In the present chapter, we have explored the formation of Type I DES, which comprises quaternary ammonium salts (Choline Chloride) and metal (II) halides ($ZnCl_2$ and $SnCl_2$), by applying Density Functional Theory (DFT) calculations. The intermolecular interactions between choline chloride and two different metal halide salts, namely Zinc Chloride ($ZnCl_2$) and Tin Chloride ($SnCl_2$), were subjected to analysis. As an initial step, we have explored the geometries, electronic structure, charge delocalization, and the thermochemistry involved in forming the DESs. Bader's Quantum Theory of Atoms in Molecules (QTAIM) and Non-covalent interactions (NCI or RDG method) has also been employed to study the mechanism of interaction. We have used the following nomenclature for the two DES systems studied in this work: DES1 (ChCl: $SnCl_2$) and DES2 (ChCl: $ZnCl_2$), respectively. To the best of our knowledge, this is the first time that the structural and formation mechanism of Type I DES is reported.

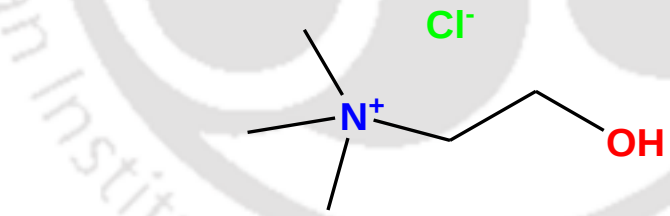

(a) Choline Chloride

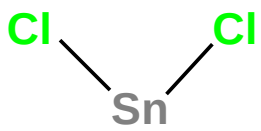

(b) Tin (II) Chloride

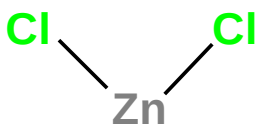

(c) Zinc (II) Chloride

Figure 3.1: Schematic representation of the molecules used in this chapter

3.3. Materials, Preparation and Experimental IR Spectroscopy

Choline Chloride (ChCl), Tin (II) Chloride ($SnCl_2$), and Zinc (II) Chloride ($ZnCl_2$) were purchased from Sigma Aldrich. Due to their inherent moisture sensitivity, the resulting compounds were dried in a high vacuum (80˚C, 2 days, 10^{-3} mbar). Both the investigated DESs, namely DES1 (ChCl: $SnCl_2$ in a molar ratio of 1:2), and DES2 (ChCl: $ZnCl_2$ in a molar ratio of 1:2) were experimentally formulated by constant stirring (≤ 500 rpm) at a temperature fixed to 100˚C and under atmospheric pressure until clear liquids were obtained. Infrared measurements on the synthesized DES mixtures were performed using the IRAffinity-1 FTIR instrument from Shimazdzu Inc.

3.4. Computational Methods

Initial DES geometries were generated by positioning individual metal halide salts ($SnCl_2$ and $ZnCl_2$) in all possible orientations around the QAS (ChCl) moiety. Preliminary geometry optimizations were carried out by employing BP86 density functional in conjunction with the triple-ζdef2-TZVP basis sets for non-heavy atoms (Choline Chloride, $ZnCl_2$-dimer, and DES2 (ChCl: $ZnCl_2$).[28-31] For heavy metal system ($SnCl_2$-dimer and DES1 (ChCl: $SnCl_2$), relativistic corrections were applied by employing the zero-order regular approximation (ZORA) approach.[32,33] During this step, the ZORA-def2-TZVP basis sets, which are relativistically recontracted version of all-electron def2-TZVP basis sets, and segmented all-electron relativistically contracted (SARC/J) auxiliary basis sets[34] were used. The resolution-of-identity (RI) approximation was applied for fast computations. [35-37] Dispersion effects were considered by applying the atom-pair-wise corrections schemes developed by Grimme *et al.* with Becke-Johnson damping (D3BJ).[38,39] The resulting stationary points were characterized as energy minima on the potential energy hypersurface by performing harmonic vibrational frequencies at the same level. The geometries were subsequently re-optimized with M06-2X

density functional[55] as it was considered as a suitable functional for evaluating thermochemical parameters for similar systems. The interaction energies of initial structures and the later formed DES was calculated using quantum chemical calculations, during which the counterpoise procedure was adopted to eliminate the basis set superposition error (BSSE).[40] All calculations were performed with ORCA version 4.0.1 quantum chemistry package.[41] The analysis of the net charge distribution on eutectic systems was performed using Natural Bond Orbital (NBO) methodologies implemented in NBO program package version 6.0,[42] and the electrostatic potential derived charges were analyzed using the CHELPG method. A frontier molecular orbital analysis was carried out to get insights into the molecular reactivity and available active sites. To further gain insights on the electronic structure and bonding in QASs, metal halide salts, and their interactions with the metal-based DESs, the Quantum Theory of Atoms in Molecules (QTAIM)[53] and non-covalent interaction (NCI or RDG) methodologies [49,50] were applied using the Multiwfn code [43]. QTAIM is an efficient approach for studying intermolecular interactions. The electron density at the bond critical points (BCPs), ρ_{BCP}, is a valuable parameter to characterize the strength of intermolecular interaction. In addition to this, the Laplacian of the electron density at BCP (∇^2_ρ) denotes regions with charge concentration (negative sign) and charge depletion (positive sign) for a chemical bond. To further validate the existence of intermolecular interactions, the non-covalent interactions analysis (NCI) have been applied to the complex structures studied. NCI analysis provides information about the distribution of electron density in molecular systems of low electron density and low gradient values. This approach is often referred to as 'reduced density gradient' (RDG) analysis.

3.5. Results and Discussions

Prior to beginning the computational investigations for this study, we performed Fourier transform infrared spectroscopy (FTIR) on both DES systems to get additional insight into the mechanism of formation of metal salt-based Deep Eutectic Solvents. The FTIR spectra of both the DES systems are presented in the Electronic supporting information (Figure 3.2 and 3.3). Figure 3.2 illustrates the FTIR spectra of pure choline chloride (Blue), tin (II) chloride (Red), and DES1 (Black). The FTIR spectrum of choline chloride reveals the distinctive bands associated with the OH, CH_2, CH_3, and C–N^+ groups at 3220 cm^{-1} (O–H stretch), 1350–1320 cm^{-1} (CH_3 and CH_2 bend), 1073 cm^{-1} (C–O stretch), and 890 cm^{-1} (C–N^+ symmetric stretching). Similarly, the FTIR spectra of pure tin (II) chloride revealed the expected broad band of stretching OH bond vibrations between 3130 and 3530 cm^{-1}, as well as bending H–O–H vibrations in the region between 1590-1600 cm^{-1}. While bands below 900 cm^{-1} are associated with Sn-Cl bonds. These spectra are consistent with previously published ones.[56] However, at 3450 cm-1, a broad vibrational band is observed that is attributed to O–H stretching. This band broadens as the interaction between QAS ions weakens and chloride pledges new interactions with the metal salt dimers, designating the formation of electrostatic interactions. The bending H–O–H vibration appears in the region between 1597–1605 cm^{-1}, and the absorption corresponding to C–N^+ symmetric stretching is observed at 869 cm^{-1}.

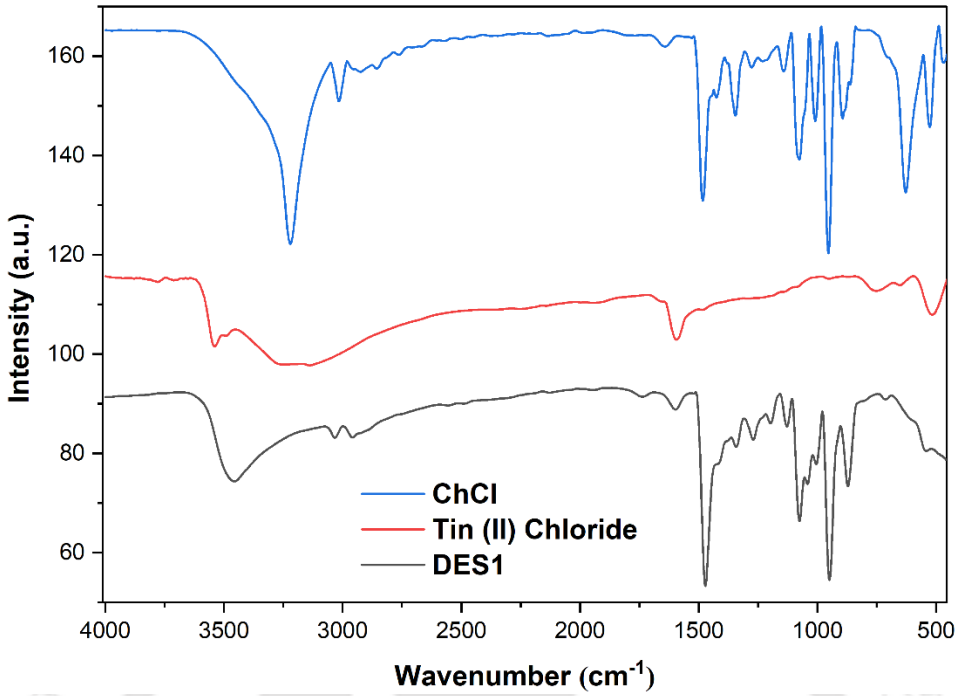

Figure 3.2: FTIR spectra of DES1 (bottom), Tin (II) Chloride (middle), and ChCl (top)

In Figure 3.3, the FTIR spectra of pure choline chloride (Blue), zinc (II) chloride (Red), and DES2 (Black) are shown. The vibrational bands for pure ChCl were determined to be within the same range as those of DES1. Similarly, the FTIR spectrum of zinc (II) chloride revealed a broad band of OH stretching at 3386 cm-1, showing the existence of OH residues due to retained moisture from the atmosphere due to the hygroscopic nature of zinc chloride salt. H-O-H bending vibration was observed at 1609 cm^{-1}, indicating the presence of water molecules. The broad peak in the range of 545-609 cm^{-1} can be attributed to the Zn-Cl stretching. Similar to DES1, DES2 also exhibits a broad vibrational band at 3340 cm^{-1}, which can be attributed to the creation of new electrostatic contacts between the QAS and metal salt dimers. The FTIR spectra was found to be in line with the earlier reported literature.[57]

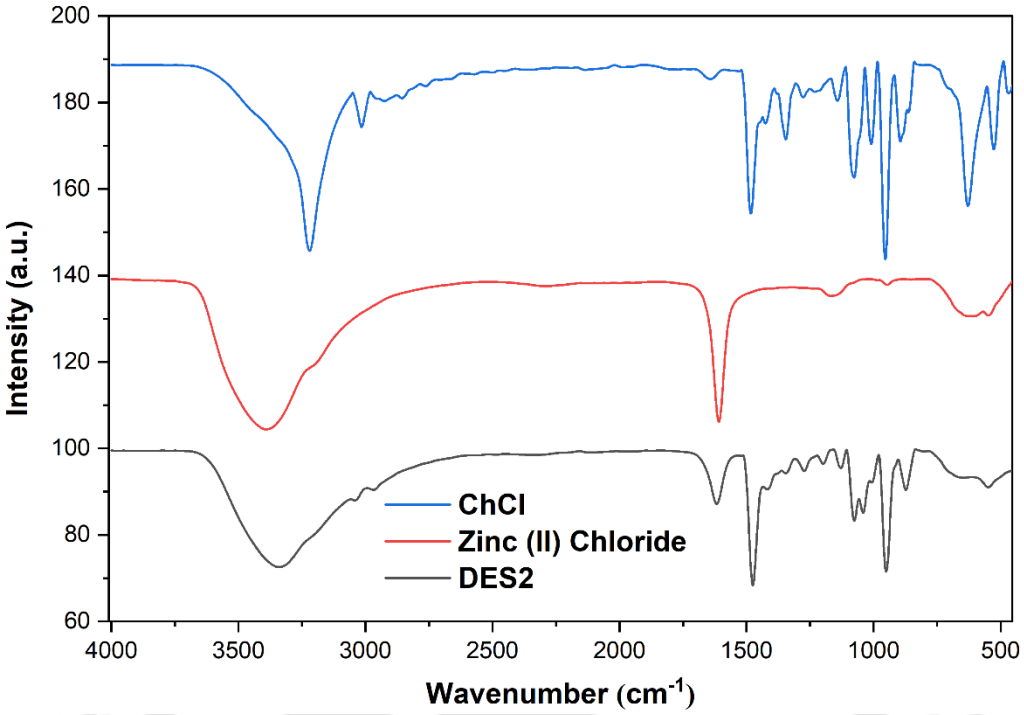

Figure 3.3: FTIR spectra of DES2 (bottom), Zinc (II) Chloride (middle), and ChCl (top)

3.5.1. Geometry Optimization

The geometries of DES complex systems were optimized using M06-2X density functional, which is reported as a suitable functional for analyzing non-covalent interactions such as hydrogen bonding. In this work, Choline Chloride is referred to as ChCl, a quaternary ammonium salt (QAS), whereas Tin (II) Chloride and Zinc (II) Chloride are well-known metal halide salts, denoted by the abbreviations MS1 and MS2, respectively. The geometric parameters (C-N, C-O, and C-C distances for choline chloride) were found to agree with the experimental results reported by Hjortas et al.[44]

For their very existence, the structural orientations of the DES are important to understand as the eutectic mixture, as the structural behavior determines their physical properties in this complex system. The DES framework consists of a network for hydrogen

bonding in which the metal halide salt molecules interact with Choline (Ch^+) cation and the anion to form a complete complex cyclic structure. In DES1, the tin atom in the metal dimer associates with the Cl^- through a single Cl-Sn⋯Cl^- with a bond distance of 2.6 Å resulting in a cyclic structure. The characteristic υ(Sn⋯Cl) is at 152 cm^{-1} and is depicted in the theoretically calculated IR spectra of DES1 (cf. Figure 3.5b). A relatively weak ionic interaction is observed in Sn⋯Cl^-⋯Sn after the formation of DES, with the Sn⋯Cl^- distance amounting to 2.9 Å (cf. Figure 3.5a) in comparison to 2.7 Å estimated in the dimer geometry of tin (II) Chloride (cf. Figure 3.4b). The $[Sn_2Cl_5]^-$ ionic species formation is well compatible with experimental studies recorded by Abbott et al. As similar to DES1, DES2 exhibits three interactions between zinc and chlorine (Zn⋯Cl^-) moieties (between the Cl^- of choline chloride and zinc atom of the dimer at a distance of 2.2 Å). Additional interactions between zinc and chloride atoms occur in the dimer geometry at a distance of 2.4 Å. The calculated IR vibrational frequency at 164 cm^{-1} can be attributed to the (Zn⋯Cl^-) interaction, which leads to the formation of $[Zn_2Cl_5]^-$ ionic species. Abbott et al. demonstrated the formation of metal salt Deep Eutectic Solvents using functionalized quaternary ammonium salts and zinc and tin metal salts in their work. Mass spectrometry (FAB-MS) and potentiometry were used to identify and quantify the complex anions. $ZnCl_2$-based DESs have been examined in greater depth than other systems, and it was found that $ZnCl_3^-$, $Zn_2Cl_5^-$, and $Zn_3Cl_7^-$ species are present in the liquid in quantities that depend on the composition of the QAS and the metal salt. They have dissimilar dimensions and charge densities and exhibit peculiar electrostatic interactions with the cation. For instance, because $ZnCl_3^-$ ions are smaller and have stronger electrostatic interactions, the freezing point of the system increases. Small variations in the concentrations of each of the complex anions are likely to have a significant effect on the ion-ion interactions, which in turn affects the freezing point. Similarly, once the concentration of $ZnCl_2$ exceeds a mole fraction of 66%, the freezing point increases. It is implied that this occurs as a result of the increased concentration

of $Zn_3Cl_7^-$ and its larger molecular mass.[10] This explains why the DES prepared at molar ratios of 1:1 and 1:3 solidify at room temperature and have greater freezing points than those prepared at a molar ratio of 1:2 in the studied systems. Similarly, for eutectic solvents containing $SnCl_2$, alike results were obtained.[54] For the same instance, the studied DES systems were optimized in different molar ratios from 1:1 to 1:3. The optimized geometries of the DESs in the molar ratio of 1:1 and 1:3 for both DESs are presented in Figure 3.6. The structural features for the documented DES systems are consistent with the experimental findings described previously.[54]

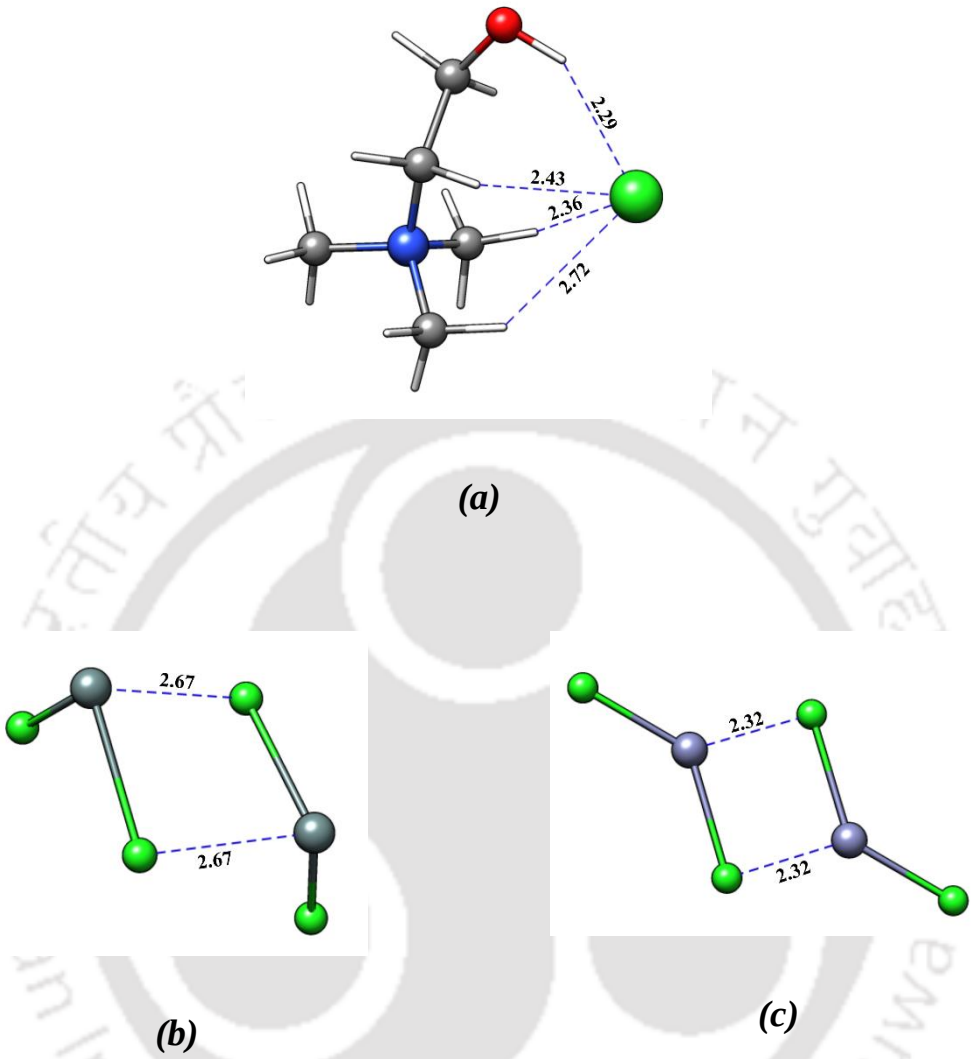

Figure 3.4: Optimized geometries of the isolated species (a) Choline Chloride, (b) Tin (II) Chloride dimer at the M06-2X/ ZORA-def2-TZVP level and (c) Zinc (II) Chloride dimer, at M06-2X/def2-TZVP level.

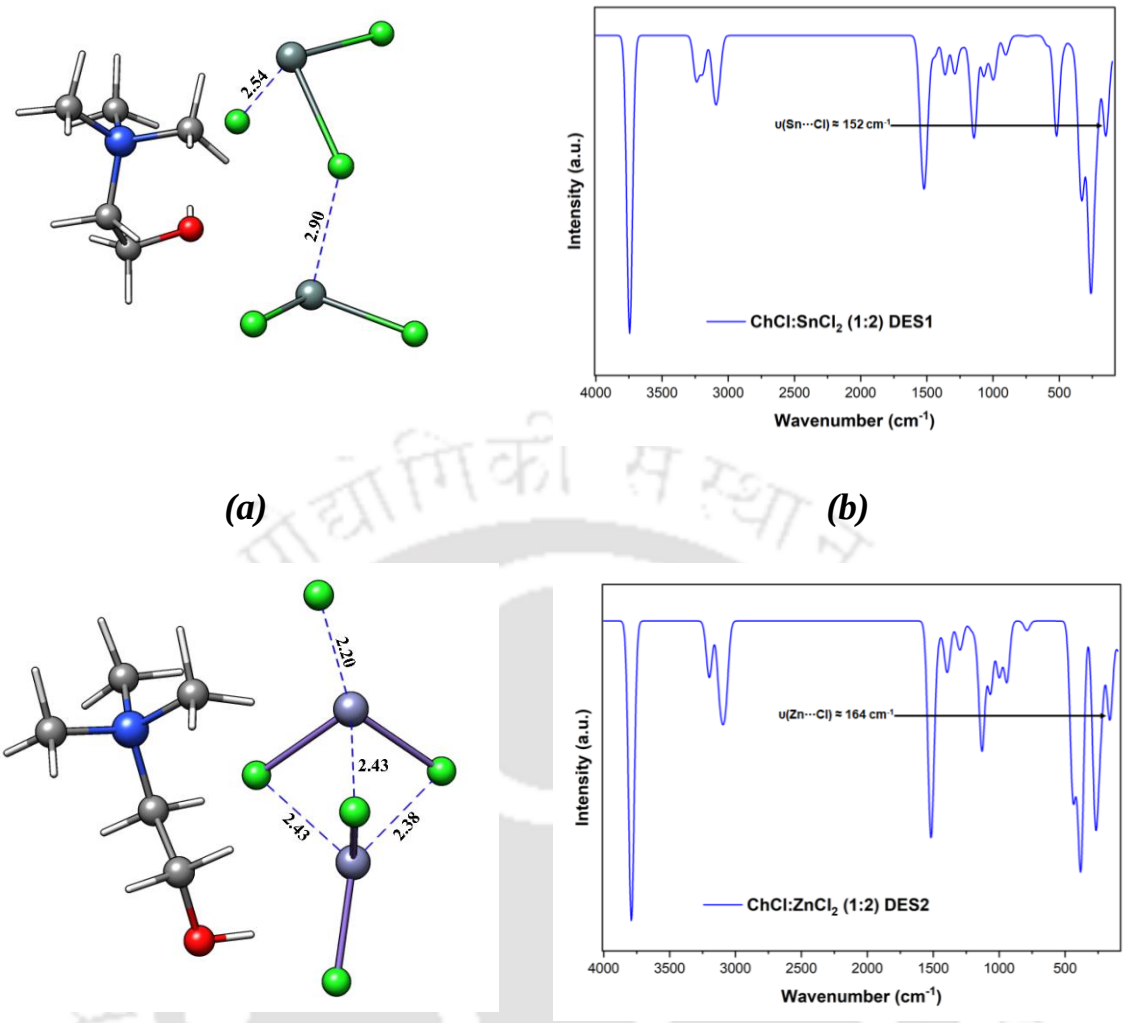

Figure 3.5: Optimized geometries of the (a), (c) DESs and (b), (d) simulated IR spectrum at the M06-2X/def2-TZVP level of theory.

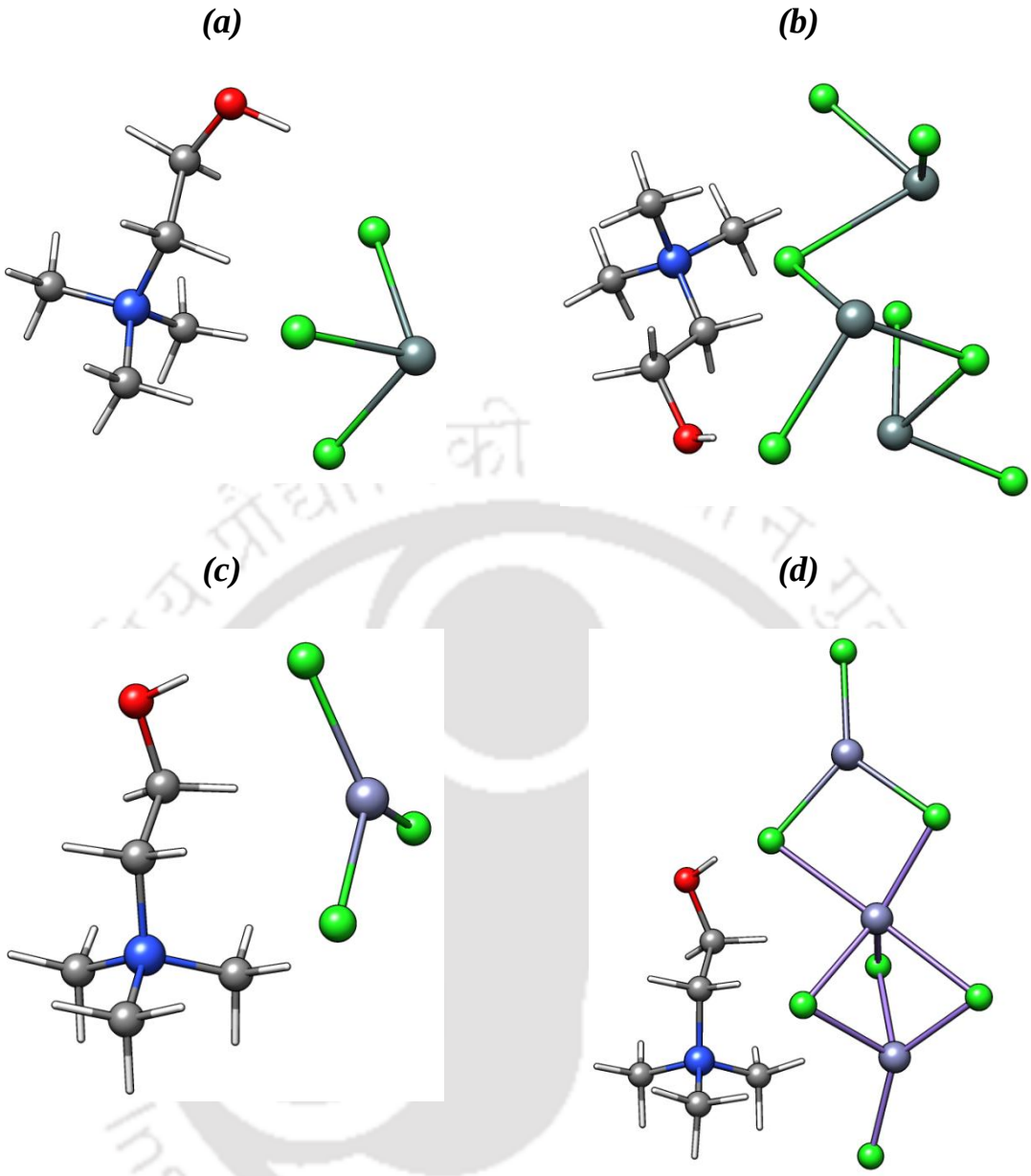

Figure 3.6: Optimized geometries of the (a) DES1 at a molar ratio of 1:1, (b) DES1 at a molar ratio of 1:3 at the M06-2X/ZORA-def2-TZVP level of theory (b) DES2 at a molar ratio of 1:1, and (d) DES2 at a molar ratio of 1:3 at the M06-2X/def2-TZVP level of theory.

3.5.2. Charge Transfer Analysis

The delocalization of charge between anion and metal halide salts occurs via hydrogen bonding interactions. This is responsible for the depression of the freezing point in DES, as suggested by Carriazo et al.[45] The intensity of the ionic hydrogen bond interactions is related to the amount of charge transfer from the QAS to the metal halide salt.[46]

In the present study, the CHELPG partial charge method and NBO charge analysis were used to understand the proposed charge delocalization in our metal-based DES systems. Note that the charge on chloride ion of Choline Chloride is reduced considerably (from -0.74 to -0.39e) in conjunction with a significant increase in the negative charge on the metal chloride donor molecules (cf. Table 3.1). In the instance of NBO charge analysis, a qualitatively distinct pattern was observed. As a result, no correlation between CHELPG and NBO charge analysis can be established for the investigated systems. When the charge distribution of the metal-based DES system is compared to that of its constituents, it is observed that the positive charge on the cationic core increases while the negative charge on the hydroxyl group of the choline cation decreases. On the contrary, the charge analysis indicates a substantial reduction in the anion's net negative charge, increasing the negative charge on metal salt dimers. In the case of DES1, a slight decrease in the positive charge on the choline moiety (Ch^+) can be attributed to the structure of the studied DES systems. As illustrated in Figure 3.5 ((a) and (c)), the optimized geometries of both examined DESs reveal that DES1 forms an open structure whereas DES2 forms a closed cage-like structure. The open and caged-like structure alluded here is the structure of the ionic moiety formed when choline chloride and metal salt dimers are mixed ($Sn_2Cl_5^-$ in DES1 and $Zn_2Cl_5^-$ in DES2). As it is evident from the charge transfer (CT), which occurs from choline cation as well as the chloride anion to the HBDs through electrostatic interactions. With reference to the chloride anion of $Ch^+\cdots Cl^-$ moiety, the direction of the charge transfer remains the same while it differs in the amount of charge transfer due to the presence of cationic moiety in the metal salt (Sn in DES1 and Zn in DES2). The anionic moiety ($Sn_2Cl_5^-$ in DES1), due to its open-like structure, is incapable of transmitting charge uniformly. Whereas in the DES2 system, a smooth charge flow results in a higher negative charge on the metal salt dimer following DES formation (Table 3.1). The uniform charge distribution in DES2 is attributed to the cage-like structure of the $Zn_2Cl_5^-$ anionic moiety. Garcia et al. studied

the quantum chemical and topological features of different DES systems in order to propose an explanation for the depression of freezing point in DESs in support of this structural property.[22] A direct correlation between the electron density at cage critical points and the freezing point of the DESs. The low electron density at the cage critical points leads to low melting points. This behavior is consistent with the fact that the low charge concentration at cage critical points is the result of extensive charge delocalization within the cage-like structures, and that melting point depression upon mixing the DES components is primarily due to the charge delocalization process resulting from the development of the entire hydrogen bonding network. Due to the cage-like structure of DES2 systems, the charge flow is uniform, resulting in a significant depression of the solvent's freezing point. DES2 systems have a lower freezing point than DES1 systems. The charge transfer in the two examined DES systems is demonstrated via visualization of charge in optimized geometries on the various species participating in the CT process in Figures 3.7 and 3.8). These analyses demonstrate unequivocally that both functional groups are required for charge transfer between the choline cation, chloride anion, and metal salts molecules through hydrogen bonding and electrostatic interactions.

Table 3.1: CHELPG and NBO charges on Different Components before and after the formation of the metal-based DES (Ch^+/(Choline), Cl^-/Chloride, Ch_N/N^+ of Choline and Ch_O/Oxygen of Choline) (MS1: $SnCl_2$-dimer, MS2: $ZnCl_2$-dimer).

	CHELPG						**NBO**			
	Ch^+	Ch_N	Ch_O	Cl^-	MS1	MS2	Ch^+	Cl^-	MS1	MS2
DES1	0.72	0.44	-0.43	-0.39	-0.33	-	0.95	-0.68	-0.26	-
DES2	0.78	0.22	-0.58	-0.42	-	-0.36	0.96	-0.77	-	-0.18
Pure Component	0.74	0.19	-0.62	-0.74	0.00	0.00	0.89	-0.89	0.00	0.00

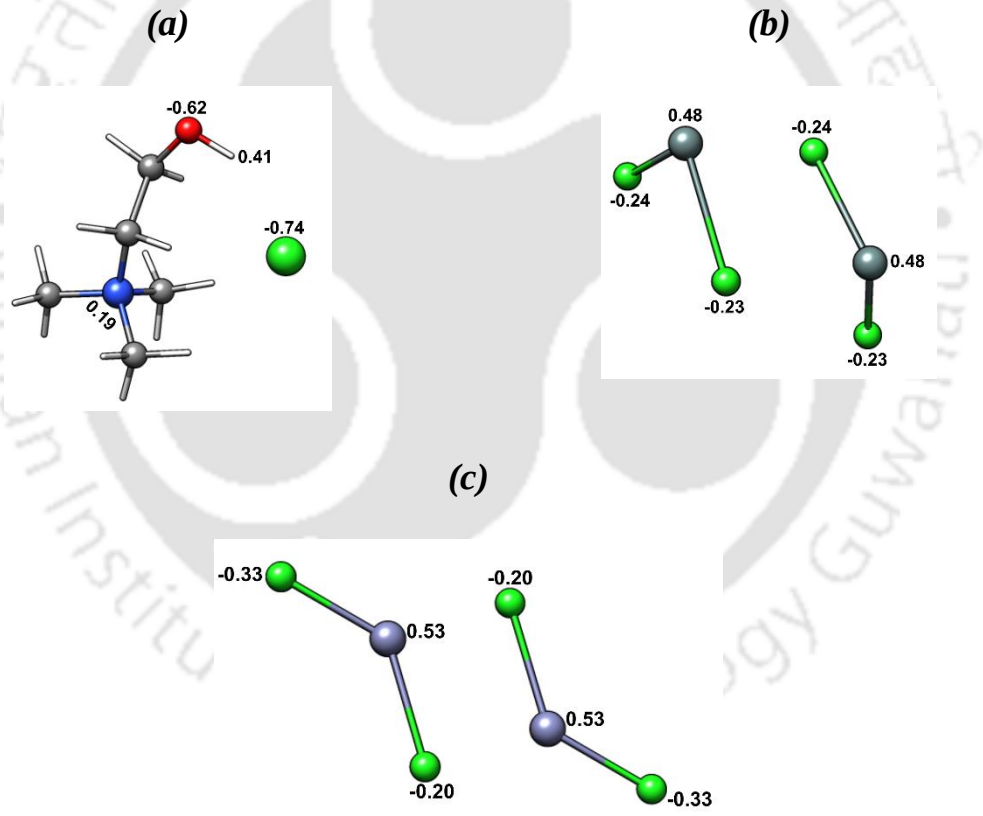

Figure 3.7: CHELPG charges of the isolated species (a) Choline Chloride, (b) Tin (II) Chloride dimer, and (c) Zinc (II) Chloride dimer.

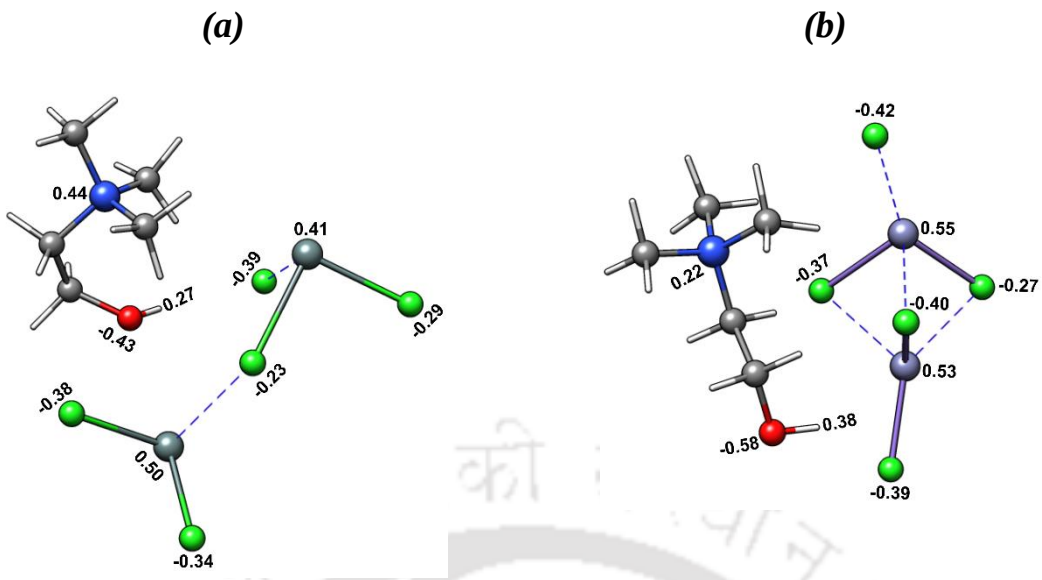

Figure 3.8: CHELPG charges of the DESs systems (a) DES1, and (b) DES2.

3.5.3. Quantum Theory of Atoms in Molecules Analysis.

The quantum theory of atoms in molecules (QTAIM) analysis has been used to provide a better understanding of intermolecular interactions between the acceptor and donor pairs in each DES. Bader's QTAIM approach is one of the well-known approaches for analyzing electron density distribution in the molecular system. The key aspect for QTAIM is the electron density, ρ, whose topology is defined by critical points (CPs) where the gradient of electron density disappears ($\nabla\rho = 0$). In QTAIM analysis, any bonding contact (bonded or interacting) between two atoms is defined by the presence of a bond critical point (BCP). The BCPs provide additional information about the nature of bonding and the mechanism of the interaction. The descriptors of BCPs, such as electron density (ρ_{BCP}), and the laplacian electron density ($\nabla^2\rho_{BCP}$), can also be used to determine the strength of interaction and help classify various weak non-covalent interactions. For instance, it was discovered that electron density properties measured at the so-called bond critical point (BCP, (3,-1)) saddle point on electron density curvature where the curvature is minimum in the direction of the atomic interaction line and maximum in the two directions perpendicular to it, can provide information about the character

of various chemical bonds, such as covalent bonds, metal-ligand interactions, different kind of H-bonds. In general, the larger the distance between the two atoms that form the bond, the smaller is the electron density in the bond's BCP, and, consequently, the weaker the bond.[58] Therefore, larger values for ρ_{BCP} indicates a stronger bonding interaction, and the sign of $\nabla^2\rho_{BCP}$ defines the characteristics of a bond. Covalent bonds and closed-shell interactions (*i.e.*, H-bond interactions, vdW interactions, and ionic bonds) can be related to negative and positive values of the Laplacian of the electron density ($\nabla^2\rho_{BCP}$), respectively.[47] The calculated values of ρ_{BCP} and $\nabla^2\rho_{BCP}$ for the intermolecular ionic and H-bonds in DES1 and DES2 are listed in Table 3.2.

Our AIM analysis indicates that both parameters (ρ_{BCP} and $\nabla^2\rho_{BCP}$) are positive (*i.e.*, a value of 0.002–0.035 a.u. was derived for the electron density, and 0.024–0.139 a.u. was estimated for the Laplacian of electron density) and indicates closed-shell interactions.[48] Figure 3.9 represents the molecular graph of both DES1 and DES2. The electron density of a BCP is to be directly proportional to the bond strength. In DES1, the electron density and the Laplacian of the electron density of the BCP1 (Sn_{24}-Cl_{27}) and BCP2 (Sn_{23}-Cl_2) correspond to ionic bonds. In contrast, the rest of the interactions correspond to the H-bonds and electrostatic interactions, indicating predominantly noncovalent weak interactions. In the case of DES2, Cl_{27}-H_{16}, Cl_{24}-H_{16}, Cl_{24}-H_{19} pairs have significantly higher electron density at the bond critical point than the other intermolecular closed-shell interactions present. Similar to DES1, the M-X (Zn-Cl) interactions (BCP 1, 2, 10, and 11) correspond to ionic bonds due to higher electron density. In both the studied DES complex systems, all our proposed hydrogen bonds and electrostatic interactions have a positive value for the electron density and the Laplacian of electron density estimated at respective BCPs.

Table 3.2: Electron Density (ρ_{BCP}) and the Laplacian of Electron Density ($\nabla^2\rho_{BCP}$) at relevant the bond critical points (BCPs) in the studied DESs.

Structure	BCP interaction	ρ_{BCP} (a.u.)	$\nabla^2\rho_{BCP}$ (a.u.)
DES1	BCP1: Sn_{24}-Cl_{27}	0.0257	0.0565
	BCP2: Sn_{23}-Cl_2	0.0540	0.1335
	BCP3: Sn_{24}-O_{21}	0.0181	0.0552
	BCP4: Cl_{27}-H_4	0.0130	0.0434
	BCP5: Cl_{28}-O_{21}	0.0141	0.0567
	BCP6: H_5-Sn_{23}	0.0097	0.0233
	BCP7: Cl_{28}-H_{17}	0.0074	0.0236
	BCP8: Cl_{28}-H_{19}	0.0098	0.0033
DES2	BCP1: Zn_{26}-Cl_2	0.0788	0.2897
	BCP2: Zn_{26}-Cl_{24}	0.0476	0.1727
	BCP3: Cl_{27}-H_{16}	0.0127	0.0416
	BCP4: Cl_{27}-H_{10}	0.0067	0.0212
	BCP5: Cl_{24}-H_{12}	0.0090	0.0282
	BCP6: Cl_{24}-H_{16}	0.0110	0.0356
	BCP7: Cl_{24}-H_{19}	0.0101	0.0332
	BCP8: Cl_{24}-H_{22}	0.0085	0.028
	BCP9: Cl_{25}-H_{22}	0.0044	0.0127
	BCP10: Cl_{27}-Zn_{23}	0.0479	0.1731
	BCP11: Cl_{28}-Zn_{23}	0.0536	0.1948

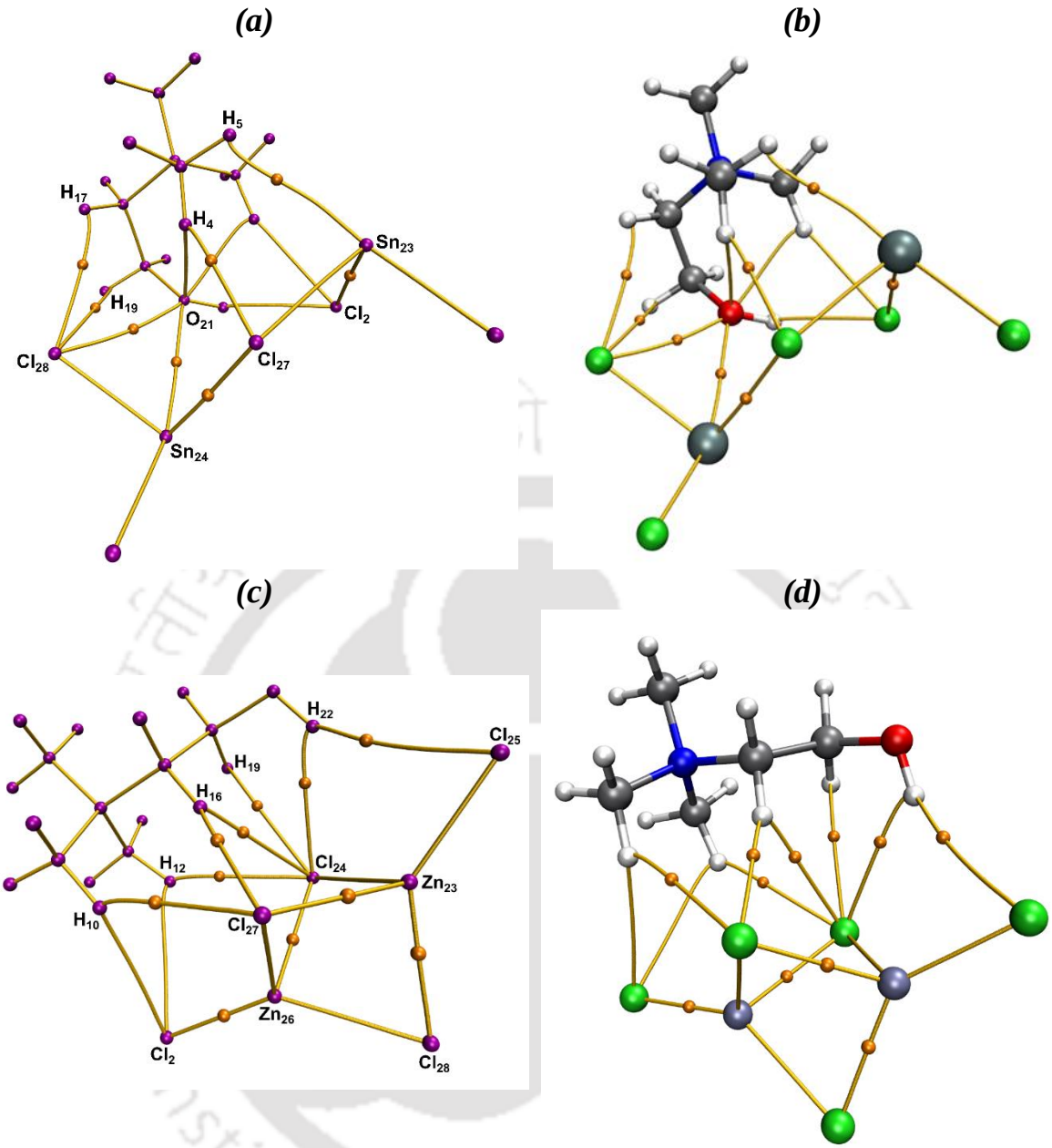

Figure 3.9: Molecular graphs of (a), (b) DES1 and (c), (d) DES2 calculated at M06 2X/def2-TZVP level.

3.5.4. Non-Covalent Interactions

A study of NCIs is employed as an alternate method to investigate the non-covalent interaction in the present work. NCI focuses on the analysis of the electron density distribution in molecular systems in the regions of low electron density and low gradient values. This method is often referred to as "Reduced Density Gradient" (RDG) analysis. Contreras-Garcia and Johnson[49] initially proposed this approach to identify the non-covalent bonds in a system (water and methane dimer). NCI can be used to interpret relationships using spikes in RDG graphs at low densities.[50] The RDG has been expressed in equation 1.

$$RDG = \frac{1}{2(3\pi^2)^{1/3}} \frac{|\nabla\rho|}{\rho^{4/3}} \quad (3.1)$$

The scatter graph maps of the reduced density gradient (RDG) plotted as a function of electron density multiplied by the sign of the electron density Hessian second eigenvalue, (sign(λ_2)ρ), one can reveal and quantify different types of weak non-covalent interactions, including hydrogen bonds. The scatter graph and isosurfaces of weak non-covalent interactions between the QAS and their related metal halide salts associated with the metal-based DESs are shown in Figure 3.10. Several RDG spikes are displayed as a function (sign(λ_2)ρ), ranging from negative to positive values, including spikes referring to the H-bonding interactions, van der Waals interactions, and steric effects. More specific details about this approach can be found elsewhere.[49] Figure 3.10 displays strong attractions, strong repulsion, and vdW interactions in blue, red, and green colour, respectively. Three kinds of spikes are evident in the RDG graph of attractive interactions, such as hydrogen bond interactions and repulsive interactions, identified as regions where $\lambda_2 < 0$ and $\lambda_2 > 0$, respectively. Furthermore, the λ_2 value approach zero for weak vdW interactions ($\lambda_2 \cong 0$). The colour blue denotes strong, attractive interactions (such as hydrogen and strong electrostatic interaction). In contrast, the

red colour indicates strong non-bonded overlap, and the transition region denotes standard van der Waals interactions such as dipole-dipole interaction, dispersion interaction, hydrophobic interaction, and so on. In general, if the RDG scatters in the range ±0.005 in spike form, weak interactions such as dispersion force exist; if the RDG scatters in the range >0.005, strong repulsive interactions exist, such as steric hindrance in aromatic rings; and if the RDG scatters in the range <0.005, strong attractive interactions exist, such as hydrogen bonds. In contrast with DES1, the sharp and dense peaks between -0.05-0.02 a.u. for DES2 is a signature of noncovalent interactions for the current system. This significant increase in the density of the spikes stems from the allegedly stable hydrogen and ionic bonds formed between the zinc and chlorine atoms of the system (DES2) and forming a complex structure. Whereas van der Waals (vdW) interaction regions (green regions) always have very small ρ, and are generally observed within the intermolecular region of both the components in studied DES systems. In addition, certain repulsive interaction peaks in the range of 0.02-0.04 a.u are present in the RDG graph of DES2, which can be attributed to chlorine atoms interactions. The strong ionic bond interactions (blue regions) are clearly indicated in the interaction of the zinc of the donor atoms with the chlorine atoms of the other donor atoms, which leads to the formation of complex species ($Zn_2Cl_5^-$)[54]. Additionally, a large flake between Ch^+ and metal chloride dimers with a transition region colour can reveal weak electrostatic interaction in the complex structure of DESs. In summary, the RDG analysis shows that the monomer structure of DESs contains both hydrogen bonds and electrostatic interactions, responsible for the decrease in freezing point and formation of the DESs.

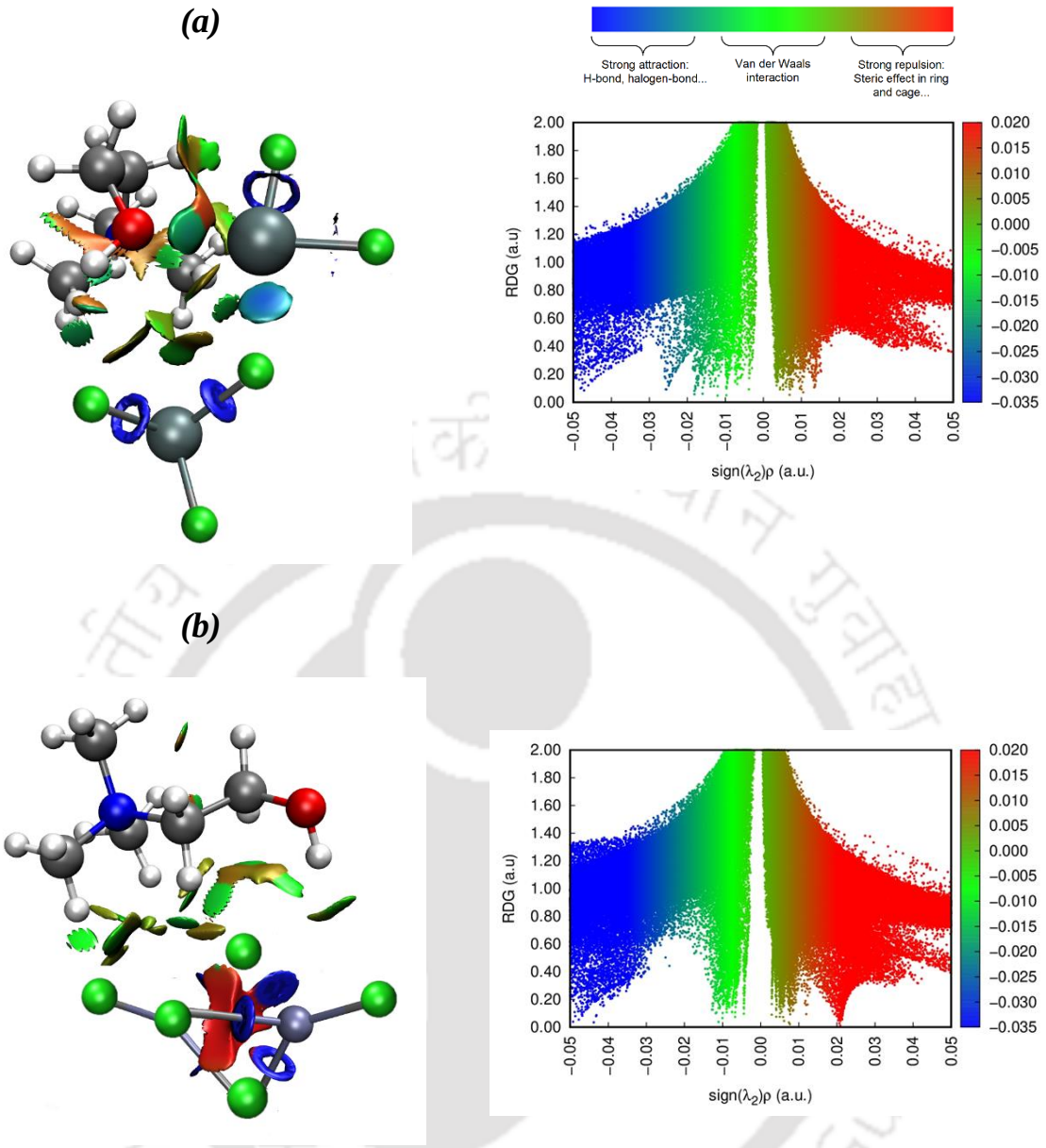

Figure 3.10: RDG isosurfaces and scatter graphs of RDG for (a) DES1 obtained at the M06-2X/ ZORA-def2-TZVP level of theory, (b) DES2 obtained at M06-2X/def2-TZVP level of theory.

3.5.5. Orbital Energies

HOMO (Highest Occupied Molecular Orbital) and LUMO (Lowest Unoccupied Molecular Orbital) energies are essential for analyzing or estimating the chemical stability of the system[51]. According to Fukui et al. [52], the discrepancy between HOMO and LUMO energy values is a central factor which provides the HOMO–LUMO energy gap and helps determine the molecular electronic transport properties. The presence of a large HOMO-LUMO gap implies a high degree of stability and resistance to charge transfer and changes in the number and distribution of electrons. As a result, hard molecules exhibit a higher HOMO-LUMO energy gap. Meanwhile, a small HOMO-LUMO gap implies a high degree of polarizability since it requires only a small amount of energy to reach the excited states. In this regard, a small HOMO-LUMO gap indicates the presence of soft molecules. The HOMO-LUMO gap indicates the species' stability via the lowest electronic excitation energy, while for pairs of molecules (such as ionic liquids and Deep Eutectic Solvents (DES)), the HOMO-LUMO gap indicates the species' reactivity via electronic hopping energy among themselves. The HOMO-LUMO energy gaps and their molecular orbital contours of the studies deep eutectic solvents (DES) are shown in Figure 3.11. The HOMO-LUMO energy gap is more for DES2 (~9.16 eV) than in DES1 (~6.97 eV), indicating a stable DES2 system. The shape and orientation of LUMO likely indicate the probable region for bond formation due to its electron acceptor nature. On the other hand, HOMO provides the potential for external interactions in terms of energy. High HOMO energy designates a high ionization potential and better electron donor properties, whereas low LUMO energy indicates high electron affinity and better electron acceptor properties. Therefore, high HOMO energy and low LUMO energy contributes toward making a molecule more stable.[52]

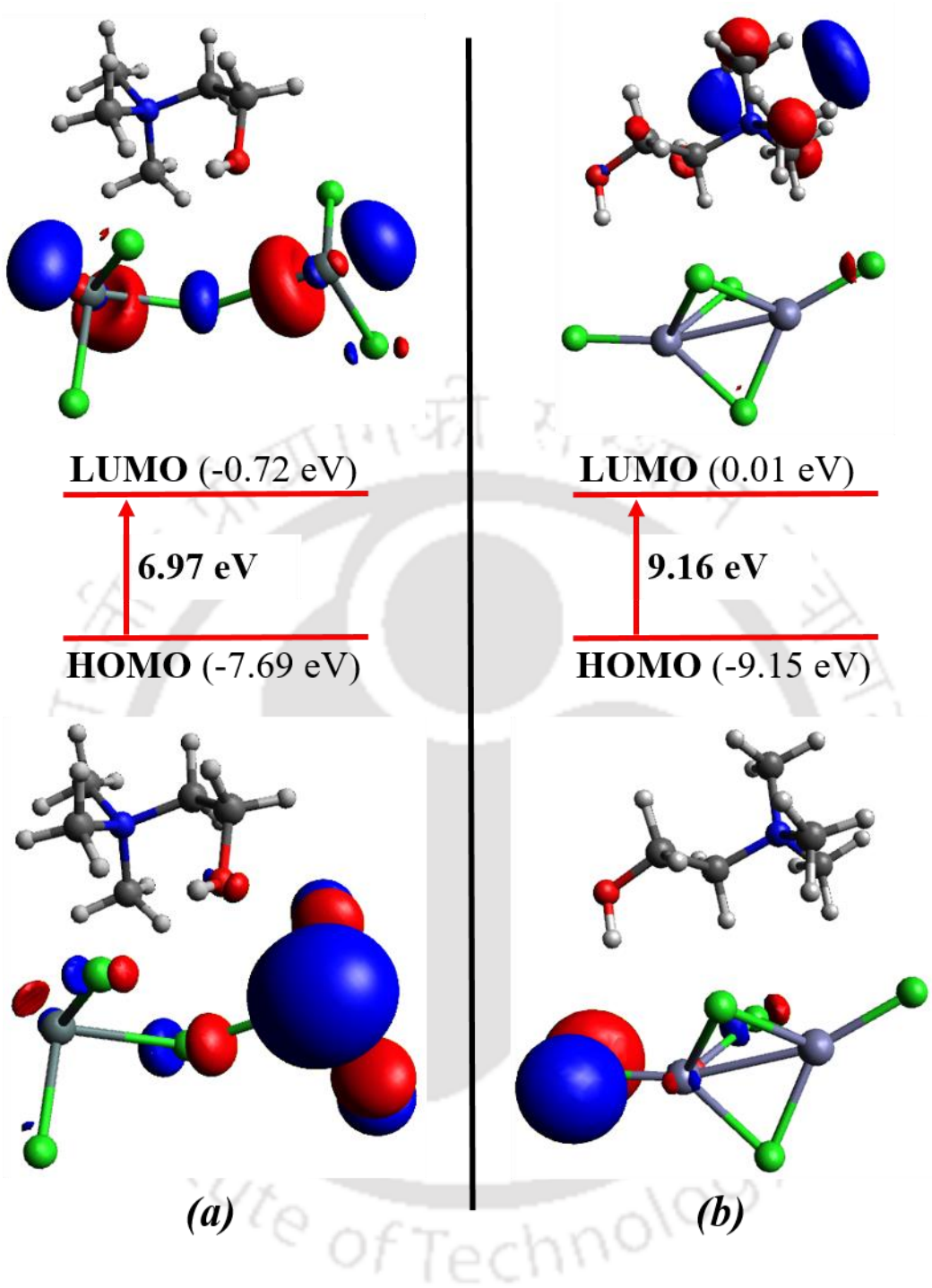

Figure 3.11: Shapes of Highest Occupied and Lowest Unoccupied Molecular Orbitals (HOMO and LUMO) for (a) DES1 calculated at the M06-2X/ ZORA-def2-TZVP level of theory, and (b) DES2 calculated at M06-2X/def2-TZVP level of theory. HOMO-LUMO energies, along with HOMO-LUMO energy differences, are also indicated (blue and red isosurfaces of HOMO and LUMO indicate positive and negative regions, respectively).

While HOMOs are primarily found over the chloride ion in QAS and metal salt dimers, LUMOs are predominantly found over the choline cation in DES2. Whereas in DES1, the LUMO orbital is placed above the metal salt dimers, which is consistent with the Tin(Sn) atom being an electron-deficient centre. As a result, the electron-rich centre readily attacks the electron-deficient Tin(Sn) atom centre efficiently. The interaction of the negatively charged chloride ion in the QAS with the electron-deficient portion of the metal salt results in the formation of the corresponding metal salt-based deep eutectic solvent. The estimated density of states (DOS) can be used to further examine the electronic properties of the interacting systems (Figure B.2). For the two systems under study, a similar DOS curve distribution is predicted, alluding to comparable interaction mechanisms in both cases.

3.6. Conclusions

In the present chapter, we have applied density functional theory calculations to investigate the formation mechanism of metal salt-based Deep Eutectic Solvents (DES) at the molecular level, their charge transfer analysis, and thermodynamics associated with its formation. The following significant conclusions are derived from the study:

(i) The H-bond and ionic interactions identified in DESs (*i.e.*, Chloride-metal salt and Choline-metal salt) exhibit strong interactions resulting in the formation of crate-like complex structures. After the formation of the DES, metal salt−chloride interaction is mainly retained, whereas Choline−Chloride interactions are deranged. The optimized geometries of the formed DESs are in line with experimental findings reported previously.

(ii) DFT calculations suggest that Cl^- serves as a charge transfer carrier between Choline cation and metal halide salts. CHELPG and NBO charge analysis demonstrate that charge transfer occurs through the cationic core of $Choline^+$ and

gets transferred to the metal salts through chloride anion through a series of hydrogen bonding and electrostatic interactions. The change in magnitude of the charges involved in CHELPG analysis predicts a higher order of charge transfer from Choline-metal salt through chloride anion.

(iii) QTAIM analysis provided significant hydrogen-bonding and ionic interaction network formed within the studied DESs systems. The represented electron density (ρ_{BCP}) and Laplacian of electron density ($\nabla^2\rho_{BCP}$) values suggest a stronger electrostatic interaction within the DES2 system as compared to the former one. The non-Covalent interaction (NCI) or RDG method was performed to analyze the main interactions involved between the QAS and metal salt complex DES systems. Strong electrostatic interactions (blue spikes) are observed between the chloride of the HBA with the zinc of the metal halide dimer in DES2 compared to DES1 within the range of -0.05 and -0.03 a.u., respectively.

(iv) A frontier molecular orbital analysis was performed to evaluate the chemical reactivity and stability of the system. A more significant HOMO-LUMO energy gap observed for DES2 indicated greater stability of the system than its eutectic counterpart, DES1.

In summary, the present chapter provides a detailed insight into the formation of the metal salt-based Deep Eutectic Solvents (DES) at the molecular level. Their application as a catalytic media in the dehydrogenation of amine boranes will be discussed extensively in the subsequent chapter.

References

(1) Hallett, J. P.; Welton, T. Room-Temperature Ionic Liquids: Solvents for Synthesis and Catalysis. 2. *Chem. Rev.* **2011**, *111* (5), 3508–3576. https://doi.org/10.1021/cr1003248.

(2) Welton, T. Ionic Liquids in Catalysis. *Coord. Chem. Rev.* **2004**, *248* (21–24), 2459–2477. https://doi.org/10.1016/j.ccr.2004.04.015.

(3) Cassity, C. G.; Mirjafari, A.; Mobarrez, N.; Strickland, K. J.; O'brien, R. A.; Davis, J. H. Ionic Liquids of Superior Thermal Stability. *Chem. Commun.* **2013**, *49* (69), 7590–7592. https://doi.org/10.1039/c3cc44118k.

(4) Villanueva, M.; Coronas, A.; García, J.; Salgado, J. Thermal Stability of Ionic Liquids for Their Application as New Absorbents. *Ind. Eng. Chem. Res.* **2013**, *52* (45), 15718–15727. https://doi.org/10.1021/ie401656e.

(5) Wu, B.; Liu, W. W.; Zhang, Y. M.; Wang, H. P. Do We Understand the Recyclability of Ionic Liquids? *Chem. - A Eur. J.* **2009**, *15* (8), 1804–1810. https://doi.org/10.1002/chem.200801509.

(6) Aschenbrenner, O.; Supasitmongkol, S.; Taylor, M.; Styring, P. Measurement of Vapour Pressures of Ionic Liquids and Other Low Vapour Pressure Solvents. *Green Chem.* **2009**, *11* (8), 1217–1221. https://doi.org/10.1039/b904407h.

(7) Santos, A. G.; Ribeiro, B. D.; Alviano, D. S.; Coelho, M. A. Z. Toxicity of Ionic Liquids toward Microorganisms Interesting to the Food Industry. *RSC Adv.* **2014**, *4* (70), 37157–37163. https://doi.org/10.1039/c4ra05295a.

(8) Abbott, A. P.; Boothby, D.; Capper, G.; Davies, D. L.; Rasheed, R. K. Deep Eutectic Solvents Formed between Choline Chloride and Carboxylic Acids: Versatile Alternatives to Ionic Liquids. *J. Am. Chem. Soc.* **2004**, *126* (29), 9142–9147. https://doi.org/10.1021/ja048266j.

(9) Smith, E. L.; Abbott, A. P.; Ryder, K. S. Deep Eutectic Solvents (DESs) and Their Applications. *Chem. Rev.* **2014**, *114* (21), 11060–11082. https://doi.org/10.1021/cr300162p.

(10) Abbott, A. P.; Capper, G.; Davies, D. L.; Munro, H. L.; Rasheed, R. K.; Tambyrajah, V. Preparation of Novel, Moisture-Stable, Lewis-Acidic Ionic Liquids Containing Quaternary Ammonium Salts with Functional Side Chains. *Chem. Commun.* **2001**, *1*

(19), 2010–2011. https://doi.org/10.1039/b106357j.

(11) Fernandez, L.; Silva, L. P.; Martins, M. A. R.; Ferreira, O.; Ortega, J.; Pinho, S. P.; Coutinho, J. A. P. Indirect Assessment of the Fusion Properties of Choline Chloride from Solid-Liquid Equilibria Data. *Fluid Phase Equilib.* **2017**, *448*, 9–14. https://doi.org/10.1016/j.fluid.2017.03.015.

(12) Zhao, X.; Zhu, G.; Jiao, L.; Yu, F.; Xie, C. Formation and Extractive Desulfurization Mechanisms of Aromatic Acid Based Deep Eutectic Solvents: An Experimental and Theoretical Study. *Chem. - A Eur. J.* **2018**, *24* (43), 11021–11032. https://doi.org/10.1002/chem.201801631.

(13) Mishra, D. K.; Pugazhenthi, G.; Banerjee, T. Ionic Liquid-Based Deep Eutectic Solvent as Reaction Media for the Thermal Dehydrogenation of Ethylene Diamine- Bis -Borane . *ACS Sustain. Chem. Eng.* **2020**, *8* (12), 4910–4919. https://doi.org/10.1021/acssuschemeng.0c00220.

(14) Häkkinen, R.; Abbott, A. Solvation of Carbohydrates in Five Choline Chloride-Based Deep Eutectic Solvents and the Implication for Cellulose Solubility. *Green Chem.* **2019**, *21* (17), 4673–4682. https://doi.org/10.1039/c9gc00559e.

(15) Perkins, S. L.; Painter, P.; Colina, C. M. Experimental and Computational Studies of Choline Chloride-Based Deep Eutectic Solvents. *J. Chem. Eng. Data* **2014**, *59* (11), 3652–3662. https://doi.org/10.1021/je500520h.

(16) Sun, H.; Li, Y.; Wu, X.; Li, G. Theoretical Study on the Structures and Properties of Mixtures of Urea and Choline Chloride. *J. Mol. Model.* **2013**, *19* (6), 2433–2441. https://doi.org/10.1007/s00894-013-1791-2.

(17) Zhekenov, T.; Toksanbayev, N.; Kazakbayeva, Z.; Shah, D.; Mjalli, F. S. Formation of Type III Deep Eutectic Solvents and Effect of Water on Their Intermolecular Interactions. *Fluid Phase Equilib.* **2017**, *441*, 43–48. https://doi.org/10.1016/j.fluid.2017.01.022.

(18) Perkins, S. L.; Painter, P.; Colina, C. M. Molecular Dynamic Simulations and Vibrational Analysis of an Ionic Liquid Analogue. *J. Phys. Chem. B* **2013**, *117* (35), 10250–10260. https://doi.org/10.1021/jp404619x.

(19) Zahn, S.; Kirchner, B.; Mollenhauer, D. Charge Spreading in Deep Eutectic Solvents.

ChemPhysChem **2016**, *17* (21), 3354–3358. https://doi.org/10.1002/cphc.201600348.

(20) Wagle, D. V.; Baker, G. A.; Mamontov, E. Differential Microscopic Mobility of Components within a Deep Eutectic Solvent. *J. Phys. Chem. Lett.* **2015**, *6* (15), 2924–2928. https://doi.org/10.1021/acs.jpclett.5b01192.

(21) Wagle, D. V.; Deakyne, C. A.; Baker, G. A. Quantum Chemical Insight into the Interactions and Thermodynamics Present in Choline Chloride Based Deep Eutectic Solvents. *J. Phys. Chem. B* **2016**, *120* (27), 6739–6746. https://doi.org/10.1021/acs.jpcb.6b04750.

(22) García, G.; Atilhan, M.; Aparicio, S. An Approach for the Rationalization of Melting Temperature for Deep Eutectic Solvents from DFT. *Chem. Phys. Lett.* **2015**, *634*, 151–155. https://doi.org/10.1016/j.cplett.2015.06.017.

(23) Zhang, C.; Jia, Y.; Jing, Y.; Wang, H.; Hong, K. Main Chemical Species and Molecular Structure of Deep Eutectic Solvent Studied by Experiments with DFT Calculation: A Case of Choline Chloride and Magnesium Chloride Hexahydrate. *J. Mol. Model.* **2014**, *20* (8). https://doi.org/10.1007/s00894-014-2374-6.

(24) Vigier, K. D. O.; Chatel, G.; Jérôme, F. Contribution of Deep Eutectic Solvents for Biomass Processing: Opportunities, Challenges, and Limitations. *ChemCatChem* **2015**, *7* (8), 1250–1260. https://doi.org/10.1002/cctc.201500134.

(25) Lin, Y. F.; Sun, I. W. Electrodeposition of Zinc from a Lewis Acidic Zinc Chloride-1-Ethyl-3-Methylimidazolium Chloride Molten Salt. *Electrochim. Acta* **1999**, *44* (16), 2771–2777. https://doi.org/10.1016/S0013-4686(99)00003-1.

(26) Abbott, A. P.; Capper, G.; Davies, D. L.; Rasheed, R. Ionic Liquids Based upon Metal Halide/Substituted Quaternary Ammonium Salt Mixtures. *Inorg. Chem.* **2004**, *43* (11), 3447–3452. https://doi.org/10.1021/ic049931s.

(27) Abranches, D. O.; Schaeffer, N.; Silva, L. P.; Martins, M. A. R.; Pinho, S. P.; Coutinho, J. A. P. The Role of Charge Transfer in the Formation of Type i Deep Eutectic Solvent-Analogous Ionic Liquid Mixtures. *Molecules* **2019**, *24* (20). https://doi.org/10.3390/molecules24203687.

(28) Becke, A. D. Density-Functional Exchange-Energy Approximation with Correct Asymptotic Behavior. *Phys. Rev. A* **1988**, *38* (6), 3098.

(29) Perdew, J. P. Density-Functional Approximation for the Correlation Energy of the Inhomogeneous Electron Gas. *Phys. Rev. B* **1986**, *33* (12), 8822.

(30) Schäfer, A.; Horn, H.; Ahlrichs, R. Fully Optimized Contracted Gaussian Basis Sets for Atoms Li to Kr. *J. Chem. Phys.* **1992**, *97* (4), 2571–2577. https://doi.org/10.1063/1.463096.

(31) Weigend, F.; Ahlrichs, R. Balanced Basis Sets of Split Valence, Triple Zeta Valence and Quadruple Zeta Valence Quality for H to Rn: Design and Assessment of Accuracy. *Phys. Chem. Chem. Phys.* **2005**, *7* (18), 3297–3305. https://doi.org/10.1039/b508541a.

(32) Van Lenthe, E.; Baerends, E. J.; Snijders, J. G. Relativistic Total Energy Using Regular Approximations. *J. Chem. Phys.* **1994**, *101* (11), 9783–9792. https://doi.org/10.1063/1.467943.

(33) Van Lenthe, E.; Snijders, J. G.; Baerends, E. J. The Zero-Order Regular Approximation for Relativistic Effects: The Effect of Spin-Orbit Coupling in Closed Shell Molecules. *J. Chem. Phys.* **1996**, *105* (15), 6505–6516. https://doi.org/10.1063/1.472460.

(34) Pantazis, D. A.; Neese, F. All-Electron Scalar Relativistic Basis Sets for the Actinides. *J. Chem. Theory Comput.* **2011**, *7* (3), 677–684. https://doi.org/10.1021/ct100736b.

(35) Sierka, M.; Hogekamp, A.; Ahlrichs, R. Fast Evaluation of the Coulomb Potential for Electron Densities Using Multipole Accelerated Resolution of Identity Approximation. *J. Chem. Phys.* **2003**, *118* (20), 9136–9148. https://doi.org/10.1063/1.1567253.

(36) Weigend, F. A Fully Direct RI-HF Algorithm: Implementation, Optimised Auxiliary Basis Sets, Demonstration of Accuracy and Efficiency. *Phys. Chem. Chem. Phys.* **2002**, *4* (18), 4285–4291. https://doi.org/10.1039/b204199p.

(37) Weigend, F.; Köhn, A.; Hättig, C. Efficient Use of the Correlation Consistent Basis Sets in Resolution of the Identity MP2 Calculations. *J. Chem. Phys.* **2002**, *116* (8), 3175–3183. https://doi.org/10.1063/1.1445115.

(38) Grimme, S.; Antony, J.; Ehrlich, S.; Krieg, H. A Consistent and Accurate Ab Initio Parametrization of Density Functional Dispersion Correction (DFT-D) for the 94 Elements H-Pu. *J. Chem. Phys.* **2010**, *132* (15). https://doi.org/10.1063/1.3382344.

(39) Grimme, S.; Ehrlich, S.; Goerigk, L. Effect of the Damping Function in Dispersion Corrected Density Functional Theory. *J. Comput. Chem.* **2011**, *32* (7), 1456–1465.

(40) Boys, S. F.; Bernardi, F. The Calculation of Small Molecular Interactions by the Differences of Separate Total Energies. Some Procedures with Reduced Errors. *Mol. Phys.* **1970**, *19* (4), 553–566. https://doi.org/10.1080/00268977000101561.

(41) Neese, F. The ORCA Program System. *Wiley Interdiscip. Rev. Comput. Mol. Sci.* **2012**, *2* (1), 73–78. https://doi.org/10.1002/wcms.81.

(42) Glendening, E. D.; Landis, C. R.; Weinhold, F. NBO 6.0: Natural Bond Orbital Analysis Program. *J. Comput. Chem.* **2013**, *34* (16), 1429–1437. https://doi.org/10.1002/jcc.23266.

(43) Lu, T.; Chen, F. Multiwfn: A Multifunctional Wavefunction Analyzer. *J. Comput. Chem.* **2012**, *33* (5), 580–592. https://doi.org/10.1002/jcc.22885.

(44) Hjortås, J.; Sørum, H. A Re-Investigation of the Crystal Structure of Choline Chloride. *Acta Crystallogr. Sect. B Struct. Crystallogr. Cryst. Chem.* **1971**, *27* (7), 1320–1323. https://doi.org/10.1107/s0567740871003935.

(45) Carriazo, D.; Serrano, M. C.; Gutiérrez, M. C.; Ferrer, M. L.; del Monte, F. Deep-Eutectic Solvents Playing Multiple Roles in the Synthesis of Polymers and Related Materials. *Chem. Soc. Rev.* **2012**, *41* (14), 4996–5014. https://doi.org/10.1039/c2cs15353j.

(46) Meot-Ner, M. The Ionic Hydrogen Bond. *Chem. Rev.* **2005**, *105* (1), 213–284. https://doi.org/10.1021/cr9411785.

(47) Solimannejad, M.; Alkorta, I.; Elguero, J. Stabilities and Properties of O3-HOCl Complexes: A Computational Study. *Chem. Phys. Lett.* **2007**, *449* (1–3), 23–27. https://doi.org/10.1016/j.cplett.2007.10.024.

(48) Robert G. Parr, W. Y. Density-Functional Theory of the Electronic. *Annu. Rev. Phys. Chem.* **1995**, *46*, 701–728.

(49) Johnson, E. R.; Keinan, S.; Mori-Sánchez, P.; Contreras-García, J.; Cohen, A. J.; Yang, W. Revealing Noncovalent Interactions. *J. Am. Chem. Soc.* **2010**, *132* (18), 6498–6506. https://doi.org/10.1021/ja100936w.

(50) Marekha, B. A.; Kalugin, O. N.; Idrissi, A. Non-Covalent Interactions in Ionic Liquid Ion Pairs and Ion Pair Dimers: A Quantum Chemical Calculation Analysis. *Phys. Chem. Chem. Phys.* **2015**, *17* (26), 16846–16857. https://doi.org/10.1039/c5cp02197a.

(51) Kumar, P. S.; Vasudevan, K.; Prakasam, A.; Geetha, M.; Anbarasan, P. M. Quantum Chemistry Calculations of 3-Phenoxyphthalonitrile Dye Sensitizer for Solar Cells. *Spectrochim. Acta - Part A Mol. Biomol. Spectrosc.* **2010**, *77* (1), 45–50. https://doi.org/10.1016/j.saa.2010.04.021.

(52) Fukui, K. Theory of Orientation and Stereoselection. In *Orientation and Stereoselection*; Springer, 1970; pp 1–85.

(53) Bader, R. F. W.; Bader, R. F. *Atoms in Molecules: A Quantum Theory*; International series of monographs on chemistry; Clarendon Press, 1990.

(54) Abbott, A. P.; Capper, G.; Davies, D. L.; Munro, H. L.; Rasheed, R. K.; Tambyrajah, V. Preparation of Novel, Moisture-Stable, Lewis-Acidic Ionic Liquids Containing Quaternary Ammonium Salts with Functional Side Chains. *Chem. Commun.* **2001**, *1* (19), 2010–2011. https://doi.org/10.1039/b106357j.

(55) Zhao, Y.; Truhlar, D. G. The M06 Suite of Density Functionals for Main Group Thermochemistry, Thermochemical Kinetics, Noncovalent Interactions, Excited States, and Transition Elements: Two New Functionals and Systematic Testing of Four M06-Class Functionals and 12 Other Functionals. *Theor. Chem. Acc.* **2008**. https://doi.org/10.1007/s00214-007-0310-x.

(56) Trujillo, S. A.; Peña-Solórzano, D.; Bejarano, O. R.; Ochoa-Puentes, C. Tin(Ii) Chloride Dihydrate/Choline Chloride Deep Eutectic Solvent: Redox Properties in the Fast Synthesis of: N -Arylacetamides and Indolo(Pyrrolo)[1,2- a] Quinoxalines. *RSC Adv.* **2020**, *10* (66), 40552–40561. https://doi.org/10.1039/d0ra06871c.

(57) Duan, Z.; Gu, Y.; Deng, Y. Green and Moisture-Stable Lewis Acidic Ionic Liquids (Choline Chloride · XZnCl2) Catalyzed Protection of Carbonyls at Room Temperature under Solvent-Free Conditions. *Catal. Commun.* **2006**, *7* (9), 651–656. https://doi.org/10.1016/j.catcom.2006.02.008.

(58) Bankiewicz, B.; Matczak, P.; Palusiak, M. Electron Density Characteristics in Bond Critical Point (QTAIM) versus Interaction Energy Components (SAPT): The Case of Charge-Assisted Hydrogen Bonding. *J. Phys. Chem. A* **2012**, *116* (1), 452–459. https://doi.org/10.1021/jp210940b.

(59) Hansen, B. B.; Spittle, S.; Chen, B.; Poe, D.; Zhang, Y.; Klein, J. M.; Horton, A.;

Adhikari, L.; Zelovich, T.; Doherty, B. W.; et al. Deep Eutectic Solvents: A Review of Fundamentals and Applications. Chem. Rev. 2021, 121 (3), 1232–1285. https://doi.org/10.1021/acs.chemrev.0c00385.

(60) Ashworth, C. R.; Matthews, R. P.; Welton, T.; Hunt, P. A. Doubly Ionic Hydrogen Bond Interactions within the Choline Chloride-Urea Deep Eutectic Solvent. *Phys. Chem. Chem. Phys.* **2016**, *18* (27), 18145–18160. https://doi.org/10.1039/c6cp02815b.

(61) Zhu, Z.; Lü, H.; Zhang, M.; Yang, H. Deep Eutectic Solvents as Non-Traditionally Multifunctional Media for the Desulfurization Process of Fuel Oil. *Phys. Chem. Chem. Phys.* **2021**, *23* (2), 785–805. https://doi.org/10.1039/d0cp05153e.

(62) Jahanbakhsh Bonab, P.; Rastkar Ebrahimzadeh, A.; Jahanbin Sardroodi, J. Insights into the Interactions and Dynamics of a DES Formed by Phenyl Propionic Acid and Choline Chloride. *Sci. Rep.* **2021**, *11* (1). https://doi.org/10.1038/s41598-021-85260-z.

Chapter 4

Deep Eutectic Solvents as Novel Solvent-cum-Catalyst Media for Thermal Dehydrogenation of Amine Boranes

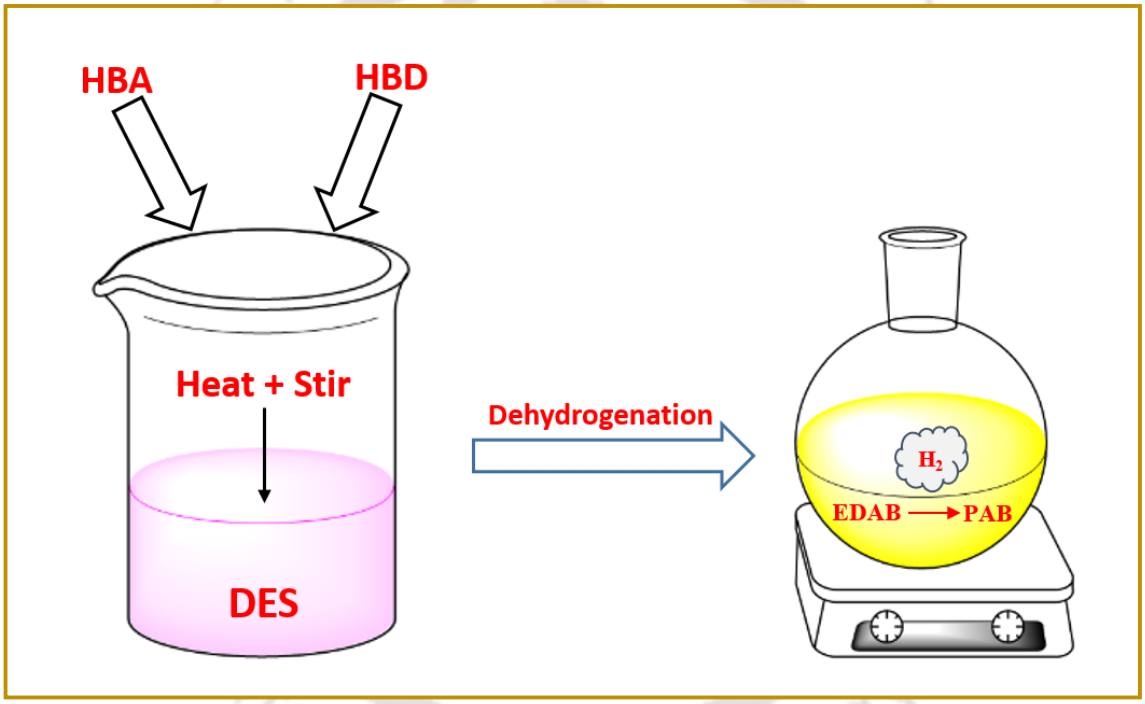

4.1. Chapter Abstract

The current chapter explores the usage of novel synthesized Deep Eutectic Solvent (DES) as a catalyst cum solvent media for the thermal dehydrogenation of chemical hydrides, namely Ammonia Borane (AB) and Ethylene diamine bisborane (EDAB). The chapter is organized into two sections; the first section investigates the thermal dehydrogenation of amine boranes utilizing type 3 Deep Eutectic Solvents; the second section investigates the dehydrogenation of amine boranes employing type 1 metal salt-based Deep Eutectic Solvents. In the first instance, the quantum chemistry-based COSMO-SAC (COnductor like Screening MOdel Segment Activity Coefficient) model was used for the selection of the pertinent solvent. 1-Butyl-3-methylimidazolium methanesulfonate: Imidazole ([BMIM][$MeSO_3$]:[Im]) (DES1), and 1-Butyl-3-methylimidazolium methanesulfonate: Urea ([BMIM][$MeSO_3$]:[Urea]) (DES2) turned out to be an ideal eutectic mixture with the highest predicted solubility with amine boranes. The DESs were synthesized by combining the hydrogen bond acceptor (HBA), 1-Butyl-3-methylimidazolium methanesulfonate, with imidazole and urea as the hydrogen bond donor (HBD) in a molar ratio of 1:2 and 1:1 at T=70°C. The formation of DES was confirmed by recording the NMR spectra.

Further, the thermal dehydrogenation study was performed at a vacuum of 4×10^{-2} mbar (gauge pressure) of AB/DES1 and EDAB/DES1 systems at 105°C, where a hydrogen equivalent of 1.40 and 2.55 was produced, respectively. In the next instance, a comparative study between Ionic Liquids (ILs) along with the DES2 for the thermal dehydrogenation of Ethylene diamine bisborane (EDAB) was performed. It was observed that the EDAB/DES2 system produced 3.2 equivalents of hydrogen with a lower induction time when compared to 3.7 equivalents of hydrogen at the same temperature (105°C) for the IL-based solvent. The residual samples were further analyzed through ^{1}H NMR analysis for the reaction mechanism and to confirm the role of ionic liquid-based DES as catalyst cum solvent media. ^{11}B NMR

analysis was further performed in order to confirm the existence of sp^2 boron moieties. In the second section of the chapter, metal salt-based DESs were employed to examine the role of type 1 based DESs in the dehydrogenation of amine boranes.

4.2. Introduction

With the advent of room temperature ionic liquids, the quest for alternative solvents has not lessened, and in the year 2003, Abbott et al. proposed one possible candidate which could replace the room temperature ionic liquids due to their easy synthesis, no generation of by-products, and low material costs making them highly economical.[1] DES is basically derived from the combination of two safe naturally occurring components (cheap, sustainable, and biodegradable) that can together form a eutectic mixture due to the reduction of excess Gibbs's free energies by the formation of hydrogen bond interactions.[2] This reduces the anion-cation interaction and thus lowers the melting point.[3] DES is typically obtained through the mixture of quaternary ammonium salt, which is the Hydrogen Bond Acceptor (HBA), and a Hydrogen Bond Donor (HBD) that has the ability to form a complex with the ammonium salt-halide anion. DES has advantages which are the same as that of IL's.[4]

The use of DES in the application of hydrogen storage and generation as additives or solvents has not been studied so far in recent years. Because of their low thermal stability compared to the traditional ILs, they are still unused in hydrogen storage applications. Deep Eutectic Solvents (DESs) with ionic liquids or salts as the HBA combined with a suitable HBD, which has substantial thermal stability compared to the traditional ILs, have been developed to counter the detriment as mentioned earlier.[5] Nevertheless, the thermal stability of a standard DES is lower than that of an IL. Therefore, an enormous scope is possible to look for a polar and highly thermal DES for thermal dehydrogenation of amine borane complexes.

This chapter reports the use of Ionic Liquid-based Deep Eutectic Solvents (IL-based DESs) as an additive for the dehydrogenation of amine borane derivatives for hydrogen

generation as ionic liquids are known to facilitate the formation of polar and ionic intermediates. The less investigated IL-based DESs have shown significant potential in a few applications to date and demonstrated various possibilities of working with them. Till date there are limited studies that describe the use of [$MeSO_3^-$] anions as eutectic solvents for ammonia sorption and CO_2 absorption.[6] From the literature, the ammonia sorption by methanesulfonate anion-based IL was found to be of the order of 0.9 g mol/ILs. A significant amount of CO_2 solubility ranged between 0.98 to 2.36 mol/kg within the same cation with the increasing length of the alkyl chains. In order to form a safe DES, [BMIM][$MeSO_3$] as HBA was combined with the economical and readily available HBDs such as urea. It should be noted that the addition of other groups such as carboxylic acid or phenols possesses disadvantages which include difficulty in recycling and its inherent toxic behavior. From the literature, the highest thermal dehydrogenation capacities were observed in the solution phase by the introduction of IL's containing imidazolium cations with anions such as [OAc^-], [HSO_4^-], [Cl^-], [Br^-].[7] Due to its remarkable mean β-value of 0.77, methanesulfonate-based Ionic liquids was preferred in this work as a hydrogen bond acceptor. The other reason is its significant ability to form hydrogen bond interactions with proton donors such as carboxylic acids, amides, and alcohols.[8]

On the other hand, the ionic characteristics of type 1 metal salt-based DESs have piqued the curiosity of researchers who are interested in using them as solvent media for a variety of applications.[9,10,11] Due to their strong polarity, metal halide-based DESs exhibit exceptional solvation properties and can be used as high-temperature electrolytes, reusable or homogenous catalysts, or as a solvent in biodiesel applications.[12] This demonstrates the broad industrial spectrum in which they can[13] play critical roles.[14,15] ChCl: $ZnCl_2$ DESs were effectively used in the transesterification of soybean to biodiesel as a low-cost and moisture-stable benign solvent. The synthesis of biodiesel utilizing zinc chloride-based DESs was shown to be

preferable to traditional ILs due to the ease with which they were prepared. Furthermore, several research groups have used metal halide-based DESs as an electrolyte in lithium-ion batteries, electric double-layer capacitors, and electrolytic media in the electropolishing of metals.[16,17]

A systematic strategy for the choice of potentially capable ILs and DESs for the dehydrogenation of AB and EDAB based on its solubility is provided in this chapter, followed by the preparation of the DES. To validate the efficacy of DES as a catalytic solvent media, a DES-induced thermal dehydrogenation experiment of AB and EDAB was conducted, revealing that DES is also similarly effective at thermal dehydrogenation of amine boranes. Later, because of EDAB's high hydrogen content, the particular hydride was used to study a more in-depth experimental approach for the same process. To predict the solubility of EDAB in ILs and DESs, COSMO-SAC model was implemented.[18] Based on the COSMO-SAC screening of a number of DES combinations, one with the highest solubility of AB and EDAB was chosen for the dehydrogenation experiment. In the present work, methanesulfonate-based DESs were chosen for dehydrogenation of the EDAB complex, and further, a comparative study with its analogue IL was made. The DES mixtures were prepared using the methanesulfonate-based IL as hydrogen bond acceptor (HBA) along with hydrogen bond donor (HBD), namely imidazole and urea.[6] The formation of the synthesized DES was analyzed using the proton NMR technique. The residual reaction mixture was characterized by ^{1}H and ^{11}B nuclear magnetic resonance (^{1}H and ^{11}B NMR) before and after dehydrogenation. Using type 1 metal salt-based DESs, a similar dehydrogenation investigation on the amine boranes was carried out in the emanating section.

4.3. Computational Details

4.3.1. Screening of IL-based Deep Eutectic Solvents

In this chapter, COSMO-SAC model is used for predicting the solubility of AB/EDAB in DESs, which can be used for amine borane complex dehydrogenation. These approaches can be helpful in examining the burgeoning set of DESs or HBA and HBD to find the applicable candidates in certain applications or to model some new DES for specific applications. Using GaussView 5.0 visualization package, the initial structures of AB, EDAB and DESs were drawn.[19] The geometry of all compounds was optimized at B3LYP level and 6-311++G(d) basis set using the Gaussian 09 package.[20,21,22] From the optimized geometry of all species, a single point energy calculation was performed with another set of DFT calculations using BVP86 level of theory for the generation of ***.cosmo*** file.[23] Thereafter ***.cosmo*** file was used to predict the IDAC value (denoted as γ^{∞}). The optimized molecule of DES along with AB and EDAB with the COSMO surface is presented in Figure 4.1. IDAC is a favored descriptor as it measures the deviation of a solution system from its ideal behavior. The solubility of a solute in a solvent can be measured by the logarithmic value of IDAC. AB and EDAB solubility in ILs and DESs is predicted on the basis of the IDAC value as the negative value of logarithmic IDAC denotes solubility whereas positive value denotes insolubility.[24,25]

Among the screen methanesulfonate-based DES, AB and EDAB have the highest solubility in DES1 and DES 2 compared to other methanesulfonate-based DES systems (Figure 4.2). Among the DES combination involving HBD, such as glycerol, ethylene glycol, imidazole, and urea, the higher solubility of [BMIM][$MeSO_3$] + imidazole, and [BMIM][$MeSO_3$] + urea initiated us in selecting the IL+DES combination for the dehydrogenation experiment of AB and EDAB. The abbreviations used for the DES systems studied in this work is as following: DES1 ([BMIM][$MeSO_3$]:Imidazole in a molar ratio of

1:2), DES2 ([BMIM][$MeSO_3$]:Urea in a molar ratio of 1:1), DES3 (ChCl:[$SnCl_2$] in a molar ratio of 1:2), and DES4 (ChCl:[$ZnCl_2$] in a molar ratio of 1:2).

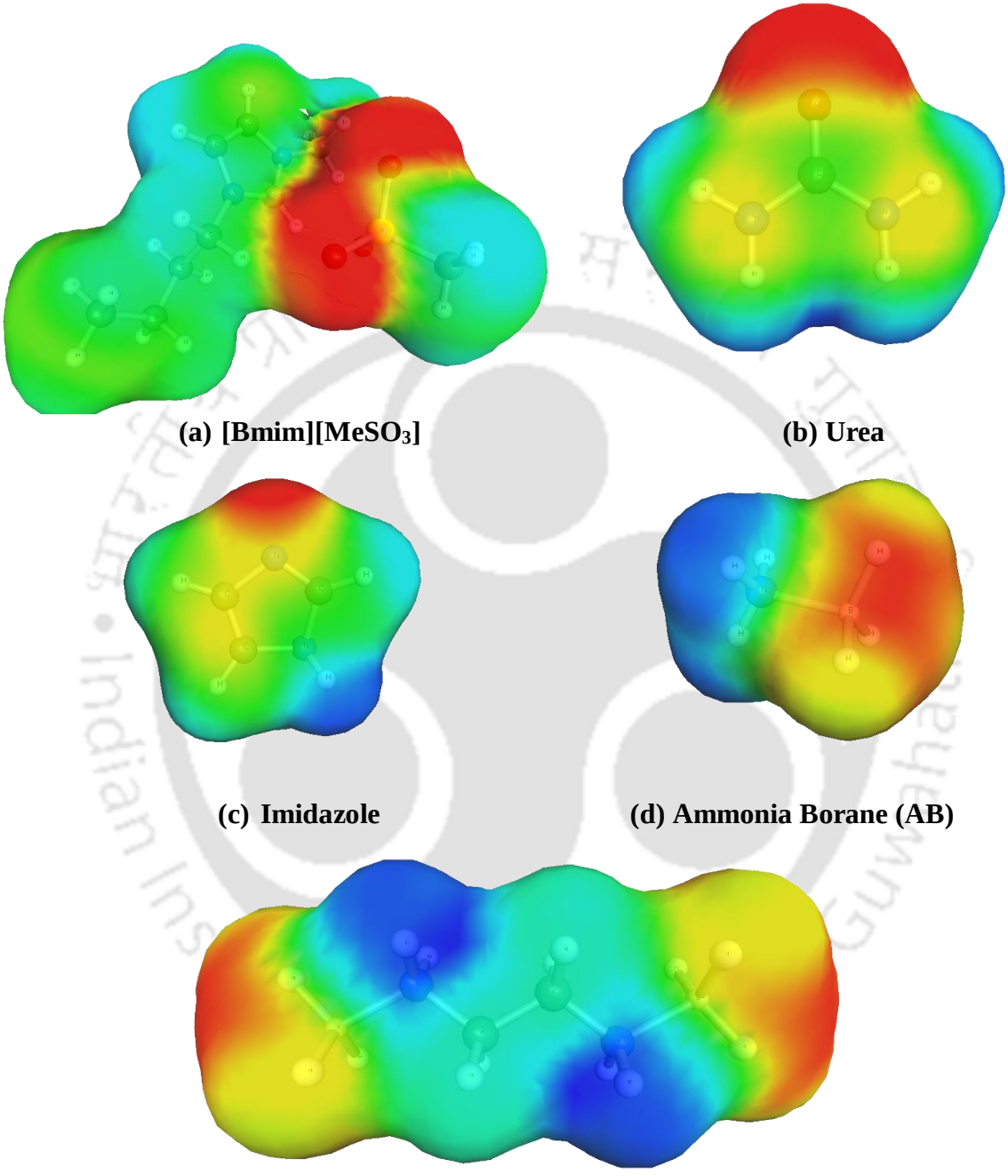

(a) [Bmim][$MeSO_3$] **(b) Urea**

(c) Imidazole **(d) Ammonia Borane (AB)**

(e) Ethylene diamine bisbornae (EDAB)

Figure 4.1: COSMO iso-surfaces generated using Gaussian 09 Package

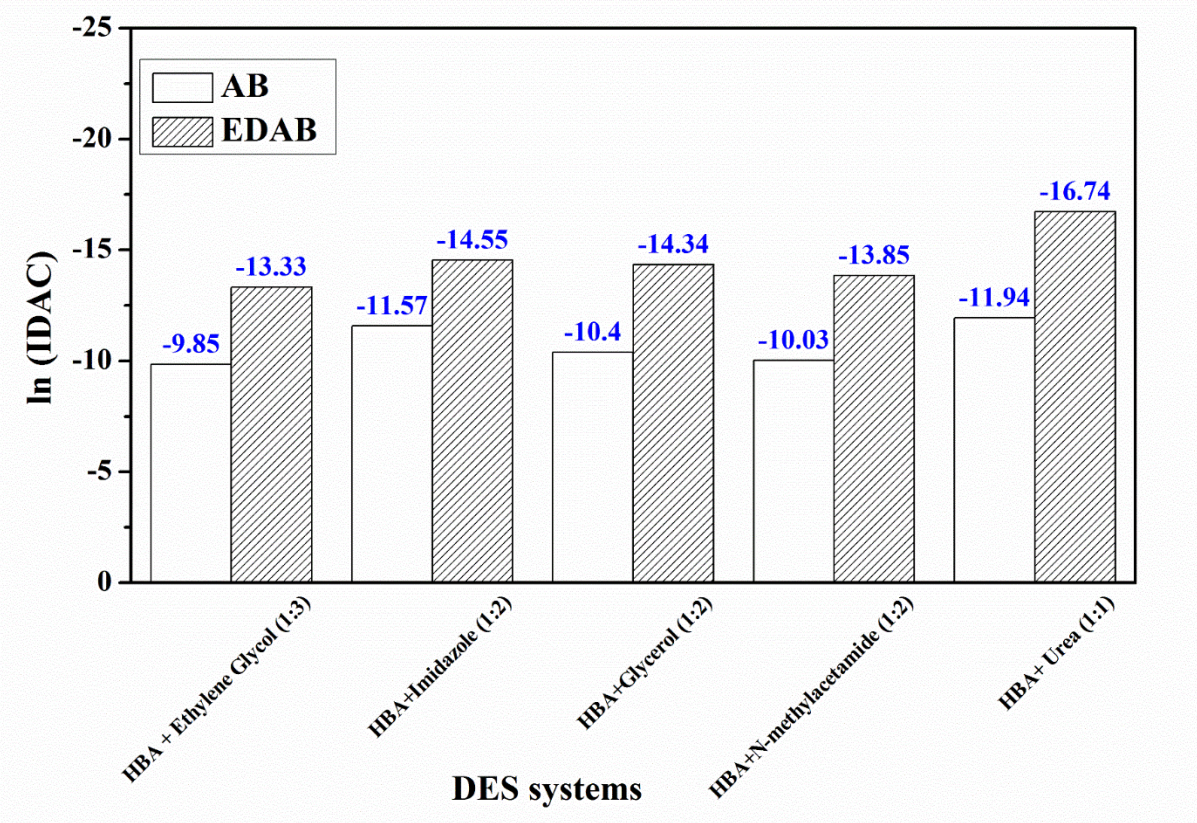

Figure 4.2: COSMO-SAC model predicted logarithmic Infinite dilution activity coefficient of AB and EDAB in DES systems at 298K.

4.4. Experimental Method

4.4.1. Material and Methods

AB (97%), (EDAB) (97%), Urea (99%), Imidazole (99%) and 1-Butyl-3-methylimidazolium methanesulfonate [BMIM][$MeSO_3$] (95%) was purchased from Sigma Aldrich. The chemical hydrides were used without further purification. The IL, [BMIM][$MeSO_3$] was purified by heating in a vacuum oven at 80°C for 24 hours. The structures of the chemical are illustrated in Table 4.1.

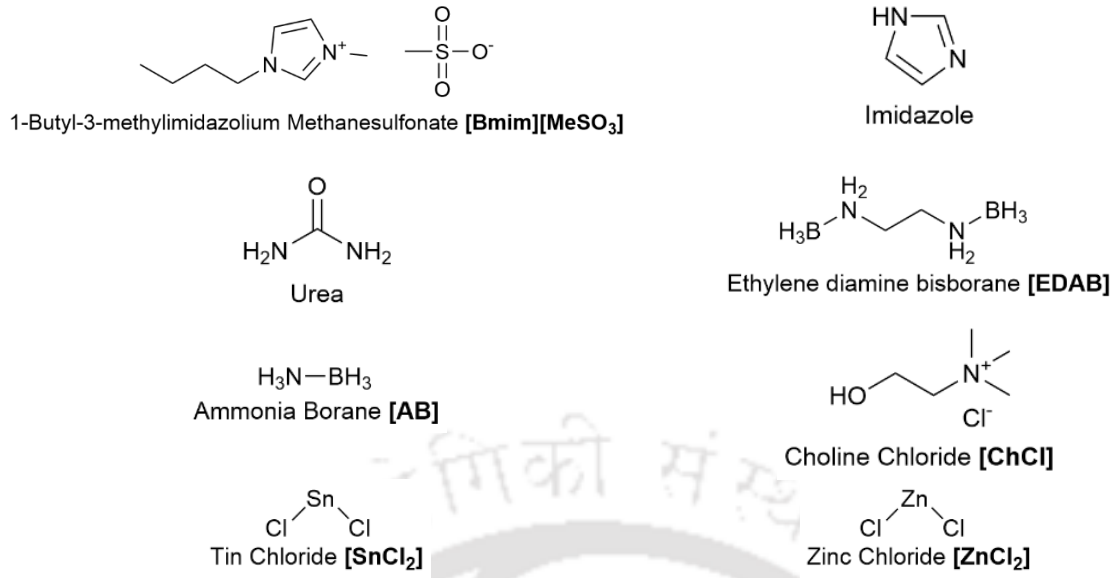

Table 4.1: List of Chemicals used in this study

4.4.2. Preparation of DES

As reported in earlier literature, the DESs were synthesized by combining two compounds, mainly HBA and HBD, in different molar ratios, respectively.[6] Here, the mixture of HBA and HBD was inserted in a 200 mL round bottom flask and was then stirred (500 r/min) and heated at 70 ºC until a uniform colorless liquid was obtained. The used IL and prepared DES were kept for vacuum drying at 70 ºC for 48 hours prior to experimentation. The water content of the synthesized DES was measured using Karl Fischer Titrator (KFT) coulometer (Metrohm 787 KF Titrino). The calculated weight % value of water in the DES is 1.02 for DES1, and 1.43 for DES2, respectively. Thereafter, the structure and purity of the newly synthesized DES were characterized by ^{1}H NMR (600 MHz NMR, Bruker, Germany). NMR Samples were prepared with chloroform ($CDCl_3$-d6) as the solvent.

4.4.3. ^{1}H NMR Characterization of DES

The first step in improving the dehydrogenation experiment is the efficient synthesis of the DES. Figure 4.3 accounts for the full range ^{1}H NMR spectra of pure IL [BMIM][$MeSO_3$]

(Figure 4.3(a)), and DES1 [BMIM][$MeSO_3$]:[Imidazole] (Figure 4.3(b)) predicting the structural feature of the newly synthesized DES1. ^{1}H NMR spectroscopy (Figure 4.3(b)) provides clear evidence about the DES structure, indicating the intermolecular hydrogen bonding between HBA and HBDs, respectively.

Pure IL [BMIM][$MeSO_3$], acting as HBA, has chemical changes attributed to protons of imidazolium cation C(2), C(4), and C(5) position at 9.48, 7.32, and 7.43 ppm. The previously described peaks change slightly downfield with the addition of imidazole, resulting in a reduction of electron density. On the other hand, the upfield shift of imidazole hydrogens in synthesized DES NMR spectra (Figure 4.3(b)) provides sufficient details on hydrogen bonds forming between the anionic part of HBA and HBD molecules.

In a similar vein, ^{1}H NMR spectra was performed to corroborate the formation of DES2. In order to obtain the intermolecular H-H interactions, Nuclear Overhauser Effect Spectroscopy technique (NOESY) was performed for a total number of twelve scans. The NMR spectra of the pure IL and pure DES is given in Figure 4.4 below. The spectra are reported as below:

[BMIM][$MeSO_3$] ^{1}H proton NMR (600 MHz, $CDCl_3$): δ (ppm) 0.70-0.73 (t, 3H, CH_3), 1.14-1.15 (m, 2H, CH_2), 1.63-1.66 (m, 2H, $NCH_2\underline{CH_2}$), 2.51 (m, 3H, $(SO_3)CH_3$), 3.81 (m, 3H, NCH_3), 4.05 (t, 2H, NCH_2), 7.32 (m, 1H, ArH), 7.43 (m, 1H, ArH), 9.48 (m, 1H, ArH).

The additional information on the DES structure can be obtained with ^{1}H proton NMR spectra (Fig.4.4 (b)), which reveals the structural relationship between HBA and the imidazolium salt (HBD). ^{1}H NMR analysis shows a slight change in peaks corresponding to the hydrogens in NCH_2 and [$(SO_3)CH_3$] groups that prove the formation of the hydrogen-bonded complex (DES2) between the HBA (IL) and HBD (Urea).

NOESY spectra is another useful technique based on a spatial mechanism to measure intra and intermolecular distances. Figure 4.5 (a) reveals the ^{1}H-^{1}H NOESY spectrum of the DES between [BMIM][$MeSO_3$] and urea at a molar ratio of 1:1. The interaction within the same molecules is represented by the diagonal peaks, whereas the cross-peaks signals suggest the interaction between the hydrogen of HBA and HBD, respectively. [BMIM][$MeSO_3$] reveals two interactions with Urea i.e. (5.65, 3.5, 0.0) and (2.41, 5.65, 0.0) respectively. The NOESY spectrum of the formed DES indicates a supramolecular structure primarily because of the H-H interactions between the active sites of HBA and HBD molecules.

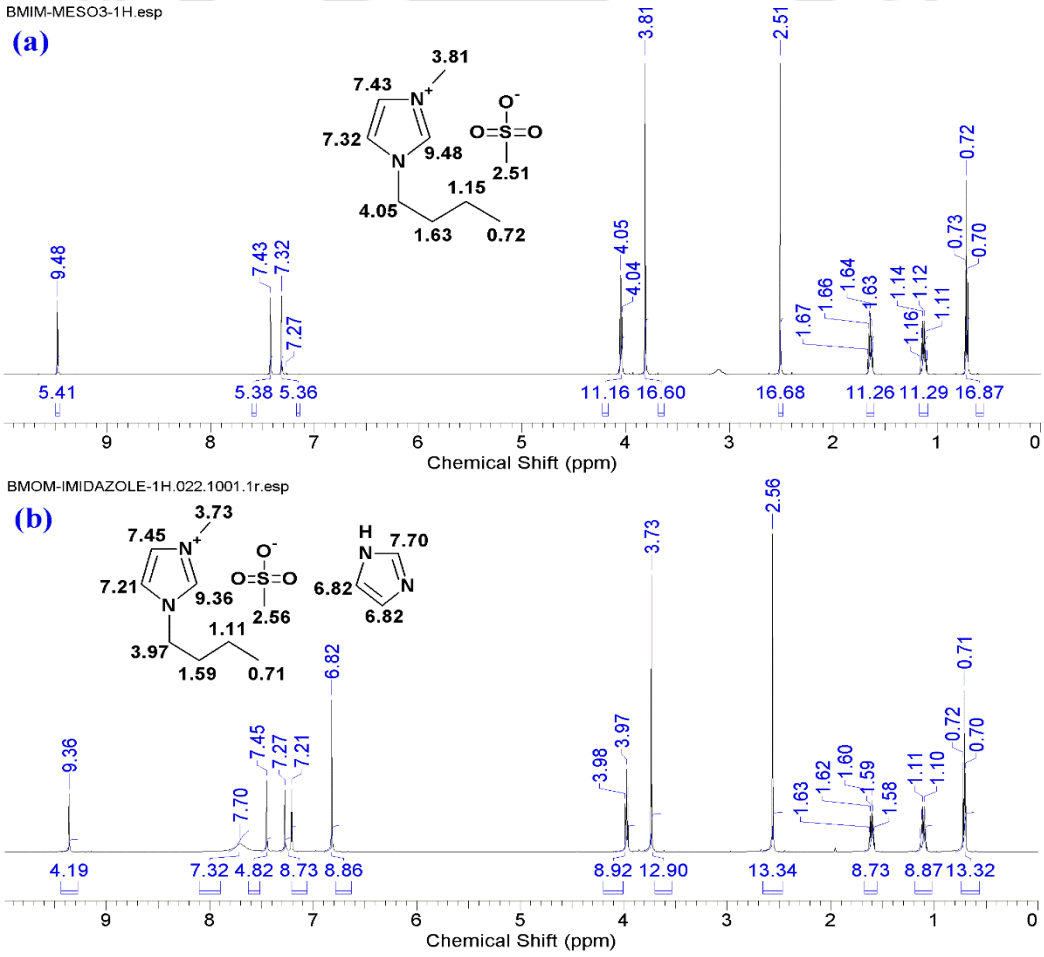

Figure 4.3: Proton NMR spectra of (a) Pure IL [BMIM][$MeSO_3$], and (b) DES1 [BMIM][$MeSO_3$]:[Imidazole]

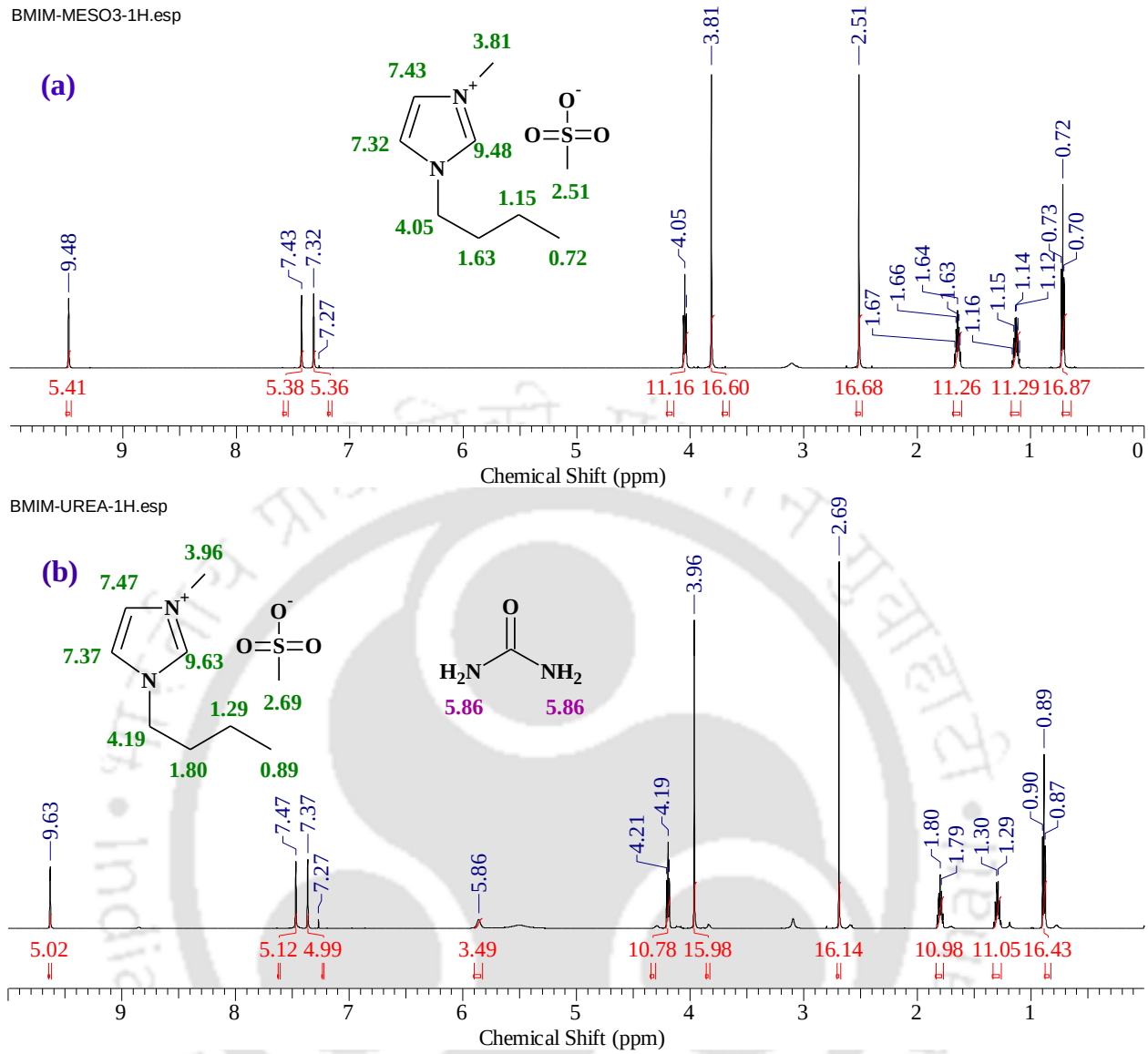

Figure 4.4: Proton NMR spectra of (a) Pure IL [BMIM][$MeSO_3$], and (b) DES2 [BMIM][$MeSO_3$]:[Urea]

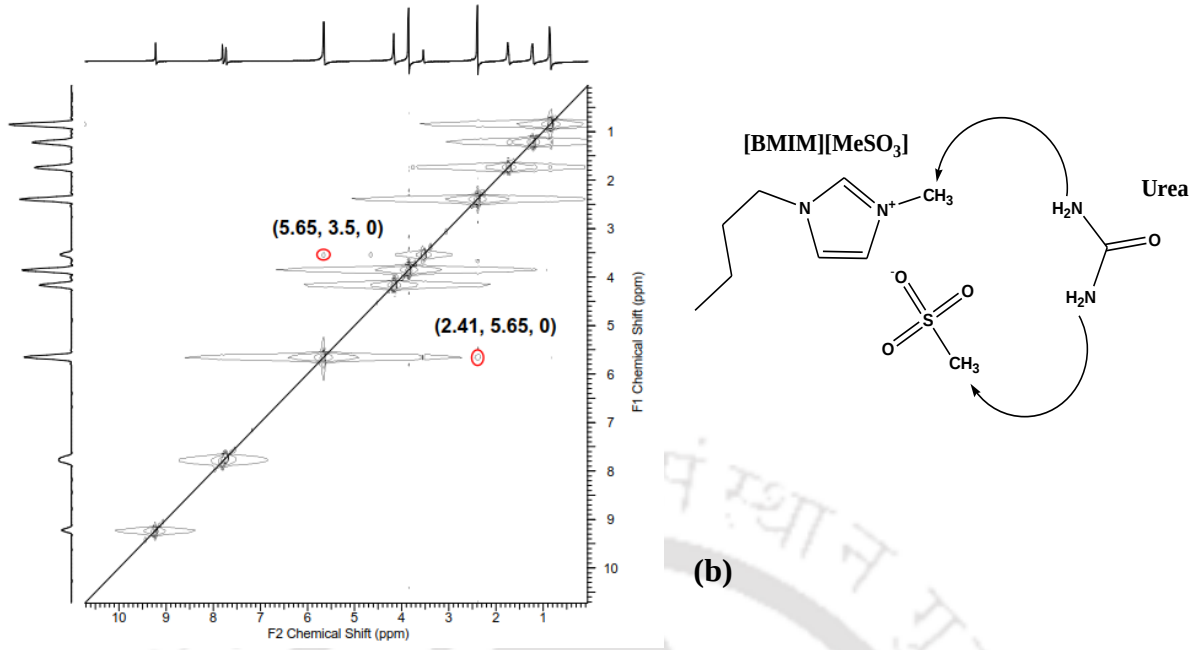

Figure 4.5: (a) NOESY spectrum of DES 2[BMIM][$MeSO_3$]:Urea at 298 K, (b) H-H Interactions

4.4.4. Dehydrogenation Experiment

Comparative dehydrogenation experiments with chemical hydrides, namely AB and EDAB, using the newly synthesized DES, were conducted at a temperature of 90°C, and 105°C at a controlled vacuum pressure of 4.0×10^{-2} mbar. The high vacuum is an integral part of the process as the influence of undesirable materials such as air and humidity is minimized. 15 mg of AB and EDAB along with 0.5 ml of vacuum-dried DES are taken into a round two-necked reactor in an oil bath at 90°C, and 105°C for a standard dehydrogenation run. The specifics of the experimental setup are available in previous chapter 2 (section 2.4.2). For further ^{1}H NMR analysis, the residual product of the dehydrogenation experiment was collected.

4.5. Results and Discussions

4.5.1. Hydrogen Equivalent Production

In our previously mentioned COSMO-SAC predicted IDAC values in section 4.3.1, [BMIM][$MeSO_3$]:[Imidazole] based DES1 was selected as an acceptable DES for the

dehydrogenation experiment. In a comparative analysis of the dehydrogenation of AB and EDAB, the same eutectic mixture was used as a catalyst cum solvent to increase the release of hydrogen equivalents. Thermal dehydrogenation of both chemical hydrides AB and EDAB was investigated systematically at 105°C. The operating temperature is nearly around the melting point of AB and EDAB, which is around 106°C and 116°C, respectively.

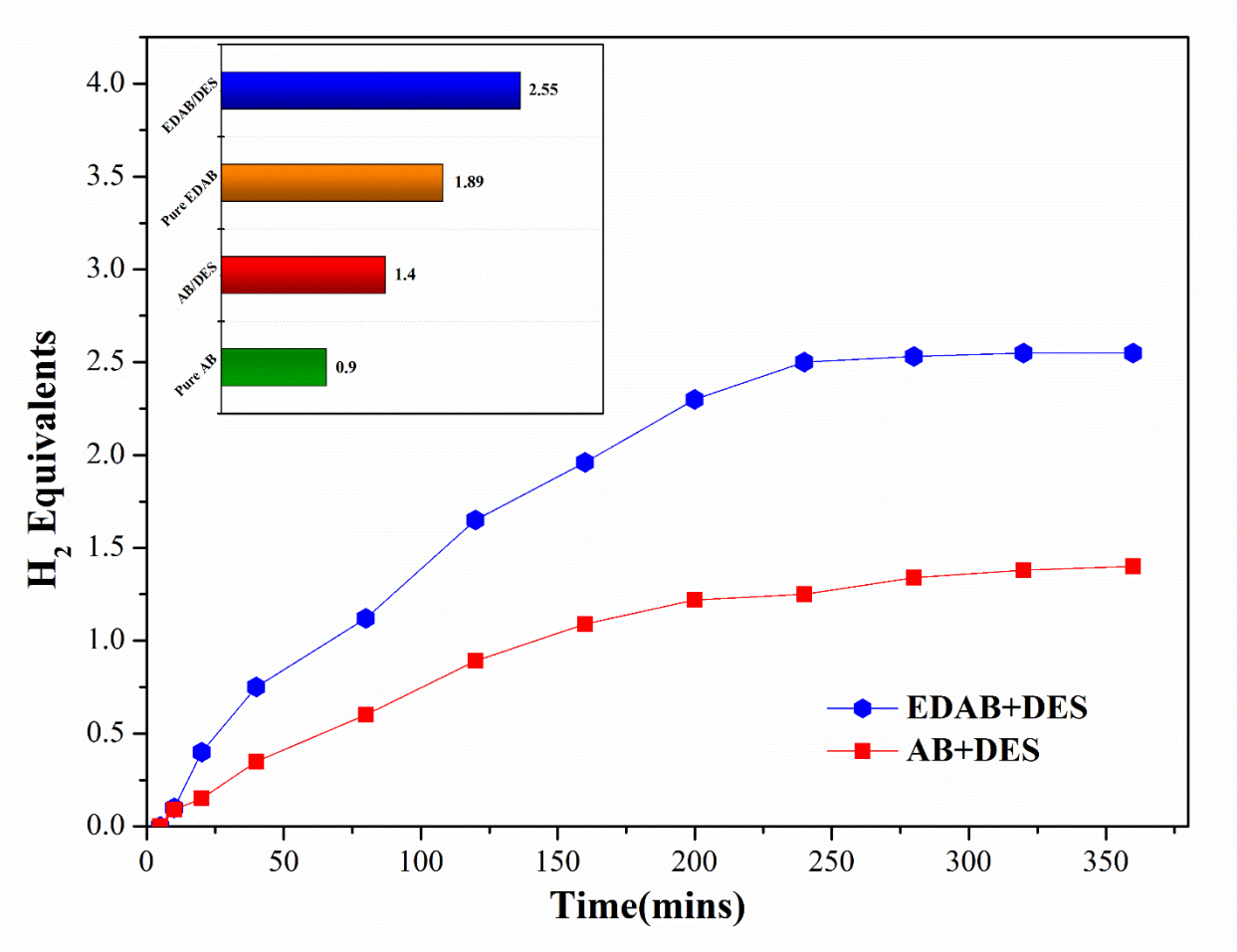

Figure 4.6: Summary of Cumulative hydrogen equivalents released at 105°C of EDAB/DES1 system, AB/DES1 system

The solid dehydrogenation of pure AB and EDAB releases 0.90 and 1.89 cumulative equivalents of hydrogen (Figure 4.7). It should be noted that for AB and EDAB, a maximum of 3 and 4 equivalents of hydrogen gas is possible. In our case with DES1 and 360 minutes of dehydrogenation, AB/DES1 system was able to release a total of 1.40 hydrogen equivalents, while in EDAB/DES1 system, 2.55 hydrogen equivalents were observed with a cumulative run

time of 250 minutes (Figure 4.6). It is noted that in its solid-state decomposition, the dehydrogenation of both AB and EDAB has an induction period, which is suppressed by the usage of deep eutectic solvent (DES). In contrast to the AB/DES1 system, the hydrogen yield of the EDAB/DES1 system is comparatively higher. The residual product of the dehydrogenation experiment was collected to perform a ^{1}H NMR analysis, which was enacted to elucidate the effect of the newly designed DES as a catalytic solvent in the dehydrogenation process. However, the absence of the NH_2 moiety ensures that EDAB is involved in the reaction that initiates the pathway for hydrogen release and that DES maintains its original structural entity (Figure 4.8(b)). This exemplifies the advantage of using DESs for the dehydrogenation of chemical hydrides. In chapter 2, a detailed reaction mechanism was proposed using an AB and EDAB as chemical hydrides with various IL systems, which is similar to the predicted reaction mechanism of IL-based DES-assisted dehydrogenation of hydrides reported in this chapter (Scheme 4.1).

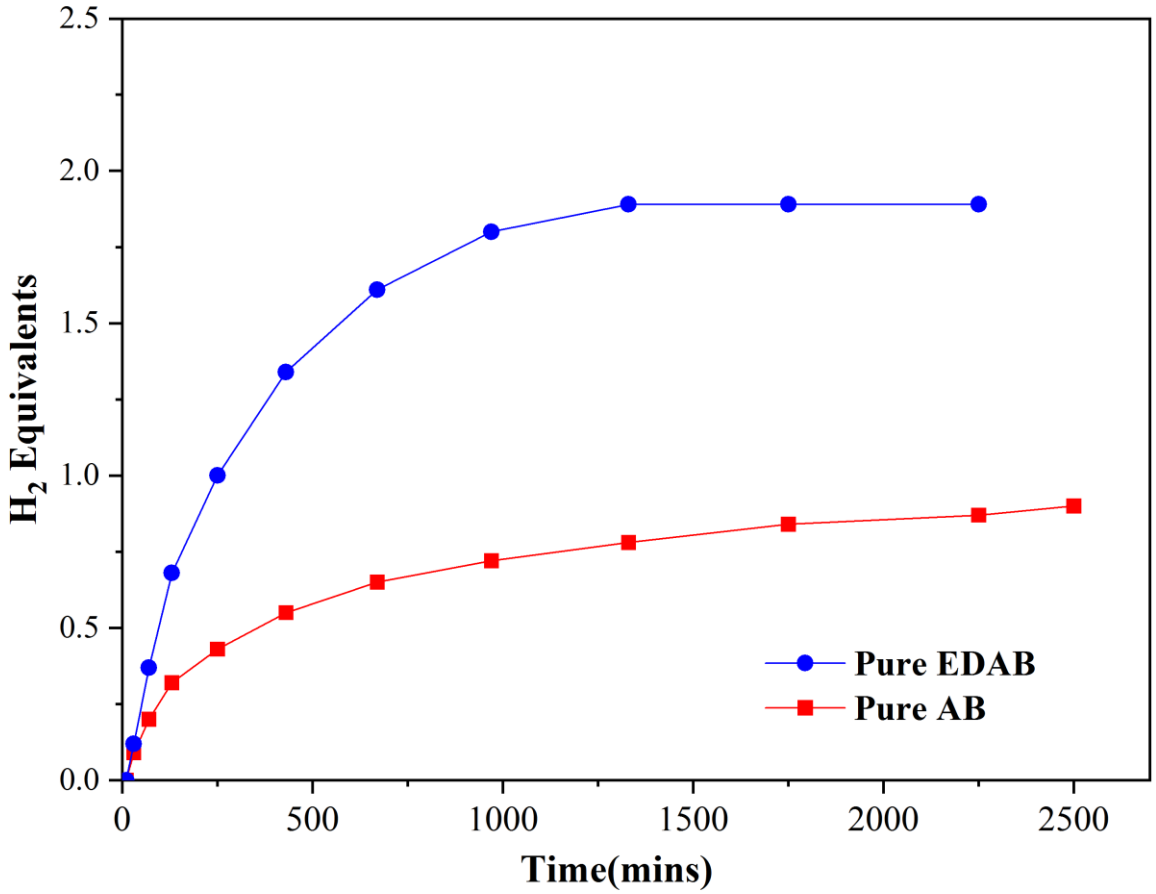

Figure 4.7: Summary of Cumulative hydrogen equivalents released at 105°C of Pure AB and Pure EDAB system

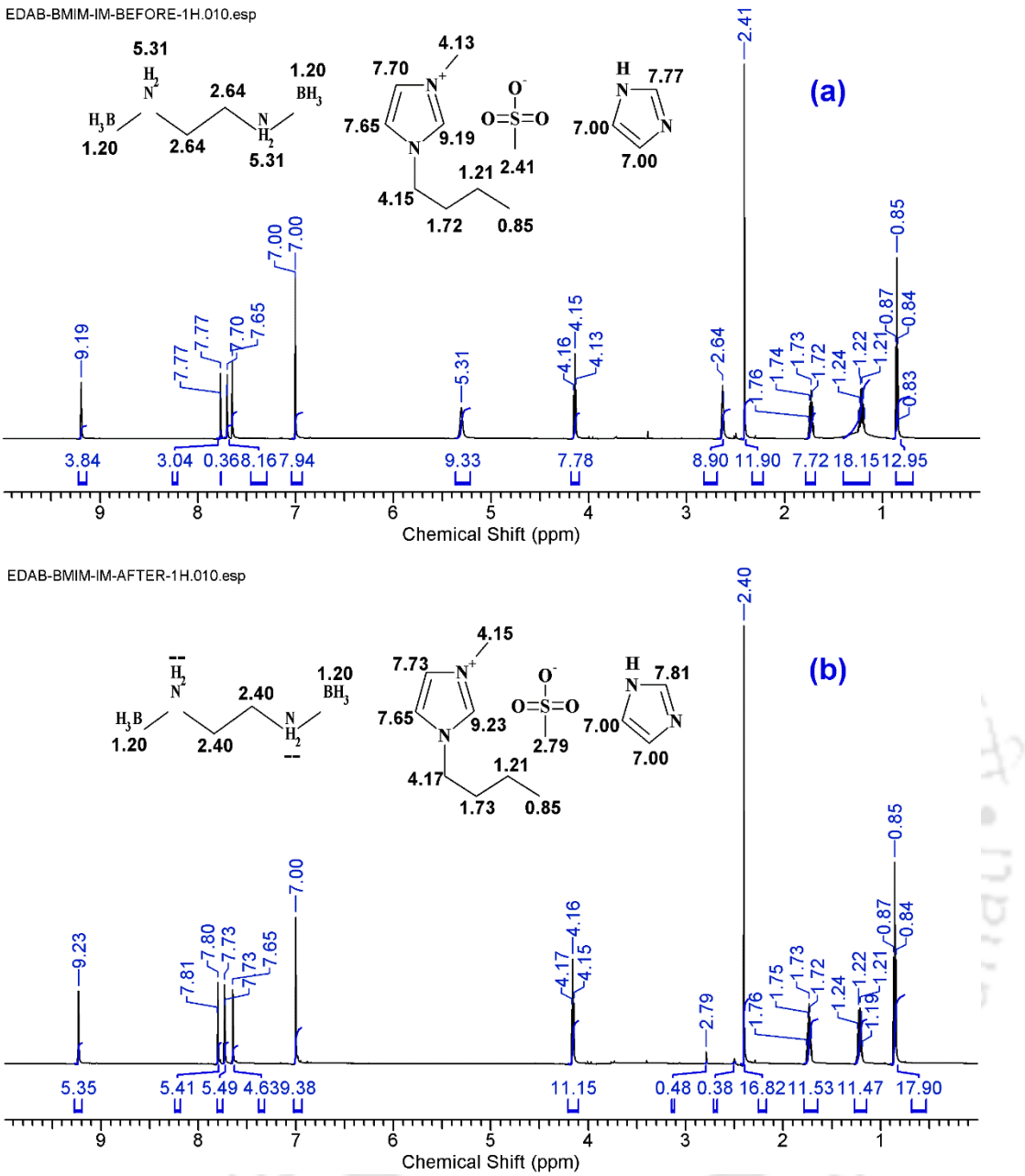

Figure 4.8: ^{1}H NMR spectra of amine borane/DES systems (a) EDAB/DES (before reaction), and (b) EDAB/DES (after reaction)

From our IDAC study (Figure 4.2), along with DES1, DES2 was also found to be one of the suitable DES for the dehydrogenation process of chemical hydrides. Because the hydrogen release from EDAB is both faster and higher than that from AB, the comparative dehydrogenation experiment utilizing IL and IL-based DES was done only on EDAB to maximize the hydrogen release. The parent IL was used in a comparative study of the dehydrogenation of EDAB as HBA and urea as HBD. Both the IL and DES have been kept in

a vacuum at 353 K for 48 h to reduce water content and reduce impurities. ^{1}H NMR spectroscopy was used to check the purity of both ILs and DESs. The NMR spectra for both the solvents (IL and DES) are provided and already discussed in Figure 4.4. It is clear that there is no reaction between EDAB-DES/IL; and HBA and HBD.

The thermal dehydrogenation of EDAB was performed separately in IL at 90°C and 105°C. The hydrogen desorption rate for both systems is nearly the same for 50 minutes. The EDAB/IL (red circle) desorption rate at 90°C is lower after 50 minutes and yields 3.2 equivalent of H_2 after a total reaction time of 360 min (Figure 4.9). The yield remains significantly larger than 1.89 equivalents of hydrogen as derived at 105°C from the dehydrogenation of solid-state EDAB (Figure 4.10). This illustrates the advantage of EDAB dehydrogenation by using ILs. By heating the same EDAB/IL mixture, 3.7 equivalents of hydrogen (dark blue triangle) are released at 105°C. The mechanism is through the development and stabilization of the intermediate product, i.e., diammoniate of diborane (DADB) known to be highly stable in ILs. This has already been documented in the previous chapters.

Overall the mechanism depends on the hydrogen bond basicity parameter of the ILs, which defines the ability of an anion to accept protons. This is probably one of the most important descriptors of the solvability of the ILs for a wide range of compounds. The solubility of chemical hydrides has been attributed to the strong hydrogen bonding interactions between the anions and nitrogen or boron atoms in hydrides. Thus to dissolve chemical hydrides in solvents such as ILs and DESs, it must have strong basic anions that can disrupt the bonding between the hydride chains and create hydrogen bonds with the solvent systems. Sahler and co-workers further related the hydrogen bond basicity (β) of several anions of ILs with the yield of hydrogen. ILs with [$MeSO_3^-$] anions have been found to be typically polar compared to those with anions such as Tf_2N and BF_4^-.[26] Further, anion's selection is strongly influenced

by its mean β-value. The mean β value follows the following trend: $[OAc^-] > [Cl^-] > [MeSO_3^-] > [BF_4^-] > [PF_6^-] > [Tf_2N]$ which is quite sufficient to explain the release of higher equivalents of H_2 using $[MeSO_3]$ based anions.

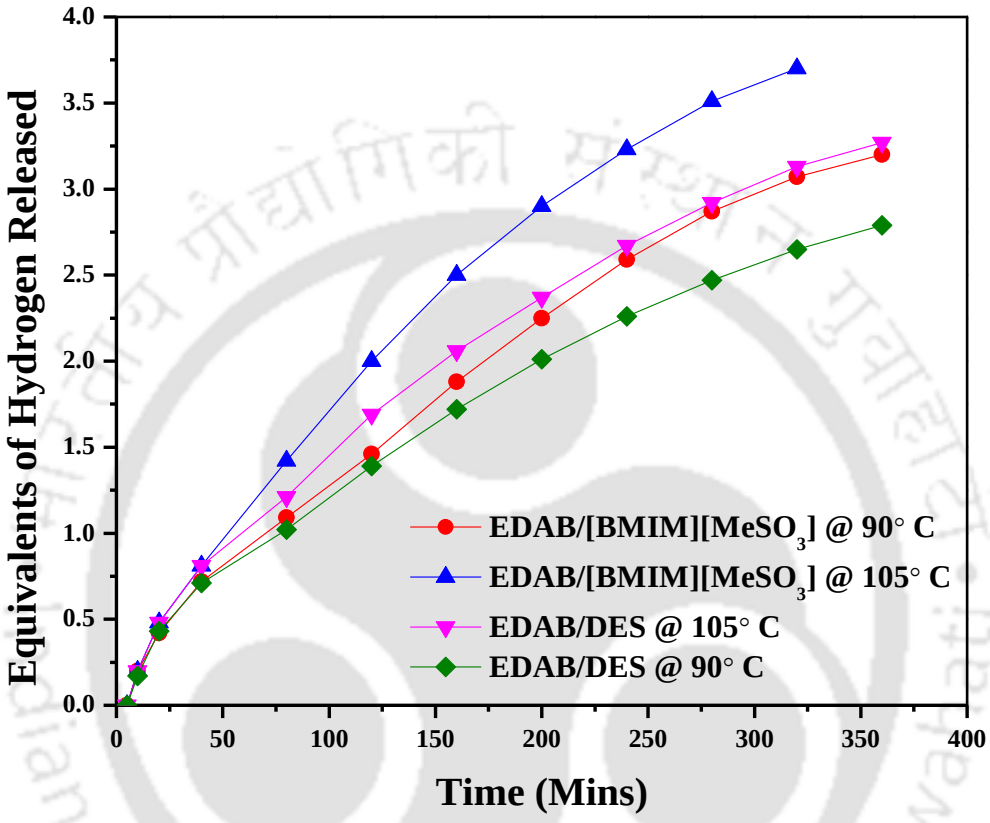

Figure 4.9: Time-resolved equivalent release of hydrogen from Pure EDAB. EDAB/IL and EDAB/DES system

On the other hand, the dehydrogenation of EDAB with the DES2 ([BMIM][$MeSO_3$]:[Urea]) was performed at two different temperatures of 90°C and 105°C. A cumulative of 2.79 and 3.27 equivalents are released at 90°C and 105°C, respectively, from the EDAB/DES systems. The hydrogen release rate at 105°C with DES2 was similar to that of IL at the same temperature until 60 mins. However, the release of hydrogen for EDAB/IL is greater than that of EDAB/DES at the same conditions (Figure 4.9) due to the higher hydrogen-bond basicity of the IL in comparison to the used DES. This, however, offsets with a less

induction time (within 10 minutes) when compared to IL. This fact highlights the catalytic role of DESs in the dehydrogenation of EDAB in comparison to solid-state dehydrogenation.

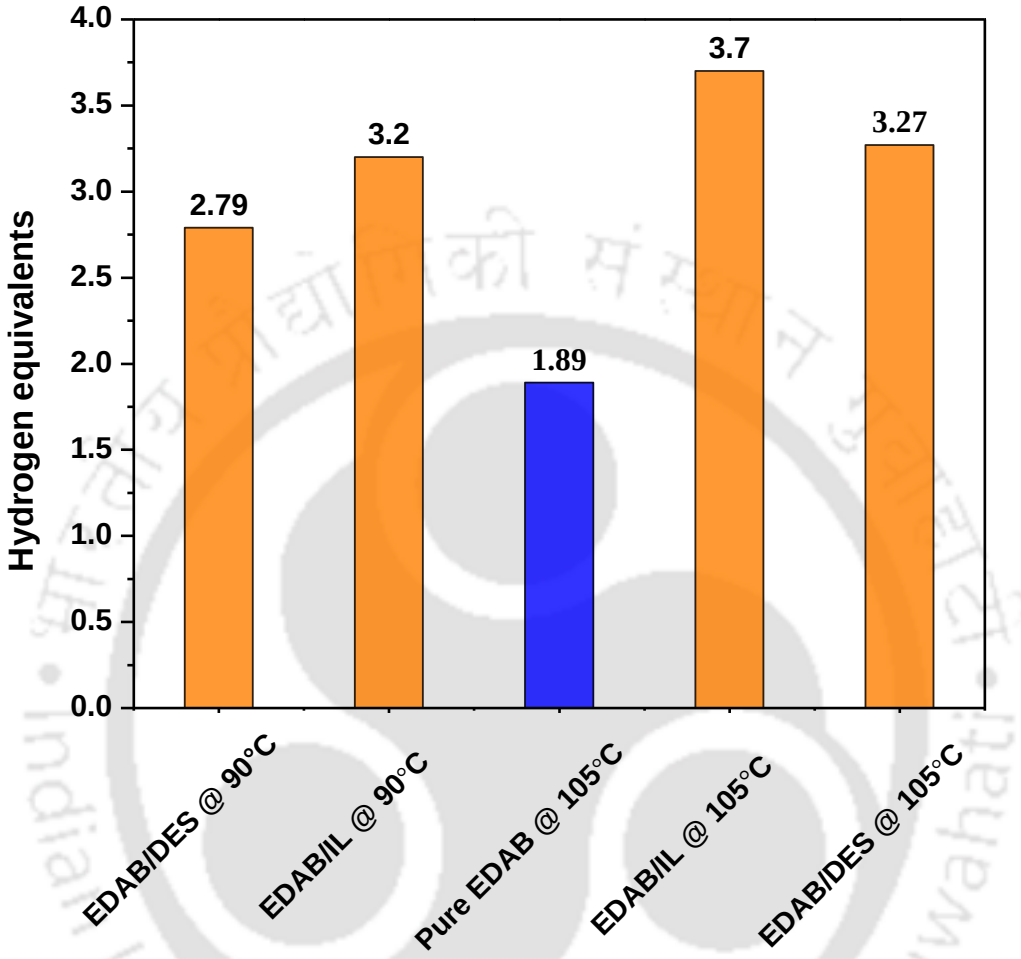

Figure 4.10: Total yield of EDAB dehydrogenation supported by various systems

Table 4.2: Viscosity (mPa.s) of IL, DES2, IL/EDAB, and DES2/EDAB systems at 25°C, 50°C, 90°C and 105°C

Systems	20°C	50°C	90°C	105°C
[BMIM][$MeSO_3$] (IL)	199.8	22.45	7.03	5.13
EDAB/[IL]	348.1	35.23	8.96	6.84
[BMIM][$MeSO_3$]:[Urea] (DES2)	369.3	32.58	7.76	6.07
EDAB/[DES2]	507.7	39.31	9.80	8.21

In order to understand the lower release with DES, the viscosity of both IL and DES were measured using a Rheometer (Physica MCR 301, Make: Anton Paar, Austria). Table 4.2 highlights the viscosity at *T*=25, 50, 90°C, and 105°C of ILs, DESs, EDAB/ILs, EDAB/DESs systems. The viscosity of the EDAB/solvent system increases with the addition of EDAB in IL and DES. Furthermore, the viscosity of both solvents and mixture systems decreases with the increase in temperature. At 20°C, EDAB/DES2 has a higher viscosity than EDAB/IL, and at 105°C, the viscosity of the former remains higher than the latter. It can be inferred that the high DES viscosity impedes the movement of EDAB molecules, resulting in delayed formation of ionic species diammoniate of diborane, resulting in lower hydrogen release equivalents when using DES as compared to pure ILs.

4.5.2. ^{1}H NMR Analysis

^{1}H NMR study was conducted to characterize EDAB/DES2 mixtures before and after the reaction. The ^{1}H NMR analysis was performed for the EDAB/DES2 complexes to re-assert the role of the newly designed DES in the dehydrogenation process as a catalytic solvent. Figure 4.11 (a) displays the ^{1}H NMR spectra for EDAB/DES2 (before reaction). The peaks for EDAB can be located at their positions as BH_3 (2.44ppm, 1.24 ppm), CH_2 at 5.42 ppm, and NH_2 (5.02 ppm, 2.93 ppm). The peaks for the DES system can also be related to their positions

as SO_3 (CH_3) (2.77 ppm), CH_3 (0.96 ppm), CH_2 (1.35 ppm), N-$CH_2$$\underline{CH_2}$ (1.86 ppm), NCH_2 (4.25 ppm), and NCH_3 (4.03 ppm). ArH can be located at (7.30 ppm, 7.39 ppm, 9.77 ppm), and NH_2 peaks of urea can be allotted at 5.82 ppm.

Figure 4.11 (b) represents the ^{1}H NMR spectra for EDAB/DES2 (after reaction). While DES has retained its original structural entity, all other peaks are within its original assigned position. Some slight changes in shift can be attributed to the addition of EDAB in DES. Nevertheless, for EDAB, an absence of BH_3 moiety ensures that EDAB is active in the reaction, which initiates a pathway for liberating hydrogen. Like the ILs, its analogue DES also functions in the same manner within the dehydrogenation reaction.

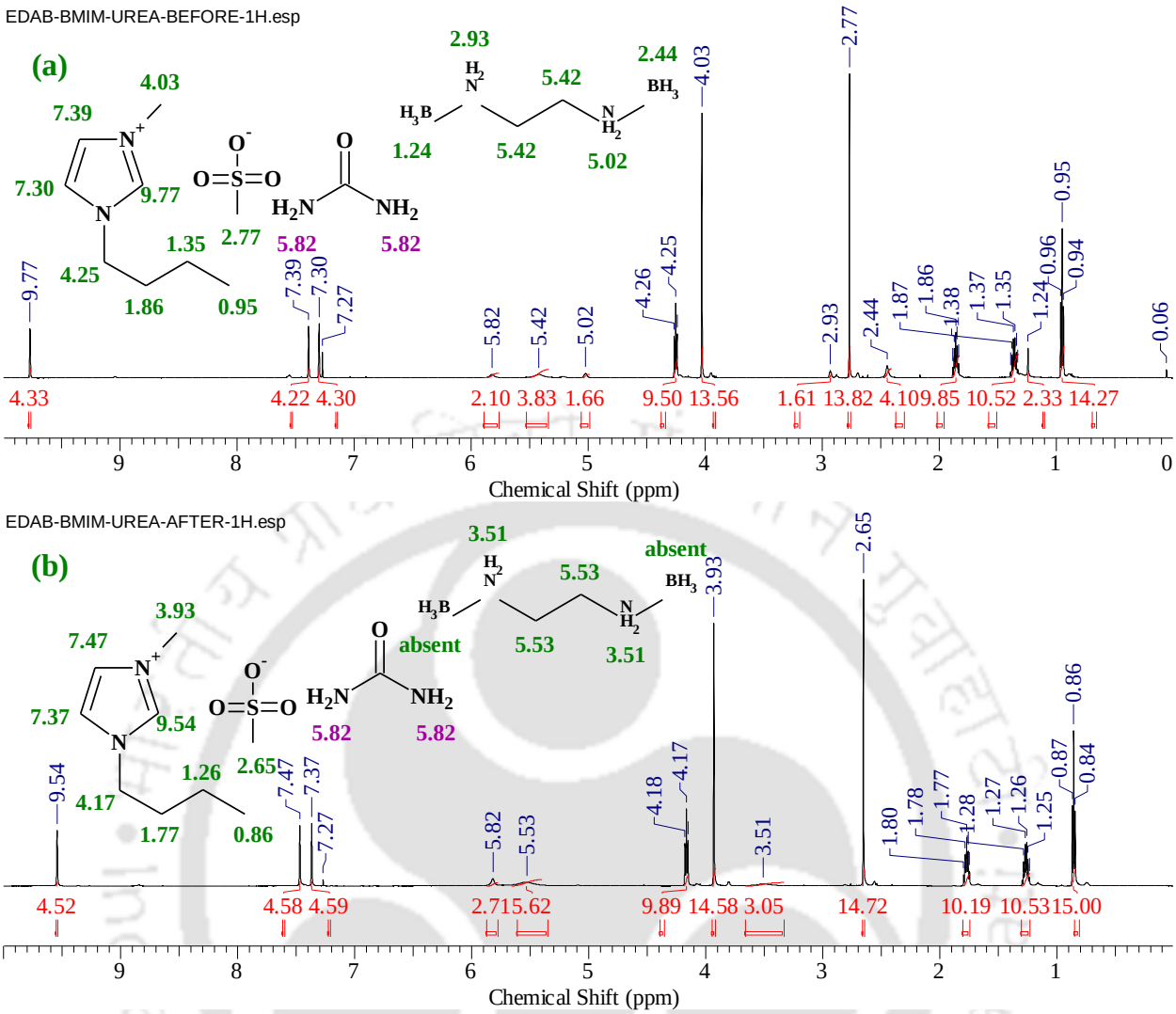

Figure 4.11: ^{1}H NMR spectra of (a) [EDAB]/DES2 (before reaction) (b) [EDAB]/DES2 (after reaction)

4.5.3. ^{11}B NMR Analysis

The effect of solvent dehydrogenation of EDAB on the boron moieties also needs to be studied and analyzed for its mechanism. A ^{11}B NMR study was performed on EDAB/DES reaction mixtures before and after the thermal dehydrogenation.[27]

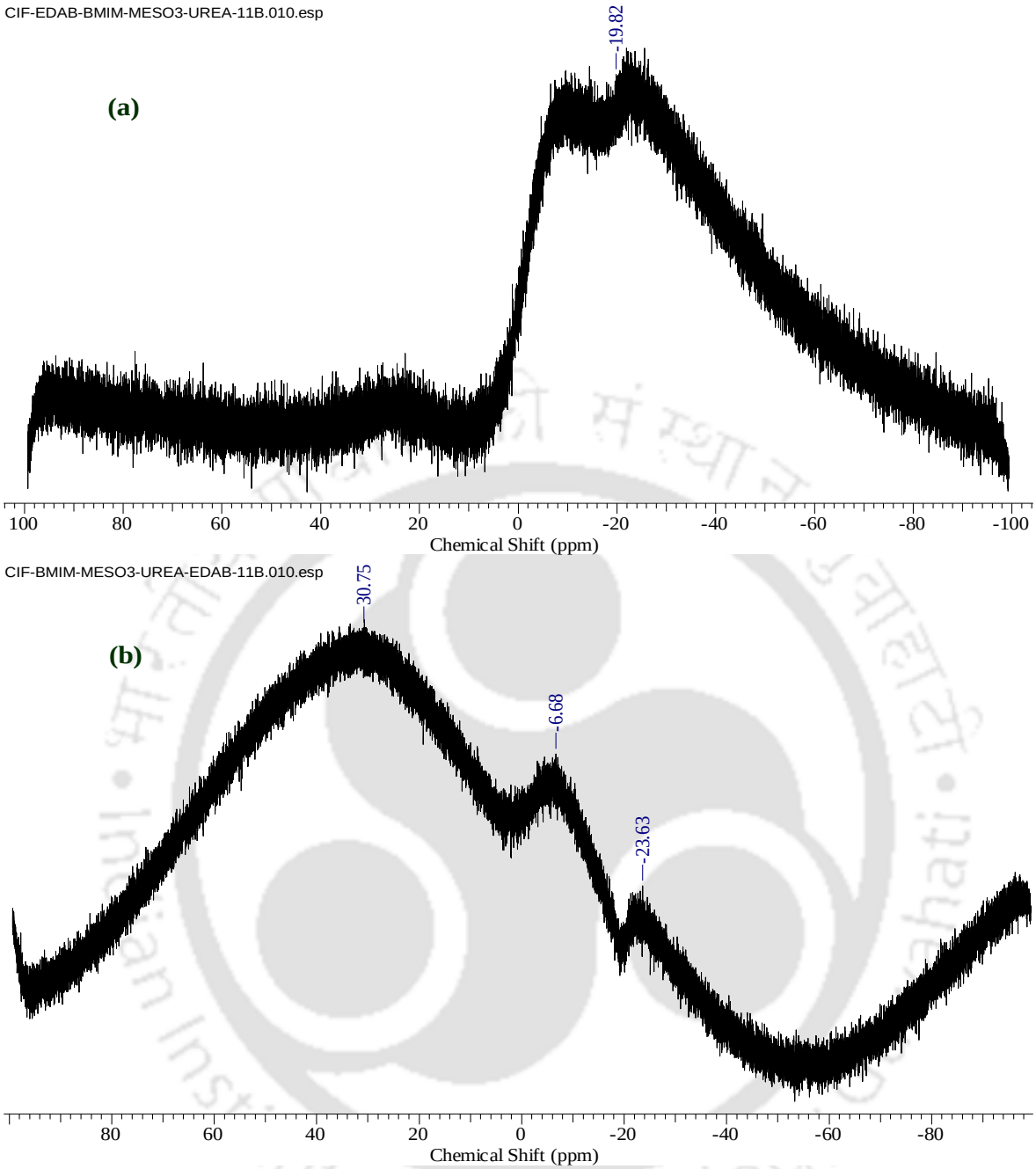

Figure 4.12: ^{11}B NMR spectra of (a) [EDAB]/DES (before reaction) (b) [EDAB]/DES (after reaction)

The ^{11}B NMR spectra of EDAB/DES before reaction (Figure 4.12(a)) confirms the presence of sp^3 –BH_3 functional group with an assigned chemical shift at -19.82 ppm, which is in line with the literature and confirms the presence of -BH_3 moiety in the reaction sample.[28] This can be attributed to the presence of unreacted EDAB species. The peak at -23.63 ppm can be attributed to the presence of polyaminoborane (PAB). An unidentified peak can be seen at

30.75 ppm which is due to the diamidoborane [$BH(NH\text{-}t\text{-}Bu)_2$]. Neiner et al. reported a chemical shift at -39 ppm, which can be assigned to ($–BH_4^-$) intermediate in dehydrogenation experiment of pure EDAB, whereas BH_2 moiety is assigned with a peak at -10 ppm, in line with the related dehydrogenation pathway of EDAB, a broad resonance at -6.08 ppm can be referred to BH_2 of EDAB dimer.[28] The products analyzed using ^{11}B NMR can predict the dehydrogenation mechanism of EDAB. This is similar to the mechanism of hydrogen release as reported by Leardini et al.[29] and Banerjee et al.[30] where the solid-state and solution-state (Ionic liquid) dehydrogenation of EDAB was reported. (Scheme 4.1).

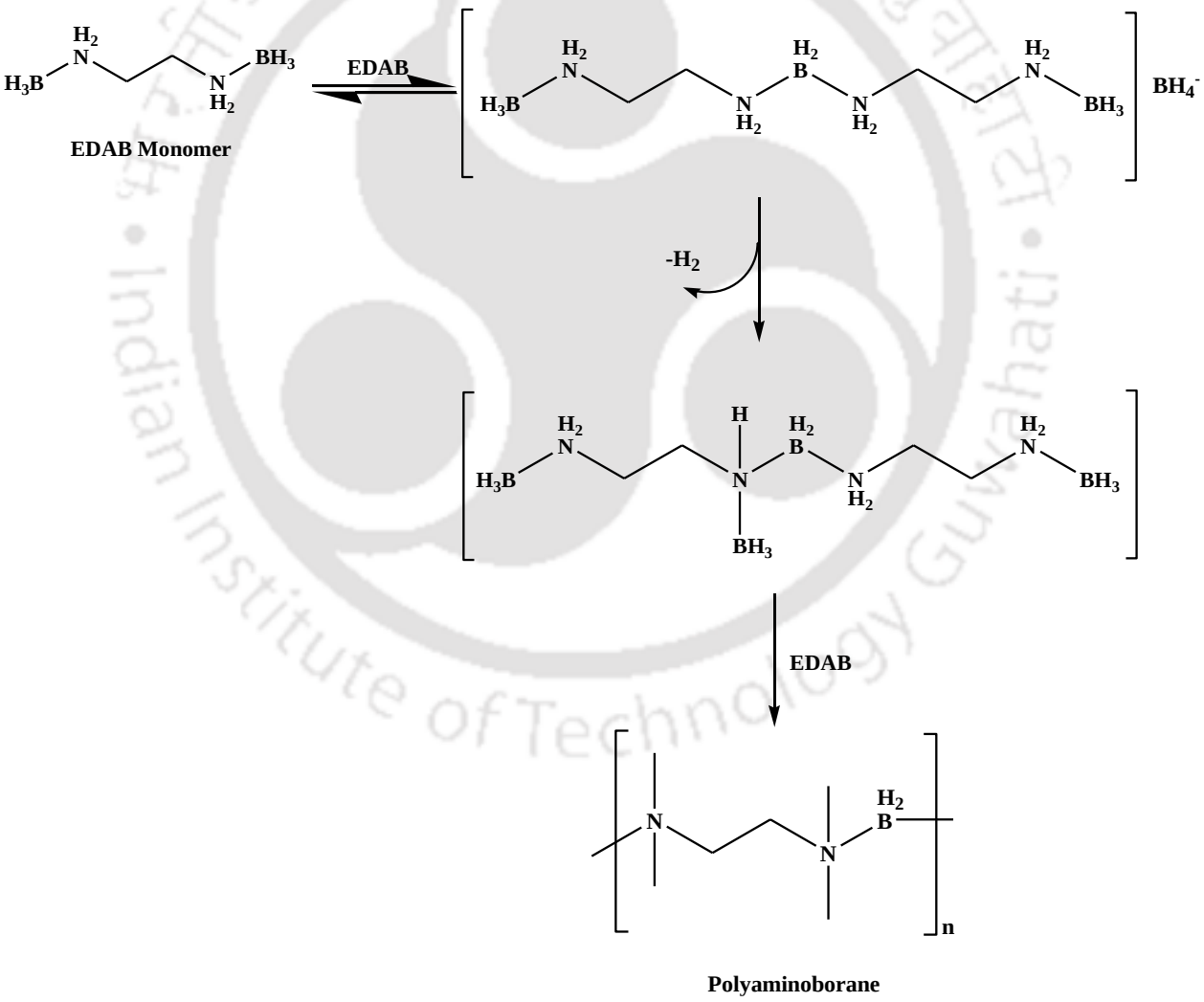

Scheme 4.1: Dehydrogenation Mechanism of the EDAB/DES System

4.5.4. Thermogravimetric Analysis

Thermogravimetric analysis (TGA) was employed to assess the thermal stability of the synthesized DESs and their pure components under the nitrogen atmosphere, using the Thermal Gravimetric Analyzer (**Netzsch** TGA **TG 209 F1 Libra**). In order to reckon the starting decomposition temperatures, a variable mode with a heating rate of 5°C min^{-1} was used at a temperature range from 25°C to 500°C. The dynamic TGA curves for the synthesized DES, its pure components, EDAB, IL, and EDAB/solvent complexes can be found in Figure 4.13 and Figure 4.14.

Since [BMIM][$MeSO_3$] is generally an acceptable thermal stable IL as it experiences a mass loss of up to 350°C.[31] Ionic liquids stability is due to the presence of high thermally stable anions, which shows a linear correlation with their coordinating nature and nucleophilicity, as non-coordinative anions follow an elimination or rearranging mechanism on degradation.[32,33] On the other hand, the onset degradation temperature of the DES1 (Figure 4.13) can be evaluated by the second peak (black), which shows a two-step degradation. The first mass loss step around 170°C can be ascribed to the decomposition of the imidazole (HBD), which can also be termed the maximum operating temperature of the DES1. The second peak of degradation can be attributed to the weight loss observed by the decomposition of HBA (IL). Finally, the synthesized ionic liquid-based DES can be concluded as a sensible alternative for dehydrogenation experiments.

The TGA curves for the DES2 and its pure components are shown in Figure 4.14 (a), i.e., IL being the HBA and urea as HBD. [BMIM][$MeSO_3$], being a highly stable IL, goes through a mass loss of up to 350°C. The second curve corresponds to that of pure DES2 shows a two-step degradation; the first step of weight loss is attributed to the onset temperature of urea which can also be considered as the DES2 onset degradation temperature (T_{onset}) that is nearly up to 150°C. The second step of weight loss from 320°C is due to the HBA (IL)

decomposition. The initial degradation temperature of DES can be referred to as the maximum operating temperature for the EDAB dehydrogenation, which is highly preferable for this work as it requires a working temperature up to 120°C, which is the melting point of EDAB.

The TGA curves for the pure EDAB and EDAB/solvent complexes are shown in Figure 4.14(b). Taking into account the pure EDAB's weight-loss activity, it can be concluded that EDAB displays a minimal weight loss up to 110°C, confirming the melting point of EDAB is in line with the literature.

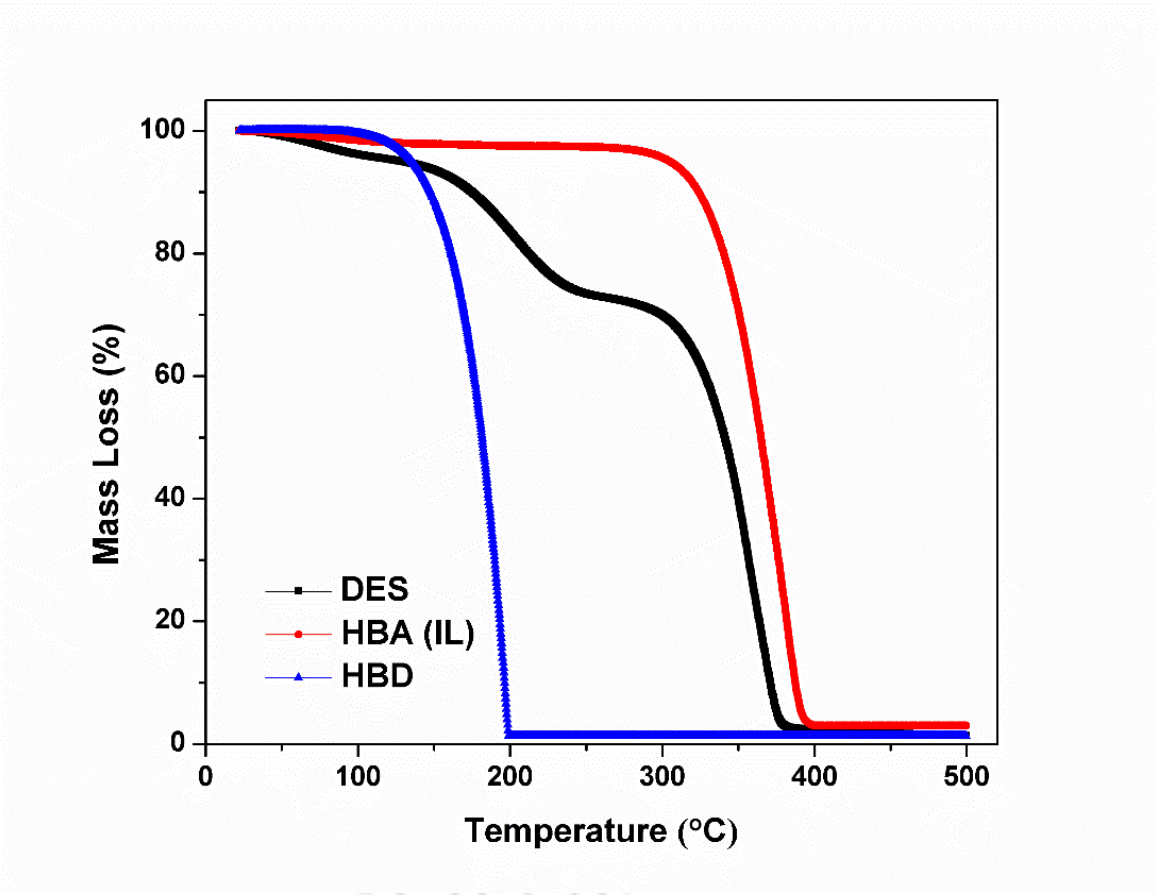

Figure 4.13: Dynamic TGA profile of the synthesized DES1 and its pure components

Comparing EDAB/IL with EDAB/DES complexes, the release of hydrogen with DESs is observed at around 120°C from the slope of TGA lines with almost no induction time, which is the main reason for the replacement with DES. In comparison with traditional highly thermal stable ILs, it can be concluded that DES goes through a rapid decomposition but propagates

the dehydrogenation reaction faster when compared to both ILs and solid-state EDAB dehydrogenation.[34]

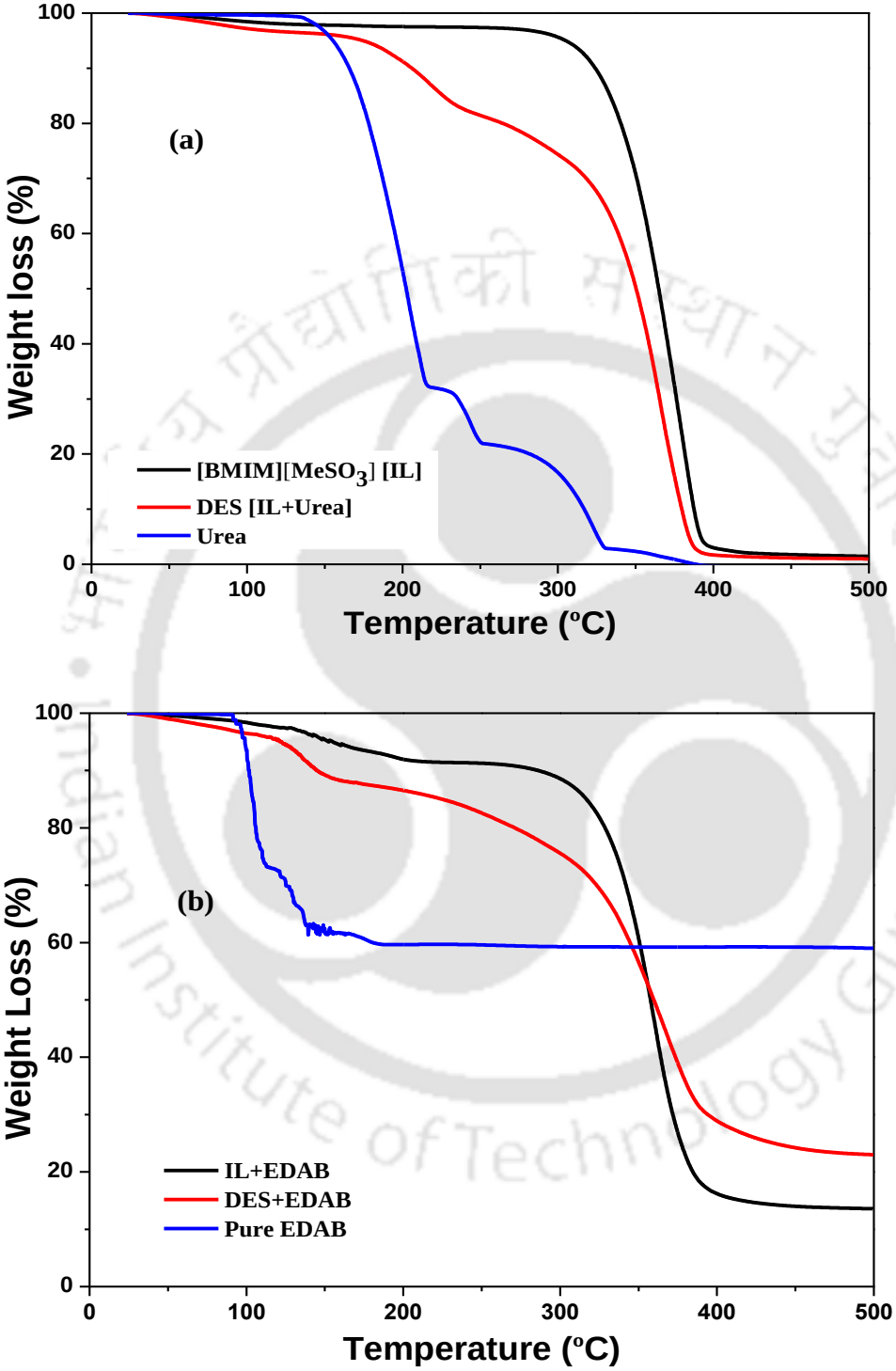

Figure 4.14: TGA Profiles of (a) pure IL, pure DES2, and pure Urea, (b) EDAB/IL, EDAB/DES2, and pure EDAB

4.5.5. Dehydrogenation Experiments with Metal Salt-Based Type 1 Deep Eutectic Solvents

Prior to the dehydrogenation studies, Deep Eutectic Solvents based on type 1 metal salts were synthesized using the same methods as previously described in the literature. Chapter 3 discusses the method of preparation in detail and its analysis.[9] Two type 1-based DESs were synthesized using choline chloride (ChCl) as the HBA and tin (II) chloride ($SnCl_2$), zinc (II) chloride ($ZnCl_2$) as metal salts in a molar ratio of 1:2. In this chapter, DES3 refers to the mixture of choline chloride and tin (II) chloride, whereas DES4 refers to the mixture of choline chloride and zinc (II) chloride.[35] The reason for concentrating on these two DES systems is that the metal salts have a higher Lewis acidity. It is well established that increasing the Lewis acidity results in an increase in the catalytic activity of a range of applications.[36] One of the primary reasons for our preference for these two DES systems is their near-room temperature melting point; these features were absent when the same HBA (ChCl) was combined with other metal salts such as $CrCl_3$, $CaCl_2$, etc.[12]

In this section, the dehydrogenation of AB and EDAB was performed in DES3 and DES4 at 80°C and 100°C. This reduction in operating temperature was to conduct the dehydrogenation studies at a lower temperature due to dual ionic components in metal salt-based DESs. Studies have shown that the ionicity and acidity of catalytic solvents promote the release of hydrogen equivalents at reduced temperatures.[38] Choline chloride has indeed been combined with a variety of metal halide salts to promote the catalytic activity of various processes at lower operating temperatures.[37] Similar to the ILs, it was presumed that the presence of ionic components in these type 1 DESs, would provide a suitable catalytic media which can stabilize the ionic intermediates.[38] Both the DESs have been kept in a vacuum at 353 K for 48 h to reduce water content and reduce impurities. As mentioned in section 4.5.1, when pure AB and EDAB are heated to 105°C, 0.90 and 1.89 equivalents of hydrogen are

released through solid-state dehydrogenation (Figure 4.7).[39] It is stated that there is an induction time in the AB and EDAB solid-state dehydrogenation, which is suppressed with the usage of DES. A negligible induction period was observed for both the amine borane-IL complexes in the presence of metal salt-based DES. However, the release of hydrogen for EDAB/DES3 as well as EDAB/DES4 from each time step was greater than that of AB/DES3 and AB/DES4 at the same conditions. A cumulative 1.8 and 1.96 equivalent hydrogen was released from AB/DES3 at 80°C and 100°C, respectively. AB/DES4 released 1.92 and 2.1 equivalent hydrogen at 80°C and 100°C, respectively (Figure 4.15). A cumulative release of hydrogen equivalents from EDAB/DES3 was found to be 3.42 at 80°C, 3.71 at 100°C; while for EDAB/DES4, it was 3.6 and 3.89 equivalents of hydrogen at 80°C and 100°C, respectively (Figure 4.16). The initial induction period observed in the dehydrogenation reaction in the presence of DES3 and DES4 can be attributed to the higher viscosity of the DES systems, which somehow hinders the application of these catalytic DES to be used at lower operating temperatures. The dehydrogenation mechanism in the presence of metal salt-based DESs usually depends on the lewis acidity of the metal salts employed in the studied DES systems. However, the dehydrogenation mechanism of amine boranes remains the same in the presence of this subcategory DESs (Scheme 4.1).

As mentioned in various studied catalytic activities of metal salt-based DESs, the higher lewis acidity of the metal salt correlates with the catalytic effect of the studied DES systems, which implies that the metal salts dominated the dehydrogenation of chemical hydrides. The catalytic activity of metal chlorides depends on their Lewis acidity. It was found that their catalytic efficiency for dehydrogenation reaction was enhanced with stronger Lewis acidity.[40] The trials to combine the electronegativity of some metal chlorides ($AlCl_3$ > $FeCl_3$ > $ZnCl_2$ > $SnCl_2$) with the catalytic efficiency for dehydrogenation of amine boranes revealed that the salts with intermediate Lewis acidity (i.e., Zn^{2+} and Sn^{2+}) provided the highest catalytic

activity.[41] Whereas metal salts with $AlCl_3$ and $FeCl_3$, when coupled with choline chloride, were unable to form a eutectic mixture at room temperature, which hinders their usage as a catalytic solvent in the same process.[12]

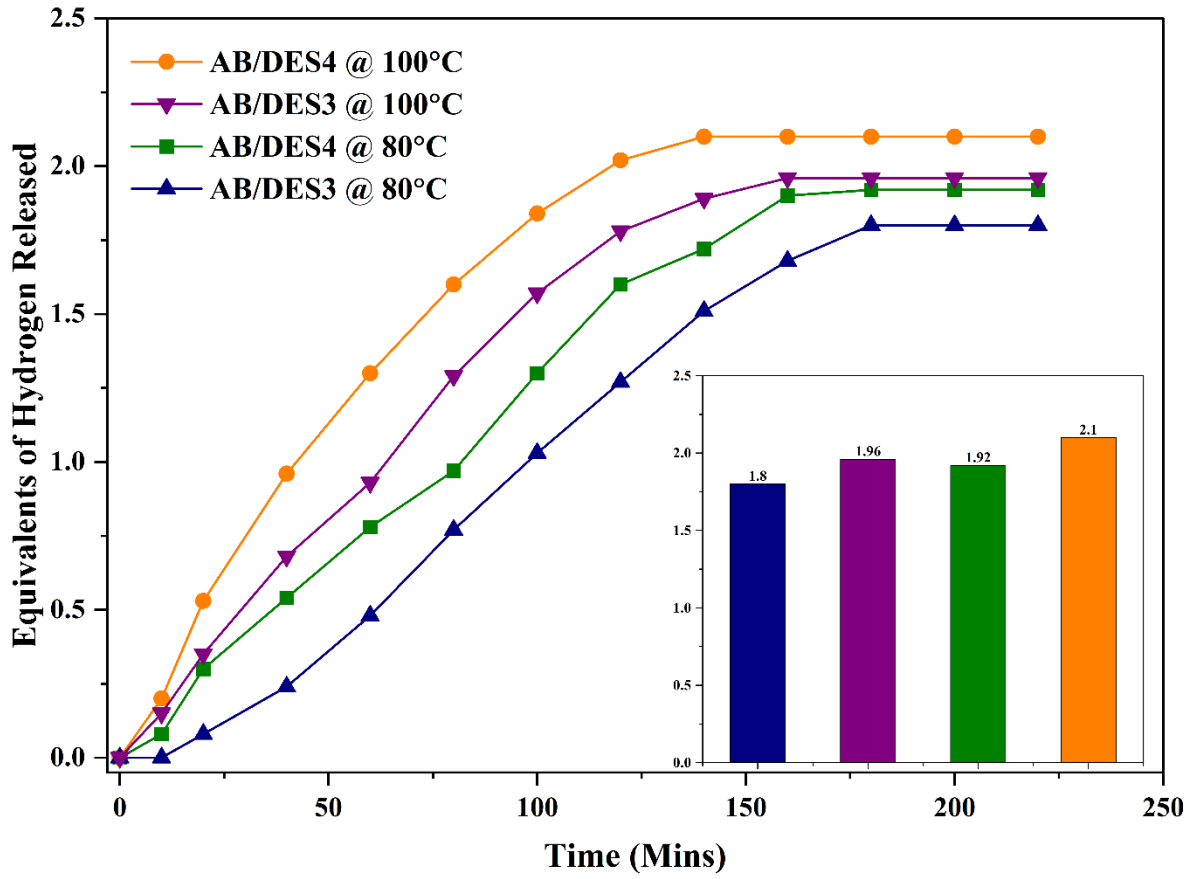

Figure 4.15: Time-resolved equivalent release of hydrogen from of AB/DES3 system, AB/DES4 system at 80°C and 100°C

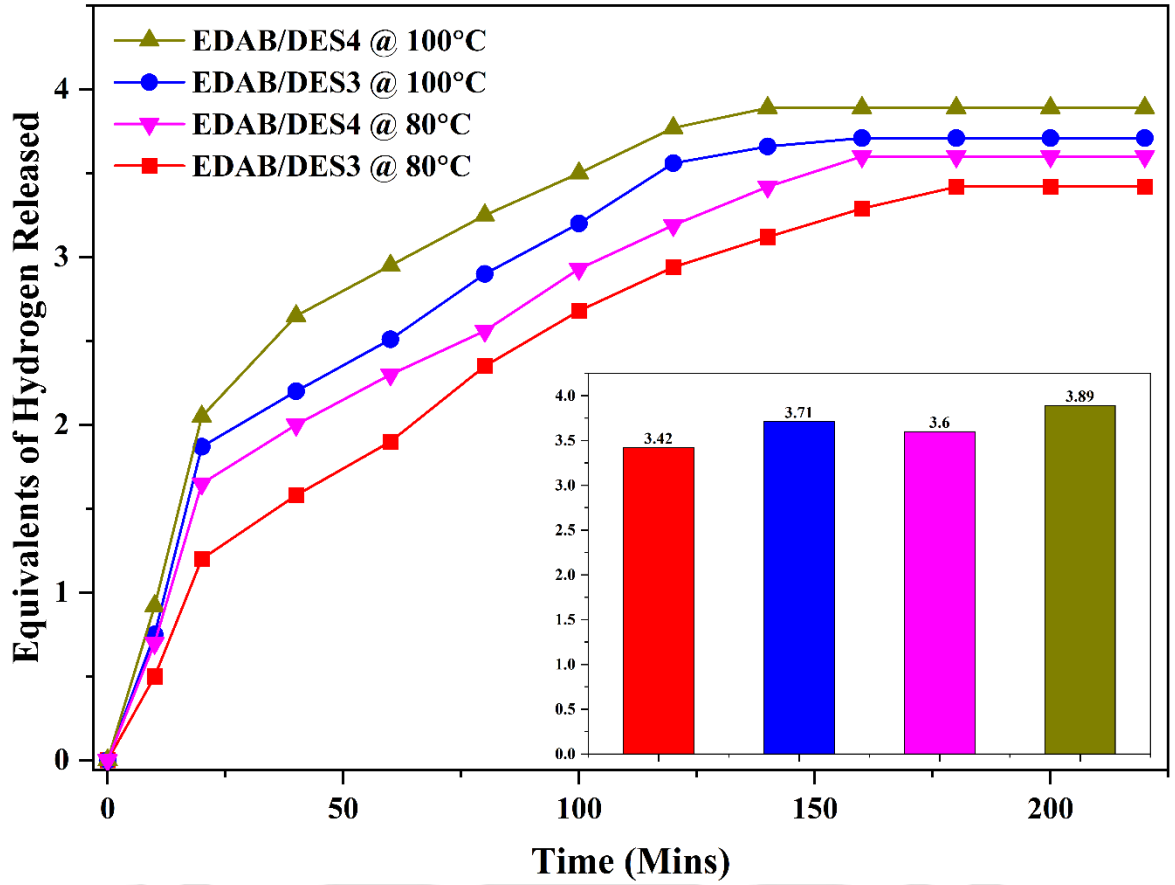

Figure 4.16: Time-resolved equivalent release of hydrogen from of EDAB/DES3 system, EDAB/DES4 system at 80°C and 100°C

4.6. Conclusions

We have reported a comprehensive study on the synthesis of novel ionic Liquid-based Deep Eutectic Solvents (IL-based DESs) and their applications in enhancing the dehydrogenation of amine boranes. DES was prepared with a thermally stable IL acting as HBA and combined with imidazole in a molar ratio of 1:2, named DES1. Another catalytic solvent named DES2 in work was formed at a molar ratio of 1:1, where IL acted as an HBA and urea as an HBD. Thermal characteristics of synthesized DESs have also been reported. The selection of the prepared DES for the dehydrogenation experiment was made using the COSMO-SAC model. A comparative analysis was conducted at 105°C for the thermal decomposition of hydrides, AB, and EDAB, promising to release 2.55 and 1.66 equivalents of hydrogen. A comparative study about the thermal decomposition of ethylene diamine bisborane (EDAB) was conducted with methanesulfonate anion-based ILs and methanesulfonate-based DES at 90°C and 105°C. The hydrogen released from EDAB/IL or EDAB/DES2 mixture were in the following increasing order: EDAB/DES2 at 90°C (2.79) < EDAB/IL at 90°C (3.2) < EDAB/DES2 at 105°C (3.2) < EDAB/IL 105°C (3.70). The equivalents of hydrogen release in the solution state of EDAB were notable in comparison to 1.89 equivalents of released hydrogen obtained in the dehydrogenation of solid-state EDAB. Confirmation of IL and DES as catalytic solvent was determined by ^{1}H NMR. The absence of the hydrogen peaks of amine borane entity, along with the integrity of the solvents (IL and DES) structure, has confirmed the fact that AB and EDAB is consumed in the dehydrogenation. ^{11}B NMR confirms the presence of trigonal boron (sp^2) BH_2, which is the only boron-containing moiety in dehydrogenation experiments. Whereas in the case of DES, the presence of diamidoborane is also reported. TGA analysis revealed the stability of EDAB/DES complexes and provided thermal stability of up to 150 °C.

In the subsequent section, the usage of metal salt-based DESs produces a highly catalytic effect on the dehydrogenation of amine boranes. Zinc-based DESs (DES4) could release 3.6 and 3.89 equivalents of hydrogen from EDAB at lower temperatures than earlier used IL and DES solvent systems in this work. This catalytic activity of zinc-based DESs can be ascribed to the higher lewis acidity of the zinc metal salts in comparison to the other system based on tin (II) chloride. The hydrogen release pattern of amine boranes in the presence of DES3 and DES4 can be correlated to its higher lewis acidity as zinc (II) chloride-based DES performs similarly in the case of AB and EDAB both. The usage of zinc and tin-based DESs proved to be a suitable catalytic solvent for the dehydrogenation process; however, their higher viscosity and freezing point are still an issue for their use as a catalytic media in the process. This investigation led to the foundation of DES systems for thermolytic dehydrogenation, and it cultivated the enormous potential of DES as a revolutionary catalytic media.

However, industrially chemical hydrides with a higher hydrogen content and controlled release are not widely available and their synthesis is cumbersome. There is a need to study other novel chemical hydrides capable of hydrogen release at moderate temperatures that are also cost-effective. In light of this, the following chapter will investigate a novel chemical hydrogen storage carrier namely Morpholine Borane(MB).

References

(1) Abbott, A. P.; Capper, G.; Davies, D. L.; McKenzie, K. J.; Obi, S. U. Solubility of Metal Oxides in Deep Eutectic Solvents Based on Choline Chloride. *J. Chem. Eng. Data* **2006**, *51* (4), 1280–1282. https://doi.org/10.1021/je060038c.

(2) Kow, K. K.; Sirat, K. Novel Manganese(II)-Based Deep Eutectic Solvents: Synthesis and Physical Properties Analysis. *Chinese Chem. Lett.* **2015**. https://doi.org/10.1016/j.cclet.2015.05.049.

(3) Francisco, M.; Van Den Bruinhorst, A.; Kroon, M. C. Low-Transition-Temperature Mixtures (LTTMs): A New Generation of Designer Solvents. *Angew. Chemie - Int. Ed.* **2013**, *52* (11), 3074–3085. https://doi.org/10.1002/anie.201207548.

(4) Wen, Q.; Chen, J. X.; Tang, Y. L.; Wang, J.; Yang, Z. Assessing the Toxicity and Biodegradability of Deep Eutectic Solvents. *Chemosphere* **2015**, *132*, 63–69. https://doi.org/10.1016/j.chemosphere.2015.02.061.

(5) Delgado-Mellado, N.; Larriba, M.; Navarro, P.; Rigual, V.; Ayuso, M.; García, J.; Rodríguez, F. Thermal Stability of Choline Chloride Deep Eutectic Solvents by TGA/FTIR-ATR Analysis. *J. Mol. Liq.* **2018**. https://doi.org/10.1016/j.molliq.2018.03.076.

(6) Akhmetshina, A. I.; Petukhov, A. N.; Mechergui, A.; Vorotyntsev, A. V.; Nyuchev, A. V.; Moskvichev, A. A.; Vorotyntsev, I. V. Evaluation of Methanesulfonate-Based Deep Eutectic Solvent for Ammonia Sorption. *J. Chem. Eng. Data* **2018**, *63* (6), 1896–1904. https://doi.org/10.1021/acs.jced.7b01004.

(7) Paul, S.; Panda, A. K. Physicochemical Investigations on the Aqueous Solution of an Ionic Liquid, 1-Butyl-3-Methylimidazolium Methanesulfonate, [Bmim][MS], in a Concentrated and Dilute Regime. *Colloids Surfaces A Physicochem. Eng. Asp.* **2012**, *404*, 1–11. https://doi.org/10.1016/j.colsurfa.2012.01.034.

(8) Abbott, A. P.; Boothby, D.; Capper, G.; Davies, D. L.; Rasheed, R. K. Deep Eutectic Solvents Formed between Choline Chloride and Carboxylic Acids: Versatile Alternatives to Ionic Liquids. *J. Am. Chem. Soc.* **2004**, *126* (29), 9142–9147. https://doi.org/10.1021/ja048266j.

(9) Abbott, A. P.; Capper, G.; Davies, D. L.; Munro, H. L.; Rasheed, R. K.; Tambyrajah, V.

Preparation of Novel, Moisture-Stable, Lewis-Acidic Ionic Liquids Containing Quaternary Ammonium Salts with Functional Side Chains. *Chem. Commun.* **2001**, *1* (19), 2010–2011. https://doi.org/10.1039/b106357j.

(10) Abbott, A. P.; Capper, G.; Davies, D. L.; Rasheed, R. Ionic Liquids Based upon Metal Halide/Substituted Quaternary Ammonium Salt Mixtures. *Inorg. Chem.* **2004**, *43* (11), 3447–3452. https://doi.org/10.1021/ic049931s.

(11) Abbott, A. P.; Capper, G.; Davies, D. L.; Rasheed, R. K.; Tambyrajah, V. Novel Solvent Properties of Choline Chloride/Urea MixturesElectronic Supplementary Information (ESI) Available: Spectroscopic Data. See Http://Www.Rsc.Org/Suppdata/Cc/B2/B210714g/. *Chem. Commun.* **2003**, No. 1, 70–71. https://doi.org/10.1039/b210714g.

(12) Ghareh Bagh, F. S.; Shahbaz, K.; Mjalli, F. S.; Hashim, M. A.; Alnashef, I. M. Zinc (II) Chloride-Based Deep Eutectic Solvents for Application as Electrolytes: Preparation and Characterization. *J. Mol. Liq.* **2015**. https://doi.org/10.1016/j.molliq.2015.01.025.

(13) Li, J.; Shou, F.; Yan, S.; Li, F.; Lu, G.; Yao, L.; Han, X. Process Optimization and Its Kinetics Analysis on Catalytic Synthesis of Biodiesel from Oleic Acid Using Deep Eutectic Solvents as Catalyst. *J. Chinese Cereal. Oils Assoc.* **2019**.

(14) Hajipour, A. R.; Nazemzadeh, S. H.; Mohammadsaleh, F. Choline Chloride/CuCl as an Effective Homogeneous Catalyst for Palladium-Free Sonogashira Cross-Coupling Reactions. *Tetrahedron Lett.* **2014**. https://doi.org/10.1016/j.tetlet.2013.11.105.

(15) Bahadori, L.; Abdul Manan, N. S.; Chakrabarti, M. H.; Hashim, M. A.; Mjalli, F. S.; Alnashef, I. M.; Hussain, M. A.; Low, C. T. J. The Electrochemical Behaviour of Ferrocene in Deep Eutectic Solvents Based on Quaternary Ammonium and Phosphonium Salts. *Phys. Chem. Chem. Phys.* **2013**. https://doi.org/10.1039/c2cp43077k.

(16) Di Pietro, M. E.; Mele, A. Deep Eutectics and Analogues as Electrolytes in Batteries. *J. Mol. Liq.* **2021**. https://doi.org/10.1016/j.molliq.2021.116597.

(17) Jach, F.; Wassner, M.; Bamberg, M.; Brendler, E.; Frisch, G.; Wunderwald, U.; Friedrich, J. A Low-Cost Al-Graphite Battery with Urea and Acetamide-Based Electrolytes. *ChemElectroChem* **2021**. https://doi.org/10.1002/celc.202100183.

(18) Wang, S.; Sandler, S. I.; Chen, C. C. Refinement of COSMO-SAC and the Applications. *Ind. Eng. Chem. Res.* **2007**, *46* (22), 7275–7288. https://doi.org/10.1021/ie070465z.

(19) Dennington, R.; Keith, T.; Millam, J. GaussView, Version 5. *Semichem Inc. Shawnee Mission. KS* **2009**.

(20) Frisch, M. J.; Trucks, G. W.; Schlegel, H. B.; Scuseria, G. E.; Robb, M. A.; Cheeseman, J. R.; Scalmani, G.; Barone, V.; Mennucci, B.; Petersson, G. A.; et al. Gaussian09 Revision D.01, Gaussian Inc. Wallingford CT. *Gaussian 09 Revision C.01*. 2010.

(21) Becke, A. B3LYP. *J. Chem. Phys.* **1993**.

(22) Becke, A. D. Density-Functional Exchange-Energy Approximation with Correct Asymptotic Behavior. *Phys. Rev. A* **1988**, *38* (6), 3098.

(23) McCullough, E. A.; Aprà, E.; Nichols, J. Comparison of the Becke-Lee-Yang-Parr and Becke-Perdew-Wang Exchange-Correlation Functionals for Geometries of Cyclopentadienyl-Transition Metal Complexes. *Journal of Physical Chemistry A*. 1997. https://doi.org/10.1021/jp963430d.

(24) Banerjee, B.; Kundu, D.; Pugazhenthi, G.; Banerjee, T. Quantum Chemical and Experimental Insights for the Ionic Liquid Facilitated Thermal Dehydrogenation of Ethylene Diamine Bisborane. *RSC Adv.* **2015**, *5* (104), 85280–85290. https://doi.org/10.1039/c5ra10625g.

(25) Kundu, D.; Chakma, S.; Pugazhenthi, G.; Banerjee, T. Effect of Thiocyanate-Based Ionic Liquids on the Dehydrogenation of Amine Boranes: Experimental and Molecular Modeling Studies. *Asia-Pacific J. Chem. Eng.* **2019**. https://doi.org/10.1002/apj.2357.

(26) Sahler, S.; Konnerth, H.; Knoblauch, N.; Prechtl, M. H. G. Hydrogen Storage in Amine Boranes: Ionic Liquid Supported Thermal Dehydrogenation of Ethylene Diamine Bisborane. *Int. J. Hydrogen Energy* **2013**, *38* (8), 3283–3290. https://doi.org/10.1016/j.ijhydene.2012.12.150.

(27) Jaska, C. A.; Temple, K.; Lough, A. J.; Manners, I. Catalytic Dehydrocoupling of Amine-Borane Adducts to Form Aminoboranes and Borazines. *Phosphorus, Sulfur Silicon Relat. Elem.* **2004**, *179* (4–5), 733–736. https://doi.org/10.1080/10426500490426683.

(28) Neiner, D. .; Karkamkar, A. .; Bowden, M. .; Joon Choi, Y. .; Luedtke, A. .; Holladay,

J. .; Fisher, A. .; Szymczak, N. .; Autrey, T. . Kinetic and Thermodynamic Investigation of Hydrogen Release from Ethane 1,2-Di-Amineborane. *Energy Environ. Sci.* **2011**, *4* (10), 4187–4193. https://doi.org/10.1039/c1ee01884a.

(29) Leardini, F.; Valero-Pedraza, M. J.; Perez-Mayoral, E.; Cantelli, R.; Bañares, M. A. Thermolytic Decomposition of Ethane 1,2-Diamineborane Investigated by Thermoanalytical Methods and in Situ Vibrational Spectroscopy. *J. Phys. Chem. C* **2014**, *118* (31), 17221–17230. https://doi.org/10.1021/jp501964r.

(30) Banerjee, B.; Pugazhenthi, G.; Banerjee, T. Experimental Insights into the Thermal Dehydrogenation of Ethylene Diamine Bisborane Using Allyl-Based Ionic Liquids. *Energy and Fuels* **2017**, *31* (5), 5428–5440. https://doi.org/10.1021/acs.energyfuels.6b02823.

(31) Zaitsau, D. H.; Yermalayeu, A. V.; Pimerzin, A. A.; Verevkin, S. P. Imidazolium Based Ionic Liquids Containing Methanesulfonate Anion: Comprehensive Thermodynamic Study. *Chem. Eng. Res. Des.* **2018**. https://doi.org/10.1016/j.cherd.2018.07.003.

(32) Meine, N.; Benedito, F.; Rinaldi, R. Thermal Stability of Ionic Liquids Assessed by Potentiometric Titration. *Green Chem.* **2010**. https://doi.org/10.1039/c0gc00091d.

(33) Chancelier, L.; Boyron, O.; Gutel, T.; Santini, C. Thermal Stability of Imidazolium-Based Ionic Liquids. *French-Ukrainian J. Chem.* **2016**. https://doi.org/10.17721/fujcv4i1p51-64.

(34) Rodriguez Rodriguez, N.; Van Den Bruinhorst, A.; Kollau, L. J. B. M.; Kroon, M. C.; Binnemans, K. Degradation of Deep-Eutectic Solvents Based on Choline Chloride and Carboxylic Acids. *ACS Sustain. Chem. Eng.* **2019**. https://doi.org/10.1021/acssuschemeng.9b01378.

(35) Trujillo, S. A.; Peña-Solórzano, D.; Bejarano, O. R.; Ochoa-Puentes, C. Tin(Ii) Chloride Dihydrate/Choline Chloride Deep Eutectic Solvent: Redox Properties in the Fast Synthesis of: N -Arylacetamides and Indolo(Pyrrolo)[1,2- a] Quinoxalines. *RSC Adv.* **2020**, *10* (66), 40552–40561. https://doi.org/10.1039/d0ra06871c.

(36) Ünlü, A. E.; Arlkaya, A.; Takaç, S. Use of Deep Eutectic Solvents as Catalyst: A Mini-Review. *Green Process. Synth.* **2019**. https://doi.org/10.1515/gps-2019-0003.

(37) Kundu, D.; Chakma, S.; Saikrishnan, S.; Pugazhenthi, G.; Banerjee, T. Molecular

Modeling and Experimental Insights for the Dehydrogenation of Ethylene Diamine Bisborane Using Hydrogen Sulfate Based Ionic Liquid. *J. Ind. Eng. Chem.* **2019**. https://doi.org/10.1016/j.jiec.2018.11.010.

(38) Kundu, D.; Pugazhenthi, G.; Banerjee, T. Low- To Room-Temperature Dehydrogenation of Dimethylamine Borane Facilitated by Ionic Liquids: Molecular Modeling and Experimental Studies. *Energy and Fuels* **2020**. https://doi.org/10.1021/acs.energyfuels.0c01896.

(39) Rizzi, V.; Polino, D.; Sicilia, E.; Russo, N.; Parrinello, M. The Onset of Dehydrogenation in Solid Ammonia Borane: An Ab Initio Metadynamics Study. *Angew. Chemie - Int. Ed.* **2019**. https://doi.org/10.1002/anie.201900134.

(40) Juneidi, I.; Hayyan, M.; Hashim, M. A. Evaluation of Toxicity and Biodegradability for Cholinium-Based Deep Eutectic Solvents. *RSC Adv.* **2015**. https://doi.org/10.1039/c5ra12425e.

(41) Nian, B.; Liao, G.; Song, Y.; Su, Y. Z.; Cao, C.; Liu, Y. Ionic Hydrogen-Bonding Interaction Controlled Electrophilicity and Nucleophilicity: Mechanistic Insights into the Synergistic Catalytic Effect of Lipase and Natural Deep Eutectic Solvents in Amidation Reaction. *J. Catal.* **2020**. https://doi.org/10.1016/j.jcat.2020.02.011.

Chapter 5

Catalytic Effect of Ionic Liquid Induced H_2-Release from Morpholine Borane Complex: A Novel and Efficient Hydrogen Storage Carrier

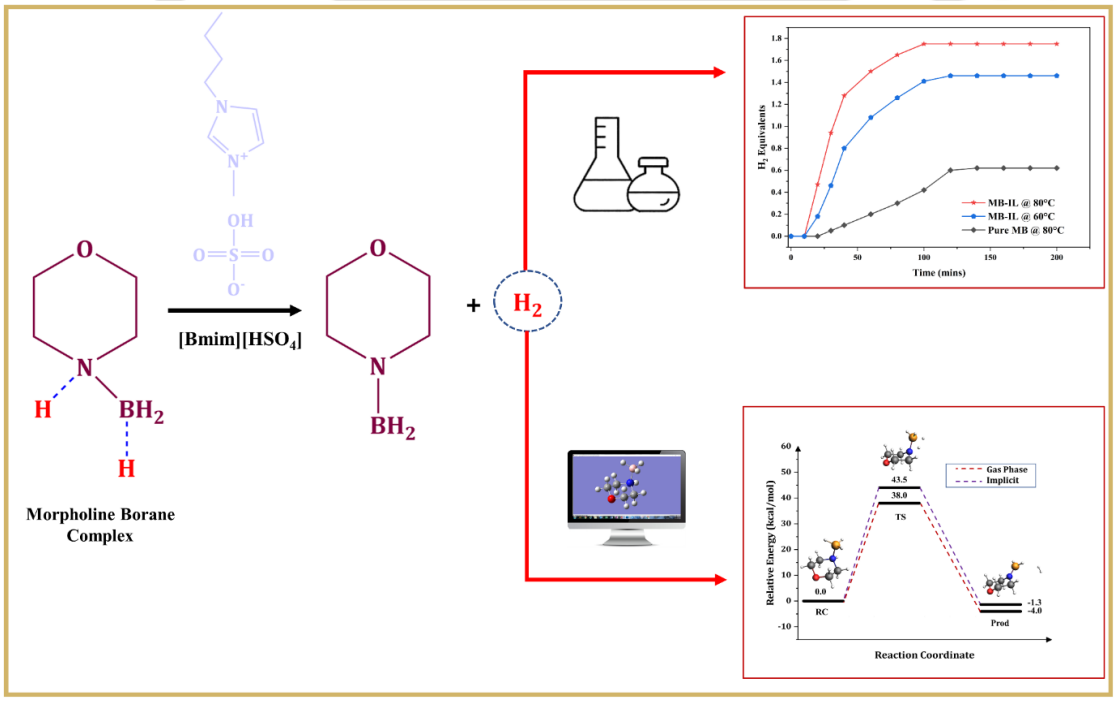

5.1. Chapter Abstract

The demand for effective and secure chemical hydrogen storage systems impedes hydrogen's usage as an alternative energy carrier. This chapter reports the use of morpholine borane (MB) as a novel, efficient, and widely viable chemical hydrogen storage material for mobile applications. Herein, for the first time, hydrogen generation from the thermolytic dehydrogenation of MB in the presence of ionic liquid (IL) media is reported. Initially, the COSMO-SAC model was utilized to determine the most appropriate solvent. [Bmim][HSO_4] proved to be an excellent catalytic cum solvent media with the maximum solubility in the morpholine borane complex. Thermal dehydrogenation experiments were conducted separately on solid-state and MB-IL systems at 60 and 80 ℃ in a vacuum-sealed experimental setup. After a prolonged heating period, the solid-state dehydrogenation of MB complex released 0.62 equivalents of hydrogen, whereas the dehydrogenation of the MB-IL system at 60 and 80 ℃ released 1.75 and 1.46 equivalents of hydrogen in a shorter time. The residue products were characterized using ^{1}H and ^{11}B NMR. ^{1}H NMR validated IL's activity as a catalytic solvent without affecting its structural identity, whereas ^{11}B NMR helped to establish an intra- and intermolecular dehydrogenation mechanism connected with MB. As confirmed by the DFT-based transition state calculations, the intramolecular dehydrogenation pathway results in a dehydrocoupled product with minimal energy required for the dehydrogenation reaction.

5.2. Introduction

Hydrogen storage and conversion are essential subjects because of their enormous potential in alleviating energy and environmental challenges. Because of its clean and sustainable nature, hydrogen has long been considered a suitable successor to fossil fuels.[1] Recently, the development of convenient, cost-effective, and highly efficient methods of

obtaining hydrogen energy has come to the top of the research priority list.[2] To attain high volumetric and gravimetric hydrogen density, the chemical storage method must be highly efficient. So, chemical hydrides leap to the top of the heap as a promising hydrogen storage solution. To achieve this, a low-cost and lightweight solid chemical hydrogen storage material with a high volumetric/gravimetric hydrogen density and a relatively quick hydrogen release kinetics must be developed.[3]

Many other commercially available compounds, especially boron-based compounds, which can also be referred to as carbon-based amine borane derivatives, have been tested as chemical hydrogen storage materials.[4] Among the materials that have been tested are ethylene diamine bisborane, hydrazine bis(borane), and dimethylamine borane.[5,6] A high hydrogen content (19.6 wt%), nontoxicity, and exceptional stability have made ammonia borane (AB) the preferred hydrogen storage material among a variety of other hydrogen storage options. AB has a number of disadvantages, including the possibility of an induction period and the documented formation of toxic gaseous products such as ammonia and borazine gas during solid-state dehydrogenation.[7] The dehydrogenation of AB in the presence of nanoparticles, scaffolds, metal-based catalysts, and catalytic solvents such as ionic liquids (ILs) and Deep Eutectic Solvents (DESs) tends to increase the rate and yield of hydrogen generation.[8,9,10,11,12,13,14,15] The search for alternative boron-based chemical storage materials for AB is underway in order to solve the difficulties associated with AB. Additionally, this pursuit is critical in a broad range of contexts, including the high cost of AB and the complexities associated with recycling dehydrogenated products. One recent study by Can et al. appraised the economics of hydrogen release from MB. Irrespective of MB's lower hydrogen content than AB, the study concluded that MB produces H_2 gas at a cheaper cost than AB.[16] Sodium borohydride ($NaBH_4$), dimethylamine borane (DMAB), and morpholine borane (MB) are the least expensive chemical hydrogen storage materials currently accessible.[10,16]

However, because of the lower melting point of DMAB and the ongoing debate about $NaBH_4$'s safety, it is determined that MB should be considered for use as a hydrogen storage material because of its many advantages, including its high hydrogen concentration (up to 12 wt%), low cost, and lack of toxicity.[16]

Morpholine-borane is a crystalline material with a melting point of 98°C with good thermal stability (Figures 5.4 and 5.5).[17] Its color ranges from white to yellow. Additionally, it is stable in aqueous solution for months without releasing hydrogen (Figure 5.2). However, despite multiple studies showing that MB can be used to synthesize metal nanoparticles (NPs) and organic synthesis, no study has revealed that MB can be thermally dehydrogenated to serve as a chemical hydrogen storage material, which encourages us to carry out the current research in light of these concerns.[18] It has been demonstrated that thermal dehydrogenation of amine-borane complexes in the presence of ionic liquids (ILs) improves both hydrogen yield and reaction rate. Bluhm and co-workers initial study presented a credible argument for the involvement of ILs in increasing the rate and extent of ammonia borane dehydrogenation.[8]

These advantages of the novel hydrogen storage material, morpholine borane (MB), prompted us to investigate its chemical dehydrogenation in the presence of an ionic liquid (IL) media. We report here that ILs provide advantageous media for morpholine borane (MB) dehydrogenation in which both the extent and the rate of hydrogen release are significantly increased.

Ionic liquids are salts that are liquid at room temperature. These salts have unique properties that make them attractive substitutes for organic solvents in hydrogen storage systems, including (a) negligible vapor pressure, (b) higher thermal stability, and (c) weakly coordinating anions and cations that provide inert reaction media and stabilize polar transition states.[19]

The solid-state dehydrogenation of morpholine borane (MB) is depicted in Figure 5.6. It was ensured that both solid-state and solution-state reactions occurred in a vacuum-sealed environment. The primary purpose of using a vacuum atmosphere in our experimental setup is to eliminate air and moisture, which might impact the reaction. The solid-state reaction was initiated by adding 25 mg of MB to a 50 mL evacuated two-neck reactor coupled to the vacuum-sealed experimental setup. Additionally, the reactor was immersed in a silicone oil bath heated to the desired temperature. At the conclusion of the reaction, the sealed valves were opened, and the evolved gases were allowed to pass through the reactor to a gas collecting flask. The evolved hydrogen was then passed via a liquid nitrogen trap to isolate any volatile non-hydrogen products or by-products. The evolved hydrogen gas was then quantified in volume using a gas buret. The specifications of the experimental glass setup can be found in our preceding chapter (Chapter 2, section 2.4.2).[9]

As illustrated in Figure 5.6, solid-state reactions conducted at 80°C yielded negligible hydrogen after 100 minutes, with only 0.3 equivalents of hydrogen gas released after 4 hours of heating. A total of 0.62 hydrogen equivalents was released after 7 hours of heating. Even after 10 hours of continual heating at the same temperature, no more hydrogen release was observed. The operating temperature in this work is close to the melting point of MB, which is around 98°C (Figure 5.4). Thus, while a minimal amount of hydrogen gas was released after prolonged heating of MB, this concern prompted us to investigate MB dehydrogenation in the presence of a catalytic solvent such as ionic liquids (ILs). Protic ionic liquids (PILs), a subclass of conventional ionic liquids, contain an exchangeable proton and display bronsted acidity, enabling their usage as solvents in various catalytic processes. Additionally, these solvents have been shown to enhance the dehydrogenation reaction by warping the intramolecular and intermolecular dihydrogen bonds inside the chemical hydrides.[20] With the enormous potential of PILs as solvent media, the current study was conducted in their presence.

5.3. Experimental Methods

5.3.1. Materials

Morpholine borane (MB) complex (97%) and 1-Butyl-3-methylimidazolium hydrogensulfate [Bmim][HSO_4] (95%) was purchased from Sigma Aldrich. Further purification was not performed on the hydride before usage. The IL, [Bmim][HSO_4], was purified by heating for 24 hours at 80°C in a vacuum oven. The chemical's structure is depicted below in Figure 5.1.

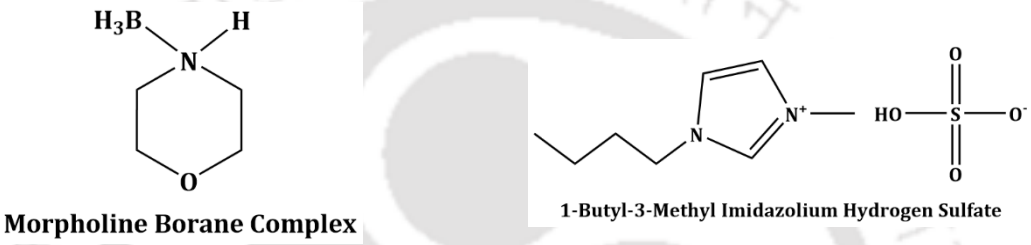

Figure 5.1: Structures and details of chemicals used in this chapter

5.3.2. NMR Analysis

The initial sample, pure morpholine borane (MB) complex, was investigated using ^{1}H and ^{13}C NMR spectroscopy. Following that, the ^{1}H and ^{13}C NMR spectra of the MB were used to determine the structure and purity of the compound (600 MHz NMR, Bruker, Germany) (Figure 5.2). The solvent used in the preparation of the NMR samples was deuterated chloroform ($CDCl_3$-d_6).

In the following step, MB/IL mixtures were characterized using ^{1}H and ^{11}B NMR before and after the reaction, respectively. The ^{1}H NMR study of the MB/IL complexes was undertaken to reassert IL's catalytic role in the dehydrogenation process. Dimethyl sulfoxide (DMSO) was used as the solvent for the NMR samples.

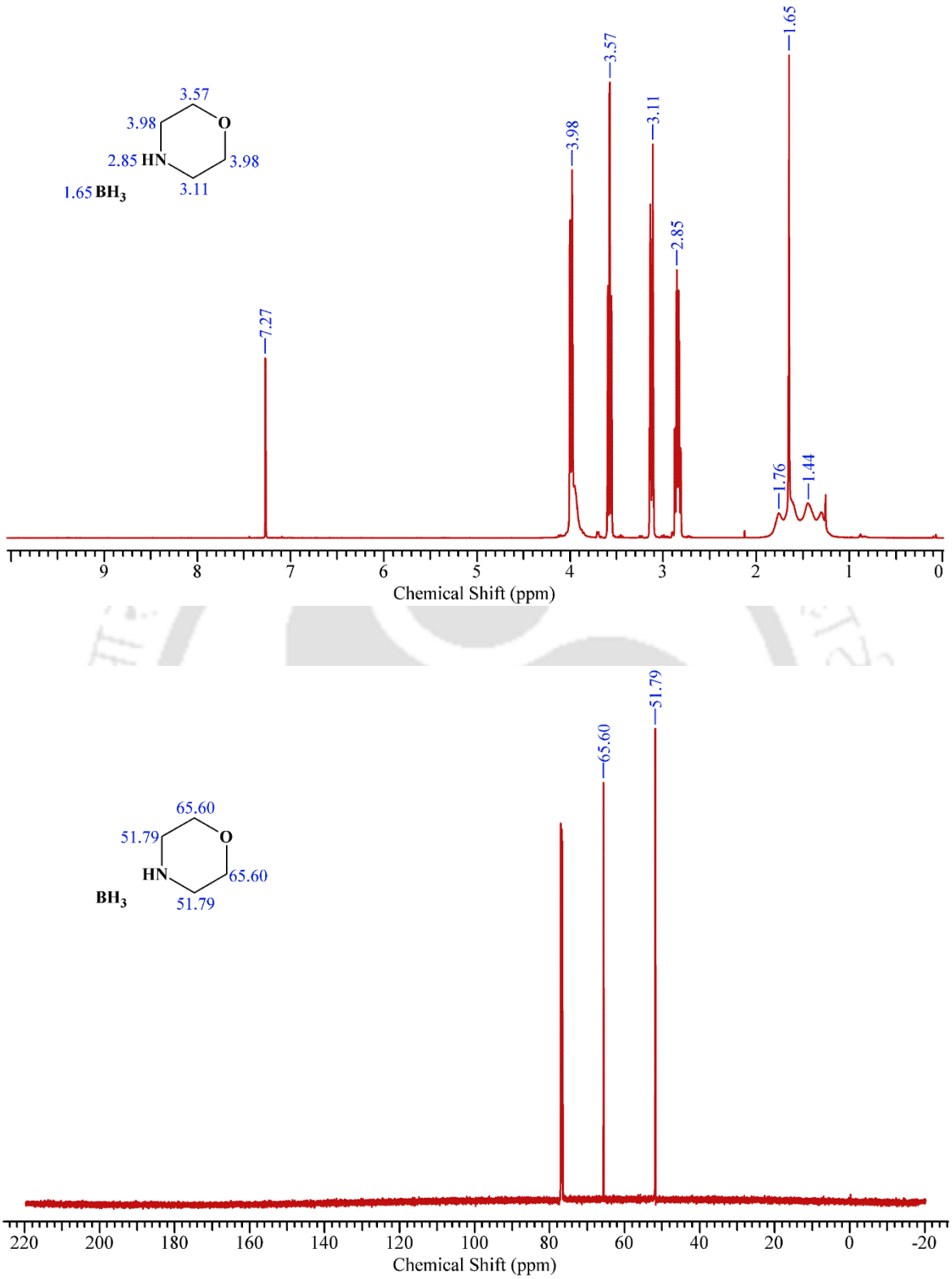

Figure 5.2: ^{1}H NMR and ^{13}C NMR spectra of pure morpholine borane complex

5.3.3. Computational Details

All molecular calculations are carried out utilizing density functional theory (DFT) implementations in the Gaussian 09 package.[2] The visualizations were performed using GaussView 5.0 visualization package.[3] The initial structures of the reactant complexes and dehydrogenated product were optimized using density functional theory based B3LYP/CCSD(T) level of theory in conjunction with a 6-311++G(d,p) basis set. To begin, several reactant complex orientations were investigated to determine a structure with a minimum. After providing a suitable TS guess, the transition state calculations were performed. The reactant complex and TS guess structures were combined with the dehydrogenated product, and a saddle point was found using a Synchronous Transit-Guided Quasi-Newton (STQN) technique. A frequency calculation was performed on the resulting TS structure, which indicated the presence of an imaginary (negative) frequency, confirming the integrity of the TS structure. Additionally, IRC calculations were performed on the TS structure to derive the reaction coordinate.

An implicit IEFPCM solvation model was employed to employ solvent as a continuum, which presents an informative detail of the interacting system. The continuum solvent employed is the IL [Bmim][HSO_4], used as a catalytic solvent in the present investigation. Following that, the relative energy of the gas phase and implicit solvation were compared. However, the DFT calculations performed here are intended to demonstrate the feasibility of testing mechanistic possibilities suggested by the experimental data.

5.4. COSMO-SAC Based Screening of ILs

In light of the large variety of available protic ionic liquids (PILs), choosing the most appropriate IL for the dehydrogenation experiment was vital before moving forward. In their work, Banerjee et al. demonstrated the COSMO-SAC model, which is based on quantum

mechanical computations, to determine the solubility of a solute in a solvent.[21] In the first instance, the COSMO-SAC calculation is implemented to predict Infinite Dilution Activity Coefficient (IDAC) values of MB in a range of PILs. These values indicate a solvent's (PILs) suitability for extracting or solubilizing a solute (MB) when its composition in the liquid phase is near zero. The IDAC values produced are used to predict the solubility of chemical hydrides in ILs; a negative logarithmic IDAC value suggests solubility, whereas a positive logarithmic IDAC value shows insolubility. The COSMO-SAC theory in its entirety can be found elsewhere.[22] The logarithmic IDAC values of MB in various PIL systems are summarized in Figure 5.3, and it is predicted that MB has the maximum solubility in hydrogen sulfate anion-based IL. All anions are coupled with 1-Butyl-3-methylimidazolium [Bmim]-based cations. [Bmim][HSO_4] is the abbreviation for the investigated IL system.

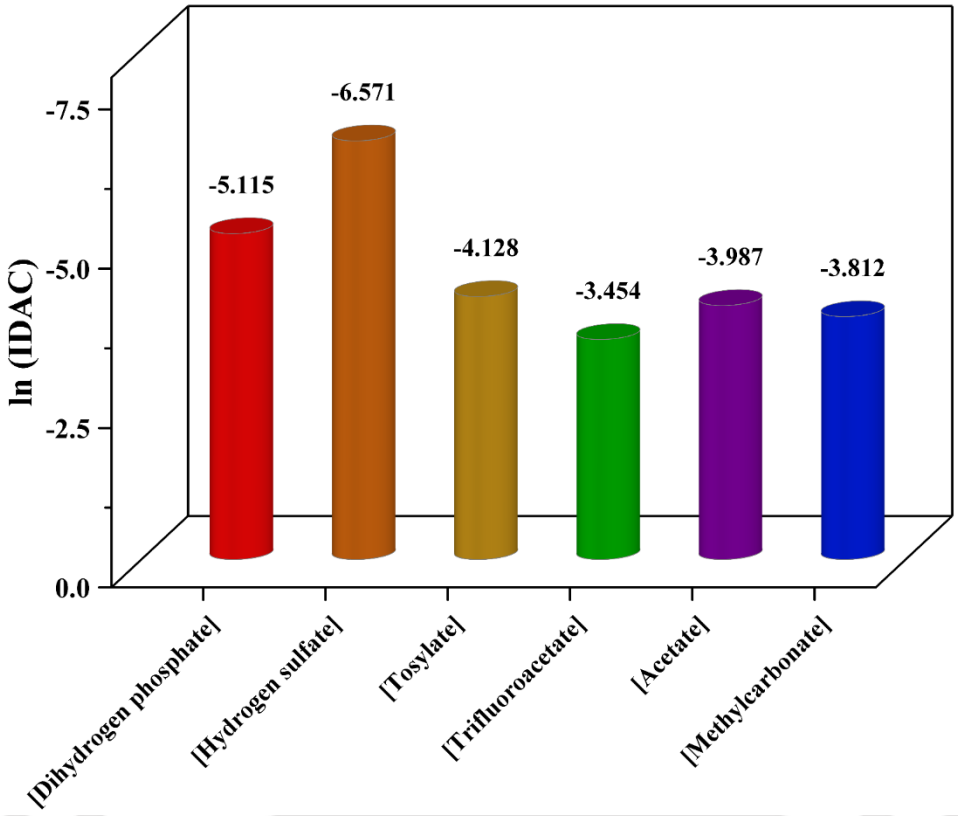

Figure 5.3: COSMO-SAC model predicted logarithmic IDAC values of MB in 1-Butyl-3-methylimidazolium [Bmim]-based ILs. All the anions are coupled with a common 1-Butyl-3-methylimidazolium-based cation.

5.5. Results and Discussions

5.5.1. Thermal Analysis

Thermal characterization of the novel hydrogen storage carrier was critical to understand the material's thermal behavior. To determine the melting point and breakdown temperature of morpholine borane (MB), differential scanning calorimetry (DSC) and thermo-gravimetric analysis (TGA) were performed on the MB complex as purchased.

The DSC analysis was carried out on NETZSCH DSC STA 449F3 equipment by heating the samples in the presence of flowing nitrogen. The samples were transported and placed into the apparatus in an inert atmosphere. The data were acquired by heating the samples

under nitrogen gas from room temperature to 200°C at a rate of 2°C min^{-1}, starting at room temperature (25°C). The DSC data is shown in Figure 5.4 below. The DSC trace of MB heated at a rate of 2°C min^{-1} reveals a strong exotherm between 98°C and 100°C, validating the previously reported melting temperature of the MB complex.[1] A thermo-gravimetric TGA (TGA (TG 209 F1 Libra; Make: M/s Netzsch, Germany) analysis of the MB complex in its solid-state was carried out to ascertain the thermal stability of the novel hydrogen storage carrier. The investigation was carried out for the MB complex in its solid-state throughout a wide temperature range (20°C to 800°C) at a heating rate of 10°C min^{-1} in a nitrogen atmosphere. The stability of amine borane complexes carries over to the MB complex, which undergoes mass loss up to 150°C. The inclusion of a ring in the MB complex can be ascribed to the complex's increased stability. Apart from the first onset peak, the TGA curve (Figure 5.5) demonstrates that the compound suffers significant mass variations around 180°C, revealing that the MB complex has a breakdown temperature of between 180°C and 200°C.

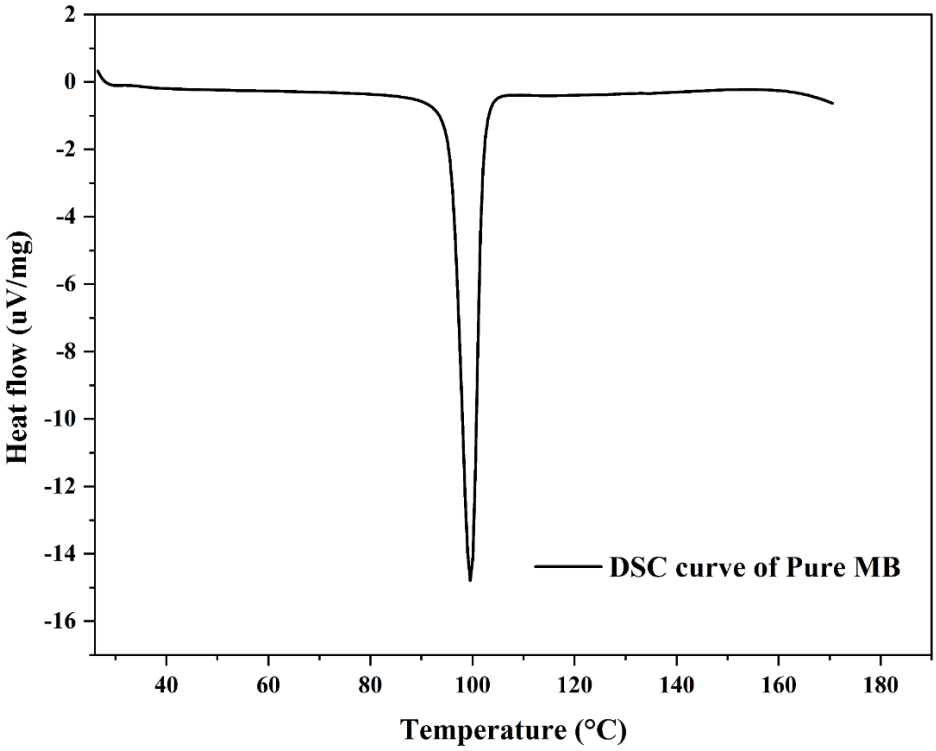

Figure 5.4: DSC curve of pure morpholine borane complex

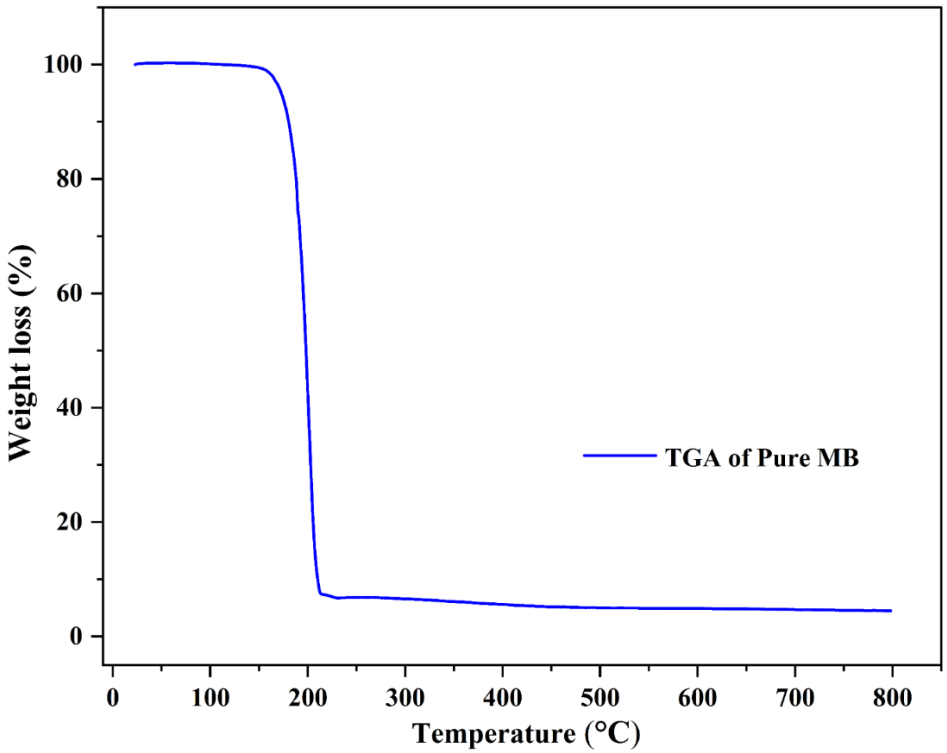

Figure 5.5: TGA curve of pure morpholine borane complex

5.5.2. IL Facilitated Thermal Dehydrogenation of Morpholine Borane Complex

In comparison to the solid-state reactions, the dehydrogenation of morpholine borane [MB] in [Bmim][HSO_4] exhibited a shorter induction time (Figure 5.6), with hydrogen release initiating within ten minutes of the sample being placed in the heated oil bath. This transitory induction period of MB in the presence of ILs can be attributed to the lower solubility of hydrides in the ILs (Figure 5.3). The parent amine-borane compounds AB and EDAB have been found to be more soluble in IL systems.[9,11,12] Separate samples heated at 80 and 60°C produced 1.75 and 1.46 equivalents of H_2, respectively. Compared to the solid-state dehydrogenation of MB at 80°C, which yielded 0.1 hydrogen equivalents during the first 100 minutes of the reaction, the IL-assisted dehydrogenation of MB released 1.28 equivalents of hydrogen gas at the same working temperature. However, when heated to 60°C, the MB-IL sample was capable of releasing 0.8 hydrogen equivalents in the same amount of heating period (Figure 5.6). An additional experimental study was undertaken to examine the effect of the cation on the dehydrogenation of the MB complex by lowering the alkyl chain length of the IL without affecting the anionic moiety. 1-Ethyl-3-Methylimidazolium hydrogen sulfate [Emim][HSO_4] was employed for this chore. When heated to 80°C, [Emim][HSO_4] was found to be capable of yielding 1.53 equivalents of hydrogen gas (Figure 5.7), which was notably less than [Bmim][HSO_4]. This reduced release of hydrogen equivalents in the presence of a lower alkyl chain cation might be attributed to a stronger interaction between the cationic and anionic moieties of the IL([Emim][HSO_4]) in contrast to the higher alkyl chain length cation IL ([Bmim][HSO_4]). A weaker interaction within the ions of [Bmim][HSO_4] tends to establish strong interactions between the anionic moieties of ILs and the chemical hydrides, resulting in a higher release of hydrogen equivalents. It is worth noting that the dehydrogenation of MB has an induction period in its solid-state, which is reduced by the utilization of ionic liquids

(ILs). In the solution state, the release of hydrogen gas was substantially higher than the 0.62 equivalents obtained in the solid-state processes.

In a recent study, the hydrolysis of the MB complex in the presence of polymer-stabilized water-soluble nanoparticles was found to be capable of releasing higher equivalents of hydrogen gas compared to the MB complex's thermolysis in the presence of IL, as demonstrated in the present work.[16] This outcome is explained by the fact that the MB complex is less soluble in the class of IL employed. The effect of solubility on the dehydrogenation process with an induction period prior to the release of hydrogen equivalents was extremely noticeable.

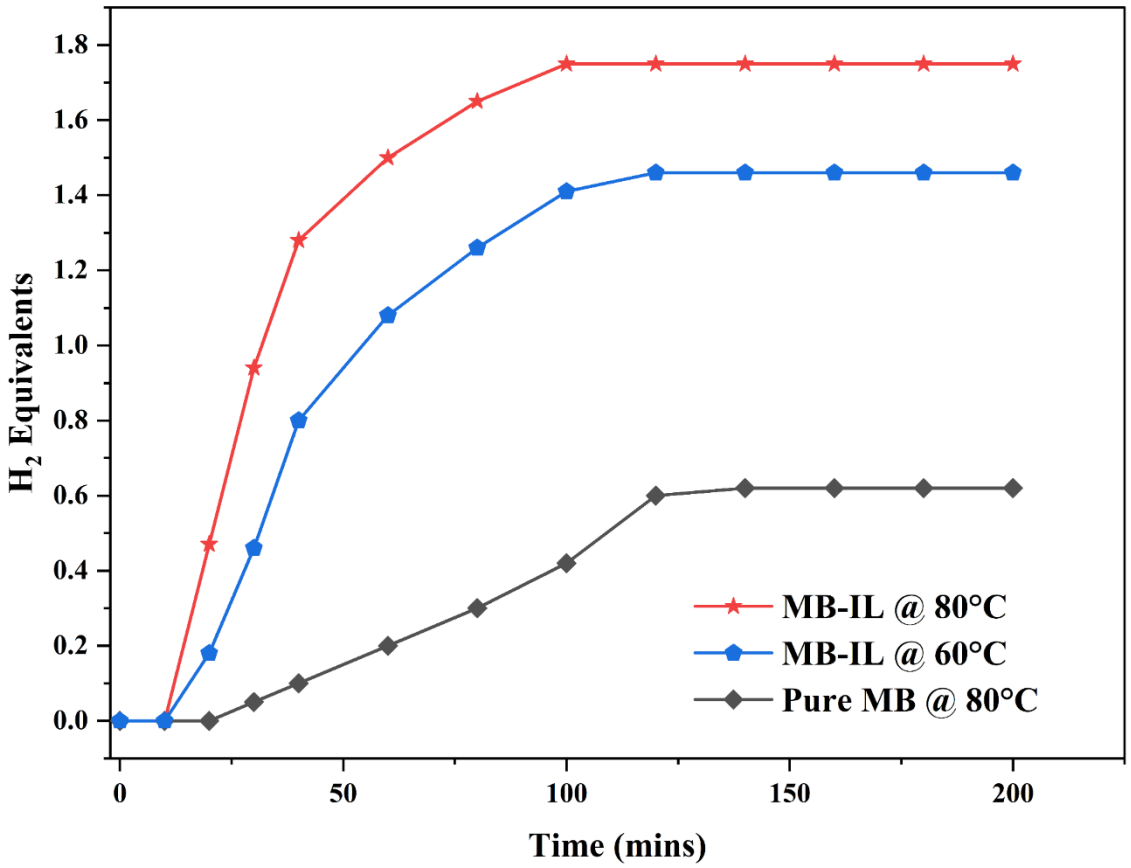

Figure 5.6: Equivalents of hydrogen released from solid MB and MB-IL systems at 80 and 60 °C

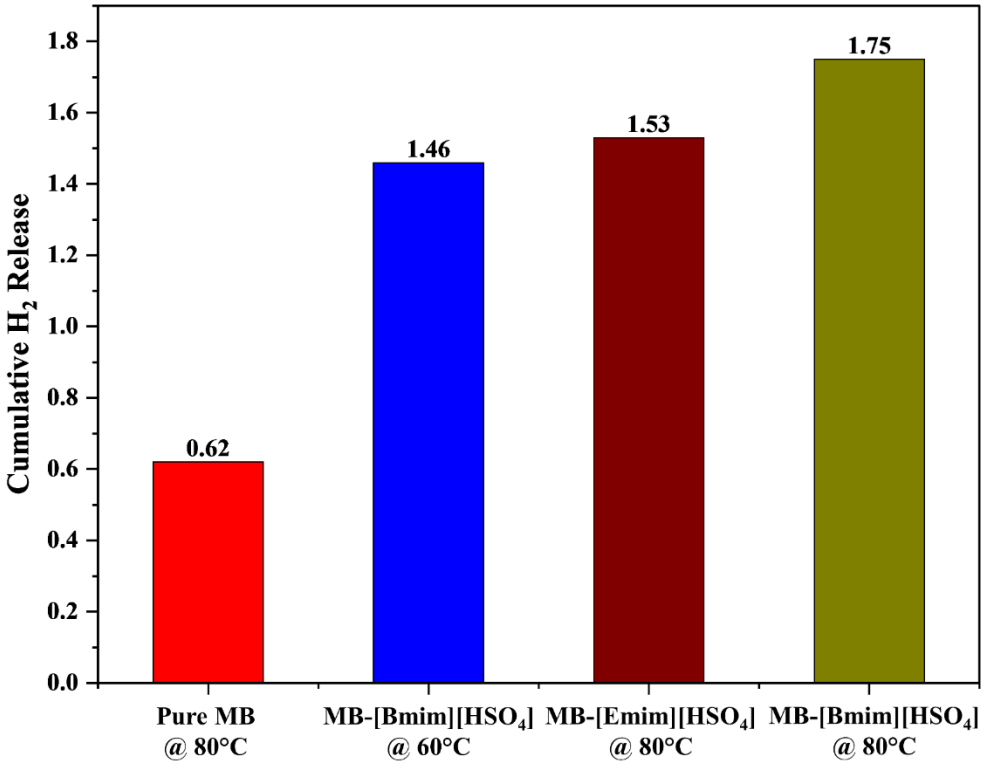

Figure 5.7: Cumulative hydrogen release from solid MB and MB-IL systems at 80 and 60 °C

5.5.3. ^{1}H and ^{11}B NMR Analysis

The residual reaction products were collected and analyzed using ^{1}H and ^{11}B NMR to confirm the catalytic activity of the IL system and to predict the dehydrogenation mechanism. This was conducted by collecting pre-and post-treatment samples and examining them using the ^{1}H NMR spectroscopy technique. The purpose of the ^{1}H NMR investigation was to assess the effect of IL on the reaction as a catalytic media in the dehydrogenation process. The ^{1}H NMR analysis revealed that the spectra of IL moieties are comparable. Still, chemical shifts of –NH are absent, along with a significant reduction in the area of peaks of $–BH_3$, signifying that the released hydrogen was obtained from the morpholine borane complex (Figure 5.8) and that IL retained its original structural entity.

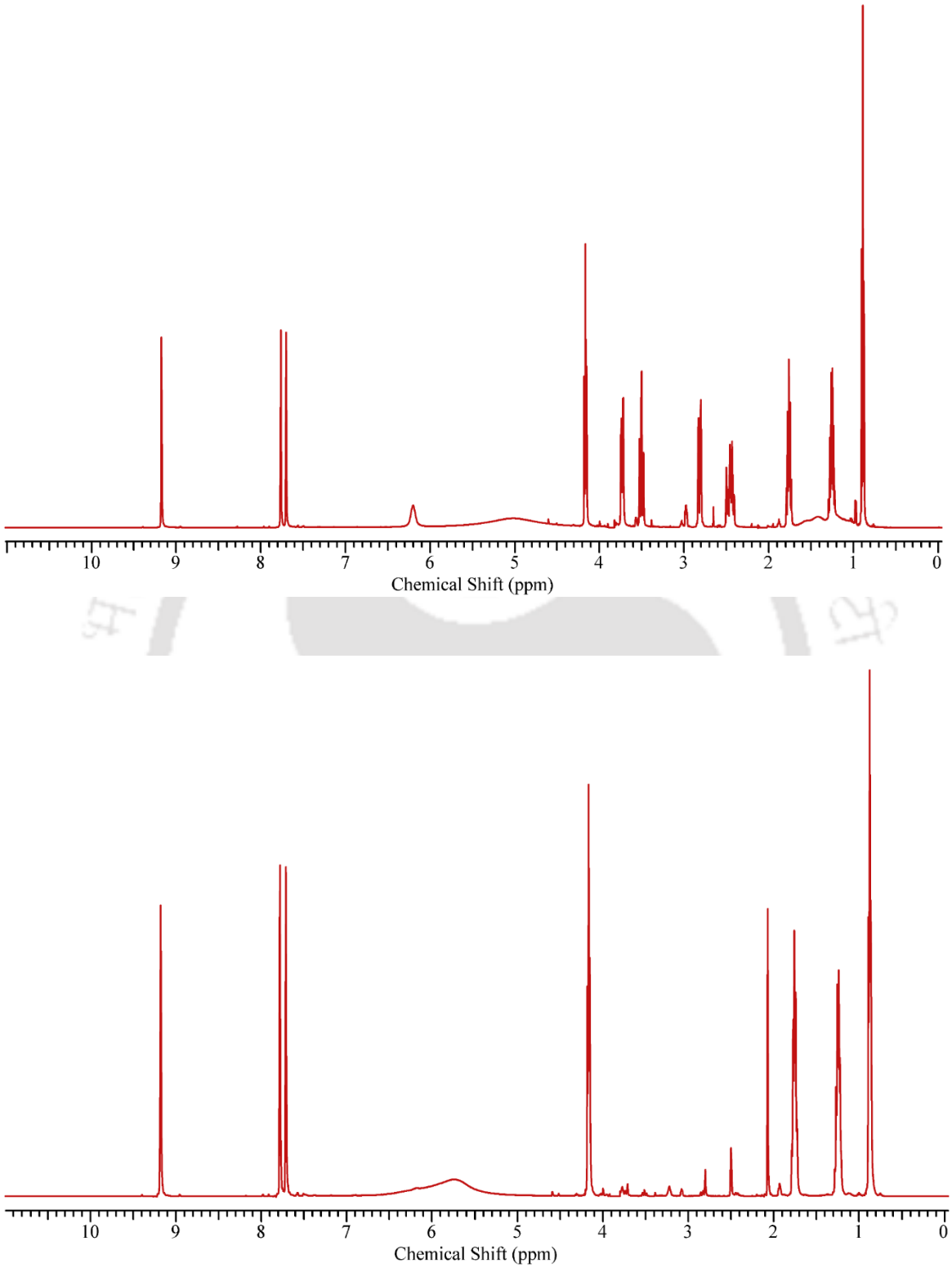

Figure 5.8: ^{1}H NMR spectra of MB/[BMIM][HSO_4] (Before and After reaction)

The ^{11}B NMR spectra of pristine MB and MB-IL reaction residues are compared in Figure 5.9. The solid MB and MB-IL initial solution spectrum revealed only unreacted morpholine borane (−14.71 and −14.84 ppm), with a slight fluctuation in the peaks due to the MB complex's interaction with the IL system. It is noted that the first few spectra are consistent with previous literature, which assigns the peak positions to the sp^3 $–BH_3$ functional group of the MB complex.[16,23] The third spectrum corresponds to the MB-IL system's residue following the release of one hydrogen equivalent, with a broad resonance at −3.12 ppm. In the presence of ILs, this chemical shift at −3.12 ppm is noteworthy. This shift can be attributed to the $–BH_2$ moiety, which ensures that one hydrogen equivalent is released. Additionally, this peak is stable and exhibits just a slight variation. IL-mediated dehydrogenation of AB produces a $−BH_2$ signal at $\delta = −5.46$ ppm.[24] As a result of its proximity to the signal, the resonance at −3.12 ppm is ascribed to the dehydrogenated MB complex's BH_2 moiety. A new strong peak at −14.71 ppm is identified with the emission of one equivalent of hydrogen, corresponding to the interaction of a new MB monomer. The presence of protic ionic liquid will enhance the affinity of protic hydrogen of MB toward the electronegative oxygen atom of hydrogen sulfate IL.[19,20] The weakening of the B-N bond as a result of the non-covalent interaction triggers the hydrogen release to occur with a shorter induction period. The spectra of the MB-IL reaction residues for the 1.3 and 1.75 hydrogen equivalents released samples were very similar to the third spectrum, exhibiting similar resonances and moderate peak shifting. These findings demonstrated unequivocally that the release of hydrogen equivalents in morpholine borane could occur via intra- and intermolecular pathways. Identical to the intramolecular mechanism, the intermolecular dehydrogenation pathway begins with the release of H_2 from the monomer. The dehydrogenated MB complex $[(CH_2)_4ONBH_2]$ associates with a new MB complex following the release of one equivalent of hydrogen gas. As a result of this dimerization, the second hydrogen equivalent is released. A comprehensive dehydrogenation study is currently being

conducted and will be included in our future work. The probable intra- and intermolecular dehydrogenation mechanisms are illustrated in Scheme 5.1.

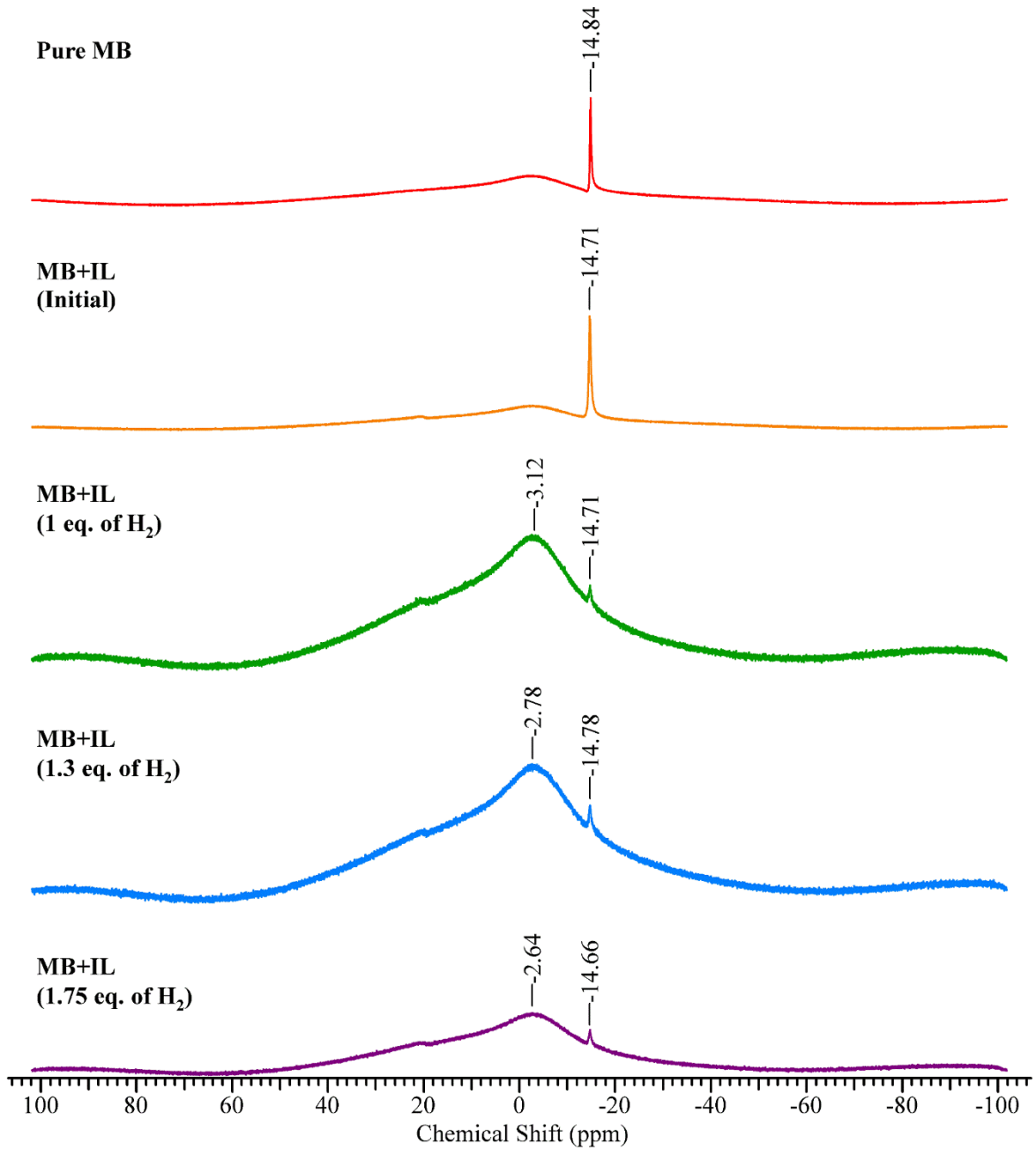

Figure 5.9: In-situ ^{11}B NMR spectra of the residues of IL aided morpholine borane dehydrogenation

(a)

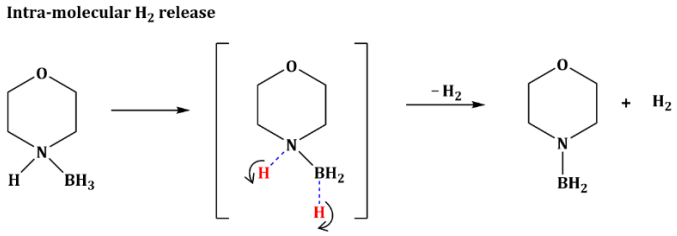

(b)

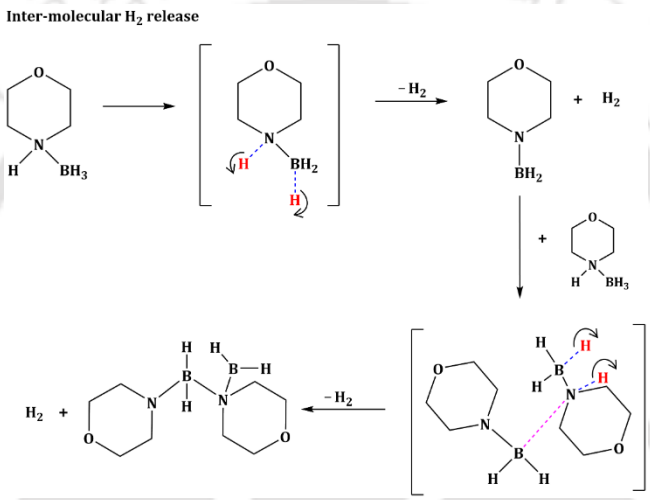

Scheme 5.1: Proposed Intra- and Intermolecular pathway for the hydrogen release from MB complex

5.6. Transition State Calculations

To better understand the mechanism of the hydrogen release processes in this system, which is considered a feasible option for chemical hydrogen storage, we investigated a probable reaction pathway (Figure 5.10) leading towards intramolecular dehydrogenation using the accurate CBS-QB3 approach.[25] Molecular bond lengths critical to hydrogen release reactions are addressed (Table 5.1). The pathway is the dehydrogenation of RC (MB) to give the dehydrogenated product (Prod) (Figure 5.11). Using the STQN method, a transition structure ($TS_{gas\text{-}phase}$, Figure 5.11) was found at the saddle point connecting the reactant

complex (RC) and the product (Prod).[26] This pathway has an activation barrier of 42.1 kcal mol^{-1} to produce a low-lying and more stable product (Prod) with a lower energy of -0.5 kcal mol^{-1} relative to the reactant complex (RC). The N–H and B–H bonds in the $TS_{gas\text{-}phase}$ structure are elongated by 0.22 Å and 0.11 Å, respectively, in comparison to the reactant complex (RC). As a result, a H–H dihydrogen bond with a theoretical distance of 0.74 Å is formed.[27] Formation of dihydrogen bonds has previously been considered to occur before the release of a hydrogen equivalent. The dehydrogenated product is predicted to form following the cleavage of N–H and B–H bonds, resulting in a shorter B–N bond in the product (B–N=1.39 Å) than in the reactant complex (B–N=1.68 Å). This intramolecular approach implies that the dehydrogenation reaction requires very minimal energy, which can be further decreased in the presence of catalytic solvents.[19,28] To infer the use of IL as a solvent media, an implicit IEFPCM solvation model was used to comprehend the interactions between the MB complex and the examined IL system. This pathway is akin to the gas-phase intramolecular approach. The reactant proceeds with the formation of a transition structure by decreasing the barrier from 42.1 to 39.3 kcal mol^{-1}, which is a favorable energy barrier. This decrease in the energy barrier can be imputable to the prominent interactions between the MB complex and IL. Moreover, in the presence of IL, this result can be explained in terms of the reduction in ground state energy of the MB complex, which is lower in magnitude than the reduction in transition state energy. The energy of the systems in gas and solvent phases is presented in Table 5.3, and it is concluded that the MB complex is more stable in the presence of solvent. This leads to a lower activation energy in the presence of solvent media, which can significantly be correlated with the experimental studies. The smaller reduction in the implicit pathway's activation energy can be attributable to the shorter induction period observed in the experimental investigation. This induction period is primarily concerned with the formation of TS, which triggers the subsequent hydrogen equivalent release. However, the $TS_{implicit}$ has a more favorable structure

than the $TS_{gas\text{-}phase}$, with a predicted H–H distance of 0.97 and extended N–H and B–H bonds of 0.41 and 0.16, respectively (Table 5.2). The dihydrogen interaction is more pronounced in this phase than in $TS_{gas\text{-}phase}$ (Figure 5.12). This pathway has the shortest interatomic distances and also demonstrates the critical role of [Bmim][HSO_4] as an effective catalyst in the dehydrogenation process, as shown in the other amine borane systems stated previously.[23] The reaction pathways in the gas and solvent phases were confirmed with an IRC calculation. Nonetheless, further study is necessary to evaluate the dehydrogenation mechanism and probable hydrogen release pathways from MB. A comprehensive analysis of this nature will be carried out as part of our future work.

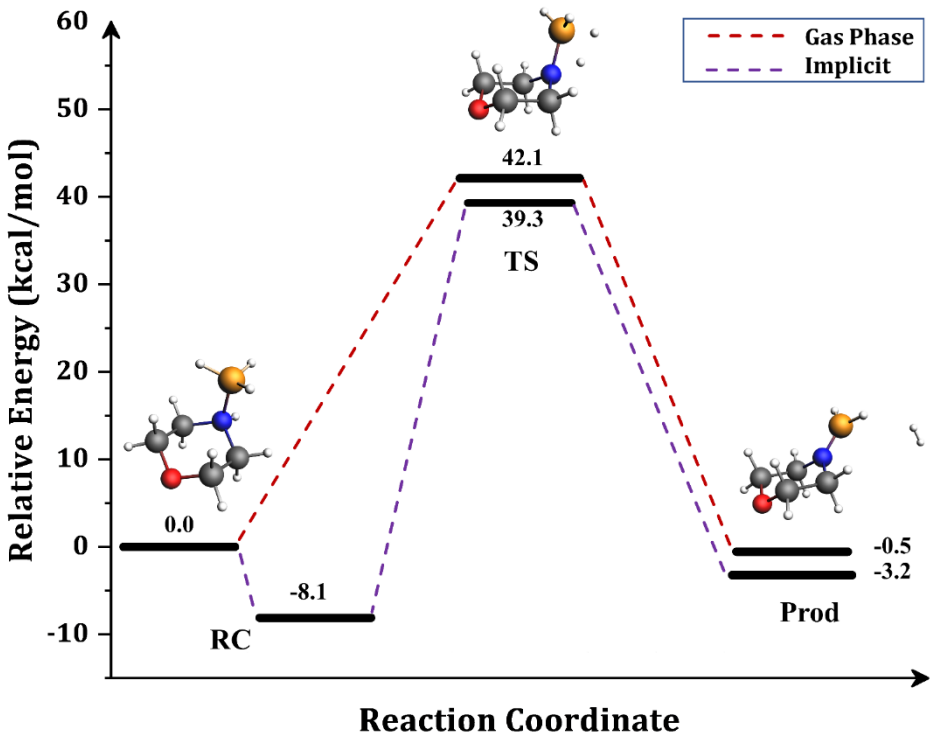

Figure 5.10: Relative energy profile for the intra-molecular dehydrogenation of morpholine borane complex (MBC) at the CCSD(T) level of theory. Relative energies are given in kilocalories per mole (kcal/mol).

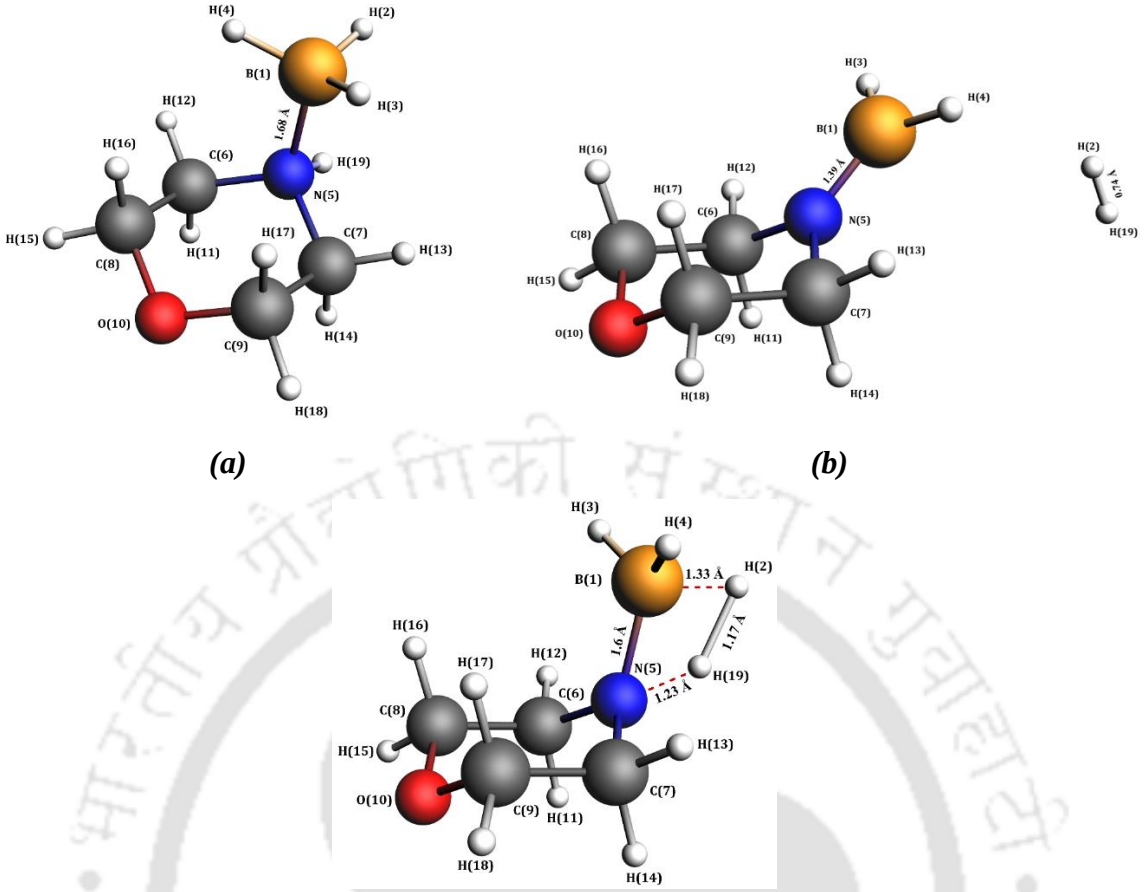

Figure 5.11: (a) The optimized structure of the morpholine borane complex, RC, (b) the lowest-energy ground-state structure of the dehydrogenated product, (Prod), and (c) transition-state structure for the dehydrogenation of morpholine borane complex in implicit solvation phase ($TS_{Gas\text{-}phase}$).

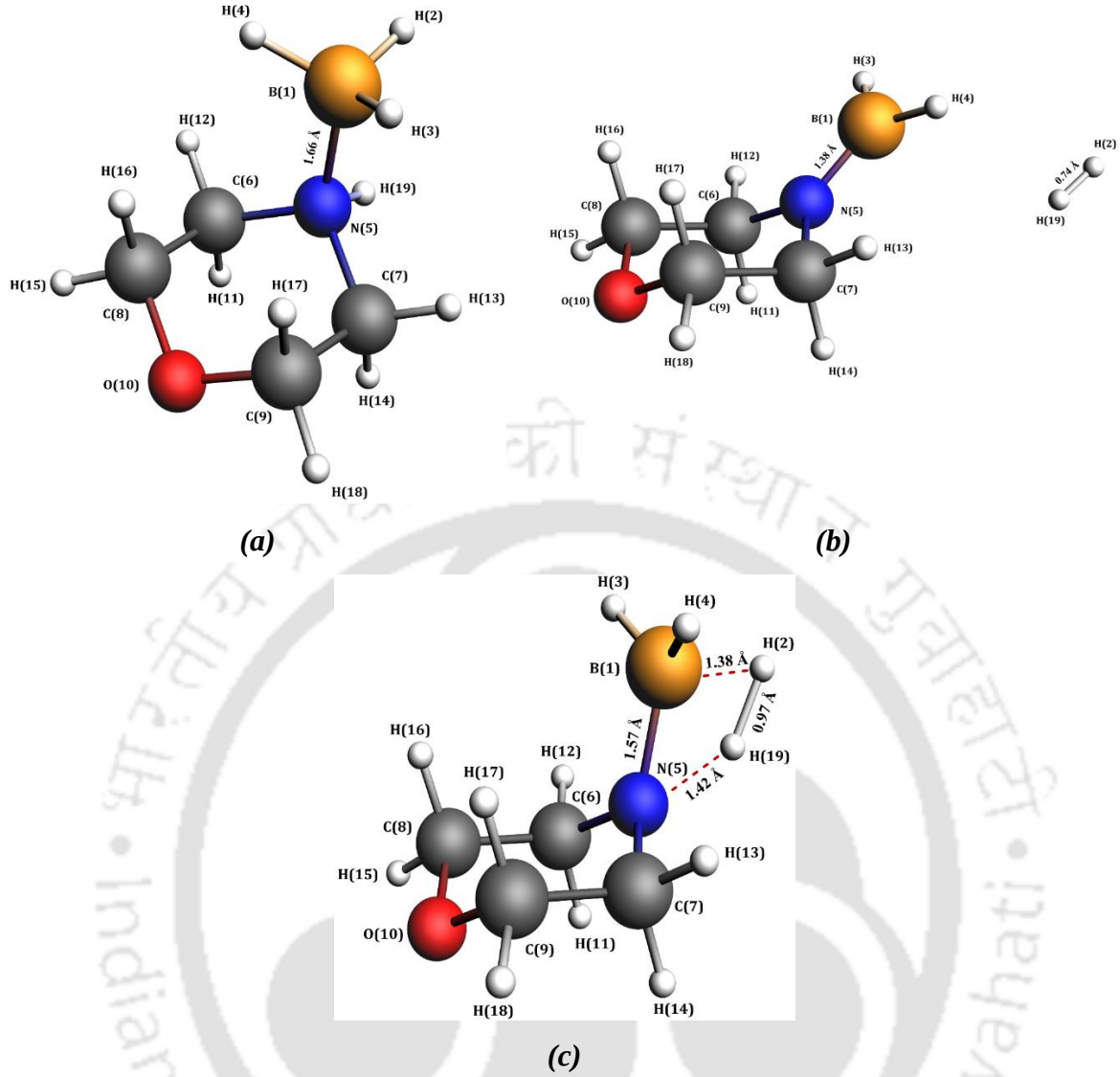

Figure 5.12: (a) The optimized structure of the morpholine borane complex, RC, (b) the lowest-energy ground-state structure of the dehydrogenated product, (Prod), and (c) transition-state structure for the dehydrogenation of morpholine borane complex in Gas-phase ($TS_{implicit}$).

Table 5.1: Bond lengths involved in the dehydrogenation reaction predicted at CCSD(T) level of theory in the gas-phase for Reactant (RC), TS, and Product (Prod).

Bond Distance	RC	TS	Prod
r (N-H)	1.02	1.23	---
r (B-H)	1.21	1.33	---
r (B-N)	1.68	1.6	1.39
r (H-H)	---	1.17	---

All distances are in Å.

Table 5.2: Bond lengths involved in the dehydrogenation reaction predicted at CCSD(T) level of theory in the implicit solvent phase for Reactant (RC), TS, and Product (Prod).

Bond Distance	RC	TS	Prod
r (N-H)	1.02	1.42	---
r (B-H)	1.21	1.38	---
r (B-N)	1.66	1.57	1.38
r (H-H)	---	0.97	---

All distances are in Å.

Table 5.3: Comparison of energy (kcal/mol) between gas phase and implicit calculation. The values highlighted in red represent the relative energy barrier.

Total Energy	RC	TS	Prod
Gas Phase Calculation	-196856.9921 **[0.0]**	-196814.8617 **[+42.1]**	-196857.5342 **[-0.5]**
Implicit Calculation	-196865.1056 **[-8.1]**	-196817.7037 **[+39.3]**	-196860.2023 **[-3.2]**

5.7. Conclusions

In summary, we have conducted a comparative study of solid-state and ionic liquid-mediated dehydrogenation of morpholine borane complex (MBC) for the first time. The COSMO-SAC model was used to determine the potential ionic liquid solvent for the dehydrogenation experiment. A comparative study of the thermal dehydrogenation of MB in ionic liquid media at 60 and 80°C reported the release of 1.46 and 1.75 equivalents of hydrogen, respectively. The release was substantially higher than the amount of hydrogen released via solid-state dehydrogenation of the hydride, which was an insignificant 0.62 equivalent of hydrogen. ^{1}H NMR characterization revealed the catalytic activity of IL. In-situ ^{11}B NMR was performed to anticipate the intra- and inter-dehydrogenation mechanism responsible for the hydrogen release from MB. Using density functional theory (DFT)-based transition state calculations, it was possible to provide additional validation for the intramolecular mechanism of hydrogen release from the MB complex. To establish MB as a chemical hydrogen storage material, this study will pave the way for future research in this sector; additional work on this issue is underway, including testing various novel ionic liquids (ILs) and Deep Eutectic Solvents (DESs) as a solvent media.[28]

References

(1) Stephens, F. H.; Pons, V.; Tom Baker, R. Ammonia–borane: The Hydrogen Source Par Excellence? *J. Chem. Soc. Dalt. Trans.* **2007**, No. 25, 2613–2626. https://doi.org/10.1039/b703053c.

(2) Hassmann, K.; Kühne, H. M. Primary Energy Sources for Hydrogen Production. *Int. J. Hydrogen Energy* **1993**, *18* (8), 635–640. https://doi.org/10.1016/0360-3199(93)90115-Q.

(3) Biniwale, R. B.; Rayalu, S.; Devotta, S.; Ichikawa, M. Chemical Hydrides: A Solution to High Capacity Hydrogen Storage and Supply. *Int. J. Hydrogen Energy* **2008**, *33* (1), 360–365. https://doi.org/10.1016/j.ijhydene.2007.07.028.

(4) Hamilton, C. W.; Baker, R. T.; Staubitz, A.; Manners, I. B-N Compounds for Chemical Hydrogen Storage. *Chem. Soc. Rev.* **2009**, *38* (1), 279–293. https://doi.org/10.1039/b800312m.

(5) Neiner, D. .; Karkamkar, A. .; Bowden, M. .; Joon Choi, Y. .; Luedtke, A. .; Holladay, J. .; Fisher, A. .; Szymczak, N. .; Autrey, T. . Kinetic and Thermodynamic Investigation of Hydrogen Release from Ethane 1,2-Di-Amineborane. *Energy Environ. Sci.* **2011**, *4* (10), 4187–4193. https://doi.org/10.1039/c1ee01884a.

(6) Mal, S. S.; Stephens, F. H.; Baker, R. T. Transition Metal Catalysed Dehydrogenation of Amine-Borane Fuel Blends. *Chem. Commun.* **2011**, *47* (10), 2922–2924. https://doi.org/10.1039/c0cc03585h.

(7) Smythe, N. C.; Gordon, J. C. Ammonia Borane as a Hydrogen Carrier: Dehydrogenation and Regeneration. *Eur. J. Inorg. Chem.* **2010**, No. 4, 509–521. https://doi.org/10.1002/ejic.200900932.

(8) Bluhm, M. E.; Bradley, M. G.; Butterick, R.; Kusari, U.; Sneddon, L. G. Amineborane-Based Chemical Hydrogen Storage: Enhanced Ammonia Borane Dehydrogenation in Ionic Liquids. *J. Am. Chem. Soc.* **2006**, *128* (24), 7748–7749. https://doi.org/10.1021/ja062085v.

(9) Mishra, D. K.; Pugazhenthi, G.; Banerjee, T. Ionic Liquid-Based Deep Eutectic Solvent as Reaction Media for the Thermal Dehydrogenation of Ethylene Diamine- Bis -Borane . *ACS Sustain. Chem. Eng.* **2020**, *8* (12), 4910–4919.

https://doi.org/10.1021/acssuschemeng.0c00220.

(10) Kundu, D.; Pugazhenthi, G.; Banerjee, T. Low- To Room-Temperature Dehydrogenation of Dimethylamine Borane Facilitated by Ionic Liquids: Molecular Modeling and Experimental Studies. *Energy and Fuels* **2020**. https://doi.org/10.1021/acs.energyfuels.0c01896.

(11) Mishra, D. K.; Banerjee, B.; Pugazhenthi, G.; Banerjee, T. Metal-Free, Ionic Liquid-Mediated Hydrogen Release from Amine Borane Complexes: An Experimental and Density Functional Theory Investigation. *Ind. Eng. Chem. Res.* **2021**, *60* (27), 9764–9776. https://doi.org/10.1021/acs.iecr.1c01507.

(12) Mishra, D. K.; Pugazhenthi, G.; Banerjee, T. Ionic Liquid-Based Deep Eutectic Solvents as Novel Solvent-Cum-Catalyst Media for Thermal Dehydrogenation of Chemical Hydrides. *Int. J. Hydrogen Energy* **2021**. https://doi.org/10.1016/j.ijhydene.2021.02.012.

(13) Rossin, A.; Peruzzini, M. Ammonia-Borane and Amine-Borane Dehydrogenation Mediated by Complex Metal Hydrides. *Chemical Reviews*. 2016. https://doi.org/10.1021/acs.chemrev.6b00043.

(14) Rossin, A.; Tuci, G.; Luconi, L.; Giambastiani, G. Metal-Organic Frameworks as Heterogeneous Catalysts in Hydrogen Production from Lightweight Inorganic Hydrides. *ACS Catal.* **2017**. https://doi.org/10.1021/acscatal.7b01495.

(15) Luconi, L.; Tuci, G.; Giambastiani, G.; Rossin, A.; Peruzzini, M. H2 Production from Lightweight Inorganic Hydrides Catalyzed by 3d Transition Metals. *International Journal of Hydrogen Energy*. 2019. https://doi.org/10.1016/j.ijhydene.2019.08.017.

(16) Can, H.; Metin, Ö. Hydrogen Generation via the Catalytic Hydrolysis of Morpholine-Borane: A New, Efficient and Cost-Effective Hydrogen Storage Medium. *Int. J. Hydrogen Energy* **2019**. https://doi.org/10.1016/j.ijhydene.2019.08.043.

(17) Ja'O, A. M.; Wann, D. A.; Rankine, C. D.; Polson, M. I. J.; Masters, S. L. Utilizing the Combined Power of Theory and Experiment to Understand Molecular Structure-Solid-State and Gas-Phase Investigation of Morpholine Borane. *Aust. J. Chem.* **2020**, *73* (8), 794–802. https://doi.org/10.1071/CH19492.

(18) White, S. S.; Kelly, H. C. Kinetics and Mechanism of the Morpholine-Borane Reduction

of Methyl Alkyl Ketones. *J. Am. Chem. Soc.* **1970**. https://doi.org/10.1021/ja00717a013.

(19) Hallett, J. P.; Welton, T. Room-Temperature Ionic Liquids: Solvents for Synthesis and Catalysis. 2. *Chem. Rev.* **2011**, *111* (5), 3508–3576. https://doi.org/10.1021/cr1003248.

(20) Greaves, T. L.; Drummond, C. J. Protic Ionic Liquids: Properties and Applications. *Chemical Reviews*. 2008. https://doi.org/10.1021/cr068040u.

(21) Banerjee, T.; Sahoo, R. K.; Rath, S. S.; Kumar, R.; Khanna, A. Multicomponent Liquid-Liquid Equilibria Prediction for Aromatic Extraction Systems Using COSMO-RS. *Ind. Eng. Chem. Res.* **2007**. https://doi.org/10.1021/ie060647d.

(22) Wang, S.; Sandler, S. I.; Chen, C. C. Refinement of COSMO-SAC and the Applications. *Ind. Eng. Chem. Res.* **2007**, *46* (22), 7275–7288. https://doi.org/10.1021/ie070465z.

(23) Banerjee, B.; Pugazhenthi, G.; Banerjee, T. Experimental Insights into the Thermal Dehydrogenation of Ethylene Diamine Bisborane Using Allyl-Based Ionic Liquids. *Energy and Fuels* **2017**, *31* (5), 5428–5440. https://doi.org/10.1021/acs.energyfuels.6b02823.

(24) Banerjee, B.; Kundu, D.; Pugazhenthi, G.; Banerjee, T. Quantum Chemical and Experimental Insights for the Ionic Liquid Facilitated Thermal Dehydrogenation of Ethylene Diamine Bisborane. *RSC Adv.* **2015**, *5* (104), 85280–85290. https://doi.org/10.1039/c5ra10625g.

(25) Simmie, J. M. A Database of Formation Enthalpies of Nitrogen Species by Compound Methods (CBS-QB3, CBS-APNO, G3, G4). *J. Phys. Chem. A* **2015**. https://doi.org/10.1021/acs.jpca.5b06054.

(26) Řezáč, J.; Šimová, L.; Hobza, P. CCSD[T] Describes Noncovalent Interactions Better than the CCSD(T), CCSD(TQ), and CCSDT Methods. *J. Chem. Theory Comput.* **2013**. https://doi.org/10.1021/ct3008777.

(27) Peng, C.; Schlegel, H. B. Optimizing to a Transition State or Higher-Order Saddle Point Transition State Optimizations Using Synchronous Transit-Guided Quasi. *J. Comp. Chem* **1994**.

(28) Bakhmutov, V. I. *Dihydrogen Bonds: Principles, Experiments, and Applications*; 2007. https://doi.org/10.1002/9780470226759.

(29) Hansen, B. B.; Spittle, S.; Chen, B.; Poe, D.; Zhang, Y.; Klein, J. M.; Horton, A.; Adhikari, L.; Zelovich, T.; Doherty, B. W.; et al. Deep Eutectic Solvents: A Review of Fundamentals and Applications. *Chem. Rev.* **2021**, *121* (3), 1232–1285. https://doi.org/10.1021/acs.chemrev.0c00385.

Chapter 6

Research Conclusions and Future Scope

6.1. Research Conclusions

The primary conclusion of this thesis are discussed below:

In the initial part of the thesis, i.e., chapter 2, dehydrogenation of amine borane complexes in ionic liquids was carried out using experimental and theoretical methodologies at temperatures ranging from 95 to 105°C. The solubility of amine borane complexes, ammonia borane (AB), and ethylene diamine bisborane (EDAB) in ILs was performed using the thermodynamic based COnductor like Screening MOdel (COSMO-SAC). Ammonium and pyrrolidinium-based cations were used for IL-based dehydrogenation since they were less commonly used as catalytic solvents. The selection of anion was determined by the hydrogen bond basicity (β) parameter of the anion moiety, which gauges an anion's ability to take protons through hydrogen bonding. The solubility investigations indicated that [TBMA][CH_3CO_3] had a greater dissolving capacity than [Bmpyr][CH_3CO_3]. The solubility studies corroborated the dehydrogenation experiments, which revealed that [TBMA][CH_3CO_3] tends to release more equivalents of hydrogen gas from AB and EDAB at 95°C and 105°C, respectively. Furthermore, quantum chemical simulations were carried out to confirm the same trend as observed in the experimental experiments and to better understand the mechanism of the dehydrogenation process at the micro-scale.

In the second chapter, theoretical investigations predicted the interaction energies using density functional theory (DFT) and HOMO-LUMO analysis. The latter revealed the fact that the anionic moieties of ILs are the regulating components, as they initiate the dehydrogenation of amine boranes via hydrogen-bond interactions between the protic moieties of amine boranes and the anionic moieties of the ILs. However, the preliminary investigation was insufficient to draw a conclusion and was unable to be replicated to earlier experimental findings indicating that highly basic anions produce a higher amount of hydrogen equivalents. The ability of the

anions possessing higher basicity gave higher equivalents of hydrogen. This was attributed to their interaction with imidazolium-based cations, which readily stabilize the ionic intermediates generated during the reaction. A combined experimental and computational technique was employed to investigate the dehydrogenation of amine borane complexes to confirm the same effect. Three anions were utilised in order of decreasing basicity: $[MeSO_4]$ > $[BF_4]$ > $[PF_6]$. These anions were combined with a higher alkyl chain cation, i.e. $[Bmim]^+$, which has been shown to be effective in catalytic processes. The prominent influence of anions' basicity in IL systems was established using a quantum chemical approach, which revealed the fact that the basicity of ILs derives from anionic species.

The thesis then proceeds to elucidate the molecular and spectroscopic mechanisms behind the formation of Type 1 metal salt-based DESs. Understanding the mechanism of DES production is essential since its features are novel and have the potential to be exploited as a catalytic solvent. The third chapter of the thesis analyses the mechanism of production of type 1 DESs using both experimental data and density functional theory (DFT) computations. The metal salt-based formulation was confirmed through the use of Fourier transform infrared spectroscopy (FTIR), which demonstrates the formation of DES. The experimental study indicated that the formation of DES is facilitated by the existence of numerous hydrogen and electrostatic interactions. The formation of DES systems at the molecular level was investigated using DFT simulations in conjunction with the quantum theory of atoms in molecules (QTAIM) and reduced gradient (RDG) analysis.

The following chapter will demonstrate the catalytic effect of neoteric solvents (DESs) on the thermal dehydrogenation of AB and EDAB. An IL-based DES was used to carry out the dehydrogenation reaction in the first case. It was found that the dehydrogenation of the amine borane in the presence of DES2 was comparable to that of IL, with the latter being

capable of releasing 3.2 equivalents of hydrogen, as opposed to the 3.7 equivalents of hydrogen released by DES2 ([Bmim][$MeSO_3$]:[Urea]). The decreased hydrogen release observed with IL-based DES was attributed to the HBDs' non-ionicity and low basicity. DESs based on choline chloride (HBAs) were employed in the second instance to overcome these concerns. Choline chloride (HBAs) was mixed with metal (II) chloride salts in a molar ratio of 1:2 to produce type 1 metal salt-based DESs, which were utilized to address the issues mentioned above. DES4 (ChCl: $ZnCl_2$) induced dehydrogenation of amine boranes tends to liberate 2.1 and 3.89 equivalents of hydrogen from AB and EDAB, respectively. The use of metal salt-based DESs, on the other hand, is preceded by an induction phase, which can be ascribed to the higher viscosity of the DESs. Nevertheless, the use of type 1 DESs paves the way for the future application of metal salt-based DESs for the dehydrogenation of amine borane complexes. This can be achieved by tweaking the various combinations of HBA and metal salts, especially those with lower viscosity and are capable of releasing hydrogen equivalents at a lower temperature and a higher reaction rate.

In the final chapter of the thesis, we investigated the potential of morpholine borane complex (MBC) as a hydrogen storage carrier. The chapter begins with a detailed examination of the MBC's thermal properties, identifying the unique material as a promising candidate for use as a hydrogen storage carrier. A protic ionic liquid (PIL), namely [Bmim][HSO_4], was used in the thermal dehydrogenation of MBC, and the results were promising. These acidic ionic liquids are well-known for their excellent performance in dehydrogenation processes. In comparison to the solid-state dehydrogenation of MB complex, the solvent-assisted thermal dehydrogenation of MB complex typically produces 1.62 equivalents of hydrogen gas, which is significantly more than the 0.62 equivalents. Additionally, it was revealed that the alkyl chain length of the IL's cation affects the dehydrogenation of the MB complex. The dehydrogenation mechanism of the MB complex also proceeds via both intramolecular and intermolecular

interactions, as demonstrated experimentally and computationally.

6.2. Future Scope

With the introduction of chemical hydrides, ILs have been found to be an effective green catalytic solvent for the dehydrogenation of amine borane complexes. This study discusses the recently discovered non-toxic, cost-effective solvents known as DESs. The introduction of DESs adds a new class of solvent that has the potential to improve the dehydrogenation efficiency of amine boranes. The lingering concerns with ILs and DESs provide us with some prospective breadth and perspective that can be addressed in future work. The following describes the future scope:

a) The regeneration of chemical hydrides on-board is a significant impediment to its use as a hydrogen storage carrier. The solubility of polymeric species within ILs and DESs precludes the solvents from being regarded as catalytic media. This problem needs to be resolved before the IL/DES-assisted dehydrogenation of chemical hydrides can be initiated on an industrial basis.

b) The recyclability of these environmentally friendly solvents is a further key issue that might be addressed in future studies. To separate reported ILs from solutes, solvents such as diethyl ether and tetrahydrofuran can be utilized. In the case of thermal dehydrogenation of chemical hydrides, however, the reaction is associated with the formation of linear poly(aminoborane)s in the presence of ILs/DESs. These oligomers cannot be isolated from their respective solute-IL/DES mixtures because they are soluble in IL/DES medium. Enhancing anti-solvents is one strategy to avoid this problem. DMSO was identified as the most promising solvent for recovering amine boranes. Our research could also advocate a similar approach for future endeavors.

c) With advancements in technology and study, it has been discovered that liquid organic

hydrogen carriers (LOHC) can also be employed as hydrogen storage. The LOHC's transport and hydrogen release processes are elementary to initiate. The LOHC process begins with the adsorption of hydrogen equivalents, which is dependent on the ability of the compound to store hydrogen molecules and concludes with the desorption of hydrogen equivalents, leaving the parent compound as the residual product. The primary difficulty that remains unresolved is optimizing operational conditions throughout the process. The research is primarily focused on minimizing the requirement for increased temperature and pressure in implying LOHC as a hydrogen storage carrier.

d) Another avenue of future research could be the use of liquid ammonia as a hydrogen storage medium that dissociates and releases hydrogen and nitrogen as a residual product, a process that is sustainable.

APPENDIX

Appendix A (Chapter-2)

Table A1: NBO charges on individual atoms for Ammonia borane (AB) at B3LYP-D3(BJ)/6-311++G(d,p) level of theory

Atom No.	Atom Type	Charge
N	1	-0.836
H	2	0.396
H	3	0.396
H	4	0.396
B	5	-0.151
H	6	-0.066
H	7	-0.066
H	8	-0.066

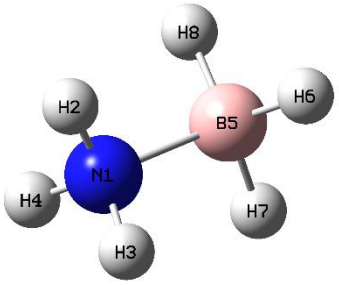

Total charge = 0.000

Table A2: NBO charges on individual atoms for Ethylenediamine bisborane (EDAB) at B3LYP-D3(BJ)/6-311++G(d,p) level of theory

Atom No.	Atom Type	Charge
N	1	-0.683
H	2	0.395
H	3	0.395
B	4	-0.155
H	5	-0.056
H	6	-0.063
H	7	-0.063
C	8	-0.188
H	9	0.209
H	10	0.209
C	11	-0.188
H	12	0.209
H	13	0.209
H	14	0.395
H	15	0.395
H	16	-0.056
H	17	-0.063
H	18	-0.063
N	19	-0.683
B	20	-0.155

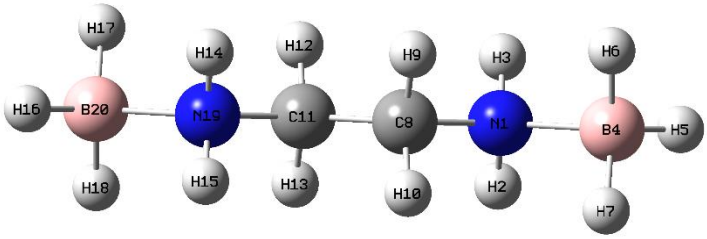

Total charge = 0.00

Table A3: NBO charges on individual atoms for AB-[BF_4^-] anion system at B3LYP-D3(BJ)/6-311++G(d,p) level of theory

Atom No.	Atom Type	Charge
B	1	1.330
F	2	-0.585
F	3	-0.585
F	4	-0.560
F	5	-0.585
N	6	-0.845
H	7	0.414
H	8	0.414
H	9	0.414
B	10	-0.170
H	11	-0.080
H	12	-0.080
H	13	-0.080

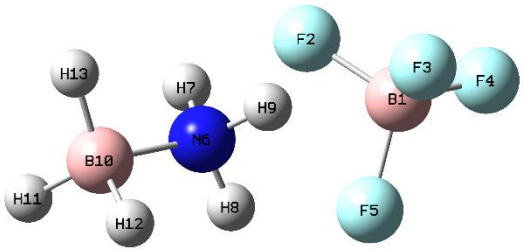

Total charge on BF_4^- anion = -0.985
Total charge on AB complex = -0.013

Table A4: NBO charges on individual atoms for AB-[PF_6^-] anion system at B3LYP-D3(BJ)/6-311++G(d,p) level of theory

Atom No.	Atom Type	Charge
F	1	-0.600
F	2	-0.580
F	3	-0.600
F	4	-0.580
P	5	2.552
F	6	-0.600
F	7	-0.580
N	8	-0.838
H	9	0.411
H	10	0.411
H	11	0.411
B	12	-0.170
H	13	-0.078
H	14	-0.078
H	15	-0.078

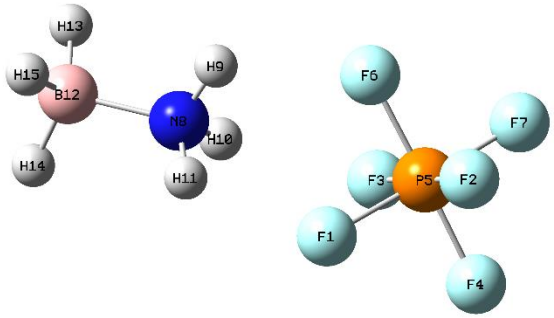

Total charge on PF_6^- anion = -0.988
Total charge on AB complex = -0.009

Table A5: NBO charges on individual atoms for AB-[$MeSO_4^-$] anion system at B3LYP-D3(BJ)/6-311++G(d,p) level of theory

Atom No.	Atom Type	Charge
S	1	2.451
O	2	-1.009
O	3	-1.009
O	4	-0.942
O	5	-0.756
C	6	-0.218
H	7	0.168
H	8	0.177
H	9	0.177
N	10	-0.864
H	11	0.375
H	12	0.432
H	13	0.432
B	14	-0.169
H	15	-0.084
H	16	-0.075
H	17	-0.084

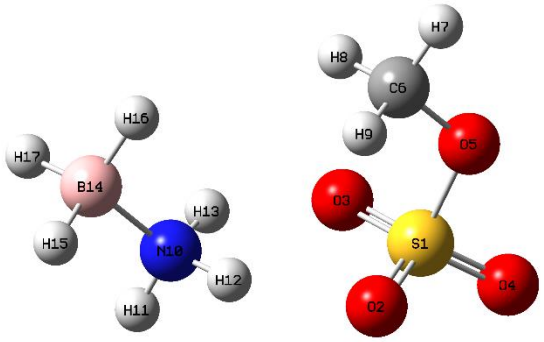

Total charge on $MeSO_4^-$ anion = -0.961
Total charge on AB complex = -0.037

Table A6: NBO charges on individual atoms for EDAB-[BF_4^-] anion system at B3LYP-D3(BJ)/6-311++G(d,p) level of theory

Atom No.	Atom Type	Charge
B	1	1.334
F	2	-0.550
F	3	-0.579
F	4	-0.589
F	5	-0.575
N	6	-0.701
H	7	0.443
H	8	0.383
B	9	-0.164
H	10	-0.068
H	11	-0.080
H	12	-0.065
C	13	-0.189
H	14	0.196
H	15	0.223
C	16	-0.197
H	17	0.196
H	18	0.238
H	19	0.378
H	20	0.439
H	21	-0.070
H	22	-0.080
H	23	-0.061
N	24	-0.696
B	25	-0.164

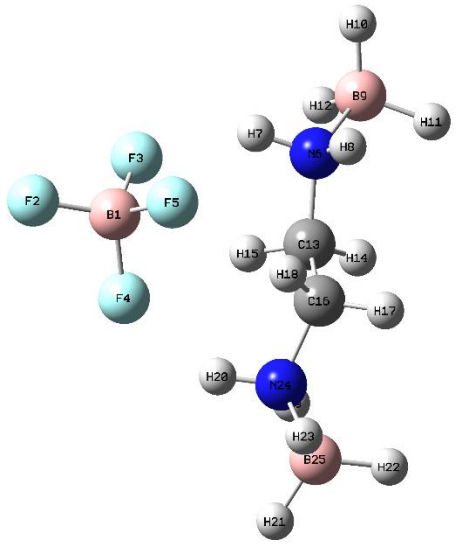

Total charge on BF_4^- anion = -0.959
Total charge on EDAB complex = -0.039

Table A7: NBO charges on individual atoms for AB-[PF_6^-] anion system at B3LYP D3(BJ)/6-311++G(d,p) level of theory

Atom No.	Atom Type	Charge
F	1	-0.611
F	2	-0.574
F	3	-0.597
F	4	-0.574
P	5	2.557
F	6	-0.597
F	7	-0.576
N	8	-0.696
H	9	0.384
H	10	0.438
B	11	-0.163
H	12	-0.066
H	13	-0.063
H	14	-0.079
C	15	-0.189
H	16	0.225
H	17	0.197
C	18	-0.194
H	19	0.234
H	20	0.197
H	21	0.431
H	22	0.381
H	23	-0.068
H	24	-0.060
H	25	-0.078
N	26	-0.691
B	27	-0.163

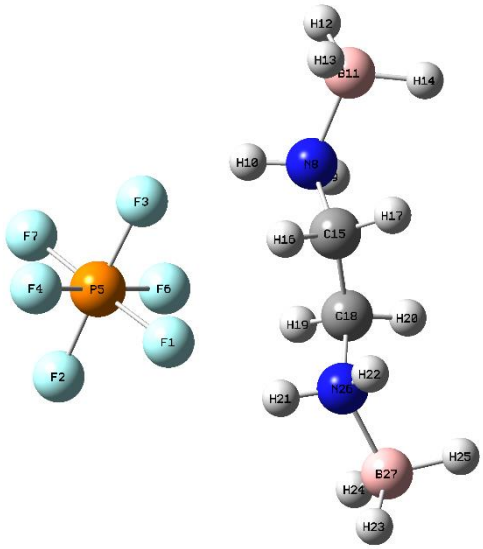

Total charge on PF_6^- anion = -0.972
Total charge on EDAB complex = -0.023

Table A8: NBO charges on individual atoms for EDAB-[$MeSO_4^-$] anion system at B3LYP-D3(BJ)/6-311++G(d,p) level of theory

Atom No.	Atom Type	Charge
S	1	2.455
O	2	-1.015
O	3	-1.015
O	4	-0.929
O	5	-0.751
C	6	-0.218
H	7	0.171
H	8	0.177
H	9	0.177
N	10	-0.679
H	11	0.384
H	12	0.384
B	13	-0.157
H	14	-0.079
H	15	-0.061
H	16	-0.061
C	17	-0.198
H	18	0.230
H	19	0.230
C	20	-0.175
H	21	0.189
H	22	0.189
H	23	0.437
H	24	0.437
H	25	-0.064
H	26	-0.078
H	27	-0.078
N	28	-0.731
B	29	-0.170

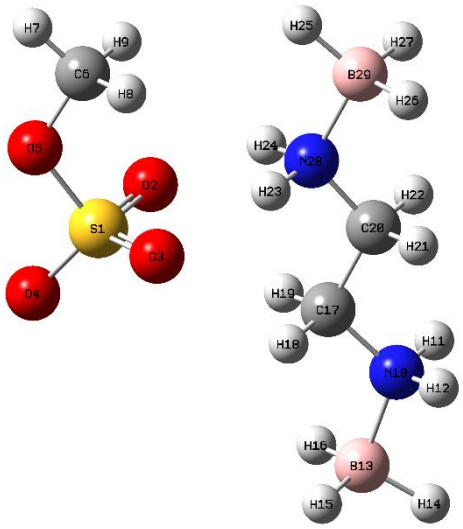

Total charge on $MeSO_4^-$ anion = -0.948
Total charge on EDAB complex = -0.051

A.1: Safety Aspects to be Followed during the Dehydrogenation process

It is vital to have a comprehensive set of laboratory safety standards in order to avoid laboratory catastrophes. Safety laws are only effective if enforced, which is why excellent laboratory management is also crucial for laboratory safety. It is also essential to understand the necessary laboratory safety signs and symbols.During the dehydrogenation experiment, the following actions must be carried out to preserve the aforementioned safety precautions.

1. Before starting the trials, safety considerations include ensuring that the system is under vacuum by ensuring the joints are properly connected.
2. Maintaining a sufficient level of vacuum to prevent IL or DES from reaching their respective vapor pressures.
3. Additionally, safety needs to be ensured on the mercury side.
4. As the system's internal pressure is high enough to cause mishaps, the gas syringe must be inserted slowly and carefully.
5. As the temperature at various portions of the apparatus varies, the equipment should be made from high-quality glass.
6. The condenser must be handled carefully because it contains nearly 1 liter of liquid nitrogen.

Appendix B (Chapter-3)

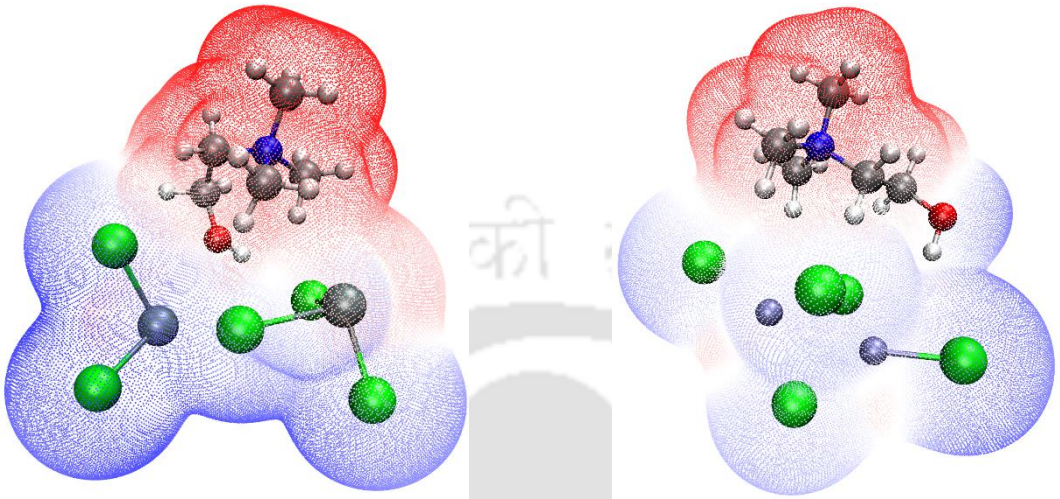

Figure B.1: Electrostatic potential (ESP) on an isosurface of electronic density (0.001 a.u.) for (a) DES1, and (b) DES2, where red color denotes positive region, and blue color denotes negative region

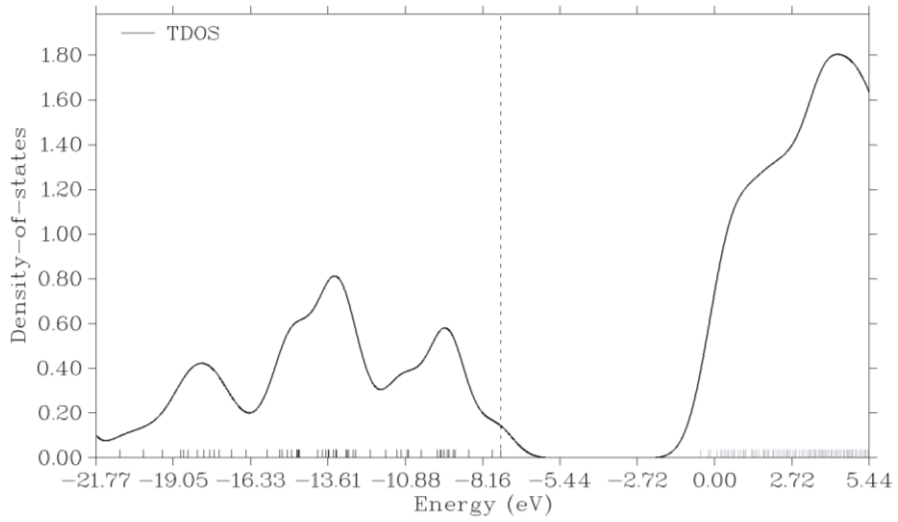

(a)

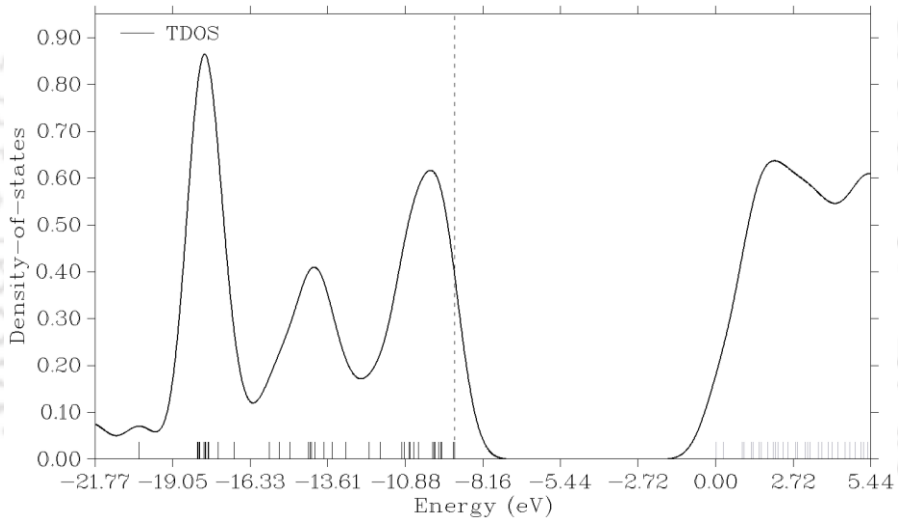

(b)

Figure B.2: Density of states (DOS) as a function of orbital energy, E, for (a) DES1, and (b) DES2

List of Publications

Published Articles

1. **Mishra, D. K.**; Pugazhenthi, G.; Banerjee, T. Ionic Liquid-Based Deep Eutectic Solvent as Reaction Media for the Thermal Dehydrogenation of Ethylene Diamine- Bis -Borane. ACS Sustainable Chem. Eng. 2020, 8, 4910−4919.
2. **Mishra, D. K.**; Pugazhenthi, G.; Banerjee, T. Ionic Liquid-Based Deep Eutectic Solvents as Novel Solvent-Cum-Catalyst Media for Thermal Dehydrogenation of Chemical Hydrides. Int. J. Hydrogen Energy 2021, 46, 15773.
3. **Mishra, D. K.**; Banerjee, B.; Pugazhenthi, G.; Banerjee, T. Metal-Free, Ionic Liquid-Mediated Hydrogen Release from Amine Borane Complexes: An Experimental and Density Functional Theory Investigation. *Ind. Eng. Chem. Res.* **2021**, *60* (27), 9764−9776.
4. **Mishra, D. K.;** Gopakumar, G.; Pugazhenthi, G.; Siva Brahmmananda Rao, C. V.; Nagarajan, S.; Banerjee, T. Molecular and Spectroscopic Insights into a Metal Salt-Based Deep Eutectic Solvent: A Combined Quantum Theory of Atoms in Molecules, Noncovalent Interaction, and Density Functional Theory Study. J. Phys. Chem. A. (2021) 9680-9690.
5. **Mishra, D. K.**; Hussain, R.; Pugazhenthi, G.; Banerjee, T. Thermal Dehydrogenation of Ionic Liquid Mediated Morpholine Borane Complex: A Novel and Efficient Hydrogen Storage Carrier. ACS Sustain. Chem. Eng. 10 (2022) 6157−6164.

Manuscripts under Revision/To be Submitted

1. **Mishra, D. K.**; Pugazhenthi, G.; Banerjee, T. An Experimental and Theoretical Elucidation: Does the Hydrogen Bond Basicity of Imidazolium-Based Ionic Liquids Affects the Thermolytic dehydrogenation of Amine Borane Complexes? (Submitted to The Journal of Physical Chemistry B, ACS Publications)
2. **Mishra, D. K.**; Pugazhenthi, G.; Banerjee, T. A Theoretical Elucidation: How and Ionic Liquid-Based Deep Eutectic Solvent is formed? (Under Revision, will be submitted)

Other Publications

1. Dutta, Arindam; **Mishra, D.K.**; Kundu, D.; Mahanta, U.; Jiang, S.P.; Silvester, D.; Banerjee, T. Examining the Electrochemical Nature of an Ionogel Based on the Ionic Liquid $[P_{66614}][TFSI]$ and TiO_2: Synthesis, Characterization, and Quantum Chemical Formulations. Ind. Eng. Chem. Res. 60 (2022).
2. Das, N.K.; **Mishra, D.K.**; Naik, P.K.; Dehury, P.; Bose, S.; Banerjee, T. Thermophysical Characterization of Dihydrolevoglucosenone based Nanofluid and its Evaluation as a Novel Heat Transfer Media: An Experimental and Density Functional Theory Study. (Submitted to Journal of Energy Storage, Elsevier)
3. Ramalingam, A.; Banerjee, T.; VIVEK , M.S.; Vatti, A.K.; **Mishra, D.K.**; Paul Mark Reji, D.J.; Nagaraj, S. Experimental and Quantum Chemical Calculation for the Production of High Purity of Ethyl Acetate. (Submitted to the Journal of Molecular Liquids, Elsevier).

International Conferences and Workshops

1. **Mishra, D. K**.; Kundu, Debasis.; Pugazhenthi, G.; Banerjee, T. Quantum Chemical Calculations for Ionic liquids assisted Thermal Dehydrogenation of Tert-Butylamine-Borane, Research Conclave IIT Guwahati 2017, 16th - 19th March, 2017, IIT, Guwahati, India
2. **Mishra, D. K**.; Pugazhenthi, G.; Banerjee, T. A Comparison of Thermal Dehydrogenation in Chemical Hydrides in Ionic Liquid and Deep Eutectic Solvent as Reaction Media, The 8th International Congress on Ionic Liquids (COIL-8), 2019 (Oral Presentation) May 13-17, 2019 Beijing China.
3. **Mishra, D. K.;** Gopakumar, G.; Pugazhenthi, G.; Siva Brahmmananda Rao, C. V.; Nagarajan, S.; Banerjee, T. Quantum Chemical Studies on Deep Eutectic Solvents Assisted Thermal Dehydrogenation of Amine-Borane Complexes. DAE First Computational Chemistry Symposium (DAE-CCS) (Poster Presentation) November 7-9, 2019 BARC, Mumbai, India (**Best Poster Award**).
4. **Mishra, D. K**.; Pugazhenthi, G.; Banerjee, T. Thermo-Gravimetric Analysis on Deep Eutectic Solvents Aided Dehydrogenation of Ammonia Borane XVI

INTERNATIONAL CONFERENCE ON THERMAL ANALYSIS and CALORIMETRY in RUSSIA (RTAC-2020) May 2020.

5. **Mishra, D. K**.; Pugazhenthi, G.; Banerjee, T. Methanesulfonate Anion Based Deep Eutectic Solvents Aided Thermal Dehydrogenation of Chemical Hydrides. FUTURE ASPECTS OF SUSTAINABLE TECH FAST 2.0. CIT Kokrajahar.
6. **Mishra, D. K**.; Pugazhenthi, G.; Banerjee, T. Ionic Liquid Based Deep Eutectic Solvents Aided Thermal Dehydrogenation of Chemical Hydrides. ASIL 9, 9th Australasian Symposium on Ionic Liquids. Melbourne, Australia
7. Attended the *Gaussian 16: Theory and Practice Workshop* organized by SCUBE Scientific Software Solutions (P) Ltd, held at Radisson Blu, 15th-19th January 2018, Delhi (Workshop)
8. Attended the Molecular Simulations Workshop organized by the Indian Institute of Chemical Engineers – Guwahati Regional Centre (IIChE-GRC), held at the Department of Chemical Engineering, IIT Guwahati, 27th Sept 2017